AD NUMBER
ADB010248
LIMITATION CHANGES

TO:

Approved for public release; distribution is unlimited.

FROM:

Distribution authorized to U.S. Gov't. agencies only; Test and Evaluation; OCT 1975. Other requests shall be referred to Army Materials and Mechanics Research Center, ATTN: AMXMR-PL, Watertown, MA 02172.

AUTHORITY

AMMRC D/A ltr, 8 Jun 1978

AD

AMMRC CTR 75-28

BRITTLE MATERIALS DESIGN, HIGH TEMPERATURE GAS TURBINE

Technical Report By:

Arthur F. McLean, Ford Motor Company, Dearborn, Michigan 48121
Eugene A. Fisher, Ford Motor Company, Dearborn, Michigan 48121
Raymond J. Bratton, Westinghouse Electric Corporation, Pittsburgh, Pennsylvania 15235
Donald G. Miller, Westinghouse Electric Corporation, Pittsburgh, Pennsylvania 15235

October, 1975

Prepared for

ARMY MATERIALS AND MECHANICS RESEARCH CENTER
Watertown, Massachusetts 02172

The findings in this report are not to be construed as an
official Advanced Research Projects Agency, Department of
the Army, or U.S. Government position, either expressed or
implied, unless so designated by other authorized documents.

Mention of any trade names or manufacturers in this report
shall not be construed as advertising nor as an official
indorsement or approval of such products or companies by
the United States Government.

DISPOSITION INSTRUCTIONS

Destroy this report when it is no longer
needed. Do not return it to the originator.

AMMRC CTR 75-28

BRITTLE MATERIALS DESIGN, HIGH TEMPERATURE GAS TURBINE

Technical Report By:

Arthur F. McLean, Ford Motor Company, Dearborn, Michigan 48121
Eugene A. Fisher, Ford Motor Company, Dearborn, Michigan 48121
Raymond J. Bratton, Westinghouse Electric Corporation, Pittsburgh, Pa 15235
Donald G. Miller, Westinghouse Electric Corporation, Pittsburgh, Pa 15235

October, 1975

Interim Report Number 8, January 1, 1975 to June 30, 1975

Contract Number DAAG 46-71-C-0162

DDC
RECEIVED
APR 14 1976
D

Prepared for:

ARMY MATERIALS AND MECHANICS RESEARCH CENTER
Watertown, Massachusetts 02172

ACCESSION for		
NTIS	White Section	☐
DDC	Buff Section	☑
UNANNOUNCED		☐
JUSTIFICATION		
BY		
DISTRIBUTION/AVAILABILITY CODES		
Dist.	AVAIL. and/or SPECIAL	
B		

i

ABSTRACT

The "Brittle Materials Design, High Temperature Gas Turbine" program objective is to demonstrate successful use of brittle materials in demanding high temperature structural applications. A small vehicular gas turbine engine and a static test rig, each using uncooled ceramic components, will be utilized in this iterative design and materials development program. Both the contractor, Ford Motor Company, and the subcontractor, Westinghouse Electric Corporation, have had in-house research programs in this area prior to this contract.

In the vehicular turbine project, design work was completed and tooling ordered for a revised Design D silicon nitride duo-density turbine rotor using radially stacked airfoil sections which reduced blade stresses by 16%. Press bonding of duo-density rotors continues to show excellent bonding between the hot pressed hub and the reaction sintered blade ring when hub-forming and bonding are accomplished in the same operation. Two hot pressed silicon nitride hubs were successfully tested through ten cycles to 1950°F and 35,000 rpm in the turbine rotor test rig with no observable deterioration in the curvic coupling rotor-to-shaft attachment. Stators of 2.55 gm/cm^3 density silicon nitride were injection molded which were free from flaws as determined visually and by x-ray radiography. Further development of 2.7 gm/cm^3 density (84.5% T.D.) injection molded silicon nitride resulted in improved moldability; test samples nitrided in an atmosphere of 4% H_2/96% N_2 had an average modulus of rupture of 43.2 ksi. This material will be used for molding of engine components.

In the stationary turbine project, a decision was made to de-emphasize the 30 Mw size turbine demonstration of ceramic stator vanes and to focus available efforts on static rig testing. The static rig was rebuilt following catastrophic failure, and incorporates a new metal combustor with additional air cooling as well as other improvements. Tensile testing of Si_3N_4 continues, with the development of a method of powder support for the specimens which considerably improved alignment. Long term static oxidation testing of hot pressed Si_3N_4 resulted in strength degradation, due to the formation of $MgSiO_3$ which chemically attacks the Si_3N_4. Hot pressed Si_3N_4 made with yttria additives was found to have poor oxidation resistance at 1800°F, although oxidation resistance was good when measured at higher temperatures.

ii

FOREWORD

This report is the eighth semi-annual technical report of the
"Brittle Materials Design, High Temperature Gas Turbine" program
initiated by the Advanced Research Projects Agency, ARPA Order Number
1849, and Contract Number DAAG-46-71-C-0162. This is an incrementally-
funded six year program.

Since this is an iterative design and materials development
program, design concepts and materials selection and/or properties
presented in this report will probably not be those finally utilized.
Thus all design and property data contained in the semi-annual reports
must be considered tentative, and the reports should be considered
to be illustrative of the design, materials, processing, and NDT
techniques being developed for brittle materials.

The principal investigator of this program is Mr. A. F. McLean,
Ford Motor Company, and the technical monitor is Dr. A. E. Gorum,
AMMRC. The authors would like to acknowledge the valuable contri-
butions in the performance of this work by the following people:

TABLE OF CONTENTS

LIST OF ILLUSTRATIONS

LIST OF ILLUSTRATIONS

Page No.

LIST OF ILLUSTRATIONS

vii

LIST OF ILLUSTRATIONS

LIST OF ILLUSTRATIONS

LIST OF TABLES

1. INTRODUCTION

As stipulated by the Advanced Research Projects Agency of the Department of Defense at the outset of this program, the major purpose is to demonstrate that brittle materials can be successfully utilized in demanding high temperature structural applications. ARPA's major program goal is to prove by a practical demonstration that efforts in ceramic design, materials, fabrication, testing and evaluation can be drawn together and developed to establish the usefulness of brittle materials for engineering applications.

The gas turbine engine, utilizing uncooled ceramic components in the hot flow path, was chosen as the vehicle for this demonstration. The progress of the gas turbine engine has been and continues to be closely related to the development of materials capable of withstanding the engine's environment at high operating temperature. Since the early days of the jet engine, new metals have been developed which have allowed a gradual increase in operating temperatures. Today's nickelchrome superalloys are in use, without cooling, at turbine inlet gas temperatures of 1800° to $1900^\circ F$. However, there is considerable incentive to further increase turbine inlet temperature in order to improve specific air and fuel consumptions. The use of ceramics in the gas turbine engine promises to make a major step in increasing turbine inlet temperature to $2500^\circ F$. Such an engine offers significant advances in efficiency, power per unit weight, cost, exhaust emissions, materials utilization and fuel utilization. Successful application of ceramics to the gas turbine would therefore not only have military significance, but would also greatly influence our national concerns of air pollution, utilization of material resources, and the energy crisis.

From the program beginning, two gas turbine engines of greatly different size were chosen for the application of ceramics. One is a small vehicular turbine of about 200 hp (contractor Ford) and the other is a large stationary turbine of about 30 MW (sub-contractor Westinghouse). One difference in philosophy between the projects is worth noting. Because the ceramic materials, fabrication processes, and designs are not fully developed, the vehicular turbine engine was designed as an experimental unit and features ease of replacement of ceramic components. Iterative developments in a component's ceramic material, process, or design can therefore be engine-evaluated fairly rapidly. This work can then parallel and augment the time-consuming efforts on material and component characterization, stress analysis, heat transfer analysis, etc. Some risk of damage to other components is present when following this approach, but this is considered out-weighed by the more rapid acquisition of actual test information. On the other hand, the stationary turbine engine is so large, so expensive to test, and contains such costly and long lead-time components which could be damaged or lost by premature failure, that very careful material and design work must be performed to minimize the possibility of expensive, time-consuming failures.

It should be noted that both the contractor and sub-contractor had in-house research programs in this area prior to initiation of this program.

1

Silicon nitride and silicon carbide had been selected as the primary material candidates. Preliminary design concepts were in existence and, in the case of the vehicular engine, hardware had been built and testing had been initiated.

At the out-set, the program was considered to be both highly innovative and risky. However, it showed promise of large scale financial and technological payoff as well as stimulation of the pertinent technical communities. This reporting period is in the fourth year of the program and major accomplishments have been achieved.

This is the 8th semi-annual report of progress. The format is the same as the last report, in that it is organized into two major sections. This was done because the technology is rather specifically related to the objectives of each project. In addition, the widespread interest from the turbine technology community centers on either the vehicular turbine project or the stationary turbine project. Each section will be complete in itself and will include its own introduction, to be of more help to the reader. The two sections are titled:

- Vehicular Turbine Project
- Stationary Turbine Project

2. INTRODUCTION AND SUMMARY-VEHICULAR TURBINE PROJECT

The principal objective of the Vehicular Turbine Project is to develop ceramic components and demonstrate them in a 200-HP size high temperature vehicular gas turbine engine. The entire hot flow path will comprise uncooled parts. The attainment of this objective will be demonstrated by 200 hours of operation over a representative duty cycle at turbine inlet temperatures of up to 2500°F. Successful completion of this program objective demonstrates that ceramics are viable structural engineering materials, but will also represent a significant breakthrough by removing the temperature barrier which has for so long held back more widespread use of the small gas turbine engine.

Development of the small vehicular regenerative gas turbine engine using superalloy materials has been motivated by its potentially superior character- istics when compared with the piston engine. These include:

- Continuous combustion with inherently low exhaust emissions

- Multi-fuel capability

- Simple machine - fewer moving parts

- Potentially very reliable and durable

- Low maintenance

- Smooth, vibration-free production of power

- Low oil consumption

- Good cold starting capabilities

- Rapid warm-up time

With such impressive potential, the small gas turbine engine using superalloys has been under investigation by every major on-highway and off-highway vehicle manufacturer in the world

In addition, the small gas turbine engine without exhaust heat recovery (i.e. non-regenerative) is an existing, proven type of power plant widely used for auxiliary power generation, emergency standby and continuous power for generator sets, pump and compressor drives, air supply units, industrial power plants, aircraft turboprops, helicopter engines, aircraft jet engines, marine engines, small portable power plants, total energy systems, and hydrofoil craft engines. While this variety of applications of the small gas turbine using superalloys is impressive, more widespread use of this type engine has been hampered by two major barriers, efficiency and cost. This is particularly so in the case of high volume automotive applications.

Since the gas turbine is a heat engine, efficiency is directly related to cycle temperature. In current small gas turbines, maximum temperature is limited not by combustion, which at stoichiometric fuel/air ratios could produce temperatures well in excess of 3500°F, but by the capabilities of the hot component materials.

Today, nickel-chrome superalloys are used in small gas turbines where blade cooling is impractical, and this limits maximum turbine inlet gas temperature to about 1800°F. At this temperature limit, and considering state-of-the-art component efficiencies, the potential overall efficiency of the small regenerative gas turbine is not significantly better than that of the gasoline engine and not as good as the Diesel. On the other hand a ceramic gas turbine engine operating at 2500°F will have fuel economies superior to the Diesel at significant weight savings.

The other major barrier is cost and this too is strongly related to the hot component materials. Nickel-chrome superalloys, and more significantly cobalt based superalloys which meet typical turbine engine specifications, contain strategic materials not found in this country and cost well over $5/lb.; this is excessively costly with respect to high volume applications such as trucks or automobiles. High temperature ceramics such as silicon nitride or silicon carbide, on the other hand, are made from readily available and vastly abundant raw materials and show promise of significantly reduced cost compared to superalloys, probably by at least an order of magnitude.

Thus, successful application of ceramics to the small gas turbine engine, with an associated quantum jump to 2500°F would not only offer all of the attributes listed earlier, but in addition offer superior fuel economy and less weight at competitive cost with the piston engine.

2.1 VEHICULAR TURBINE PROJECT PLAN

The vehicular turbine project is organized to design and develop an entire ceramic hot flow path for a high temperature, vehicular gas turbine engine. Figure 2.1 shows a schematic of this regenerative engine. Air is induced through an intake silencer and filter into a radial compressor, and then is compressed and ducted through one side of each of two rotary regenerators. The hot compressed air is then supplied to a combustion chamber where fuel is added and combustion takes place.
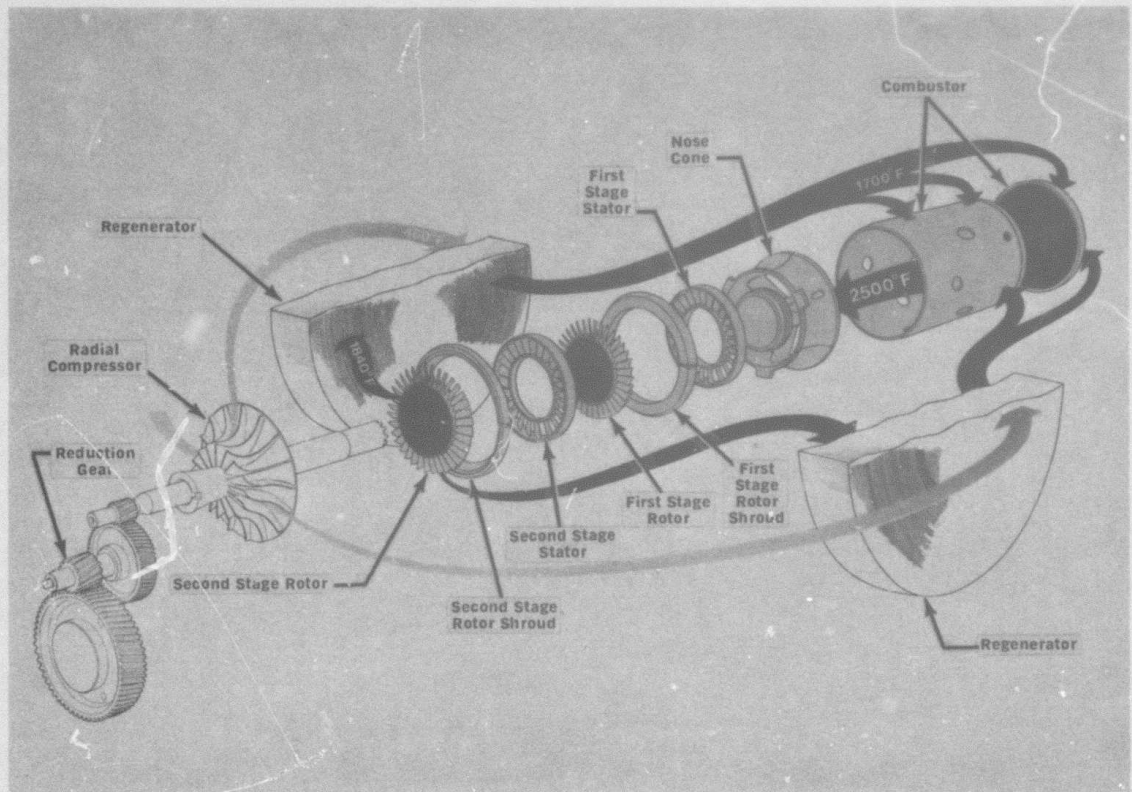
Figure 2.1   Schematic View of the Vehicular Gas Turbine Engine Flowpath

The hot gas discharging from the combustor is then directed into the turbine stages by a turbine inlet nose cone. The gas then passes through the turbine stages which comprise two turbine stators, each having stationary airfoil blades which direct the gas onto each corresponding turbine rotor. In passing through the turbine, the gas expands and generates work to drive the compressor and supply useful power. The expanded turbine exhaust gas is then ducted through the hot side of each of the two regenerators which, to conserve fuel, transfer much of the exhaust heat back into the compressed air. The hot flow path components, subject to peak cycle temperature and made out of superalloys in today's gas turbine, are the combustor, the turbine inlet nose cone, the turbine stators, the turbine tip shrouds, and the turbine rotors. These are areas where the use of ceramics could result in the greatest benefits, therefore these components have been selected for application in the vehicular turbine project.

5

Successful development of the entire ceramic flow path, as demonstrated in a high temperature vehicular gas turbine engine, will involve a complex iterative development. Figure 2.2 shows a block diagram flow chart, including the feedback loops, of the major factors involved, and serves to illustrate the magnitude of this complex and comprehensive iterative development program. Of particular importance is the inter-relationship of design, materials development, ceramic processes, component rig testing, engine testing, non-destructive evaluation and failure analysis. One cannot divorce the development of ceramic materials from processes for making parts; no more so can one isolate the design of those parts from how they are made or from what they are made. Likewise, the design of mountings and attachments between metal and ceramic parts within the engine are equally important. Innovation in the control of the environment of critical engine components is another link in the chain. Each of these factors has a relationship with the others, and to obtain success in any one may involve compromises in the others. Testing plays an important role during the iterative development since it provides a positive, objective way of evaluating the various combinations of factors involved. If successful, the test forms the credibility to move on to the next link in the development chain. If unsuccessful the test flags a warning and prompts feedback to earlier developments to seek out and solve the problem which has resulted in failure. Finally, all of the links in the chain are evaluated by a complete engine test, by which means the ultimate objective of the program will be demonstrated. It is important then to recognize that this is a systems development program--no single area is independent, but each one feeds into the total iterative system.
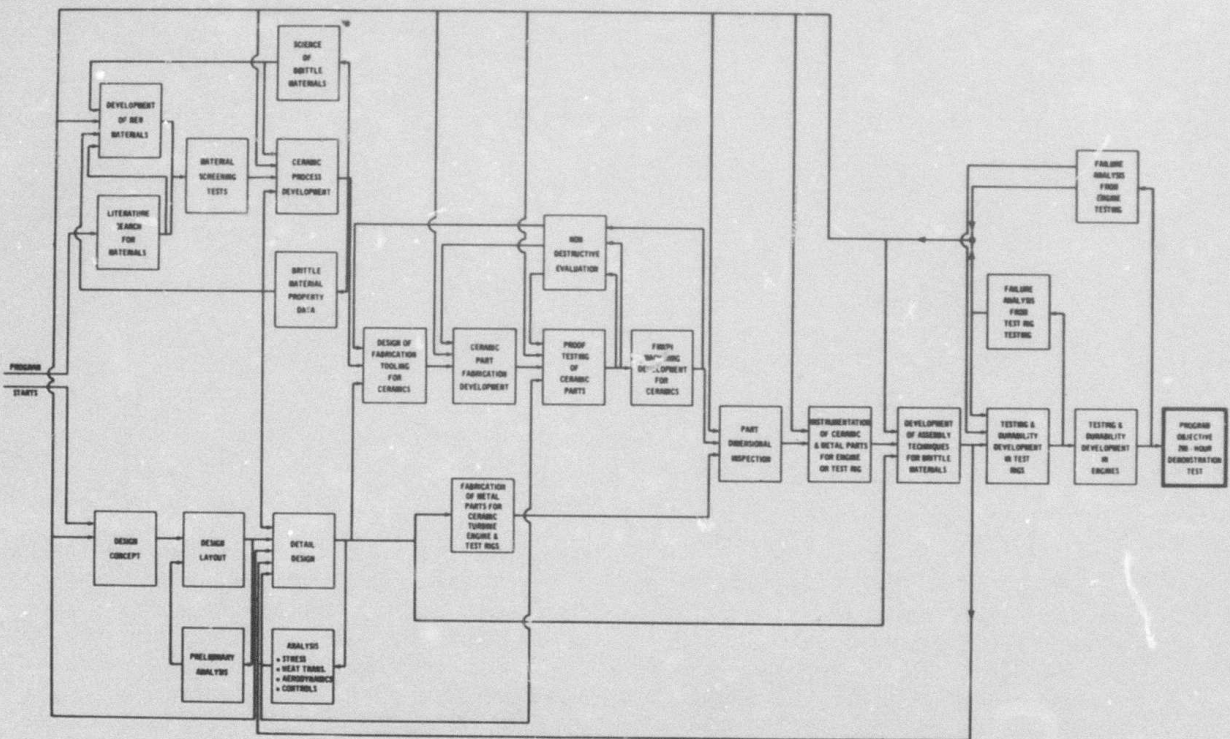
Figure 2.2   Block Diagram Flow Chart of the Iterative Development Process

2.2 PROGRESS AND CUMULATIVE STATUS SUMMARY - VEHICULAR TURBINE PROJECT

To meet the program objectives, the work has been divided into two major tasks:

1. Ceramic Component Development

2. Materials Technology

The progress and present status in each of these is summarized in Section 2.2.1 and 2.2.2.

2.2.1 CERAMIC COMPONENT DEVELOPMENT

Two categories of ceramic components are under development: rotating parts (i.e. ceramic rotors), and stationary parts (i.e. ceramic stators, rotor shrouds, nose cones, and combustors). In this iterative development, each component will pass through various phases comprising design and analysis, materials and fabrication, and testing.

Ceramic Rotors

Development of the ceramic turbine rotor is by far the most difficult task in the ARPA program. This is because of:

-   The high centrifugal stresses associated with maximum rotor speeds of 64,240 rpm.

-   The high thermal stresses associated with thermal shock and the high temperature gradients from the rotor rim to the rotor hub.

-   The high temperature of the uncooled blades associated with turbine inlet gas temperatures of up to 2500°F.

-   The very complex shape of the turbine rotor.

-   The hostile environment associated with the products of combustion from a turbine combustor.

Progress and Status

• Fully dense Si_3N_4 first and second stage integral rotors were designed and analyzed [1,2,3,4].

• A method of attaching rotors was conceived and designed [1,2].

• The following approaches for making integral rotors were investigated but discontinued:

-   • Direct hot pressing of an integral Si_3N_4 rotor [1].

-   • Ultrasonic machining of a rotor from a hot pressed Si_3N_4 billet [1,2,3].

Note: Numbers in parentheses refer to references listed in Section 8.

- • Hot pressing an assembly of individually hot pressed Si_3N_4 blades (1,2).

- • Pseudo-isostatic hot pressing of an injection molded Si_3N_4 preform (1,2,3).

- • Hot pressing using comformable tooling of preformed Si_3N_4 blades and hub (2,3,4).

- • Fabrication of a dense SiC blade ring by chemical vapor deposition (1,2,3,4).

- Electric discharge machining of a rotor from a hot pressed SiC billet (2,3,4).

• A "duo-density" Si_3N_4 ceramic rotor was conceived and designed (3).

• Tooling to injection mold Si_3N_4 blade rings was designed and procured (3).

• Hundreds of blade rings were molded for bonding experiments, cold spin tests, and developing blade ring quality.

• Over two hundred and sixty hot press bonding of duo-density rotors were carried out. These have progressed from rotors with flat-sided hubs to current fully-contoured hubs made simultaneously with the hot press bonding operation. Prior severe blade ring distortion problems have been solved by using a double blade fill technique to support the blade ring during bonding. In addition, the diffusion bond has improved to its current excellent quality as evidenced by microstructure examination. Experiments were conducted using magnesium nitrate instead of magnesium oxide as a densification aid. Excellent bonding and density was achieved, however, strength was deficient. Successful modifications were made to the graphite wedge system to reduce blade ring cracking and tearing problems. Problems which remain are some blade ring cracking, on an inconsistent basis, and also, occasional rim cracking (4,5,6,7,8).

• Over 50 cold spin tests resulted in blade failures over a range of speeds, some of which exceed full speed reqirements of the new Design D' blading. However, an improvement in consistency is required if a reasonable yield from the blade ring fabrication process is to be achieved. This emphasizes the need for three-dimensional blade stress analysis as well as development of a higher strength, better quality blade material. Cold spin testing of rotor hubs of hot pressed Si_3N_4 showed a characteristic failure speed of 115,965 rpm with a Weibull slope of 17.66. Several hot pressed hubs, made by the hot press bonding process were cold spun to distruction, and showed results consistent with the hot pressed hubs. A high speed motion picture study (3000 frames/sec) was conducted of a turbine rotor failure in the cold spin pit (8).

• A three dimensional model of the rotor blade along with heat transfer coefficients has been generated for three dimensional thermal and stress analysis (5,6,8).

• Development of better quality blade rings continues. X-ray radiography of green parts has proved effective in detecting major flaws. Slip cast Si_3N_4 test bars having a density of 2.7 gm/cm^3 show four point MOR of 40,000 psi, therefore processes to slip cast a rotor blade ring are under investigation

as are methods of achieving 2.7 gm/cm^3 density with injection molded material [6,7,8].

• Thermal shock testing simulating the engine light-off condition was conducted on rotor blade rings for approximately 2,500 cycles without damage [5,6].

• A technique to evaluate probability of failure using Weibull's theories was developed and applied to ceramic rotors [5].

• A test rig was designed and built to simulate the engine for hot spin testing of ceramic rotors [3,4,5]. A set of low quality duo-density rotors was spin tested to 20% speed and 1950°F for a short time before failure, believed due to an axial rub [7].

• A revised rotor design (Design D) was conceived, using common rotors at both first and second stage locations [7].

• A lower stress version of the Design D rotor, designated Design D', has been designed using radially stacked blade sections. Blade stresses were reduced from 21,000 psi in Design D to 13,180 psi in Design D' [8].

• The rotor test rig was rebuilt and testing initiated with hot pressed Si$_3$N$_4$ rotor hubs to evaluate the rotor attachment mechanism, and the curvic coupling mounting design was subjected to 10 operating cycles to 1950°F without damage [8].

Ceramic Stators, Rotor Shrouds, Nose Cone, and Combustors

While development of the ceramic turbine rotor is the most difficult task, parallel development of the stationary ceramic flow path components is necessary to meet the objective of running an uncooled 2500°F vehicular turbine engine. In addition, success in designing, making, and testing these ceramic components will have an important impact on the many current applications of the small gas turbine where stationary ceramics alone can be extremely beneficial. The progress and status of these developments is summarized below taking each component in turn.

Progress and Status

Ceramic Stators

• Early Design A first stage stators incorporating the turbine tip shrouds had been designed, made by assembling individual injection molded Si$_3$N$_4$ vanes, and tested, revealing short time thermal stress vane failures at the vane root [1]

• Investigations of a number of modified designs led to Design B where the rotor shroud was separated from the stator. Short time thermal stress vane failures at the vane root were eliminated [1].

• In the fabrication of stators the starting silicon powder, the molding mixture and the nitriding cycle were optimized for 2.2 gm/cm^3 density material [2,3].

• Engine and thermal shock testing of first stage Design B stators revealed a longer term vane cracking at the vane mid-span. This let to modification of the vane cord, designated the Design C configuration, which solved the vane mid-span cracking problem [3,4].

·A remaining problem in first and second stage stators was cracking of outer shrouds, believed due to the notch effect between adjacent vanes. To solve this, tooling for a one-piece first stage Design C stator was procured [4,5].

·The second stage stator could not be made in one piece due to vane overlap, so an "inverted channel" design was investigated to eliminate notches at the stator outside diameter. However, engine testing showed that axial cracking of the outer shroud remained a problem [3,4,5,6].

·Completed 50 hour duty-cycle engine test of the hot flow path components to 1930°F. The assembled first stage Design C stator was in excellent condition; some vanes in the second stage inverted channel stator had developed fine cracks [6].

·Completed 100 hour duty-cycle engine test of the hot flow path components without a second stage stator to 1930°F. The one piece first stage Design C stator successfully survived this test [7].

·Improvements in material, and processing resulted in the fabrication of flaw free one piece stators of 2.55 gm/cm^3 density [8].

·A test was devised to mechanically load stator vanes to failure which provided useful information for material and process development [8].

·Thermal shock testing of 2.7 gm/cm^3 density stator vanes revealed no detectable cracking and negligible strength degradation after 9000 cycles of heating to 2700°F and cooling in the thermal shock rig [8].

Ceramic Rotor Shrouds

·Separate first and second stage ceramic rotor shrouds, which are essentially split rings, evolved in the stator change from Design A to Design B [1].

·As a result of rig and engine testing, rotor shrouds made of cold pressed, reaction sintered Si_3N_4 were modified to have flat rather than conical side faces [2].

·Because of occasional cracking, cold pressing was replaced with slip casting for making higher density rotor shrouds, resulting in 2-3 times increase in strength (from 12 ksi up to 30-40 ksi) [3].

·Slip casting of rotor shrouds solved the cracking problem but revealed a dimensional change problem as a function of operating time. This was solved by incorporation of nitriding aids and heat treatments which reduced instability to acceptable levels [4,5,6].

·Completed 50 hour duty cycle engine test of the hot flow path components to 1930°F, after which both first and second stage rotor shrouds were in excellent condition [6].

·Further testing of rotor shrouds to 245 hours showed them to remain crack free and in excellent condition [7].

Ceramic Nose Cones

- Early Design A nose cones had been designed, made from injection molded reaction sintered Si_3N_4, and tested [1].

- The nose cone was modified to Design B to accommodate Design B first stage stators. Several Design B nose cones were made and tested in rigs and engines [2].

- Voids in molding nose cones were minimized by preferentially heating the tooling during molding [5].

- Circumferential cracking and axial cracking problems led to preslotted, scalloped nose cones designated Design C [3,4,5,6].

- Completed 50 hour duty-cycle engine test of the hot flow path components to $1930^{o}F$, after which the Design C nose cones was in excellent condition [6].

- Completed 100 hour duty-cycle engine test of the hot flow path components to $1930^{o}F$ after which the Design C nose cone was in excellent condition [7].

- Further such testing of the nose cone to 221 hours showed it to remain crack free and in excellent condition [7].

- Improvements in materials and processing resulted in the fabrication of flaw free nose cones of 2.55 gm/cm^3 density [8].

Ceramic Combustor

- Combustor tubes made of slip cast Si_3N_4 and various grades of recrystallized SiC (Crystar) cracked during light off tests in the combustor rig [4].

- A combustor tube made of reaction sintered SiC (Refel) successfully survived 171 hours of rig testing simulating the engine duty cycle with 20 hours at $2500^{o}F$ combustor outlet temperature [7]. This combustor was also successfully tested in an engine [8].

2.2.2   MATERIAL TECHNOLOGY

Materials technology forms the basis for component development including component design, component fabrication, material quality in the component as-made, and evaluation by testing. There are three major categories under materials technology---materials engineering data, materials science, and non-destructive evaluation. Progress and present status in each of these areas is summarized below:

Materials Engineering Data

•Techniques were developed and applied for correlating the strength of simple ceramic disks with bend test specimens using Weibull probability theories [5].

•Elastic property data as a function of temperature was determined for various grades of silicon nitride and silicon carbide [2,3,4,5,6,7].

•The flexural strength vs temperature of several grades of SiC and Si_3N_4 was determined [3,4,5,6].

•The compressive strength vs temperature of hot pressed SiC and hot pressed Si_3N_4 was determined [4].

•Creep in bending at several conditions of stress and temperature was determined for various grades of reaction sintered silicon nitride [4,5,6].

•The specific heat vs temperature of 2.23 gm/cm^3 reaction sintered Si_3N_4 was measured, as were thermal conductivity and thermal diffusivity vs temperature for both 2.23 gm/cm^3 and 2.68 gm/cm^3 reaction sintered Si_3N_4 [4].

•Stress-rupture data was obtained for reaction sintered silicon nitride under several conditions of load and temperature [6].

Materials Science

•A technique was developed and applied to perform quantitative x-ray diffraction analyses of the phases in silicon nitride [2].

•An etching technique was developed and used for the study of the microstructure of several types of reaction sintered Si_3N_4 [2].

•The relationship of some processing parameters upon the properties of reaction sintered Si_3N_4 were evaluated [3,4,5,6].

•The oxidation behavior of 2.2 gm/cm^3 density Si_3N_4 was determined at several different temperatures. The effect of oxidation was found to be reduced when the density of reaction sintered Si_3N_4 increased [3,7].

•The relationship of impurities to strength and creep of reaction sintered silicon nitride was studied, and material was developed having considerably improved creep resistance [4,5,6].

•Fractography and slow crack growth studies were performed on reaction sintered SiC [5] and hot pressed Si_3N_4 [6,7].

12

The development of sintered Sialon-type materials was initiated [7]. The effects of yttria additives are being studied especially in relation to the formation of glassy phases [8].

A higher density molded Si_3N_4 has been developed which will be used for component fabrication. Four point bend strengths of 43 ksi at room temperature were measured [8].

An experimental study showed that high pressures did not facilitate nitriding of relatively dense silicon compacts. A parallel theoretical study showed that to store sufficient nitrogen within the pores and avoid diffusion an impractically high pressure would be needed [8].

Non-Destructive Evaluation

Ultrasonic C-scan techniques were developed and applied for the measurement of internal flaws in turbine ceramics [1,2,3,4].

Sonic velocity measurements were utilized as a means of quality determination of hot pressed Si_3N_4 [2,3,5].

A computer-aided ultrasonic system was used to enhance the sensitivity of defect analysis in hot pressed Si_3N_4 [3,4,6].

Acoustic emission was applied for the detection of crack propagation rates and the onset of catastrophic failure in ceramic materials [1,2,5,6].

A method was developed and applied for the detection of small surface cracks in hot pressed Si_3N_4 combining laser scanning with acoustic emission [4].

X-ray radiography was applied for the detection of internal defects in turbine ceramics [2,3,4,5].

Hidden flaws in as-molded stators and rotor blade rings were located by x-ray radiography [5,6,7]. Such NDE of as-molded parts has been used to develop processes to make flaw-free components [8].

A dye penetrant has been used to detect surface cracks in components made of the higher density 2.55 gm/cm^3 Si_3N_4 [8].

A state-of-the-art summary of NDE methods as applied to the ceramic turbine programs was compiled [6].

2.3 FUTURE PLANS

While it may be concluded, from the program summarized in Section 2.2 of this report, that much has been accomplished in many portions of the vehicular turbine project, difficult problems still remain to be solved. This is particularly true in the fabrication development of ceramic turbine rotors. Future plans therefore emphasize increased effort on materials development and rotor process development. When rotors of reasonable quality can be made consistently the testing phase of the program will be emphasized to establish a statistical basis for proceeding toward 2500°F high speed testing.

Component Development

Changing design of the hot flow path to the Design D configuration discussed in the last report [7], which utilizes common stators and rotors at both first and second stage locations is expected to be highly beneficial. Since fewer difficult parts are required, more time and effort will be available for application to materials and fabrication development and for accumulation of test data on similar components, maximizing the statistical data base. Future component development work on duo-density Si_3N_4 turbine rotors will concentrate on the fabrication of molded and/or slip cast blade rings of high strength. The production of these parts in prototype quantity will be increased so that more press-bonding trials can be made, thus decreasing the turn-around time to identify and solve detailed fabrication problems. In addition, more components will become available for testing, thus increasing the feedback of test results to material and process improvements. Emphasis will be placed on identifying manufacturing flaws which result in premature failures, and on process improvement to eliminate these flaws. Non-destructive analysis techniques are expected to play an important role in flaw identification and subsequent elimination.

Based upon three-dimensional stress analyses, the turbine rotor blades have been redesigned (Design D') to reduce blade stresses. New tooling incorporating these design improvements will be procured, and will then be used for the fabrication of Design D' rotor blade rings. Further design studies will continue on an updated Design E flow path configuration which will be optimized for aerodynamic efficiency, ceramic manufacturing, and durability. This will be the final rotor design in the Ford/ARPA program, and will define the current state-of-the-art limitations in brittle material design as applied to small gas turbines.

The ceramic rotor testing program will continue to utilize room temperature spin testing to evaluate part quality and material strength. In addition, rotors will be evaluated in a hot spin rig prior to testing in a turbine rotor test rig which closely simulates the engine. Additional hot testing will be done in turbine engines, in order to increase the amount of available testing time and speed up the feedback of test information. In order to minimize the risk of rotor failure during engine testing, rotors with blades of reduced height will first be used. As improvements are made, it is anticipated that the blade heights will be increased until the correct design height is attained. Test temperatures will also be gradually increased during this engine testing sequence until 2500°F is reached.

In addition, component development will continue on the stationary flowpath components. Research on fabrication of one piece stators will continue for the

14

higher-density (2.7 gm/cm^3 Si$_3$N$_4$) which has better properties than the 2.55 gm/cm^3 density Si$_3$N$_4$ now being tested. Refinements and improvements in component quality will continue, utilizing non-destructive evaluation techniques to evaluate and control quality. Efforts will continue to achieve major objectives of completion of a 175 hour test of stationary ceramic components over the ARPA duty cycle up to 1930°F (metal turbine rotors) and completion of a 25 hour test of the components up to 2500°F in a specially designed stationary flow path test rig which does not incorporate rotating parts.

Material Technology

Feedback from engine and rig testing of stationary components made from reaction sintered Si$_3$N$_4$ indicates that improved durability could be expected if improvements in strength and oxidation resistance could be obtained. Therefore, increased emphasis will be placed on the development of higher density injection molded Si$_3$N$_4$ for rotor blade rings, nose cones, and stators. Such material would be expected to have significantly improved strength and oxidation resistance; in addition, other means of improving oxidation resistance are being studied. Another area receiving major emphasis will be processing improvements aimed at increasing the yield of acceptable parts and reducing the risk of testing unacceptable parts in both molded and slip cast reaction sintered Si$_3$N$_4$. Integral with this effort will be the application and continued development of non-destructive evaluation techniques to assist in the elimination of flaws-in particular, those flaws which are found by testing to have a critical effect upon component life.

In the final stages of the program, increasing attention will be given to material characterization, including the higher density reaction sintered silicon nitride materials currently being developed. It is expected that materials engineering data will be compiled and statistically analyzed for those materials which are utilized for the 200 hour demonstration which constitutes the major program objective.

3. PROGRESS ON CERAMIC COMPONENT DEVELOPMENT-VEHICULAR TURBINE PROJECT

3.1 CERAMIC ROTOR DEVELOPMENT

SUMMARY

The Design D turbine rotors have been revised to Design D' to reduce blade stresses and to improve fabricability. Three-dimensional analysis of Design D' showed that the required strength of the blade material could be reduced by 16% compared to Design D. The new rotors, Design D', have non-twisted, radially stacked airfoils which have been thickened to improve injection molding fabrication. Using these design constraints, several iterations of aerodynamic design and analysis were conducted leading to Design D'. The results show that Design D' will be 1.0 to 1.8 percentage points lower in efficiency than Design D.

The algorithms necessary to conduct a strength analysis of a ceramic rotor based on a probabilistic approach have been derived. Component reliability may be predicted or, conversely, goals for material strength and variability may be set. Strength analysis of the Design D' rotor is in progress and will be reported in the next period.

Effort continues on fabrication development of the duo-density rotor involving hot pressing the hub and hot press bonding to the blade ring in one operation. A double blade fill technique was developed for support of the blade ring during press bonding. The technique consists of slip casting silicon metal powder between blades, and, after drying, encapsulating this assembly in additional slip cast silicon metal. This assembly is then nitrided in one operation which reduces the blade ring processing time by two weeks.

An attempt was made to improve the homogeneity of the hot pressed Si_3N_4 hubs by substituting magnesium nitrate for the MgO powder previously used as a a densification aid. The Si_3N_4 powder and magnesium nitrate additive was wet milled for seven days to achieve homogeneity and powder particle size below 2μ. Several turbine wheels were press bonded using this material; however, subsequent cold spin testing of the hubs produced failure speeds significantly lower than those made with magnesium oxide additive. Accordingly, use of magnesium nitrate has been discontinued and magnesium oxide is again being used as the densification aid.

Deficiencies in the graphite wedge system used to hot press bond turbine wheels resulted in fracture of the graphite restraining sleeve and subsequent fracture of the blade ring. Several modifications to the graphite system were made to improve turbine wheel quality. The most effective consisted in extending the width of the blade rim so that the contoured piston, in its final position at the end of press-bonding, over-laps the blade ring by the amount of the extension. Thus, the piston no longer drags on the restraining graphite sleeve and graphite breakage is eliminated.

Development of the shell mold slip casting process at Georgia Institute of Technology Experiment Station continued with concentration on weakening the mold to enhance removal without part damage after nitriding, and on mold filling techniques. The most successful mold material is carbon bonded with polyvinyl alcohol. Mold filling was best accomplished by centrifugal casting under vacuum. However, shrinkage cracking in the blades was experienced and attention was turned

17

to slip casting blade rings. Blade rings were formed without cracking or breaking of blades. It is evident that quality control of slip parameters must be developed for an acceptable yield of good blade rings.

The program on high pressure nitriding of high green density silicon metal components at Battelle was continued with experiments on the effect of higher nitriding temperatures, to 1450°C, and longer nitriding times. In high green density samples, nitriding to full density occurred only in a surface skin approximately 0.025 inches thick with substantial amounts of unreacted silicon in the core. Evidence of uncontrolled exothermic reaction was seen and it appears that optimization of the parameters controlling the reaction kinetics is difficult. A theoretical study of nitriding shows that it is not possible to store sufficient nitrogen in closed pores to complete the reaction at practical pressure levels, and therefore it was decided to discontinue this effort.

During this period many tests were conducted in the cold spin pit for evaluation of the strength of reaction sintered silicon nitride turbine blades. Blade ring segments, epoxied to metal or silicon nitride hubs, and complete blade rings were tested. The highest speed attained was 58,100 rpm or 91% maximum speed with Design C blades. This is equivalent to 69,000 rpm for the shorter Design D blades. In 50 tests comparing over 350 blades, scatter in breaking strength was only 8%. Data from the blade tests were statistically analyzed to determine distribution of failure speeds, characteristic speed, and Weibull modulus m.

Six hot pressed silicon nitride rotor hubs made from duo-density turbine wheels were spun to destruction in the cold spin pit. The highest failure speed was 113,570 rpm and review of the test results indicate that hub strengths are comparable to those made by a separate hot pressing operation.

A high speed motion picture study was conducted of the failure of a ceramic rotor spun to destruction at 55,540 rpm in the cold spin pit. Film speed was 3000 frames/second and the actual rotor disintegration was recorded in only 4 frames. Cracking progressed radially outward from the bore. Some circumferential movement of crack propagation was observed in the throat area.

The turbine rotor test rig was rebuilt after the last failure and operated with two hot pressed silicon nitride hubs at speeds to 35,000 rpm and temperature to 1950°F. The purpose of the test was to check the rig rebuild as well as the curvic coupling rotor-to-shaft attachment. The latter test comprising 10 thermal cycles was successful with no observed deterioration of the curvic coupling teeth.

In the previous report the efficiency of load transfer from the rotor bolt installation tool to the rotor nut was reported as 80% of predicted value. Recalibration of the fixture load cell showed this efficiency to be 95%.

18

3.1.1   DESIGN AND ANALYSIS

Introduction

A new low-stress turbine rotor, Design D' (D prime), has been analyzed
to determine the affects on engine performance, blade and rotor stress levels,
and material strength requirements. Results of aerodynamic analyses are presented
along with the full speed mechanical loading stress analysis and material strength
requirements. Mechanical and thermal stress distributions at maximum speed con-
ditions for the rotor disk, plus a three dimensional mechanical loading stress
distribution for the second stage airfoil were also determined.

Mechanical Design of the D Flowpath

The Design D flowpath, discussed earlier and shown in Figure 3.1, is composed
of common first and second stage stators, and first and second stage rotors, which
have been machined from the same as-hot-pressed, duo density rotors. A revision
of the blading of the Design D rotors has been designed to reduce blade stresses
and improve fabricability. This revision has been designated Design D' (D prime).
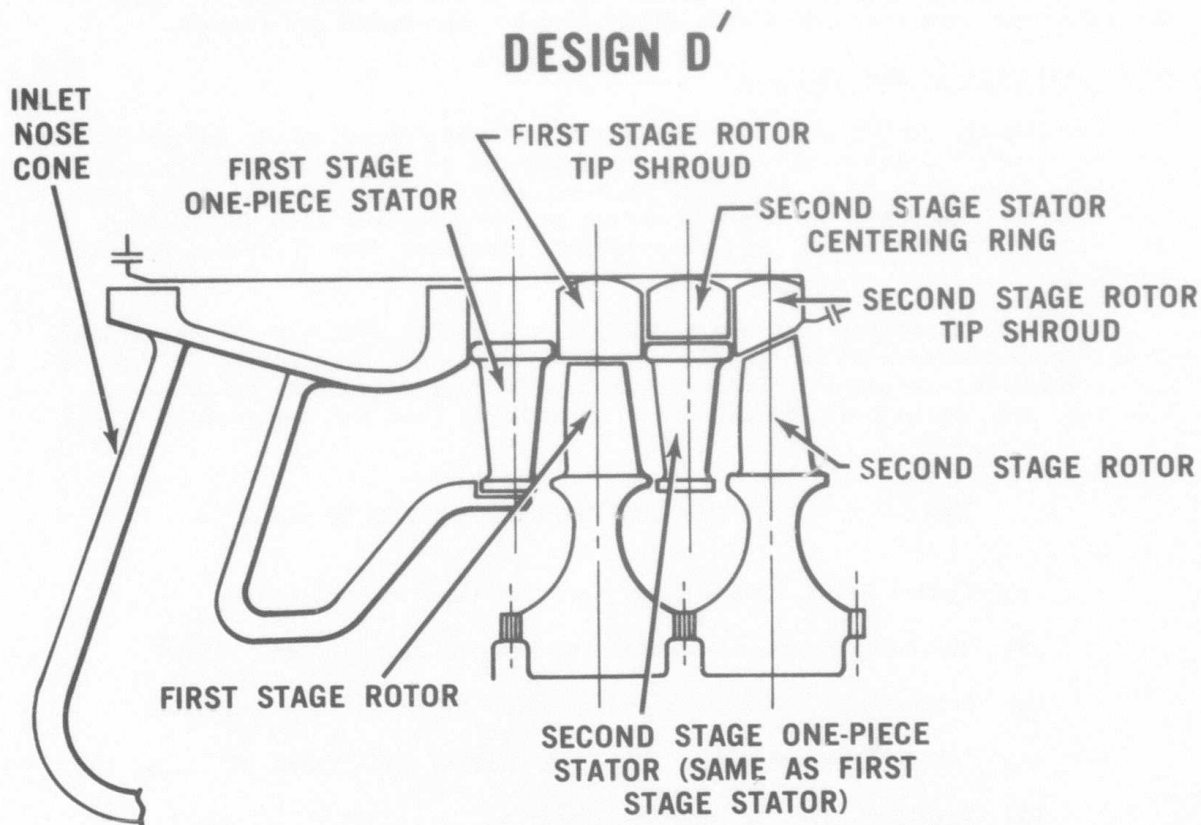
DESIGN D'

Figure 3.1   Schematic Cross-Section View of Design D' Hot Flow
Path Configuration

The blade was designed so that the maximum average centrifugal stress would not exceed 13,000 psi at 110% speed, and the trailing edges were thickened to facilitate the injection molding of the higher strength 2.7 gm/cm^3 Si$_3$N$_4$ material now being developed (Ref. Section 4.1 of this report). This was accomplished by using an airfoil design with non-twisted, radially stacked blade sections. The trailing edge thickness varied linearly from 0.022 inches at the tip to 0.034 inches at the blade root. This blade configuration minimized bending and torsional stresses while improving blade fill characteristics during the molding operation.

Because the D' rotor required new blade ring injection molding tooling, it was also possible to reduce the diameter of the rotor platform so that it provides a smooth transition with the inner shroud of the stators, thus improving efficiency. This change also required that new tooling be used for the hot-pressed hub contours. The accuracy of the press-bonded hubs has been improved so that much of the final machining has been eliminated. The only machined surfaces remaining on the rotors are the bore, the blade tips, the curvic coupling, and the axial faces of the rotor platform.

The stationary flowpath components and the attachment hardware are identical for both Designs D and D'. This allows the rotors to be interchanged, and minimizes the number of components which must be fabricated and stocked.

Aerodynamic Design and Analysis

Aerodynamic design and analysis studies were performed on the Design D' turbine rotor in order to minimize any degradation of aerodynamic efficiency resulting from changing to the lower stressed design. This was desirable not only from the standpoint of overall engine performance, but also to minimize the increase in turbine exit gas temperatures resulting from decreased turbine efficiency.

The physical design restraints which most directly affected the aerodynamic design are summarized in Table 3.1. The helical camberline stacking is the aspect which most strongly differentiates the D' design from the preceding D design. The concept of helical stacking requires that the camberlines of all

TABLE 3.1   DESIGN CONSTRAINTS - D' TURBINE ROTOR

(a) Common Rotor - same blade profiles used in both stages

(b) Helically Stacked - radial stacking of section camberlines

(c) Centroidally Stacked - radial stacking of section centroids

(d) Section Area Distribution - one dimensional stress of 13,000 psi

(e) Trailing Edge Thickness - linear variation 0.034" at hub to 0.022" at tip

(f) Design D Stators - common stator in both stages

(g) Minimal alteration to existing envelope

(h) Manufacture by means of "Radial Draw" tooling

20

radial sections be connected in a fixed relationship. For the parabolic camberlines used in this and previous designs, the result is a family of parabolas through a common origin whose ordinates are related through the ratio of the section radii. One implication of this in blade design is that once one camberline is fixed (e.g. the hub section), the camberlines at all other radial sections are fixed and variations of blade angles can only be achieved by "sliding" the blade section along the given camberline. However, in order to maintain centroidal stacking of the total blade, the amount of "sliding" which can be done has been found to be relatively small, thereby producing a blade with minimal hub to tip variation. It was therefore not possible to achieve the large hub to tip variations of blade inlet angles necessary to match the flow leaving the current design stators.

The procedures employed in the aerodynamic design of D' relied heavily on computerized techniques, from the initial basic blade definition through the final drawing of the section profiles. An in-house computer program was used to define the blade sections with respect to angles and thickness distributions. Another computer program, utilizing the minimum curvature spline technique, was used to determine section areas and centroid locations, and to smooth out pressure side irregularities. These two computer programs were used jointly in an iterative process to define a helically stacked blade which met the physical constraints such as area distribution and centroidal stacking, and at the same time provided acceptable blade inlet angles and gas exit angles. Once blade geometry was defined, turbine performance and interstage flow conditions were obtained using a non-free vortex version of an in-house turbine performance computer program. Blade surface velocity distributions and blade boundary layer data were obtained from the NASA computer programs TSONIC [9] and BLAYER [10]. Performance and velocity analyses were conducted for the 55% and 100% engine speed conditions using $1930^{\circ}F$ and $2500^{\circ}F$, respectively, as the turbine inlet temperatures. In the design process, three major configurations were analyzed, the different configurations being summarized in Table 3.2.

TABLE 3.2   AIRFOIL CONFIGURATIONS WHICH WERE ANALYZED IN
THE CERAMIC BLADE REDESIGN

Configuration	Description
1	Radial stacking without centroidal stacking of the blade sections. Trailing edge thickness of 0.015 inches from the mean section to the tip.
2	Same as configuration (1) except that the trailing edge thickness had a linear taper of 0.034 inches at the hub to 0.022 inches at the tip to facilitate the injection molding of the blade.
3 (Low Stress Design D')	Both radial and centroidal stacking of the blade sections, and having the trailing edge thickness distribution of configuration (2).

21

Another computer program was used to automatically draw blade sections using a Gerber drafting machine. Figure 3.2 shows an example of four stacked radial sections of two adjacent blades as viewed along the indicated radial line passing between the two blades. Pictures of this type permit ready evaluation of the capability of fabricating such blading by radial draw molding techniques. Additionally, non-projected individual sections were drawn separately to produce a final fabrication drawing.

In summary, a low stress ceramic turbine rotor blade has been aerodynamically designed and analyzed for use in both the first and second stage rotors. The design (called D') is a compromise to satisfy the Design D flowpath, which utilizes the present design one piece stators in both the first and second stage locations. The efficiency of the D' design was calculated to be 1.0 to 1.8 percentage points lower in efficiency than the D design which it replaces.

Two Dimensional Rotor Analysis

This section presents a summary of the two-dimensional heat transfer and stress analysis work done on the rotor assembly model and the first and second stage turbine rotor models. Computations in this report were based on a turbine inlet temperature of 2500°F combined with a centrifugal speed of 110 percent. This 10 percent additional speed is to allow for possible overspeed.

The finite element model of the rotor attachment assembly previously reported [2] was modified to the D-prime rotor profile configuration. The platform radius was modified slightly and is now the same for both the first and second stage. The platform was shifted in the axial direction to accommodate the D' blade. The bond joint is now at a radius of 1.486 inches, while the blade ring radius is 1.562 inches. The finite element grids used to model the discs, shown in a previous report [6], were modified to the D' configuration. The D' blade loads were input to the axisymmetric finite element program as pressure loads. The axial pressure distribution was determined from the three-dimensional finite element program. The clamping load of the rotor attachment bolt was included as a pressure load. The rotor assembly model was again used to determine thermal boundary conditions for the individual rotor models as discussed in previous reports [2,4].

The model for circulation in the common cavity proposed in the last report [7] has been disproved experimentally; measured air temperatures in the cavity were much lower than those predicted by the model with circulation. Therefore the heat transfer assembly model was restored to the point where the heat transfer in the cavity is considered to be by conduction through the air. This gave more accurate predictions of disc temperatures.

Radiation heat transfer was added to the annular space between the rotor hub and the tie-bolt. This was done by calculating radiation equivalent conduction properties for the elements. The equivalent elements have an overall heat transfer equal to the sum of the radiation heat transfer plus the conduction heat transfer in the air. The addition of radiation causes the bolt to run at higher temperatures, since the cooling air flow in the bolt has been held constant. The effect of this elevated bolt temperature is being evaluated.

Blade surface and blade channel heat transfer coefficients were computed for the D' blades using the method previously reported [6]. These values were then used to calculate an effective heat transfer coefficient which included the fin effectiveness of the blade.

22

2.6" RADIUS

2.3" RADIUS

2.0" RADIUS

1.7" RADIUS

RADIAL LINE
OF VIEWING

1.7" RADIUS

2.0" RADIUS

2.3" RADIUS

2.6" RADIUS
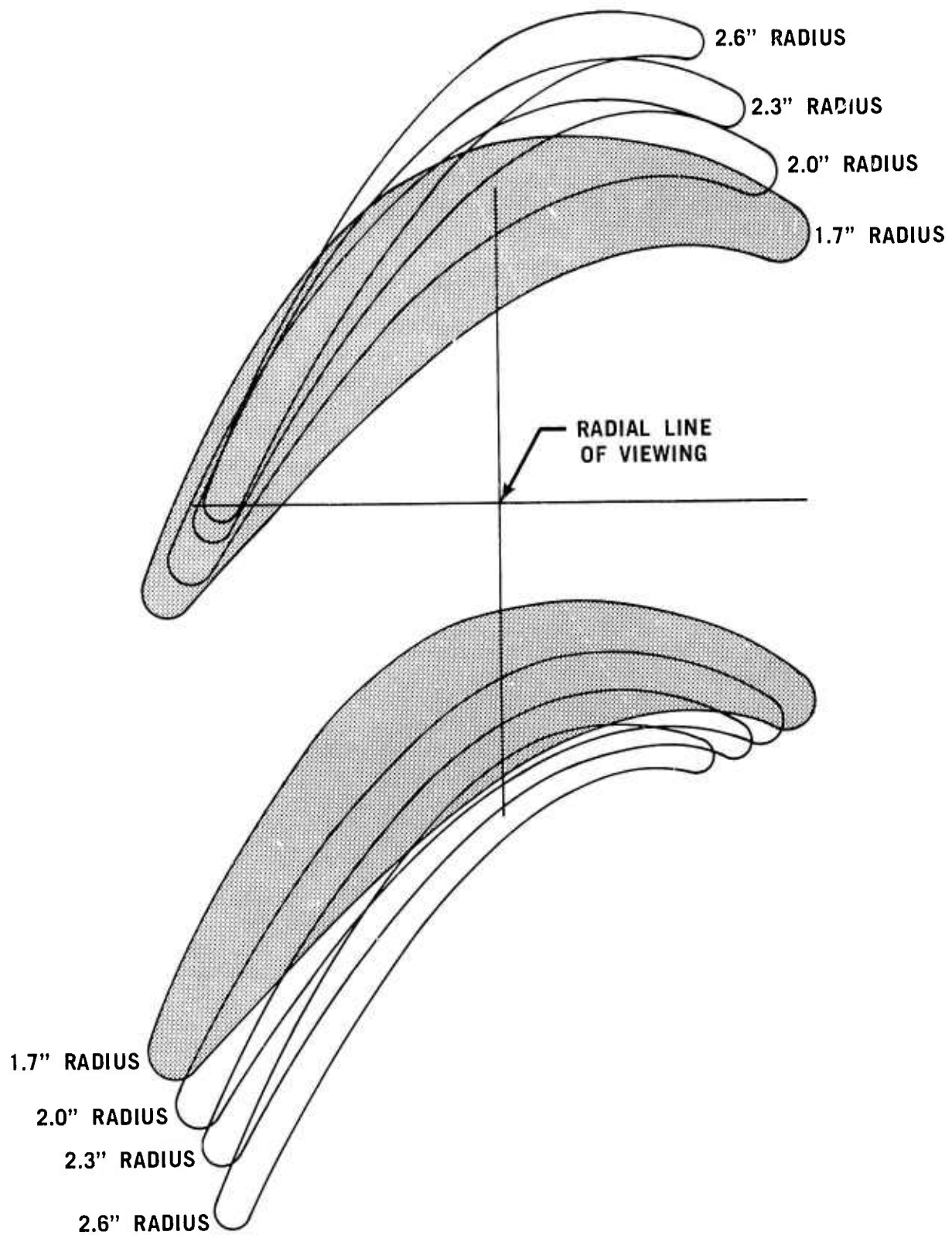
Figure 3.2   Computer Drawn D' Rotor Blade Cross-Sections

The results of the analysis are shown in Figures 3.3 through 3.6, Figures 3.3 and 3.4 being for the first stage rotor. Figure 3.3 shows the temperature distribution in isotherms of 20 degrees, using a maximum disk temperature of 2300°F. Figure 3.4 shows the stress distribution in isobars of 1000 psi. The maximum stress of 42,000 psi occurs at the bore, where the temperature is 1650°F. The stress distribution is the result of imposing the temperature distribution shown in Figure 3.3 with the blade and disk centrifugal loads at 110 percent speed and the clamping load.

Figures 3.5 and 3.6 show the same information for the second stage. Maximum disk temperature is 1940°F. Maximum stress is at the bore and is 39,000 psi with a temperature of 1330°F.

Three Dimensional Rotor Analysis

The new blade design, D' (D prime), features both radially and centroidally stacked blade elements as previously mentioned so as to minimize parasitic bending and torsional stresses that are normally present in twisted airfoils. In addition, it is anticipated that a pure radial draw, which is possible with this blade, will favor the fabrication of the rotor and thus improve its quality.

A total of three airfoil configurations were evaluated, as discussed in the preceding section. To expedite the evaluation, the blade was modeled as fixed at the platform. Earlier analyses of similar structures verified that this technique will closely simulate the complex blade-platform interaction while providing a very economical tool for a parametric design study such as this. The results of this study of the three configurations shown in Table 3.2 are given on Tables 3.3, 3.4 and 3.5 covering the tabulation of stresses in the critical portion of the blade immediately above the fillet.

As seen from these tabulations, all three configurations meet the objective of reduced stress levels in addition to a drastic reduction in parasitic torsion and bending stresses. Configuration 3 was selected as the best on the basis of the greatest reduction in stress (from 21,000 psi in the Design D to 13,180 psi) and consequently lowered the strength requirements for a candidate material by approximately 16%.

Having established an acceptable blade design, the three-dimensional model of the airfoil was extended to incorporate the repetitive disk segment of the rotor into the throat. The techniques used in developing this portion of the model were explained in an earlier report [6]. An isometric view of the complete model is shown in Figure 3.7.

The present in-house version of the SAP III computer program does not have the capability of analyzing a structure with truly repetitive boundaries [11]. Considering, however, that the blade airfoil sections have been radially stacked, and as a result the bending and twisting were minimized, a good approximation can be achieved using skewed sliding boundaries whereby the sides of the wedge are free to slide in the radial direction only. To simulate the restraint of the throat of the disk, the axial and radial deflections from the axisymmetric analysis were used as nodal point displacement data at that boundary. Figure 3.8 shows these input criteria.

24

HOT GAS FLOW

REACTION SINTERED
Si$_3$N$_4$ BLADES
DENSITY = 2.70 GM / CM^3

HOT PRESSED Si$_3$N$_4$ DISK
DENSITY = 3.18 GM / CM^3

2200

2100

2000

1900

1800

1700

1600
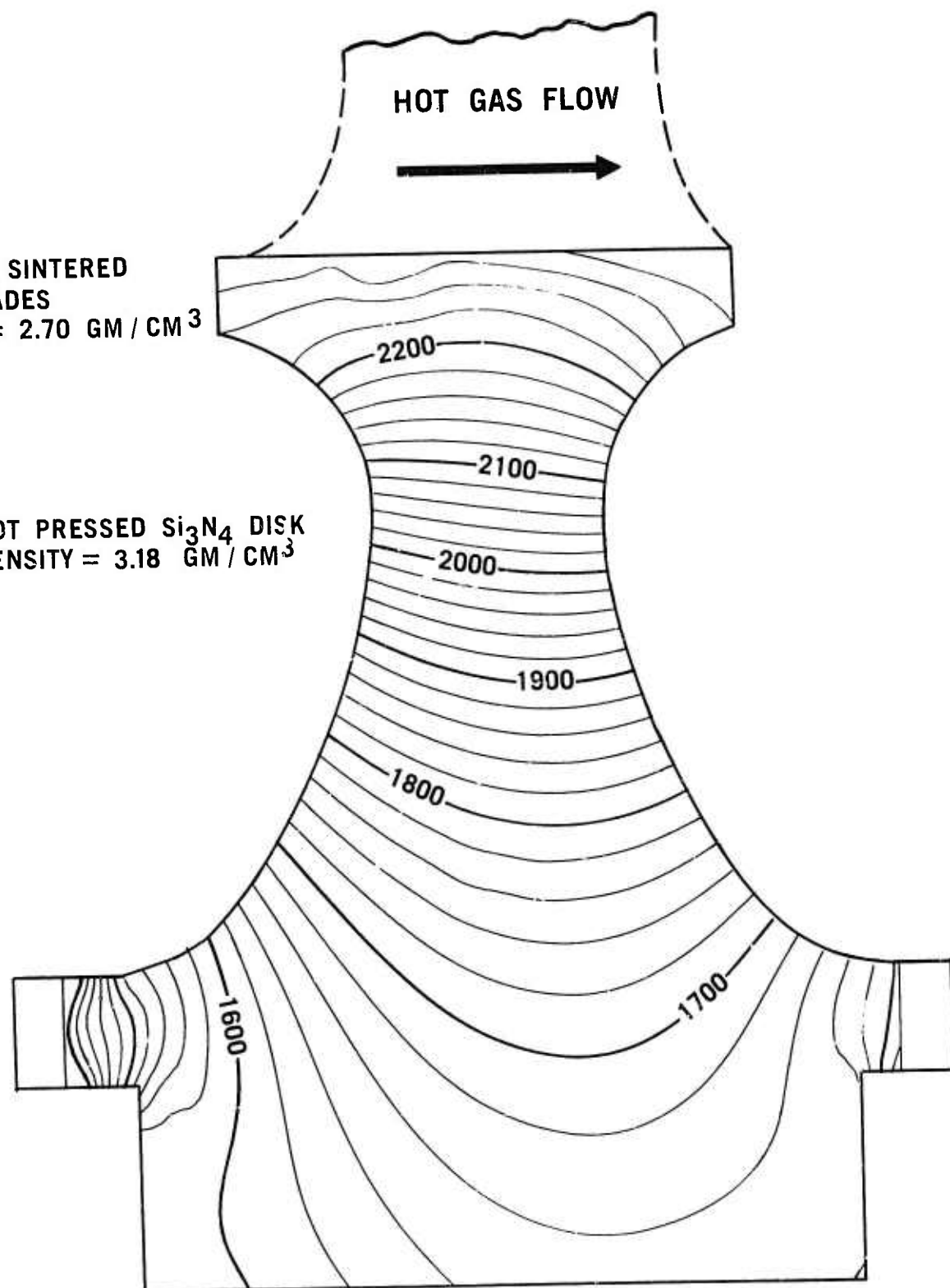
Figure 3.3   Isotherms ($^{\circ}$F) in First Stage Rotor at 100% Steady
State Speed Temperature Boundary Conditions

HOT GAS FLOW

REACTION SINTERED
Si_3N_4 BLADES
DENSITY = 2.70 GM / CM^3

HOT PRESSED Si_3N_4 DISK
DENSITY = 3.18 GM / CM^3
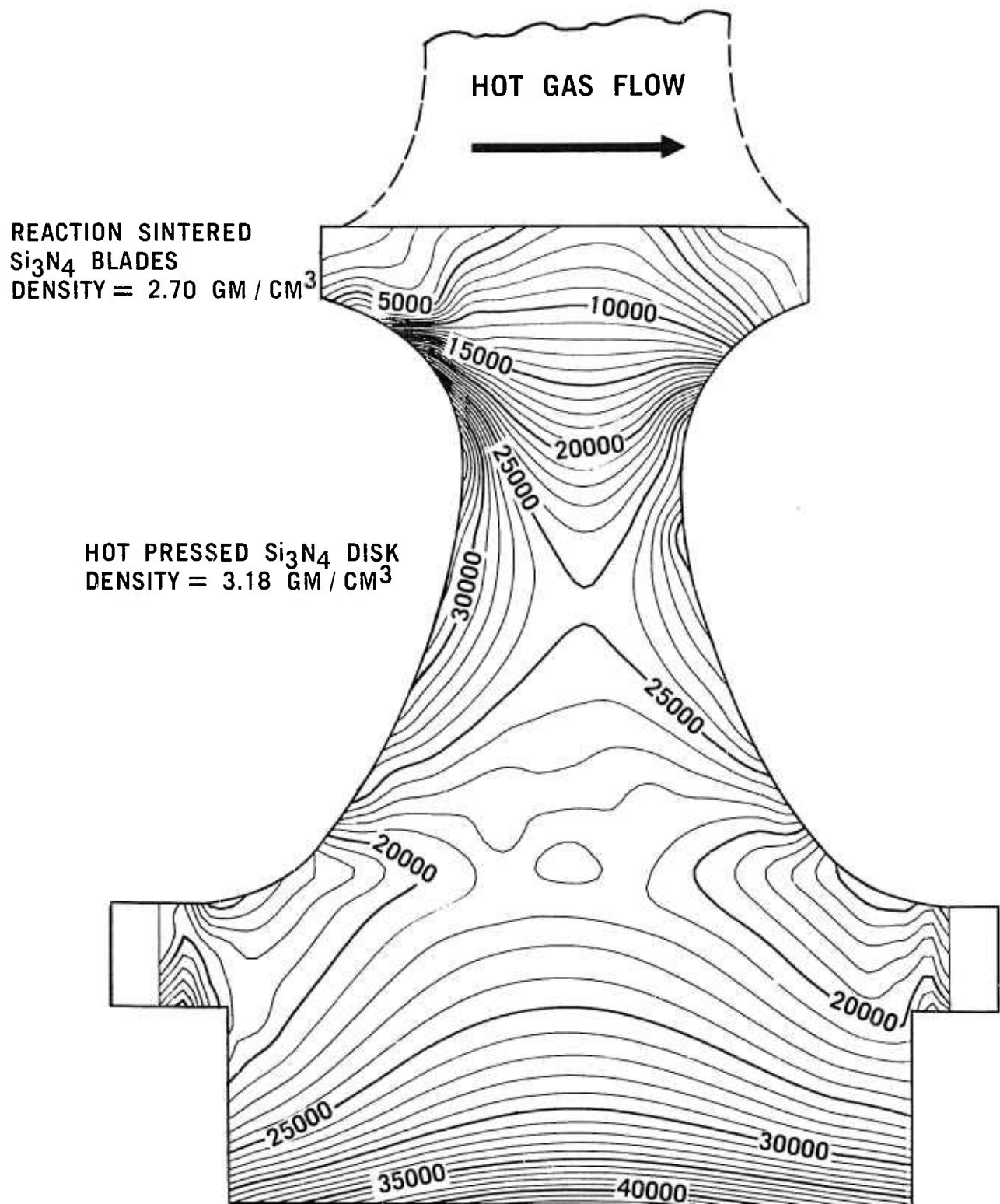
Figure 3.4   Maximum Principal Stresses (psi) in First Stage Rotor,
Combining Thermal Stresses at 100% Speed and Centrifugal
Stresses at 110% Speed
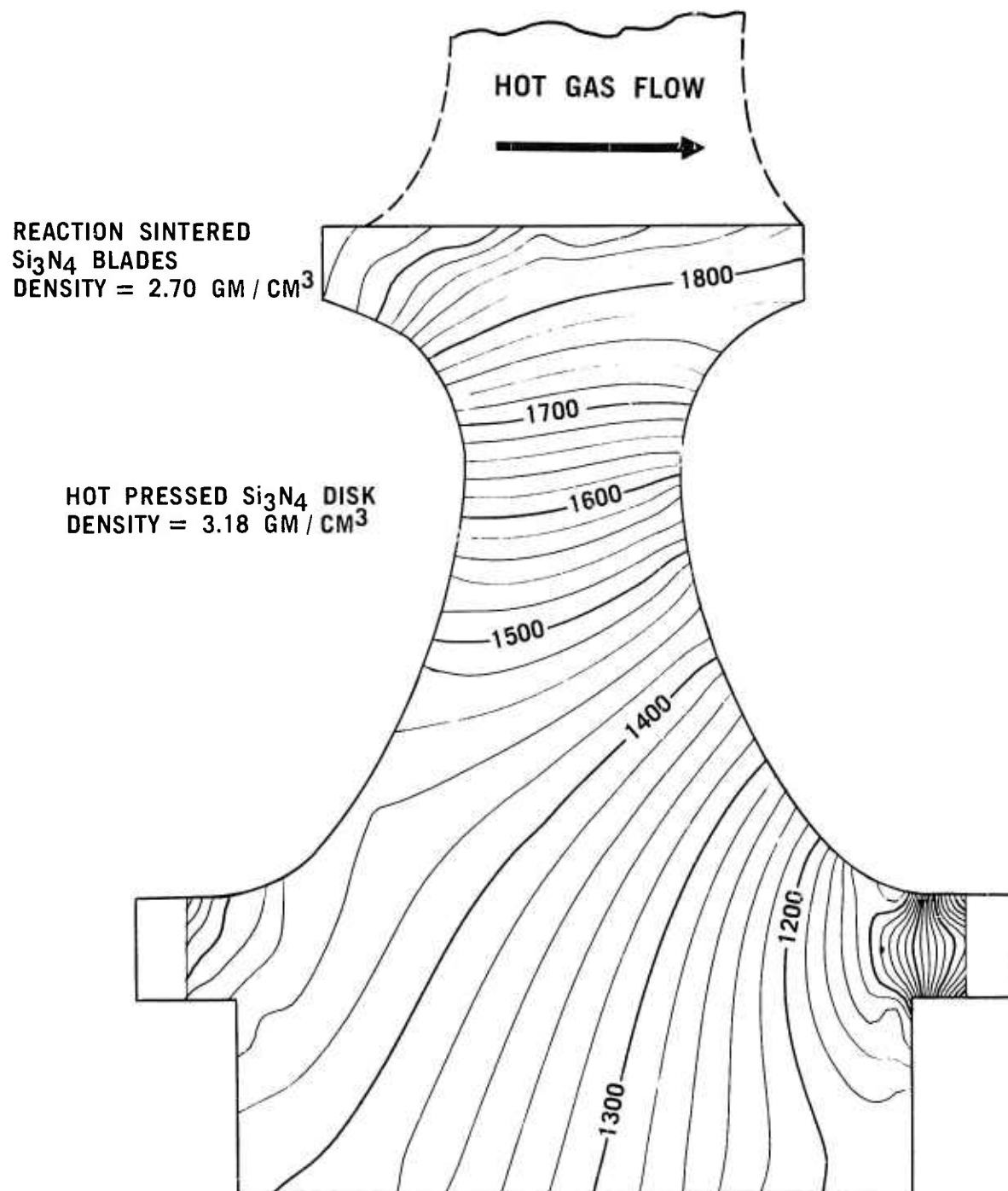
Figure 3.5   Isotherms (°F) in Second Stage Rotor at 100% Steady
State Speed Temperature Boundary Conditions
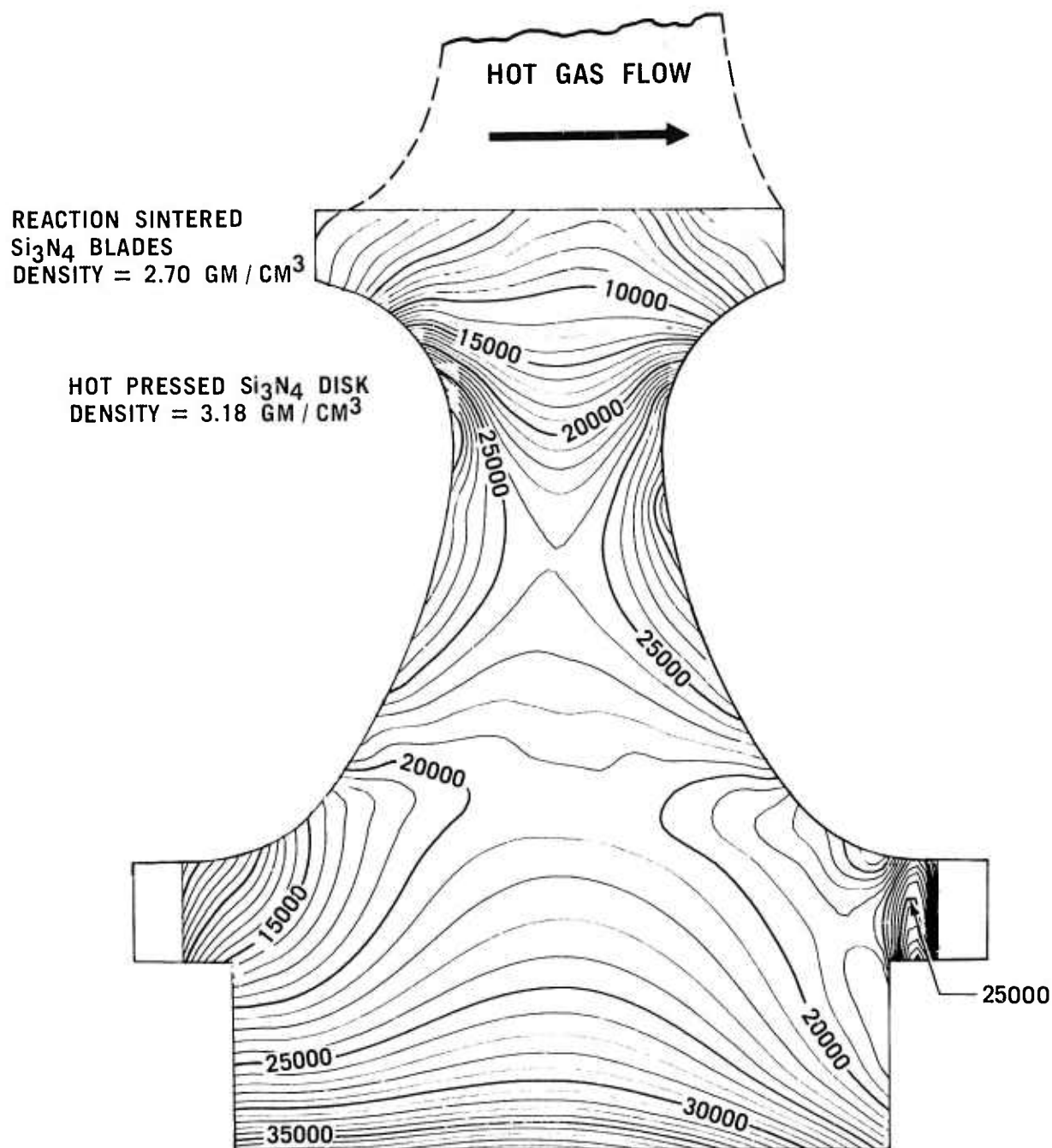
Figure 3.6   Maximum Principal stresses (psi) in Second Stage Rotor,
              Combining Thermal Stresses at 100% Speed and Centrifugal
              Stresses at 110% Speed

28

TABLE 3.3   CENTRIFUGAL STRESSES AT 70,680 RPM (110% SPEED)
              FOR ROTOR CONFIGURATION 1

| | T.E. | | | | | | | L.E. |
Axial Location	1	2	3	4	5	6	7	8
1.660 Radius								
Centroidal	14,650	14,050	13,580	13,040	12,280	11,360	10,310	8,880
Pressure	14,320	14,210	13,650	12,940	11,790	10,440	9,340	8,210
Suction	15,050	14,200	13,690	13,170	12,360	11,520	10,650	9,310
1.750 Radius								
Centroidal	14,070	13,950	13,390	12,780	12,040	11,060	9,960	8,570
Pressure	13,610	13,250	12,640	12,060	11,210	10,250	9,400	8,320
Suction	14,520	14,660	14,160	13,380	12,470	11,480	10,260	8,710
1.850 Radius								
Centroidal	13,330	13,340	12,900	12,320	11,590	10,550	9,370	7,870
Pressure	12,860	12,670	12,000	11,200	10,560	9,800	9,020	7,840
Suction	13,820	14,040	13,690	13,210	12,410	11,050	9,530	7,820

TABLE 3.4   CENTRIFUGAL STRESSES AT 70,680 RPM (110% SPEED)
              FOR ROTOR CONFIGURATION 2

| | T.E. | | | | | | | L.E. |
Axial Location	1	2	3	4	5	6	7	8
1.660 Radius								
Centroidal	17,070	15,720	14,790	13,970	12,930	11,820	10,700	9,310
Pressure	16,360	15,910	14,850	13,680	12,470	11,050	9,890	8,830
Suction	17,880	15,840	14,770	14,180	13,130	11,960	10,940	9,550
1.750 Radius								
Centroidal	15,570	15,190	14,510	13,610	12,640	11,490	10,280	8,820
Pressure	14,960	14,470	13,800	12,860	11,790	10,700	9,800	8,630
Suction	16,210	16,010	15,320	14,230	13,150	11,920	10,550	8,930
1.850 Radius								
Centroidal	13,880	14,030	13,590	12,980	12,140	11,000	9,700	8,110
Pressure	13,280	13,210	12,770	12,100	11,290	10,290	9,250	8,010
Suction	14,480	14,850	14,330	13,660	12,800	11,470	9,920	8,120

TABLE 3.5   CENTRIFUGAL STRESSES AT 70,680 RPM (110% SPEED)
FOR ROTOR CONFIGURATION 3

Axial	T.E. 1	2	3	4	5	6	7	L.E. 8
1.660 Radius								
Centroidal	13,080	12,050	12,010	12,040	12,190	12,300	12,110	12,310
Pressure	13,180	12,310	12,210	12,030	12,050	11,980	11,860	12,300
Suction	12,880	11,840	11,830	11,990	12,440	12,780	12,350	12,340
1.750 Radius								
Centroidal	11,980	12,110	12,040	12,010	11,850	11,660	11,500	11,400
Pressure	12,060	12,170	11,860	11,550	11,240	10,970	10,770	10,770
Suction	11,860	11,900	11,920	12,150	12,180	12,120	12,080	11,980
1.850 Radius								
Centroidal	11,700	11,800	11,800	11,650	11,450	11,120	10,720	10,050
Pressure	11,710	11,700	11,460	11,150	10,860	10,540	10,250	9,750
Suction	11,700	11,860	11,990	11,910	11,790	11,530	11,120	10,320
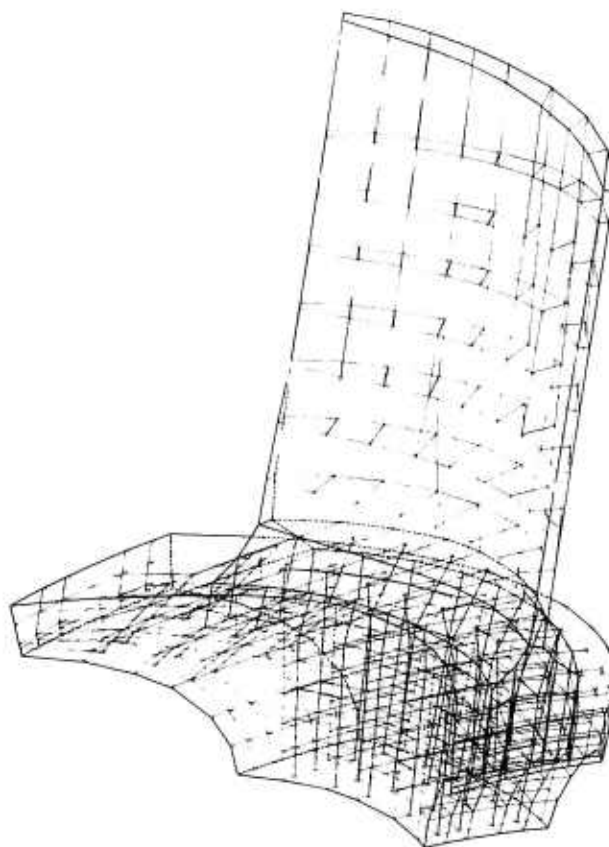
Figure 3.7   Isometric View of the Three Dimensional Model of the
Second Stage Turbine Rotor Blade and Repetitive Disk
Segment Extending Down to the Throat
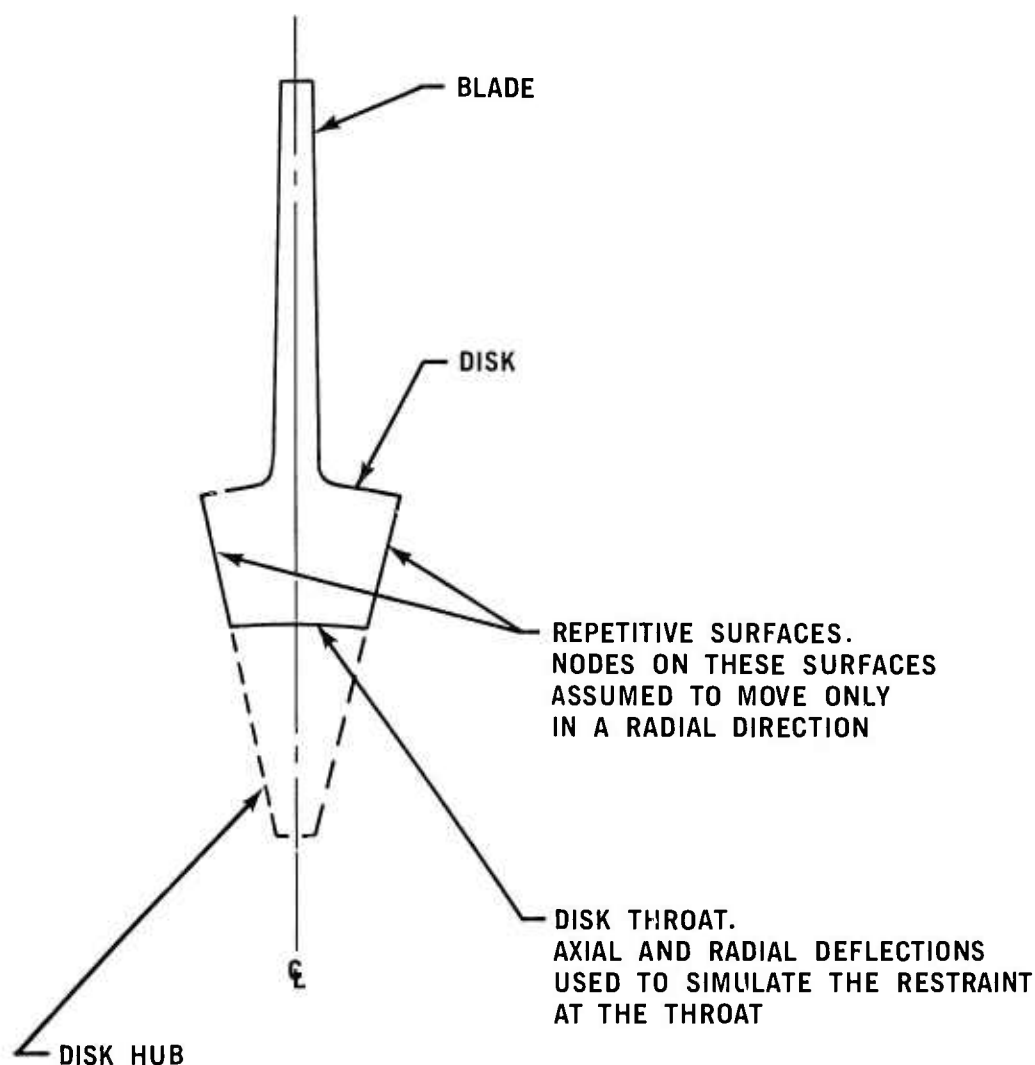
Figure 3.8   Sketch of the Three Dimensional Rotor Model Parallel
              to the Rotor Centerline Showing the SAP III Input
              Criteria

Figure 3.9 shows the correlation of the maximum principal stresses from the
2-D and 3-D analyses for several locations in the disk due to centrifugal loading.
As shown, there is good agreement between the stress figures for all regions
except the disk rim where the discrete blade loadings induce localized stress
concentrations not apparent in the axisymmetric analysis which averages the
circumferential responses of the structure (stresses, temperature and deformations).
Figures 3.10 and 3.11 show respectively the centrifugal stress contours on the
camber line plane and on the pressure and suction surfaces of the second stage
airfoil at 70,680 rpm (110% speed).

Strength Requirements

The necessary relationships have been derived between the working stress
and the material strength as required to meet a specified reliability level.
To account for the variability in material strength, Weibull's statistical model
described in an earlier report [5] was used.

31
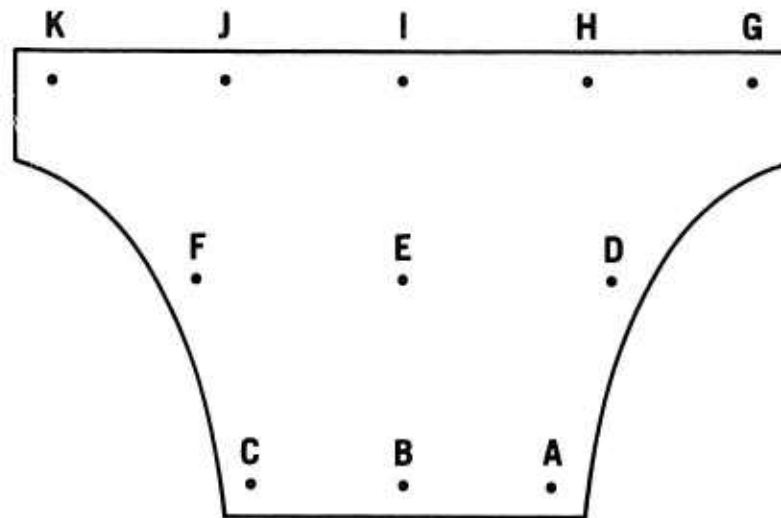
LOCATION	A	B	C	D	E	F	G	H	I	J	K
SAP III; 3D, (KSI)	21.79	15.99	22.98	15.59	15.10	15.87	8.77	10.01	14.40	10.38	8.61
AXISYMMETRIC; 2D, (KSI)	20.41	17.32	22.12	14.91	14.71	15.56	7.61	7.84	7.75	7.71	8.10

Figure 3.9   Comparison of Maximum Stresses as a Result of Centrifugal Loading at 110% Speed From Both SAP III and Axisymmetric Analyses at Various Rotor Disk Locations
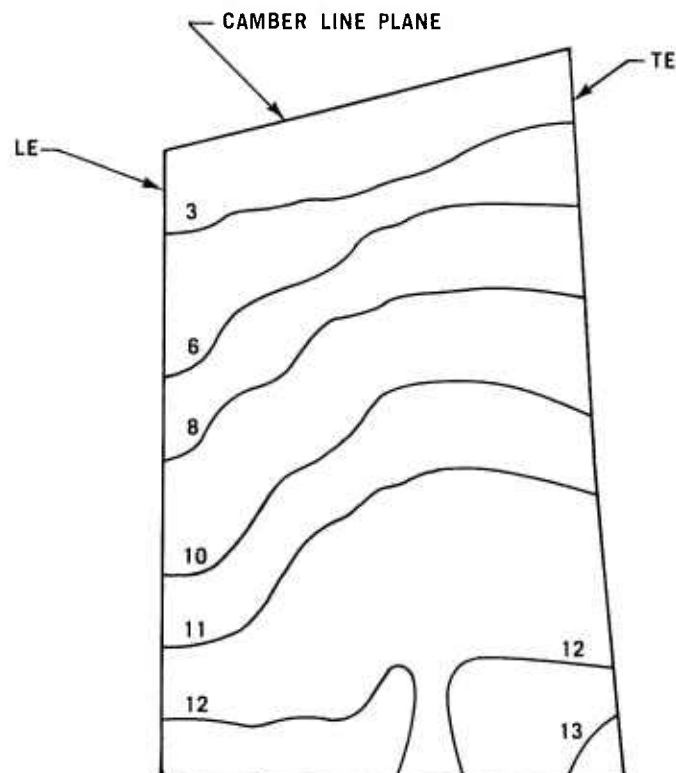
Figure 3.10   Centrifugal Stresses (ksi) at 110% Speed in Design D' Second Stage Rotor Blade

32
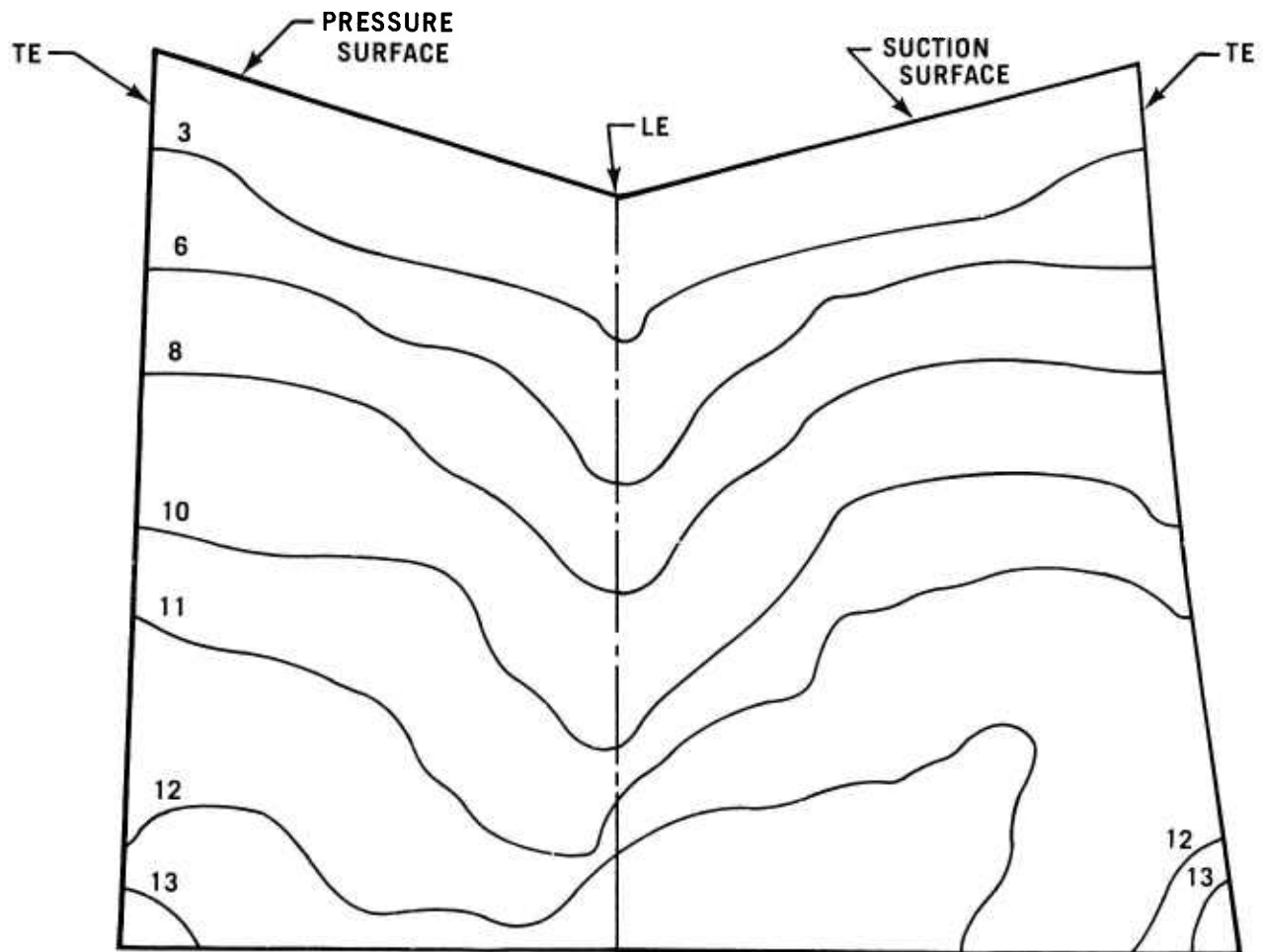
Figure 3.11   Centrifugal Stresses (ksi) at 110% Speed in Design D'
Second Stage Rotor Blade

The reliability or the probability of survival of the blade can be expressed in a normalized form in terms of a reference stress, usually the maximum stress σ_m in the blade, and the effective volume.

$$R = \exp\left[-\left(\frac{\sigma_m - \sigma_u}{\sigma_o}\right)^m V_{eff}\right] \tag{1}$$

where $\left(\dfrac{\sigma_m - \sigma_u}{\sigma_o}\right)^m$ is the Weibull function with Weibull parameters

σ_u, σ_o, and m corresponding to material properties at operating conditions (temperature, etc.) at σ_m.

V_{eff} is the effective volume of the blade, i.e. the equivalent volume subjected to a uniform tensile stress σ_m and which exhibits the same failure statistics as the blade.

33

Since the strength properties of the material are normally obtained from the MOR or similar tests, the strength of the blade can be related to the strength of the test (MOR) specimens at equal probabilities of failure.

$$(\sigma_m - \sigma_u)_{Blade} = (\sigma_m - \sigma_u)_{Test} \left(\frac{V_{eff\ Test}}{V_{eff\ Blade}} \right)^{\frac{1}{m}} \tag{2}$$

For an uniaxial tensile test specimen $V_{eff\ Test}$ is equal to the actual volume of the test section. Rearranging equation (1):

$$\frac{1}{\sigma_o^m} \qquad V_{eff} = \frac{\ln\left(\frac{1}{R}\right)}{\left(\sigma_m - \sigma_u\right)^m}$$

If the probability of survival, R_p, corresponds to a reference stress level of σ_{m_p}, (1) can be rewritten in terms of R_p and σ_{m_p}:

$$R = \exp\left[- \ln\left(\frac{1}{R_p}\right) \left(\frac{\sigma_m - \sigma_u}{\sigma_{m_p} - \sigma_u}\right)^m \right] \tag{3}$$

Furthermore, if $\bar{\sigma}_m$ is the mean value of the reference stress σ_{m_p} at fracture, it is given according to Weibull by:

$$\bar{\sigma}_m = \sigma_u + \int_{\sigma_u}^{\infty} \exp\left[-\ln\left(\frac{1}{R_p}\right) \left(\frac{\sigma_m - \sigma_u}{\bar{\sigma}_m - \sigma_u}\right)^m \right] d\sigma_m \tag{4}$$

Integrating:

$$\bar{\sigma}_m = \sigma_u + \left(\bar{\sigma}_m - \sigma_u\right) \left(\frac{1}{m}\right) \left[\ln\left(\frac{1}{R_p}\right) \right]^{-\frac{1}{m}} \Gamma\left(\frac{1}{m}\right)$$

Rearranging:

$$\left[\ln\left(\frac{1}{R_p}\right) \right]^{\frac{1}{m}} = \left(\frac{1}{m}\right) \Gamma\left(\frac{1}{m}\right) = \Gamma\left(1 + \frac{1}{m}\right)$$

$$\ln\left(\frac{1}{R_p}\right) = \left[\Gamma\left(1 + \frac{1}{m}\right) \right]^m \tag{5}$$

34

where $\Gamma\left(1 + \dfrac{1}{m}\right)$ is the gamma function of $\left(1 + \dfrac{1}{m}\right)$

Introducing for the blade:

$$\beta = \frac{\text{Allowable level of reference stress } {}^{\sigma}\text{all. at required reliability, } R}{\text{Mean value of reference stress at fracture}} = \frac{1}{\text{F.S.}}$$

$$\beta = \frac{\left(\sigma_{\text{all.}} - \sigma_u\right)_{\text{Blade}}}{\left(\bar{\sigma}_m - \sigma_u\right)_{\text{Blade}}} \tag{6}$$

where F.S. is the factor of safety

From equation (2):

$$\left(\bar{\sigma}_m - \sigma_u\right)_{\text{Blade}} = \left(\bar{\sigma}_m - \sigma_u\right)_{\text{Test}} \left(\frac{V_{\text{eff}_{\text{Test}}}}{V_{\text{eff}_{\text{Blade}}}}\right)^{\frac{1}{m}}$$

Substituting into equation (6):

$$\beta = \frac{\left(\sigma_{\text{all.}} - \sigma_u\right)_{\text{Blade}}}{\left(\bar{\sigma}_m - \sigma_u\right)_{\text{Blade}}} = \frac{\left(\sigma_{\text{all.}} - \sigma_u\right)_{\text{Blade}}}{\left(\bar{\sigma}_m - \sigma_u\right)_{\text{Test}}} \left(\frac{V_{\text{eff}_{\text{Test}}}}{V_{\text{eff}_{\text{Blade}}}}\right)^{-\frac{1}{m}} \tag{7}$$

Substituting equations (5) and (7) into (3):

$$R = \exp\left[-\left\{\Gamma\left(1 + \frac{1}{m}\right)\beta\right\}^m\right] \tag{8}$$

Solving equation (8) for β and substituting into equation (7):

$$\beta = \frac{\left(\sigma_{\text{all.}} - \sigma_u\right)_{\text{Blade}}}{\left(\bar{\sigma}_m - \sigma_u\right)_{\text{Test}}} \left(\frac{V_{\text{eff}_{\text{Test}}}}{V_{\text{eff}_{\text{Blade}}}}\right)^{-\frac{1}{m}} = \left[\ln\left(\frac{1}{R}\right)\right]^{\frac{1}{m}} \frac{1}{\Gamma\left(1 + \frac{1}{m}\right)}$$

Thus, the allowable level of the reference (maximum) stress in the blade at a required reliability level R to the mean strength of test specimens can be expressed as:

$$\sigma_{all.} = \sigma_u + \left(\bar{\sigma}_m - \sigma_u\right)_{Test} \left(\frac{V_{eff\ Test}}{V_{eff\ Blade}}\right)^{\frac{1}{m}} \frac{\left[\ln\left(\frac{1}{R}\right)\right]^{\frac{1}{m}}}{\Gamma\left(1 + \frac{1}{m}\right)} \quad (9)$$

And, in the special case when $\sigma_u = 0$

$$\sigma_{all.} = \bar{\sigma}_{m\ Test} \left(\frac{V_{eff\ Test}}{V_{eff\ Blade}}\right)^{\frac{1}{m}} \frac{\left[\ln\left(\frac{1}{R}\right)\right]^{\frac{1}{m}}}{\Gamma\left(1 + \frac{1}{m}\right)} \quad (10)$$

Solving for the mean strength of the test specimens:

$$\bar{\sigma}_{m\ Test} = \sigma_{all.} \ \Gamma\left(1 + \frac{1}{m}\right) \left[\frac{V_{eff\ Test}}{V_{eff\ Blade}} \ln\left(\frac{1}{R}\right)\right]^{-\frac{1}{m}}$$

Where $V_{eff\ Test}$ is related to the size of the MOR bars tested.

Figure 3.12 shows equation (11) plotted for several values of m for the Design D' second stage turbine blade when centrifugally loaded. This figure gives the materials engineer two options to achieve the same reliability level. When the process yields a large material variability (low value of m) he must strive for a high mean failure strength. On the other hand, a low variability (high m) permits a lower mean strength requirement.

Stress and strength studies of both rotor stages are in progress for the 100% and the 55% steady-state and the cold-start transient conditions. Temperature distributions are being calculated using TAP, a 3-D heat transfer computer code described in earlier reports [6,7]. Currently, TAP is being modified to allow for variables of material properties with temperature and to permit repetitive structures.

$$\bar{\sigma}_{m_{MOR}} = \frac{\sigma_{BLADE}\, \Gamma\left(1 + \frac{1}{m}\right)}{\left\{\dfrac{Veff_{MOR}}{Veff_{BLADE}}\, \ln\left(\frac{1}{R}\right)\right\}^{\frac{1}{m}}}$$
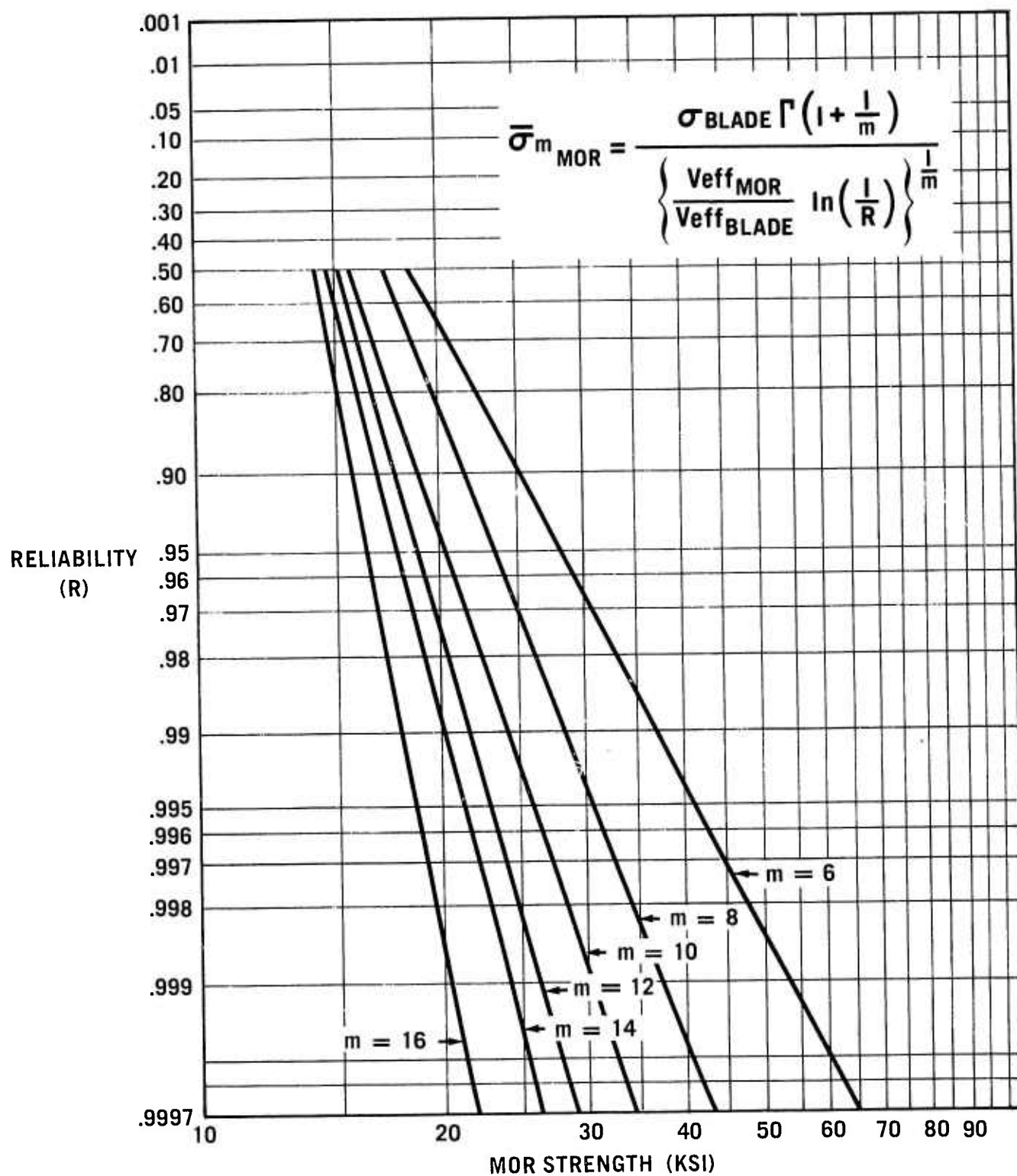
RELIABILITY (R)

MOR STRENGTH (KSI)

Figure 3.12   Modulus of Rupture Strength Requirements vs Reliability for the Design D' Second Stage Rotor Blade, Centrifugal Loading Only

37

3.1.2 MATERIALS AND FABRICATION

Introduction

The primary in-house effort on fabrication of ceramic turbine rotors continues to be directed at the silicon nitride duo-density concept. Improvements in the graphite assembly system and hot pressing furnace materials and designs have enabled the fabrication of several rotors in which both the distortion and damage in the blade rings during hot-press bonding have been significantly reduced.

The development of slip casting of silicon nitride rotor blade rings, using a modified investment casting technique, has resulted in improvements in mold removal following nitriding. Additional work was done on casting parameters.

A process for high pressure nitriding of high density slip cast silicon shapes to obtain near-theoretical density Si_3N_4 was applied to thin sections typical of blades used for duo density turbine rotors. Difficulties still remained in achieving complete nitridation, and coupled with theoretical studies which indicate that an inadequate amount of nitrogen can be stored in the compact's pores, resulted in deemphasizing this approach.

Duo Density Silicon Nitride Rotors

The duo density rotor is the primary approach being investigated for fabricating a ceramic turbine rotor. In this concept, the high strength of the hot-pressed Si_3N_4 is utilized in the hub region where stresses are highest but temperatures are moderate and, therefore, creep problems are minimized. Creep resistant reaction sintered Si_3N_4, which can be formed into complex airfoil blade shapes, is utilized for the blades. The blades are generally exposed to higher temperatures but lower stress levels than the turbine rotor disk.

Work on developing duo-density rotors during this reporting period was directed toward further refining the graphite wedge hot-pressing system [4,5,6,7] for bonding a theoretically dense Si_3N_4 hub to the reaction sintered Si_3N_4 blade ring. Since the thin rim of the blade ring has insufficient strength to support the applied pressure during hot-press bonding, a double blade fill technique [6] was developed. This technique consists of first filling the space or cavities between the blades with slip cast silicon metal. Each blade cavity insert is independent of one another. A second blade fill of slip cast silicon metal is applied entirely encasing both the turbine blades and blade cavity inserts. Both the first and second silicon metal blade fills are simultaneously converted to Si_3N_4 by nitriding. Combining the nitriding steps of both blade fills has reduced the blade ring processing time by two weeks. Boron nitride is used to prevent the various blade fill materials from bonding to each other and to the turbine blades.

The theoretically dense Si_3N_4 contoured hub region was fabricated from AME alpha Si_3N_4 powder with MgO added as a densification aid. The concentration of MgO has been varied from 2 to 5 w/o and both magnesium oxide and magnesium nitrate have been used as a source for MgO. The adoption of the simultaneous hot-pressing-press bonding technique, described in the last report [7] which involves both hot-pressing the contoured Si_3N_4 hub and hot-press bonding the hub to the reaction-sintered blade ring in one operation, continued in use and exhibited good bonding. It was postulated that a more homogeneous distribution of magnesium oxide in the

Si_3N_4 powder could be obtained by dissolving magnesium nitrate in anhydrous methyl alcohol (the liquid milling media) rather than using MgO powder. This would hopefully allow the hot-pressing pressure for forming the hub to be reduced from the normally used pressure of 5,000 psi. Magnesium nitrate was added to produce a MgO concentration equivalent to 2 w/o. The Si_3N_4 powder with the magnesium nitrate additive was wet ball milled with alumina balls for seven days to reduce the powder particle size below 2μ and to homogeneously mix in the magnesium nitrate.

The milled mixture was dried and loaded into the hub cavity of the graphite restraining sleeve (Figure 3.13.) Normal procedures involve hot-pressing the Si_3N_4 powder at $1750^{\circ}C$ and 2,500 psi for 2 hours to densify the hub region while simultaneously effecting bonding to the blade ring. The graphite wedge system enables the encased blade ring to be restrained at the O.D. by applying pressure independently to this area through the compression rig [5]. As reported previously [7], complete bonding over the entire height of the blade rim was achieved without bowing the rim. However, subsequent spin test results showed the hubs to be of low strength as failure occurred at approximately 80,000 rpm. As a basis for comparison, this is a significant decrease from the characteristic burst speed of approximately 116,000 rpm for hot pressed Si_3N_4 - 5 w/o MgO contoured hubs reported previously [7].

Microstructural analysis showed the hubs to be theoretically dense as evidenced by the absence of porosity. However, chemical analysis indicated an excessive increase in the aluminum contamination, due to reaction with the alumina grinding media. The silicon nitride powder processed with the magnesium nitrate additive also exhibited unusual pressing characteristics in that densification proceeded at both a faster rate and at a $100^{\circ}C$ lower temperature. Theoretically dense Si_3N_4 hubs were also produced at pressures as low as 1,500 psi from this powder. Although characterization of this hub material is incomplete, the preparation of Si_3N_4 powder with magnesium nitrate has been discontinued because of the poor performance in spin testing. Magnesium oxide is again being used as the densification aid.

Further work was done to improve the graphite wedge hot press bonding system shown in Figure 3.13. This technique utilizes an encapsulated Si_3N_4 blade ring ("A", Figure 3.13) in which the graphite wedges ("B" and "C") restrain the outside of the blade ring. Silicon nitride powder with 5 w/o MgO as the additive is simultaneously hot-pressed to theoretical density and bonded to the blade ring. However, several problems have been encountered with this technique. Due to piston drag and some bonding of the Si_3N_4 powder to the lower edge of the restraining sleeve ("D") a bending moment resulted causing severe fracture of the graphite restraining sleeve and subsequent fracture of the blade ring ("A").

To eliminate this problem, the inside diameter of the restraining sleeve was enlarged to allow the insertion of a thin graphite sleeve (wall thickness of 0.080 inches). Although fracture of the graphite restraining sleeve was greatly reduced, drag of the contoured piston on the thin inner sleeve resulted in sufficient pressure exerted on the rim of the blade ring to cause deformation and crushing of the rim. In addition, at the fabrication temperature of $1750^{\circ}C$, sufficient magnesium silicate glass migrated from the Si_3N_4 hub into the reaction-sintered blade rim which enhanced the deformation of the blade rim under pressure.
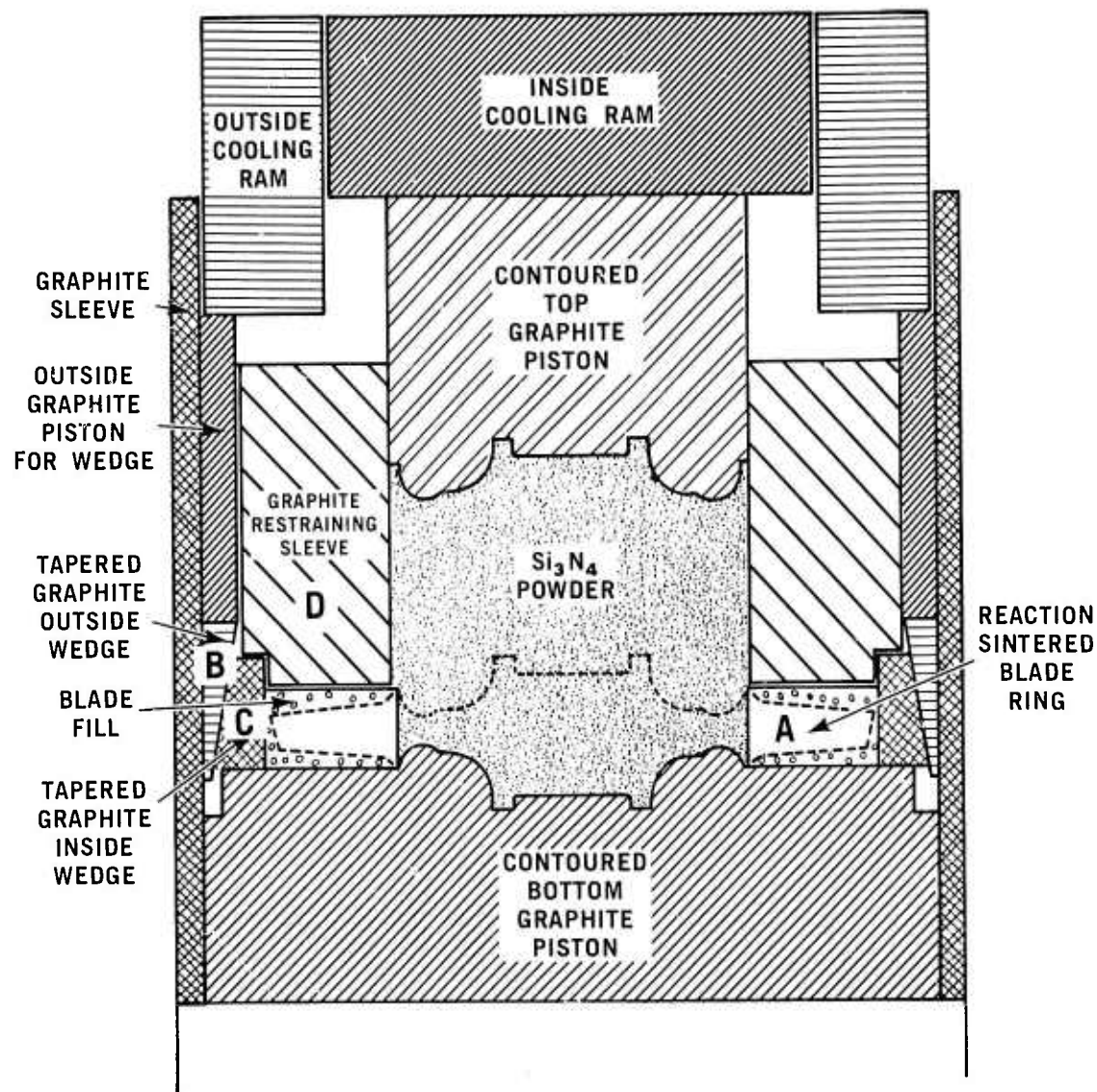
Figure 3.13   Hot Press Bonding Assembly for Simultaneous Forming and
                Bonding a Silicon Nitride Rotor Hub to a Blade Ring

Figure 3.14 illustrates densification of the rim as indicated by the dark areas
between the blades. In addition, small deformation ridges between the blades
and at the leading edge blade root are observed.

Although the inner sleeve greatly improved the rotor quality, modifications
of the assembly were required to eliminate applied pressure to the rim by the
thin inner sleeve. Two modifications are being evaluated which are shown in
Figures 3.15 and 3.16.

Figure 3.15 shows a modified version of the hot-press bonding assembly which
utilized a short inner graphite ("E") sleeve at the lower inner diameter of the
graphite restraining sleeve ("F"). The inner diameter of the reaction sintered
blade ring ("G") was machined to 3.070 inches while the inner diameter of the short
inner sleeve and outer diameter of the top contoured piston ("H") was 3.000 inches.

Figure 3.14   Densification of the Reaction Sintered Si_3N_4 Rim, as
Indicated by Dark Color

Although some drag of the piston on the short inner sleeve occurred, a point is
reached where pressure is exerted by the Si_3N_4 powder on the bottom edge of the
short inner sleeve ("E") counteracting the drag. This system greatly reduces
but does not eliminate pressure exerted on the blade rim. Fracture of graphite
has not been observed using this system.

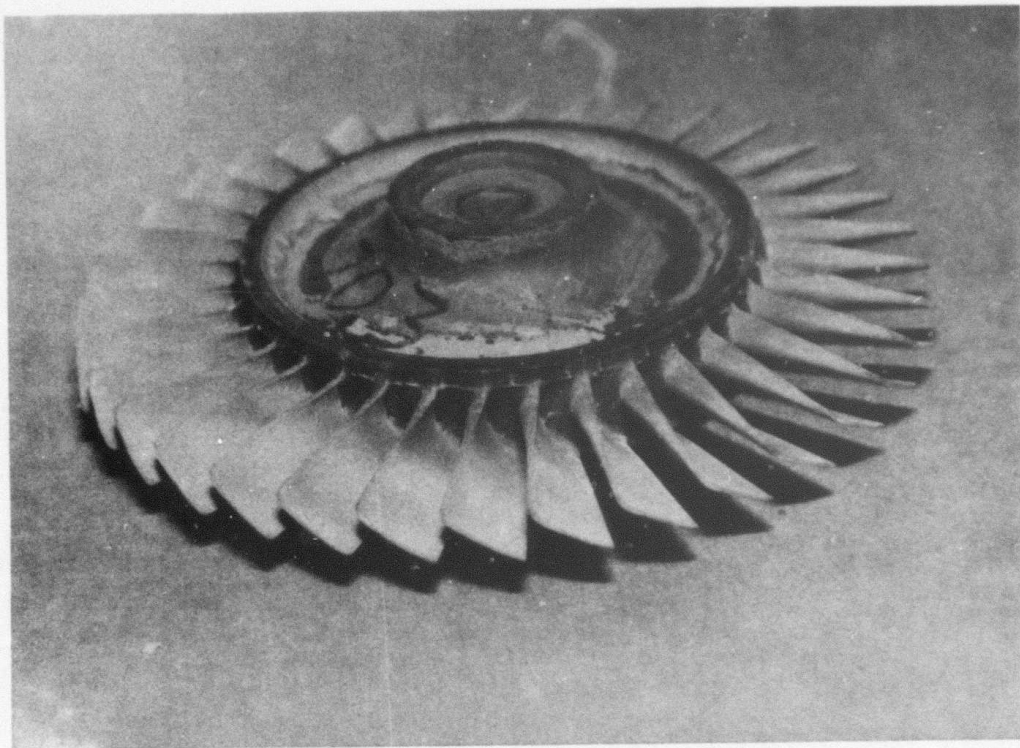Figure 3.16 shows another modified version of the hot-press bonding graphite
assembly, which completely eliminates the inner sleeve. This technique utilized
a reaction sintered Si_3N_4 blade ring ("J") with an extended rim height of 0.200
inches which is completely reinforced with blade fill material. When the Si_3N_4
powder in the hub region is completely densified, as illustrated by the dotted
line in ("K") Figure 3.16, the top contoured piston ("L") extends into the inner
diameter of the blade ring. This eliminates both the drag and the bonding to the
graphite restraining sleeve and subsequently eliminates its fracture. Since there
is no inner graphite sleeve, pressure is not exerted on the rim and there is one
less part in the assembly to handle.

Because of the success of eliminating both the axial and circumferential
cracks, this latter process is being further developed and refined. In addition
only occasional blade root cracks are observed. However, slight deformation of
the blade rim persists which results in small tears in the rim. Potential
solutions to this problem which will be investigated are an increased rim thick-
ness, lower MgO concentration in the hub region to minimize diffusion into the
rim, and further improvements in blade support.
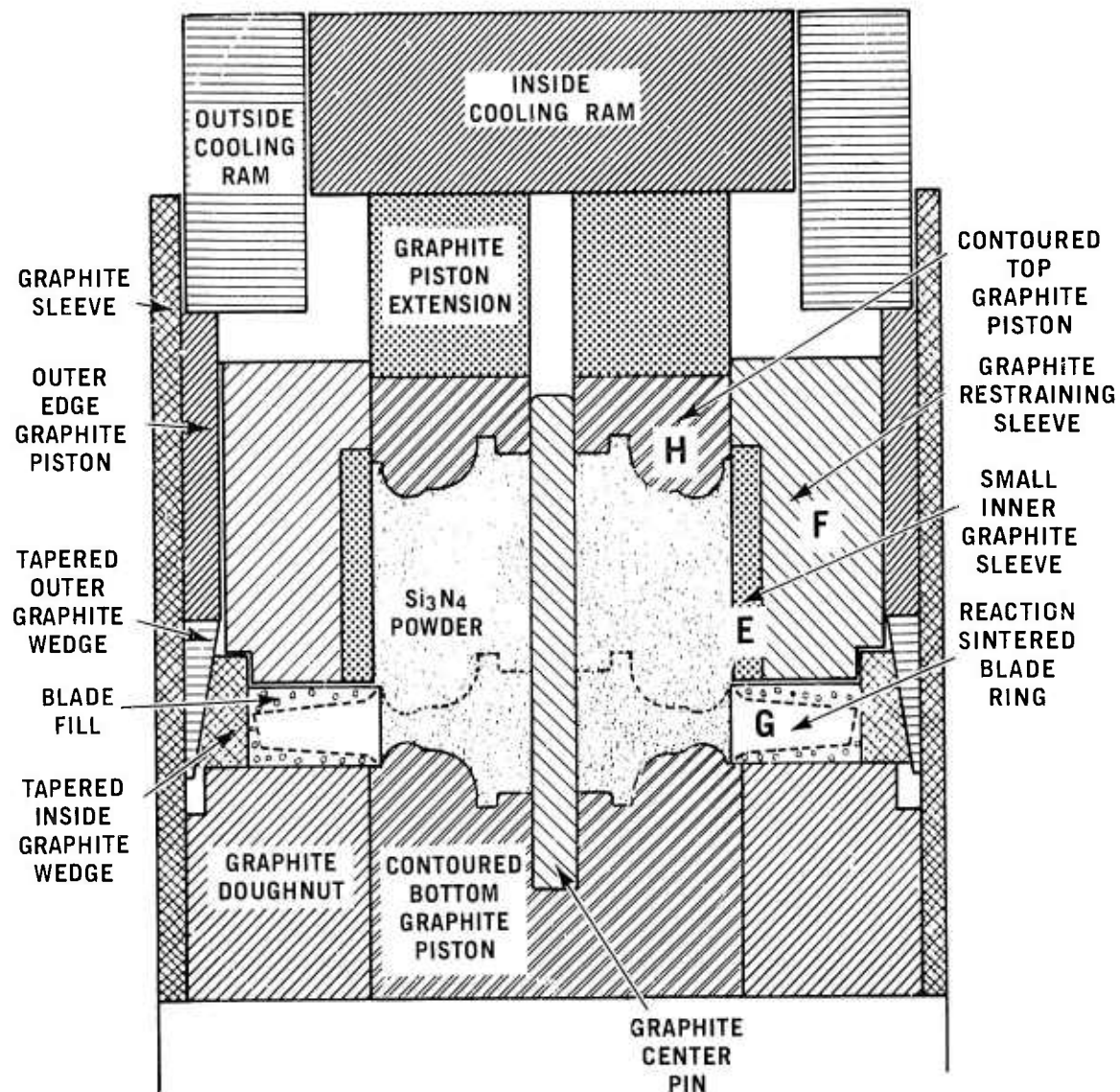
Figure 3.15   Modified Hot Press Bonding Assembly with a Small Inner
Graphite Sleeve

One Piece Turbine Rotors

Precision Cast Ceramic Rotors

Progress on a program at the Georgia Institute of Technology Experiment
Station, directed at the development of investment casting techniques for forming
precision cast ceramic shapes, has been previously reported [5,6,7]. Recent
emphasis had shifted towards slip casting a complete blade ring from silicon
slip in a fused silica shell mold and subsequently removing the shell mold after
the shape has been nitrided. Such a blade ring could have a density significantly
higher than the injection molded blade rings available earlier and would constitute
a major improvement in blade ring strength. A problem had been encountered in the
transition from single blades to full blade rings in that the silica shell molds
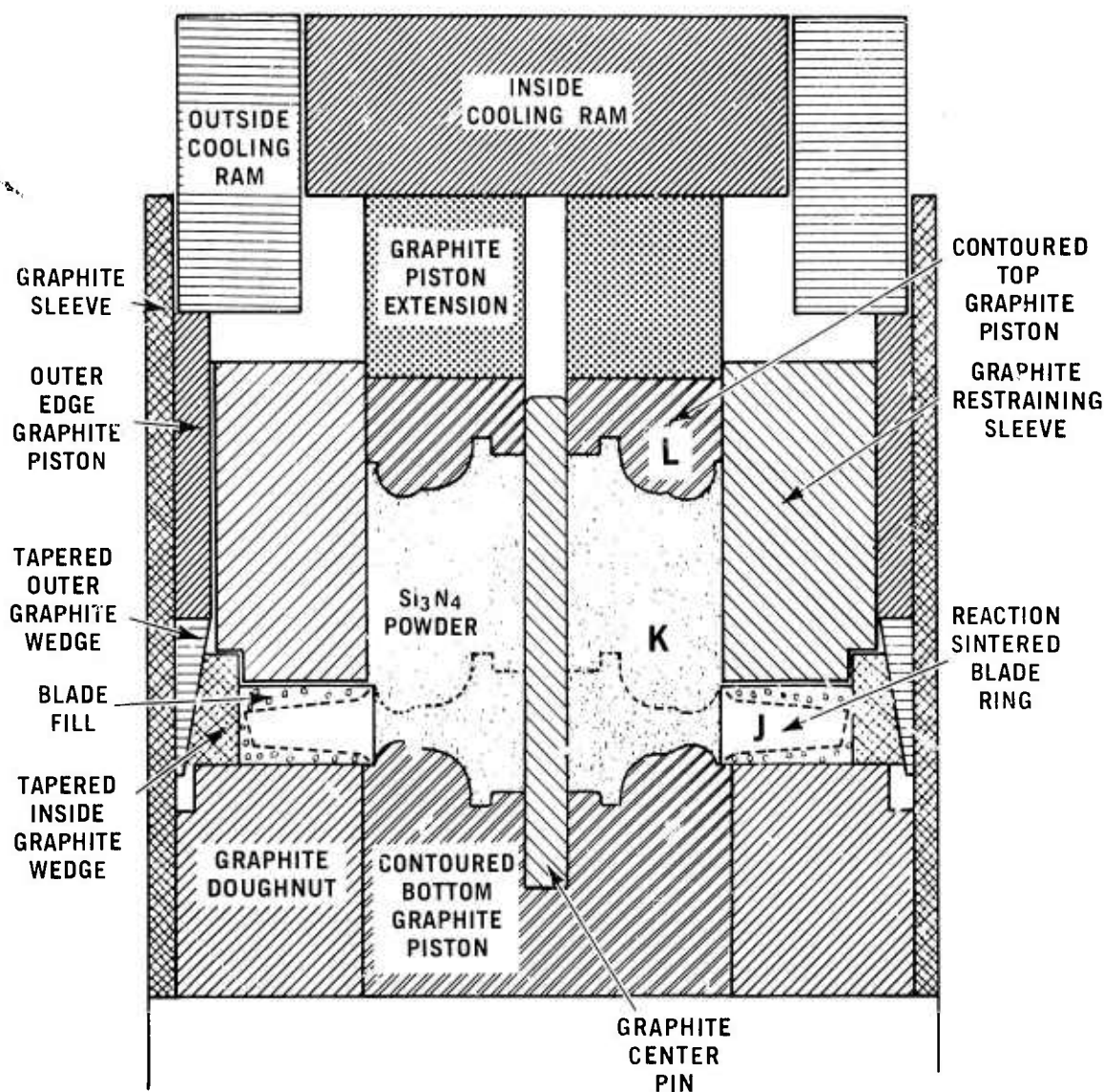
Figure 3.16   Modified Hot Press Bonding Assembly with No Inner
Sleeve

exhibited too high a fired strength for complete removal of the mold without some blade damage after nitriding.

Several approaches were investigated aimed at decreasing the strength of the mold. These included, 1) additives to cause devitrification of the silica on cooldown from the nitriding temperature, 2) a refractory second phase to decrease sintering and cause expansion mismatch microcracking to reduce strength and 3) a switch from the silica system to an organic bonded carbon system. In addition, a chemical method of removing a silica mold by treatment with hot concentrated sodium hydroxide solutions was evaluated.

The most successful method from a mold removal point of view was the carbon molds bonded with polyvinyl alcohol (PVA). The wax pattern from which the mold is formed may be readily removed by microwave heating and after the shape was cast, dried, and nitrided, the remaining carbon could be brushed away or rinsed off under running water.

The chemical method of removing the silica mold after nitriding was also fast and effective. However, the more severe hot concentrated sodium hydroxide treatments reduced the strength of 3/4" diameter by 6" long slip cast silicon nitride test bars by as much as 25% as measured by a four point bend test.

The mold filling process that appeared most effective was centrifical casting aided by a moderate vacuum. Casting of the full one-piece rotor with the contoured hub was never completely successful because of shrinkage cracking of the hub. This was therefore abandoned in favor of blade forming without the hub. Blade rings were formed without cracking of the ring and without breaking of the blades. However, a delicate balance of the slip parameters of solids content and viscosity is necessary in order to completely fill the thin blade cavities and yet avoid shrinkage cracks. A dual casting process has shown promise by using a slightly different slip for each portion of the casting, however, optimum parameters for the best end result have not yet been established.

High Pressure Nitriding of Reaction Sintered Silicon Nitride

High pressure nitriding of preformed silicon parts is a concept being investigated to produce a theoretically dense, one piece Si_3N_4 turbine rotor. This technique for forming a one-piece Si_3N_4 turbine rotor, if successful, would offer fabrication advantages over the duo-density rotor concept. Silicon metal compacts have been slip cast to green densities of 1.91 gm/cm^3 which would be equivalent to 3.18 gm/cm^3 density (T.D.) when fully converted to Si_3N_4. However, experience has shown that complete nitriding can not be accomplished for silicon compacts having green densities in excess of 1.65 gm/cm^3 (equivalent to 2.8 gm/cm^3 Si_3N_4) under conventional ambient pressure nitriding conditions.

Work previously reported [7] indicated that nitriding times in excess of 10 hours at 10,000 psi nitrogen pressure had little if any effect on the degree of nitriding. However, increasing the nitriding temperatures to 1350°C significantly increased the degree of nitridation but required very careful pre-nitriding at lower temperature to prevent a runaway exothermic reaction.

Although significant nitridation of the silicon compacts was accomplished at 1350°C, the major portion of nitriding occurred at the outer edge while high concentrations of silicon metal remained at the specimen core. The microstructure of a silicon compact nitrided at 1350°C for 5 hours at 10,000 psi nitrogen pressure is shown in Figures 3.17 and 3.18, illustrating the edge and center of the compact, respectively. Figure 3.17 indicates that complete nitriding can be attained up to approximately 0.025 inches from the specimen surface. Figure 3.18 illustrates the amount of silicon metal remaining after high pressure nitriding at the specimen center. Although some nitriding occurred as evidenced by the gray areas, substantial amounts of silicon metal (white area) remain. This microstructure was typical for all the 90, 95, and 100% equivalent density silicon compacts.
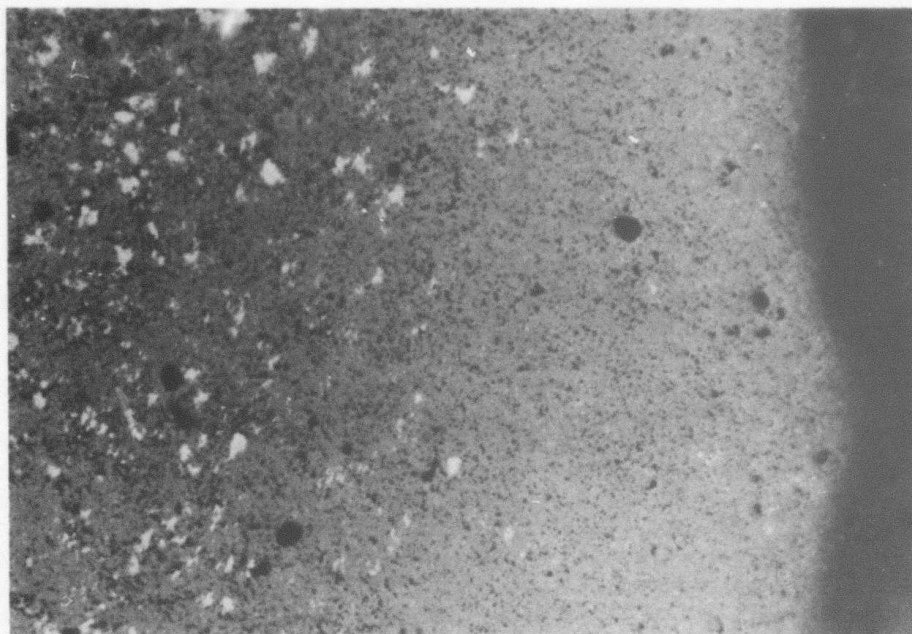
44

Figure 3.17   Microstructure of the Surface of Silicon Compact
               Nitrided at 1350°C (2462°F) for Five Hours at 10,000
               psi Nitrogen Pressure (100X)
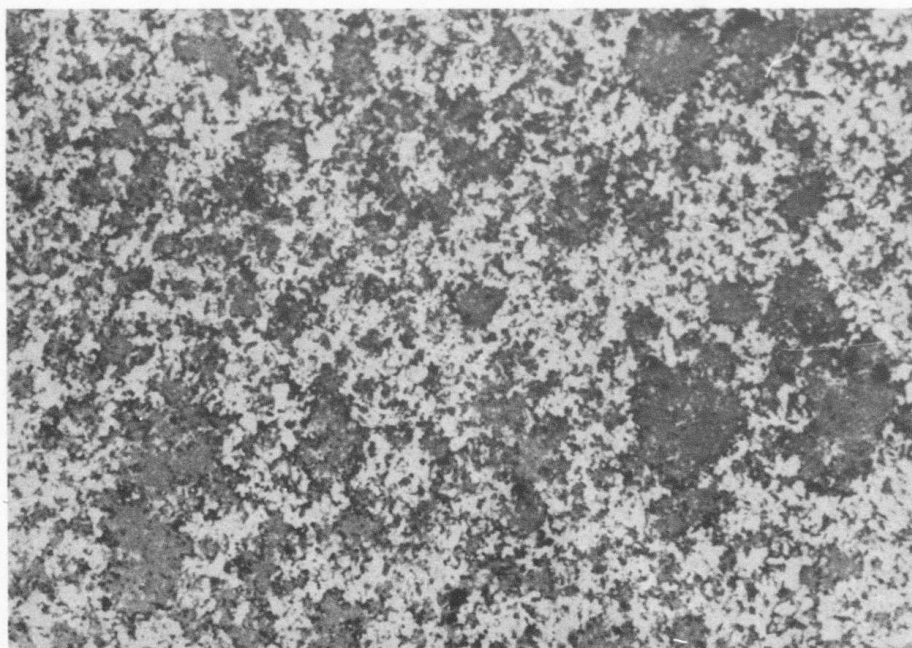

Figure 3.18   Microstructure of the Interior of a Silicon Compact
               Nitrided at 1350°C (2462°F) for Five Hours at 10,000
               psi Nitrogen Pressure (100X)

45

Based on these results, high pressure nitriding runs were made at $1450^{\circ}C$ and 10,000 psi nitrogen pressure for 5 and 15 hours respectively. Several slip cast silicon specimens at equivalent density levels of 90, 95, and 100% were prepared. The silicon metal specimens were 0.75 inches in diameter by 0.75 inches long, and were placed on Si_3N_4 powder in unsealed molybdenum cans. Several specimens contained Fe_2O_3 as a nitriding aid. The nitrogen gas was passed through a getter prior to specimen contact to remove traces of oxygen. The silicon samples were pre-nitrided at 1 atm. nitrogen pressure prior to processing in the autoclave.

The results showed that the 90% equivalent density compacts (both with and without the Fe_2O_3 additive) were essentially completely converted to Si_3N_4. This results in only a slight density improvement over typical results obtained under ambient conditions and therefore does not justify the expense and complication of high pressure nitriding. The 95 and 100% equivalent density compacts, although completely nitrided at the surface, exhibited a gradual decrease in nitridation toward the center region of the specimen. Both of these higher density specimens exhibited silicon metal cores at the center with only slight nitridation in this region. These results indicate an exothermic reaction to some degree and that optimization of the parameters for controlling the reaction kinetics is difficult and would involve an extensive program. In parallel with the high pressure nitriding experiments, a theoretical study of nitriding was undertaken and showed that it was not possible to store enough nitrogen in the pores of a silicon powder compact to permit complete nitridation using available equipment, as explained in more detail in Section 4.2 of this report. As a consequence of this study and the disappointing experimental results, it was apparent that high pressure nitriding of green compacts sufficiently dense to yield near-theoretical density Si_3N_4 was not close at hand. Accordingly further effort on this approach was terminated.

46

3.1.3   ROTOR TESTING

Introduction

Primary emphasis during this reporting period has been on cold spin testing of reaction sintered Si_3N_4 rotor blade segments. Additional efforts in the cold spin pit have been directed toward developing techniques for testing complete blade rings. A high speed motion picture was taken of a ceramic rotor at the instant of failure. The spin pit was also used to measure the strength of the revised hot pressed Si_3N_4 rotor hubs.

The turbine rotor test rig was rebuilt with hot pressed Si_3N_4 rotor hubs (duo-density rotor without blades) and a series of tests conducted to evaluate the rotor attachment mechanism. The major efforts were directed toward evaluation of the curvic couplings and the experimental determination of the rotor bolt cooling air requirements.

Cold Spin Testing

The equipment and the technique used in cold spin testing of ceramic turbine rotors have been discussed in a previous report [6]. Ceramic blade rings and turbine rotor hubs are spin tested at room temperature in a partial vacuum at speeds gradually increased at the rate of 400 rpm/sec. until destruction.

During this reporting period most of the testing has been concentrated on reaction sintered Si_3N_4 blades. In order to determine the blade strength, some tests were conducted with blade rings which were sectioned into several segments. Each blade ring segment consisted of 3-4 blades. Figure 3.19 shows a metal test hub and two segments, at the instant of failure, at the highest failure speed attained during this report period of 58,100 rpm or 91% of maximum speed.

Perhaps the most important conclusion derived from the 50 tests of over 350 blades was the good uniformity of blade strength, since the scatter in breaking strength was only 8%. It was necessary to develop an improved epoxy bonding material for fastening the blade segments to the test hub, since some spin tests resulted in failure of the epoxy. For example, Figure 3.20 was taken at the instant of failure which occurred at 55,650 rpm (87% of maximum speed) and was directly attributable to a poor epoxy bond. Improvements resulted when a one part-heat cured epoxy was used to bond the Si_3N_4 blade ring segment to a hot pressed Si_3N_4 test hub, rather than a metal test hub.

Rotor Blade Failure Statistical Analysis

The results of cold spin testing of reaction sintered Si_3N_4 rotor blades were statistically analyzed in order to determine the distribution of failure speeds, characteristic speed, and Weibull modulus, m. The characteristic speed is the speed at which 63.3% of the blades will have failed. The method of analysis was the use of order statistics with the Weibull distribution which utilizes the suspended test items to adjust the observed failure distribution to obtain the population failure distribution, as discussed in an earlier report [6].
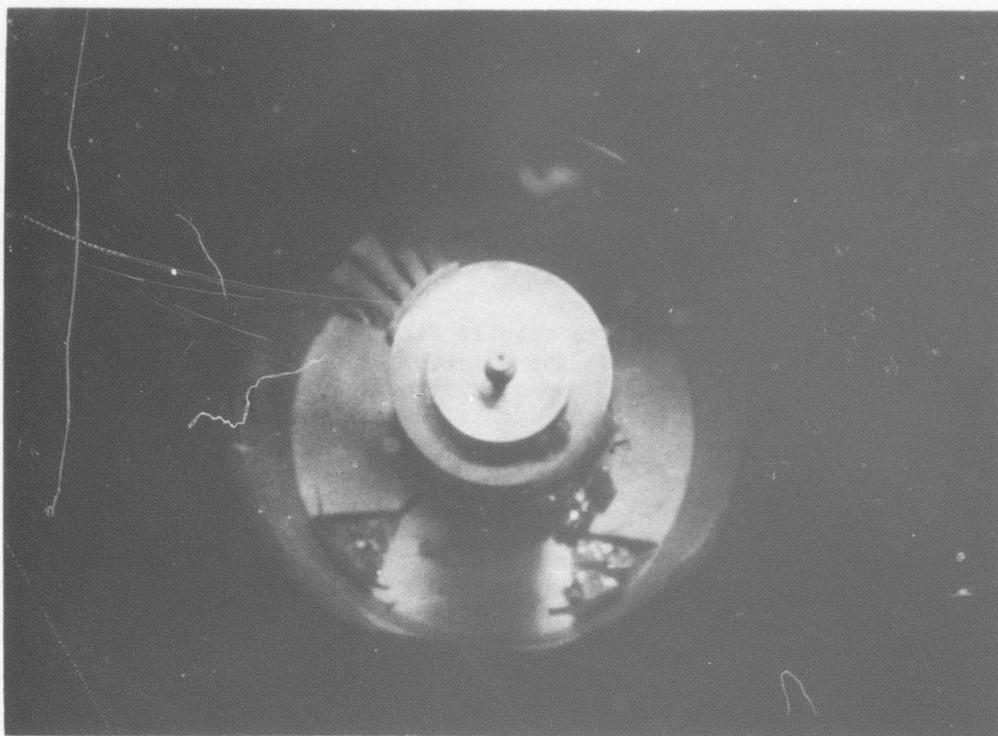
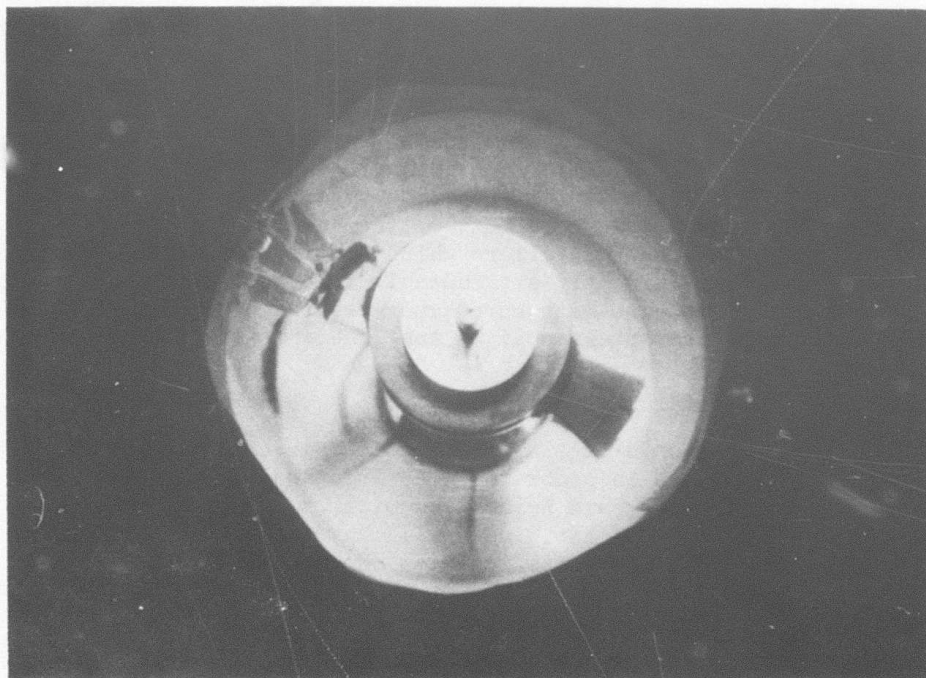Figure 3.19   Photograph of a Blade Failure at 58,100 RPM

Figure 3.20   Photograph of the Failure of the Epoxy Bond at 55,650 RPM

48

TABLE 3.6   SPIN TEST DATA FOR SECOND STAGE ROTOR BLADES

Test Group Size	Failure Speed RPM
1	32550
1	32560
1	39460
1	41070
4	43100
5	46660
3	54880
7	57380
4	58100

The data for this analysis is shown in Table 3.6. The blade segments were selected from several blade rings. The selection of blades used in this analysis was based on the assumption that the manufacturing process would be developed to the point where all the blades on a blade ring would be the same quality as those selected for testing, and only those parts having no visible flaws were selected for testing. Test groups consisting of more than one item, as shown in Table 3.6, had one blade failure with the remaining blades considered statistically as suspensions.

The failure distribution is shown in Figure 3.21 for individual blades. The suspended blades in the test results shown in Table 3.6, shifts the median and characteristic speeds to higher values than indicated by the test result data shown in Table 3.6. If the suspended items could have been tested to failure, the resulting median and characteristic speeds would be those shown in Figure 3.21. The suspensions were caused when one blade in the group failed and destroyed the remaining blades. In addition, the blades tested were Design C, and were 0.22 inches longer than the Design D blades. Applying a correction for the Design D blades results in further increases in median and characteristic speeds.

Cold Spin Testing of Hot Pressed Silicon Nitride Rotor Hubs

Six hot pressed Si_3N_4 rotor hubs, fabricated using the duo-density press bonding technique, were processed for strength evaluation tests. All of the blades were removed and the reaction sintered Si_3N_4 was machined off the hubs for destructive tests. Figure 3.22 shows a hub at the highest failure speed attained of 113,570 rpm. The e tests have shown that the current hot press/press-bonding parameters yield rotor hub strengths comparable to the previously reported [7] hub strengths fabricated using the original rotor forming technique which separated hub fabrication and blade ring bonding.

Cold Spin Test Using High Speed Photographic Techniques

The spin pit was also used to conduct a high speed motion picture study of crack propagation and how it develops during the failure of a second stage Design C injection molded Si_3N_4 blade ring bonded to a slip cast Si_3N_4 contoured hub, made specifically for this test. The special 16 mm camera running at 3000
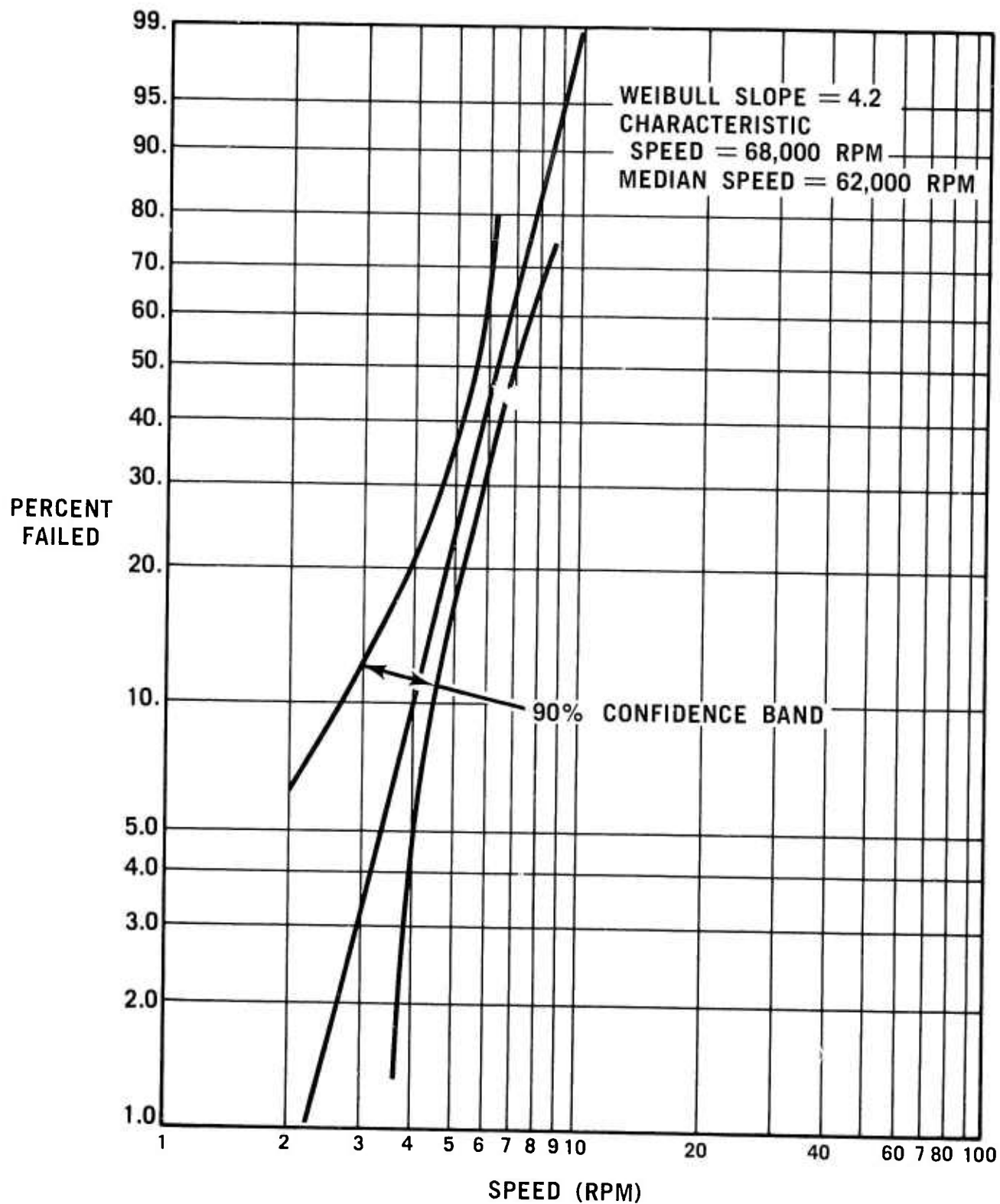
Figure 3.21   Failure Distribution of Single Reaction Sintered
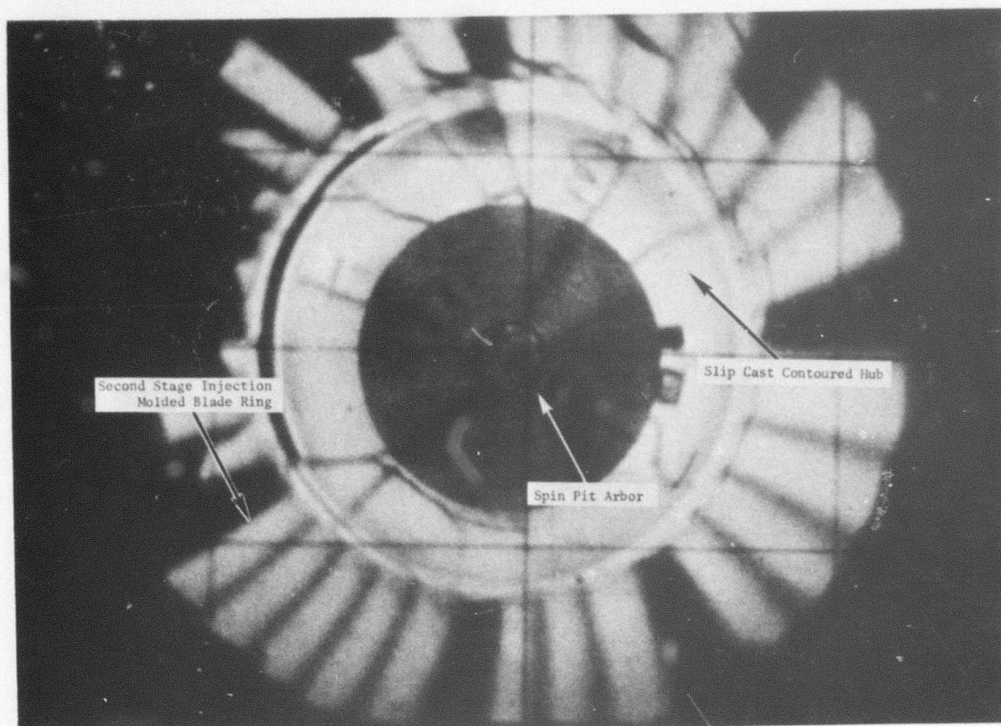Si$_3$N$_4$ Rotor Blades

Figure 3.22   High Speed Motion Picture Frame of a Rotor Failure
at 55,540 RPM

frames/second captured the failure at 55,540 rpm or 86% of maximum speed. The
exposed film from start to finish amounted to 3,068 frames, only four of which
were needed to show the entire fracture. Figure 3.23 shows one of those four
frames of the rotor at burst. The irregular lines in the hub are the multiple
crack paths at the exact instant of failure. Individual blade failures occurred
during the run-up to destruction. Since these failures actually occurred between
frames, they were not photographed. This film dramatically indicates that failure
of a ceramic turbine rotor occurs very rapidly and will be difficult to document.
The hub cracks originated in the bore and traversed radially outward to the rim.
Some circumferential cracking can be observed at the neck area of the hub. As
the cracks reached the rim, they appeared to go directly through in places where
bonding was sound and then travelled circumferentially through the bond joint
where bonding was poor. This film and others like it exposed at faster film speeds
may provide a useful investigative tool for development of ceramic turbine rotors.

Turbine Rotor Test Rig Testing at Temperature

Following failure of the turbine rotor, in the turbine rotor test rig as
noted in the last report [7], all salvageable test rig parts were inspected and
replaced as necessary. The high speed shaft showed no damage. The pattern
between the mating teeth of the rotor curvic spline and the shaft curvic spline
was satisfactory. After rebuild with two hot pressed Si_3N_4 rotor hubs and
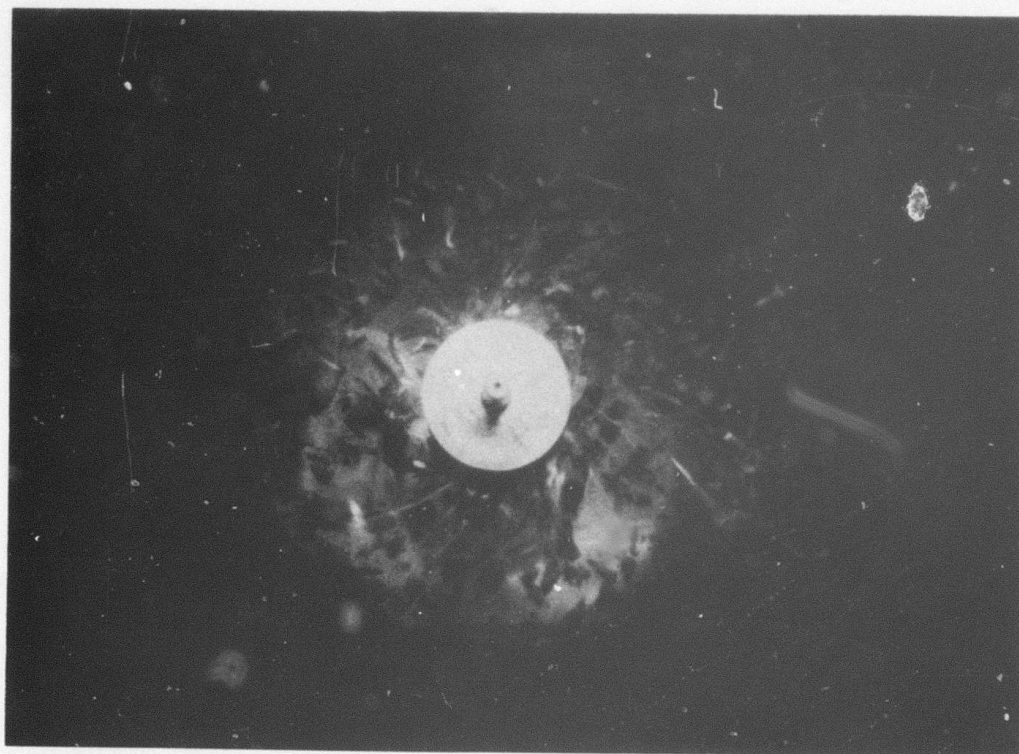
51

Figure 3.23   Photograph of a Hot Pressed Si_3N_4 Contoured Hub
                Failure at 113,570 RPM

installation in the test cell, the rig was operated under both steady state
and cyclic conditions as follows:

Condition 1   19,000 rpm $900^\circ F$ Inlet temperature

Condition 2   35,300 rpm $1950^\circ F$ Inlet temperature

The object of the test was to shake-down the rig after making a modification
in mounting of the exhaust plenum and to make a hot evaluation of curvic couplings.
The procedure consisted of slowly heating the rig inlet air to $900^\circ F$ with
a pre-heater while the shaft was rotated at 19,000 rpm. The combustor was then
fired and the turbine accelerated to Condition 2 which represents engine idle
and was considered sufficient speed and temperature to accomplish the object of
the test. This cyclic operation was repeated for 10 cycles between steady state
conditions 1 and 2. Inspection of the hardware after hot operation revealed the
following:

No chipping of the curvic teeth at any mating surface. This is
especially significant in light of wear patterns which show relative
movement between the shaft-second stage rotor hub curvic interface
and between the adaptor-first stage rotor hub curvic interface.
No permanent deformation of the rotor attachment bolt.

This testing program will continue to work toward full speed (64,240 rpm) and
$2500^\circ F$ turbine inlet temperature.

52

Rotor Bolt Testing

An important component used in the attachment of ceramic rotors to the metal shaft is the air-cooled folded bolt. Previous reports [2,4,5,6,7] have discussed the design and initial testing of this bolt and the Turbine Rotor Test Rig was used to determine the amount of cooling air required for its safe operation.

The rotor bolt cooling design is complex, and is shown schematically in Figure 3.24. As designed for engine use, compressor discharge air enters the turbine labyrinth seal and divides as follows:

Toward the rear face of the second stage turbine.
Into the engine oil sump.
Into the high speed shaft for rotor bolt cooling purposes.

Because of these three separate flow paths, it is difficult to calculate with any degree of confidence the quantity of cooling air entering the high speed shaft rotor bolt cooling passage.

Heat transfer calculations which require specification of the mass flow are also uncertain. Therefore, a means was devised to measure the mass flow rate, which is difficult because of the small size of the cooling air supply hole in the rotor bolt and the high speed rotation of the shaft.

A miniature instrumentation rake was fabricated and installed in the inner body of a Si_3N_4 nose cone, as shown in Figure 3.25. This probe consists of five total pressure probes to determine pressure distribution across the diameter of the rotor bolt supply passage, a thermocouple to measure cooling air exit temperature, and a static pressure probe. This instrumentation is adequate to determine the cooling air velocity profile which will be integrated over the cooling air supply hole area to determine mass flow rate. Data from this test program will result in the accumulation of flow rates for a wide range of engine speeds and cooling air inlet supply pressures simulating engine compressor discharge pressures. Using this data as input to analytical heat transfer analysis, bolt exit air temperatures can be calculated.

Rotor Bolt Elongation Measurement

It was reported in the last report [7] that the efficiency of the load transfer from the rotor bolt installtion tool to the rotor nut was approximately 80 percent of the predicted value. It has since been determined that the calibration of the fixture load cell was in error. It was found that the calibration is very sensitive to the concentricity of the calibration load relative to the load cell.

The load cell was recalibrated, using the actual loading fixture as the calibration hardware, and repeatability was obtained. Dimensional checks of the tension member elongation at 3900 pound load were then made resulting in values of 95 percent of the predicted elongation. The elongation checks will continue to be made as other rotor attachment hardware is put into service.
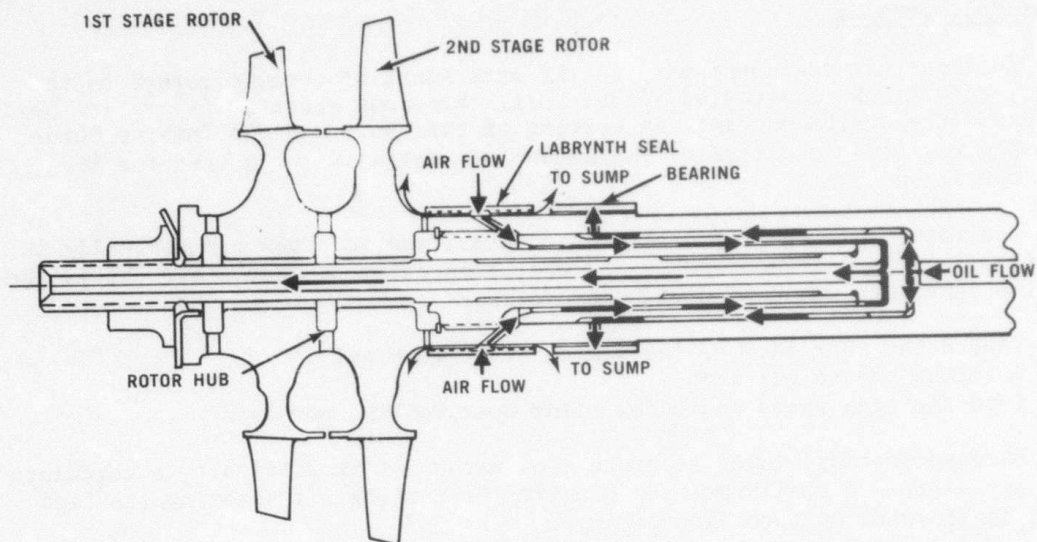
Figure 3.24   Rotors and Attachment Assembly Illustrating Cooling
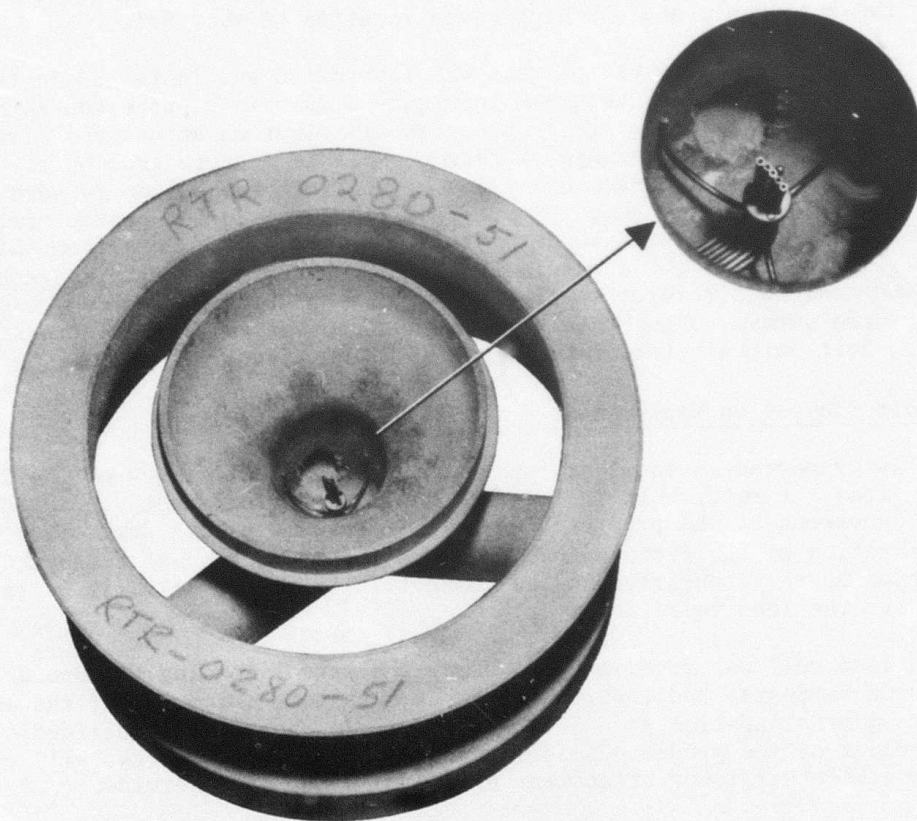Air Flow

Figure 3.25   Combination Total Pressure, Static Pressure, and
Temperature Probe Installed in Turbine Inlet Nose
Cone

54

3.2 CERAMIC STATOR, NOSE CONE AND COMBUSTOR DEVELOPMENT

SUMMARY

Stators of 2.55 gm/cm^3 density silicon nitride were injection molded which were free of detectable defects as a result of modifications to the tooling. Evacuation of the stator cavity, prior to injection, appears to have eliminated outer shroud voids produced by entrapped gases. The organic burnout process has been changed to a charcoal-wicking system which eliminated adverse distortion of the components and resulted in excellent removal of the organics prior to nitriding. A modification of this new burn-out process was also used in fabricating nose cones. Changes made to the nose cone tooling resulted in the fabrication of flaw free components of 2.55 gm/cm^3 density. Fabrication of slip cast Si_3N_4 rotor shrouds continued with no additional development work.

Continued thermal shock rig testing of 2.55 gm/cm^3 vane segments produced 2 vane cracks out of 8 vanes tested after an additional 1000 cycles to 2500°F (all segments had previously survived 3000 cycles to 2300°F). Stator vanes of higher density (2.7 gm/cm^3) survived 9000 cycles with no cracks-4000 cycles to 2300°F, 1000 cycles to 2500°F, and 4000 cycles to 2600-2700°F.

The 171 hour, 56 cold light, "Refel" reaction sintered silicon carbide combustor [6] was successfully tested for a short time in an engine under conditions of cold light-offs and transient accelerations to idle.

Recently introduced stator vane proof testing promises to be a valuable tool to monitor the quality of stator vanes. Statistical test results indicate recently fabricated stator vanes are of superior strength and quality than some previously fabricated, and are similar to engine tested stators which completed 60-100 hours of ARPA durability without vane failures [6].

A 2500°F Flowpath Test Rig has been built and installed to evaluate the stationary flowpath components at temperatures up to 2500°F. Initial checkout of the rig is progressing on schedule.

Engine testing has been directed towards qualification of the stationary ceramic flowpath components. Seven Si_3N_4 nose cones and seven Si_3N_4 one piece stators have been subjected to the qualification test. Two reaction sintered silicon carbide one piece stators also successfully passed the qualification test cycle.

3.2.1   MATERIALS AND FABRICATION

Introduction

Development efforts were directed toward obtaining flaw free one piece stators and nose cones using a new molding material system to produce silicon nitride densities of 2.55 gm/cm^3. Radiography of the as-molded components was the primary NDE method used to optimize material and molding parameters. Fabrication problems related to material flow in the die cavities, die misalignment, entrapped gas voids, and component distortion during burn-out of the organics were identified and corrected. Significant increases in the yield of parts determined to be flaw free by x-ray were obtained.

Silicon Nitride Stator Fabrication

Further development has been conducted during this reporting period on the fabrication of 2.55 gm/cm^3 stators. Several new materials have been utilized for molding, as discussed in Section 4.1 of this report. Additional research has been conducted to determine the flow characteristics of the 2.55 gm/cm^3 material as it enters the die cavity under pressure. The flow of the material using a bottom gate over a three vane area is shown in Figure 3.26. Note that the material enters and flows in both circumferential directions around the outer shroud, filling the vanes from the outside to the inside. The vanes at the top (180° from the material gate) fill last, with the top inner shroud being the last to fill. Although many void-free components have been molded, there is a tendency to entrap gas in the quadrant of the stator which fills last, therefore forming small voids.
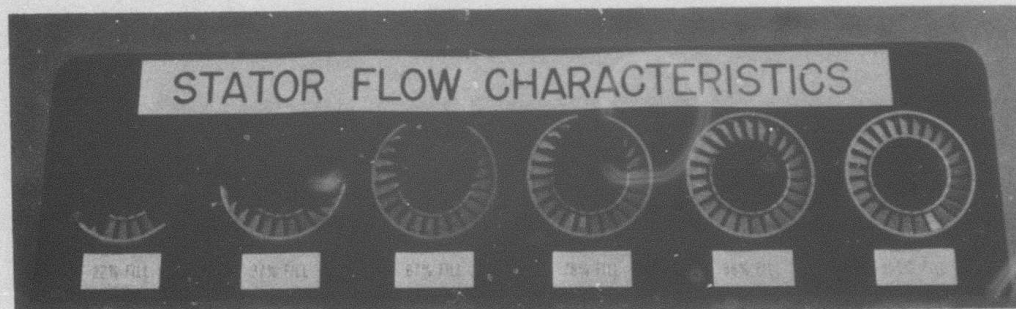

Figure 3.26   Progressive Flow of Material In Injection Molding of a One Piece Stator When Gating Through Three Adjacent Vanes

In an effort to eliminate the entrapped gas, a new sprue bushing detail is being developed which will vent the inner shroud at the top of the stator. This vent will provide a reservoir which fills after the entire stator has been filled, allowing trapped gas to flow into the reservoir-which is subsequently removed.

Evacuation is another approach which was evaluated to eliminate trapped gas and improve the material flow into the die. A new outer shroud insert has been fabricated and installed in the stator tooling. A thin 0.003 inch gap around the entire outside diameter of the stator allows the die cavity to be evacuated to 30 inches Hg, using a roughing pump. The gap is too narrow

56

to allow material flow into the vacuum system. By eliminating the air from the cavity prior to material injection, there are no pockets of compressed air to be expelled or entrapped during injection molding.

Components molded using the vacuum system appear flaw free using visual sectioning techniques. X-ray evaluation will be used to further verify the absence of voids. The vacuum has also been effective in lowering the resistance to material flow into the die cavity. Previous molding of stators was done at $170^{\circ}F$ with the cavity at atmospheric pressure. With the cavity at 30 inches of Hg vacuum, molding temperature was reduced to $150^{\circ}F$ with no loss in fluidity.

Several modifications have also been made to the tooling during this reporting period to improve the mechanical operation. Cracking of the stator at the fillet radius between the inner shroud and vane during molding was caused by slight misalignment (0.005 inches) during die opening. To correct this misalignment, new linear ball bearings were installed on die guide pins. This change alone did not entirely eliminate the problem. A stripper plate and an extractor plate were added to push and pull the stator from the die prior to the point where misalignment damage occurred. This decreased the sensitivity of the die to misalignment, and crack free components have been molded since these modifications were made.

In conjunction with the use of the 2.55 gm/cm^3 material for stators, a new binder burnout method was developed. Stators were previously packed in Al_2O_3 granules and heated at the rate of $5^{\circ}C/hr$ to $300^{\circ}C$ in order to remove organics prior to nitriding. With the 2.55 gm/cm^3 material, this cycle resulted in some distortion and cracking of the stator. Coconut charcoal of 80-200 mesh was substituted for the Al_2O_3 granules. Using Al_2O_3 granules, the component had to reach the volatization temperature of the organics before burnout began. However, charcoal absorbed the organics as soon as a liquid phase was present, which occurred below the decomposition temperature. A burnout cycle which heats the part to $450^{\circ}F$ in charcoal at furnace rate, holds for 16 hours, and cools at furnace rate to room temperature was established for stator burnouts. This procedure has successfully eliminated the distortion noted in previous Al_2O_3 burnouts. The charcoal burnout is also advantageous in that organics are wicked from the component rather than carbonized in situ. Residual carbon tests of charcoal air cycled components show levels equivalent to the starting silicon powder.

Silicon Nitride Nose Cone Fabrication

During this reporting period, advances have been made in several areas of nose cone fabrication. Material density has been upgraded to the 2.55 gm/cm^3 level, tooling rework has been completed, and NDE techniques utilized to yield nose cones of higher quality.

The nose cone tooling was realigned to ensure tight insert fit. This was required to avoid low density regions associated with areas of material leakage.

The 2.55 gm/cm^3 density Si_3N_4 material was used to fabricate nose cones and demonstrated the necessary molding shrinkage and required high green strength. These nose cones were subjected to more stringent visual and x-ray NDE than were previously the case. Many components manufactured were found to be free of detectable flaws. These components are currently being processed and tested.

The charcoal burnout procedure discussed under ceramic stator fabrication was adapted to the nose cone burnout. The cycle consists of heating at a rate of 7°F/hr with a six hour hold at a temperature of 620°F. This procedure removes approximately 95% of the organic from the nose cone, with none of the distortion and cracking which occurred with previous Al_2O_3 granule burnout procedures. Additional heating to 700°F with the nose cone free-standing in air removes the remainder of the organics.

Silicon Nitride Rotor Shroud Fabrication

No further development work was carried out on rotor shroud fabrication during this reporting period. Engine test results of rotor shrouds are given in Section 3.2.2 of this report.

3.2.2   TESTING

Introduction

The stationary hot flow path components include the combustor, turbine inlet nose cone, common first and second stage stators, and first and second stage rotor tip shrouds. In order to evaluate these components, five different types of test rigs are employed. The Thermal Shock Test Rig is used to test stator vane design modifications and materials, the Combustor Test Rig is used for combustor evaluation, the newly constructed 2500°F Flowpath Test Rig is used to evaluate all of the stationary components at temperatures up to 2500°F, Engine Test Rigs are used for light-off qualification and durability testing, and a new Stator Vane Load Test will be used to proof load stator vanes before engine testing.

Stator Vane Load Testing

Visual inspection of 2.55 gm/cm^3 Si$_3$N$_4$ density one piece stators, made early in the fabrication program described in Section 3.2.1 of this report, revealed a cracking problem in the leading edge of the vanes. This condition was not previously observed in any of the stators fabricated from lower density silicon nitride material systems.

The random occurrence of these cracks necessitated an evaluation to determine their effect on structural integrity. Individual vanes were mechanically loaded to failure on an Instron testing machine, as illustrated in Figure 3.27. A cross-head speed of 0.02 inches per minute was used and the failure load graphically recorded. Failure loads ranged from 3.6 to 22.5 pounds on 126 test vanes, with the majority of vanes which failed below 10 pounds having large defects, ranging in size from 0.010 inches to 0.100 inches long. A statistical analysis indicated a correlation exists between failure load and visual inspection before proof testing.

Changes made later in the fabrication process (refer to Section 3.2.1 of this report) greatly reduced the number and magnitude of vane defects and resulted in higher loading to produce vane failure with less scatter, as shown in Figure 3.28. Stators 764 and 784 contained a total of 45 vane defects, ranging in size from 0.010 inches to 0.100 inches, whereas more recently fabricated stator 829 and 848 contained only 3 vanes with questionable indications of flaws.

Stators which had achieved a degree of engine durability, along with one stator which sustained 5 failed and 2 cracked vanes during engine testing, were also subjected to the vane loading test. Figure 3.29 shows these results. The stator which had some earlier engine vane failures had the lowest Weibull distribution, whereas the stator which had no earlier vane failures during engine testing had higher strength distributions, as would be expected.

Future plans for load testing stator vanes to eliminate weak vanes will incorporate acoustic emission monitoring to detect the onset of damage to the vanes. Load testing will also be used as a quality control tool, and will provide a means of assessing future material and process improvements.

Thermal Shock Rig Testing

Testing of ceramic stators on the Thermal Shock Test Rig was continued during this reporting period according to the procedures previously reported [2,3,4,5,6,7].
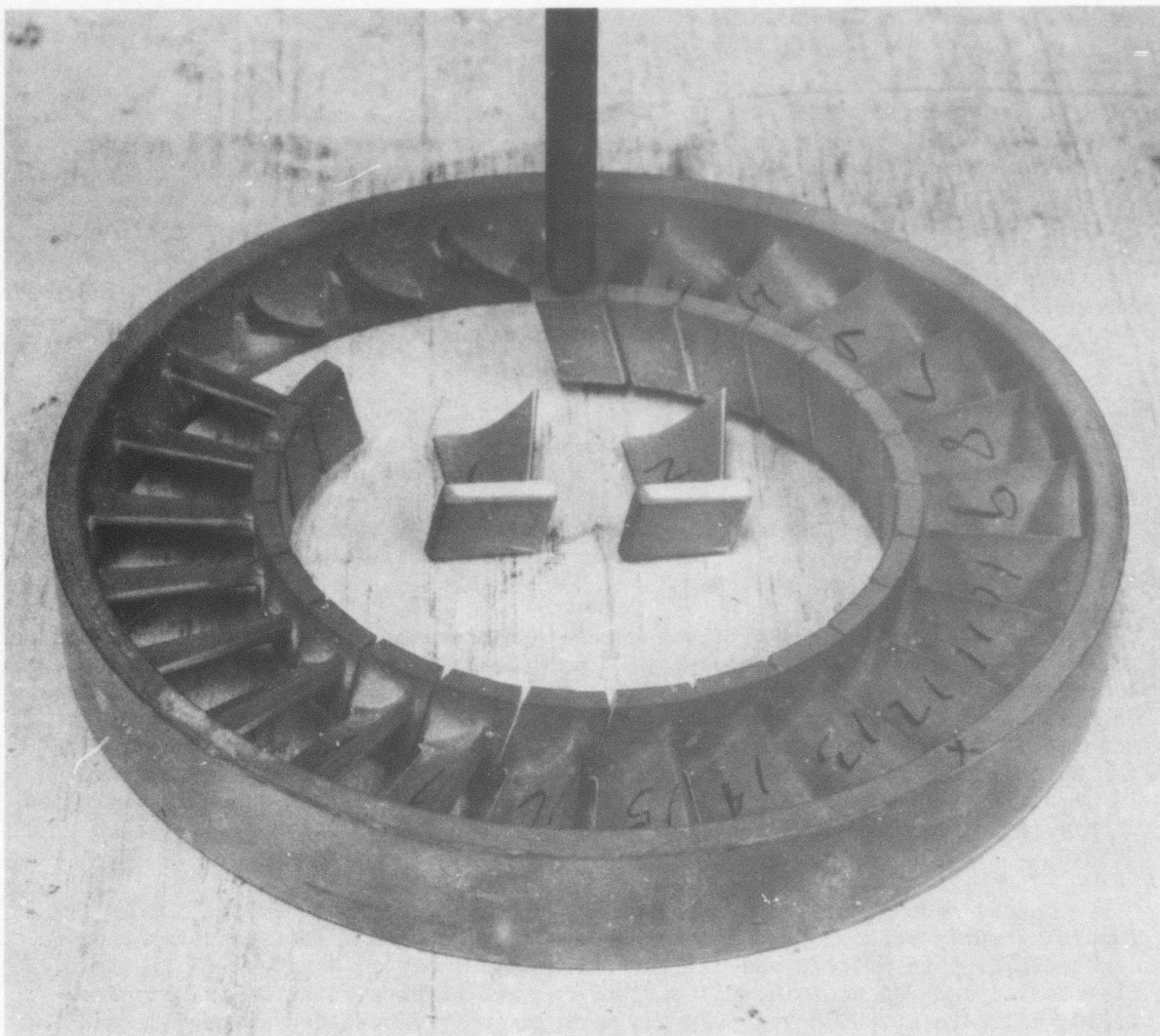
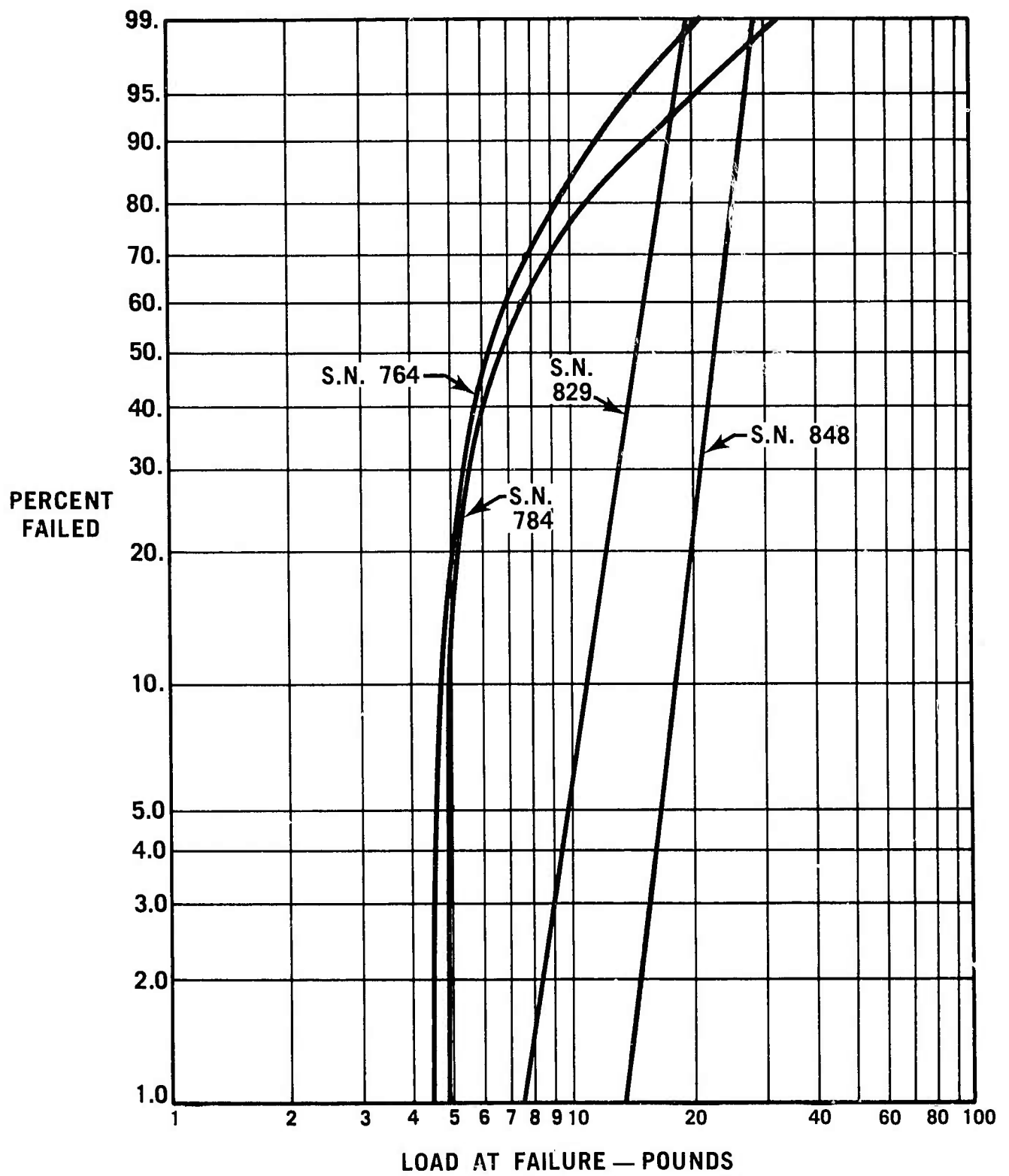Figure 3.27   Method of Mechanically Loading Stator Vanes

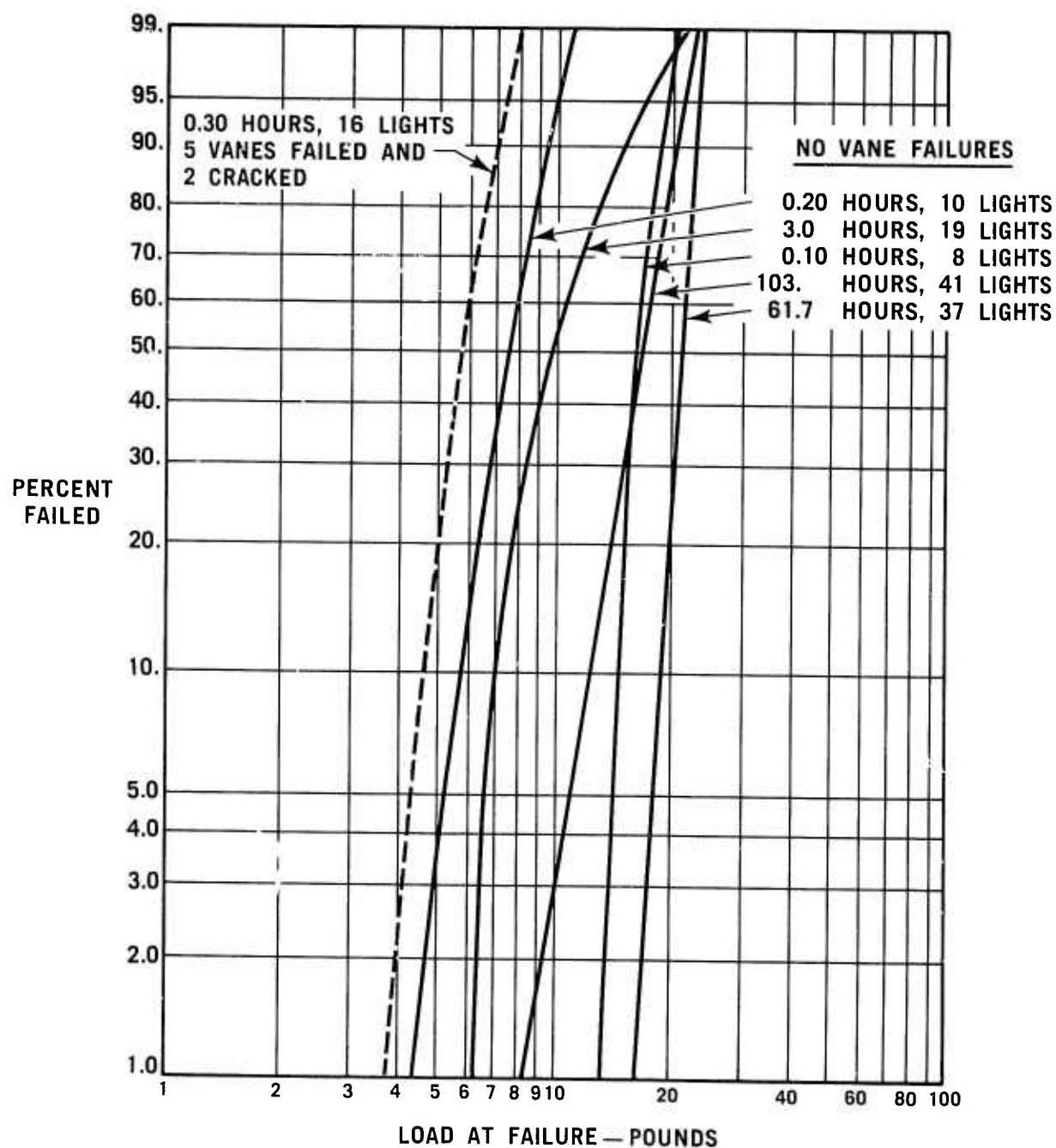Figure 3.28   Weibull Distribution of One Piece Stator Vane Failure
Loads

61

PERCENT FAILED

0.30 HOURS, 16 LIGHTS
5 VANES FAILED AND
2 CRACKED

NO VANE FAILURES

0.20 HOURS, 10 LIGHTS
3.0 HOURS, 19 LIGHTS
0.10 HOURS, 8 LIGHTS
103. HOURS, 41 LIGHTS
61.7 HOURS, 37 LIGHTS

LOAD AT FAILURE — POUNDS

Figure 3.29   Weibull Distribution of Vane Failure Loads of One Piece
                Stators Which Were Engine Tested

The Si_3N_4 stator segments of 2.55 gm/cm^3 density previously subjected to 3000 cycles of thermal shock to $2300^\circ F$ [7] were further cycled to $2500^\circ F$. The quench air was adjusted to maintain a $600^\circ F/sec$ down shock. After an additional 1000 cycles, 2 of the 8 vane segments had developed vane cracks but had not entirely separated.

Similar stator vane segments (3 vanes and corresponding segment of outer shroud) but of 2.7 gm/cm^3 density, were also tested. Preliminary test conditions were established at $2300^\circ F$ vane temperature measured at a point just inside the leading edge of the vane near the midspan. Down shocks of $600^\circ F/sec$ were maintained. The segments were subjected to 4000 cycles at $2300^\circ F$ without failure. The maximum temperature was raised to $2500^\circ F$ and a down shock of $600^\circ F/sec$ was maintained. After 1000 additional cycles no failures were noted. The temperature was raised to $2600^\circ F$ and the down shock held at $600^\circ F/sec$. During this test, vane temperature control became more difficult, and the vane temperature varied from $2600-2700^\circ F$. After an additional 4000 cycles no failures were observed. Figures 3.30 and 3.31 show vane segments which have had no thermal cycling and vane segments which have been cycled for the entire 9000 cycle test. Note there are some discolorations due to combustion products, but no apparent difference in vane geometry is visible. Under higher magnification, a slight erosion of the leading edge of the center (target) vane can be noted.
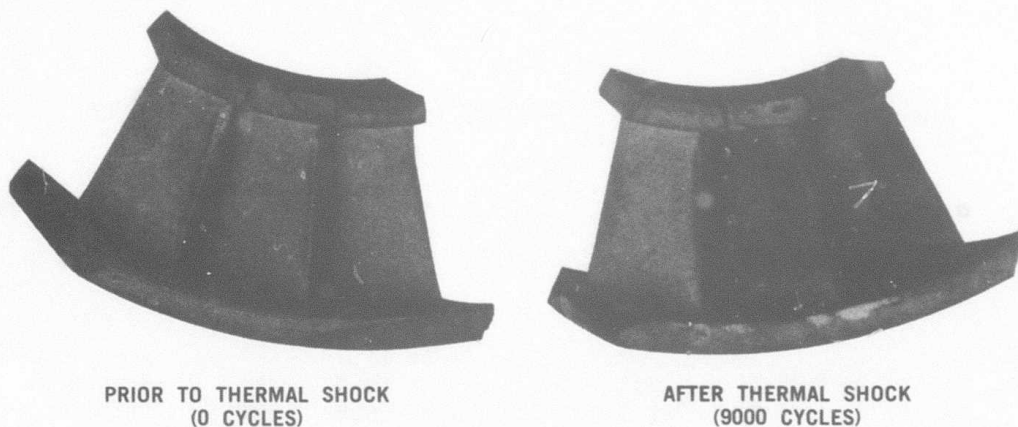

PRIOR TO THERMAL SHOCK
(0 CYCLES)

AFTER THERMAL SHOCK
(9000 CYCLES)

Figure 3.30   Stator Vane Segments Viewed Trailing Edge Up Before and After Thermal Shock Testing

PRIOR TO THERMAL SHOCK   AFTER THERMAL SHOCK
        (0 CYCLES)   (9000 CYCLES)
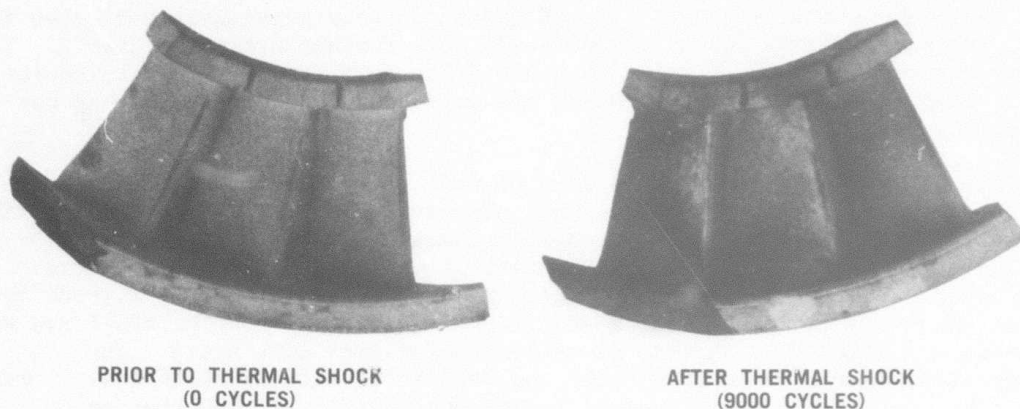

Figure 3.31   Stator Vane Segments Viewed Leading Edge Up Before and
               After Thermal Shock Testing

After the 9000 cycle test, the vanes which were thermal shocked were broken on the bend test fixture used for testing stators as described previously in this section. The strength of the cycled stators and a base-line comparison is presented in Table 3.7.

TABLE 3.7   BREAKING LOAD (POUNDS) FOR 2.7 gm/cm^3 DENSITY

Baseline	9000 Thermal Shock Cycles
6.5	5.7
6.5	6.5
6.8	6.0
7.0	11.5
7.3	13.5
11.2	AVG = 8.8
11.3	
11.7	
12.7	
AVG = 9.0	

Six of the fourteen tested vanes had subsurface flaws in the vanes at the fracture location, which was typical of earlier fabricated stators. As shown in the table, the mean strength degradation of the shocked vanes was less than 3%. A nonparametric statistical analysis, (Mann-Whitney 'U' Test), of the two sets of data concluded that they are from the same population with a high degree of confidence.

Ceramic Combustor Testing

Evaluation of ceramic combustors has been conducted by subjecting prototype components to a series of tests simulating engine conditions. Previous reports [4,6,7] discussed tests which were conducted with dense, high strength, reaction bonded silicon carbide ("Refel"), which concluded that it was the best candidate material for ceramic combustors.

A "Refel" SiC combustor was previously tested in the Combustor Test Rig [7] for 171 hours of cyclic durability at each of the steady state conditions representative of the prescribed engine duty cycle. During this reporting period, this same combustor was installed in an engine and tests were conducted, consisting of ambient temperature light-offs and transient accelerations to steady-state idle condition at a temperature of 1930°F. Two such tests were conducted of five minutes duration each. Careful inspection after completion of the tests confirmed that the "Refel" combustor was in sound structural condition with no cracks or other visually observalbe defects.

2500°F Flowpath Test Rig

A 2500°F Flowpath Test Rig has been designed, fabricated, installed, and initially checked out. This a relatively simple rig, without rotors, which will be used to more conveniently test the stationary ceramic flowpath components at temperatures up to 2500°F.

Figure 3.32 shows a cross-section of the rig, which consists of an outer stainless steel shell and an inner ceramic flowpath, separated by high temperature insulation. The rig utilizes a standard engine type combustor assembly operating with preheated, compressed air which is delivered from the test facility at temperatures up to 1100°F. Airflow, temperatures, and pressures can be manually controlled over the entire engine operating range via a series of valves not shown in Figure 3.32. The hot exhaust gas is cooled with a water spray prior to dumping into the cell exhaust system.

The rig was designed so that stationary flowpath components can be tested one at a time, all together, or any combination thereof, by utilizing substitute ceramic spacers (except for a nose cone which is required for all testing). A rear observation port provides visual inspection of the components during testing.

The combustor exit temperature is monitored by using thermocouples located at the inlet of the nose cone.

The rig has been checked out over most of the range of engine operating pressures and airflows (up to turbine inlet temperature of 1930°F). The present effort is concentrating on high temperature instrumentation to insure accuracy and durability prior to initiation of ceramic component testing.

Hot Static and Dynamic Testing of Stators, Shrouds, and Nose Cones

Evaluation of turbine inlet nose cones, first and second stage stators, and first and second stage rotor tip shrouds continues in Engine Test Rigs. Each component is first qualified by subjecting it to 10 cold lights followed by immediate engine shutdown and is then evaluated over the ARPA duty cycle [6].
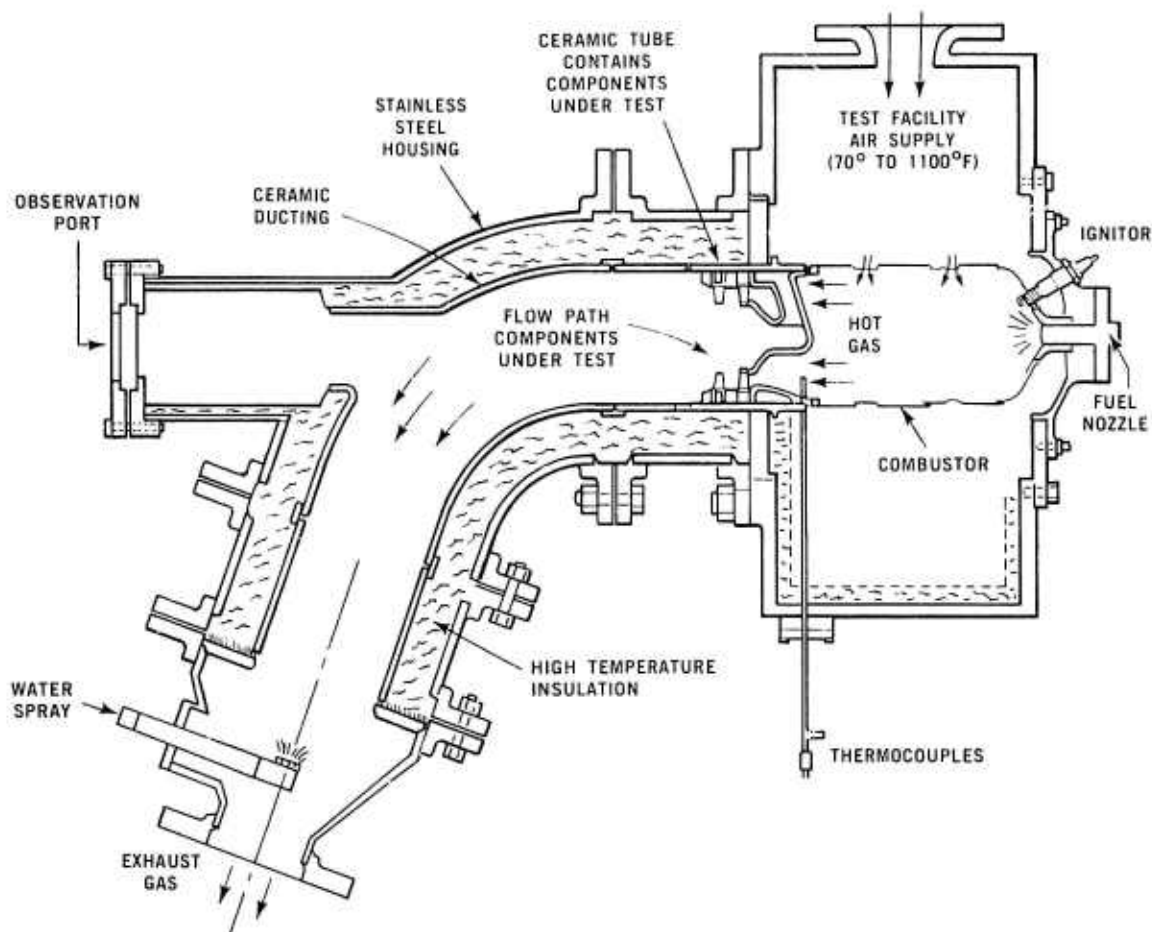
Figure 3.32   Schematic View of Static Flow Path Qualification Test Rig

Table 3.8 shows the results of engine testing on silicon nitride ceramic stationary components performed to date, with the top line indicating the target values established for each component. Testing during this reporting period has concentrated on the light-off qualification test.

Seven new nose cones have been subjected to a total of 338 lights and over 60 hours of hot running with four of the seven remaining serviceable. Two of the other three failed through molding flaws, while the other was damaged in handling.

even one piece stators have also been tested. However, only two remain serviceable, with four of the remaining five having failed through molding flaws. It should be noted that the two serviceable stators, serial numbers 841 and 848, (2.55 gm/cm^3 density Si$_3$N$_4$ stators), are representative of recent fabrication as described in Section 3.2.1.

Four second stage rotor tip shrouds have been subjected to a total of 128 lights and over 27 hours of hot running, with three of the four remaining serviceable.

In the last report, [7] the processing of one piece reaction sintered silicon carbide stators was discussed. Three of these stators, not shown in Table 3.8 were also tested during this reporting period. Two survived for 12 and 14

TABLE 3.8   ENGINE TEST RESULTS FOR Si_3N_4 COMPONENTS

Component & Serial No.	Engine Static Testing				Cyclic Testing (ARPA)					Component Status	Misc. Lights	Tests Hours	Total Part Time(Hrs)	Total Part Lights
	Lights Cold	Shutdowns Cold	Shutdowns Hot	Test Hours	Lights Cold	Lights Hot	Shutdowns Cold	Shutdowns Hot	Test Hours					
Target	10	9	1	.2	14	26	-	40	200					
Nose Cones														
73+										F	142	16.75	16.75	142
102	10	9	1	.20	44	36	21	59	221.5	S			221.70	90
103	19	17	2	.40	1	2	0	3	50.5	F,O			50.90	22
130	-	-	-	-	5	3	2	6	24.5	F,H			24.50	8
202+	10	9	1	.20	9	2	9	2	6.50	S			7.00	26
207+	6	5	1	3.50						S	2	1.5	5.00	8
304+	34	31	3	1.00						S			1.00	34
320+										F,X	10	1.15	1.15	10
321+	30	27	3	.50						F,X	29	27.50	28.00	59
807+	59	53	6	1.20						S			1.20	59
Stators														
372	10	9	1	.20	1	2	0	3	50.5	S,C			50.7	13
421+	10	9	1	.20						C,X	3	2.80	3.00	13
424+	10	9	1	.25						C,X	9	2.75	3.00	19
428	10	9	1	.20	17	14	6	25	103	F,C			103.20	41
430	10	9	1	.20	14	13	6	21	61.5	F,C			61.70	37
715+	10	9	1	.20						E,V,O	6	.1	.30	16
751+	11	10	1	.20						C,V,O,X	2		.20	13
820+	14	13	1	.30						C,X			.30	14
841+	12	11	1	.20						S			.20	12
848+	11	10	1	.20						S			.20	11
First Shrouds														
24	19	17	2	.40	1	2	0	3	50.5	S			50.90	22
111	13	12	1	.20	61	41	34	68	245	S			245.20	115
Second Shrouds														
6+										F	3	1.75	1.75	3
38	19	17	2	.40	1	2	0	3	50.5	S			50.90	22
100+					1	9	0	10	11.0	S	30	1.60	12.60	40
102+					1	9	0	10	7.8	S			7.80	10
104+										S	75	5.10	5.10	75
106	10	9	1	.20	61	41	34	68	245	S			245.20	112

+ NEW ENTRY THIS REPORTING PERIOD

Key
S = Serviceable
F = Failed
O = Failure occurred in other than ARPA duty cycle
H = Part failed during handling
C = Cracked shroud
V = Vane(s) failed
X = Internal material flaw involved in failure

67

light-offs respectively with no cracks in the vanes or shrouds. The other stator
sustained 2 vane failures, at the junction of the vane and outer shroud, on the
12th light-off. Extended light-off testing is planned for the two remaining
serviceable SiC assemblies.

3.3 GAS BEARINGS

SUMMARY

Several second generation three leaf foil bearing configurations have been designed, fabricated and tested. These incorporate ease of fabrication and assembly, and provide for development of improved damping capabilities. One arrangement was tested over the speed range up to 64,240 rpm, although further development is needed to improve the damping characteristics before this bearing system qualifies for engine operation. However, it has been decided not to include further work on gas bearings in the ARPA program, so that all available effort can be focussed on development of high temperature ceramic components.

3.3.1   GAS BEARING DESIGN AND DEVELOPMENT

Introduction

Early configurations of both single and three leaf foil gas bearings
were designed and tested. The single leaf bearing was shown to have difficult
assembly problems and the three leaf configuration had inadequate damping
capacity [6,7].

Various bearing geometry modifications of the three leaf arrangement are
being evaluated with respect to their dynamic stability.

Fabrication of Foil Gas Bearings

Three leaf foil gas bearings have been fabricated for continued testing
and development. A die, Figure 3.33, has been designed, built and is being
utilized to produce the corrugated foil support. The die includes removable
inserts so that the corrugated geometry can easily be modified.
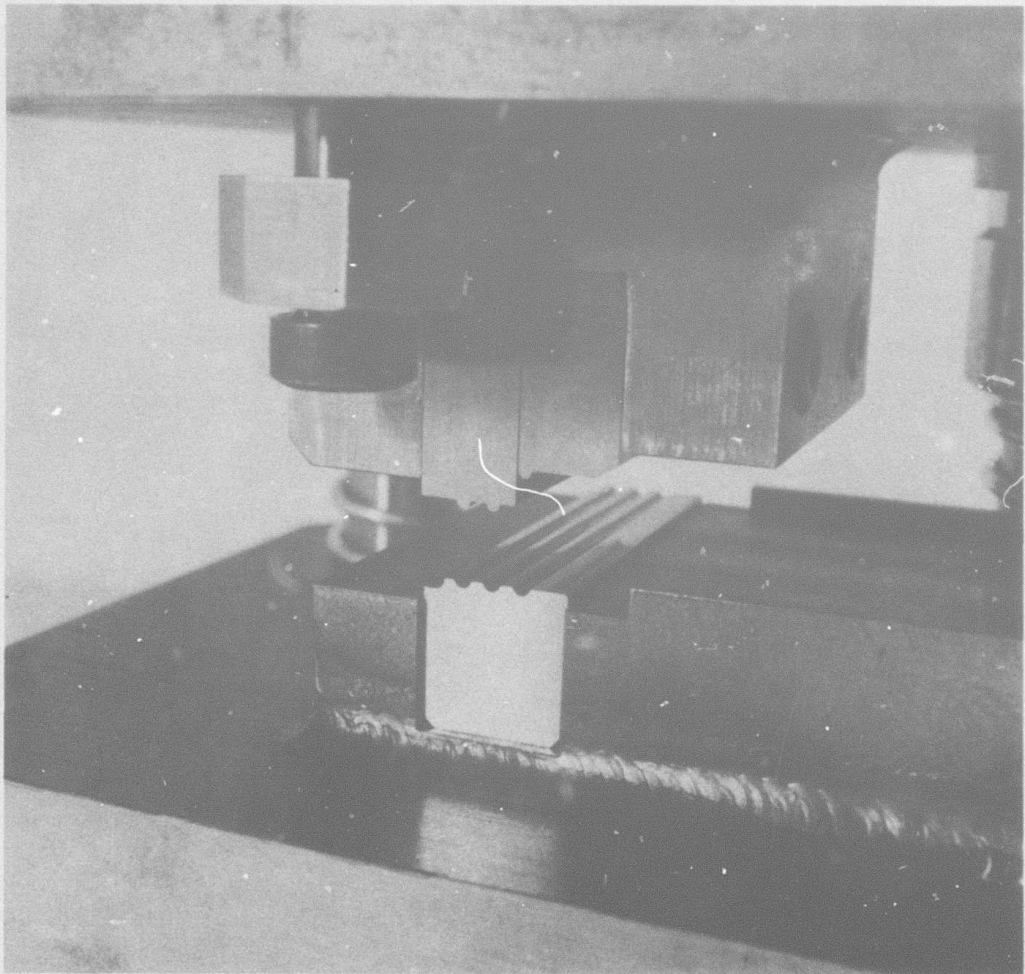
Figure 3.33   Tooling for Forming of Corrugated Foil Support

The inner foils are sprayed with molybdenum disulfide film lubricant and then heat cured. The inner foils and the corrugated foil supports are then spot welded into a machined sleeve to form the completed bearing, as shown in Figure 3.34.

Gas Bearing Testing

The dynamic simulator test rig, described in a previous report [6], was used to evaluate a three leaf foil gas bearing. A schematic view of this test rig is shown in Figure 3.35. The high speed rotor assembly was supported by one foil gas bearing (near the turbine end) and one oil lubricated journal bearing. The rotor system was tested to 64,240 rpm (100% speed) and experienced some regions of instability but was able to pass through these without exceeding established shaft orbit limits. Figure 3.36 shows shaft orbits at two axial stations with the rig operating at 64,240 rpm (100% speed).

TOP FOIL

STACKED SHIMS

BUMP FOIL

BEARING SHELL
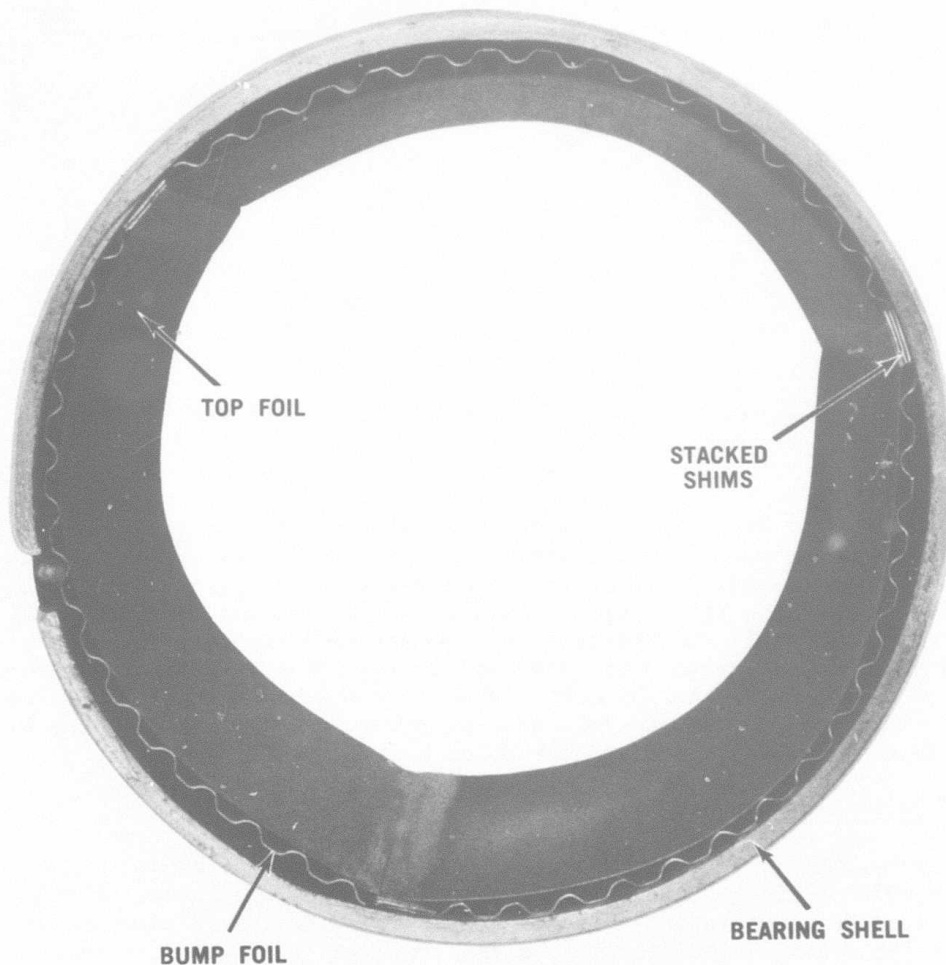
Figure 3.34   Completed Gas Bearing

**ROTOR-COMPLIANT FOIL BEARING
DYNAMIC SIMULATOR RIG**
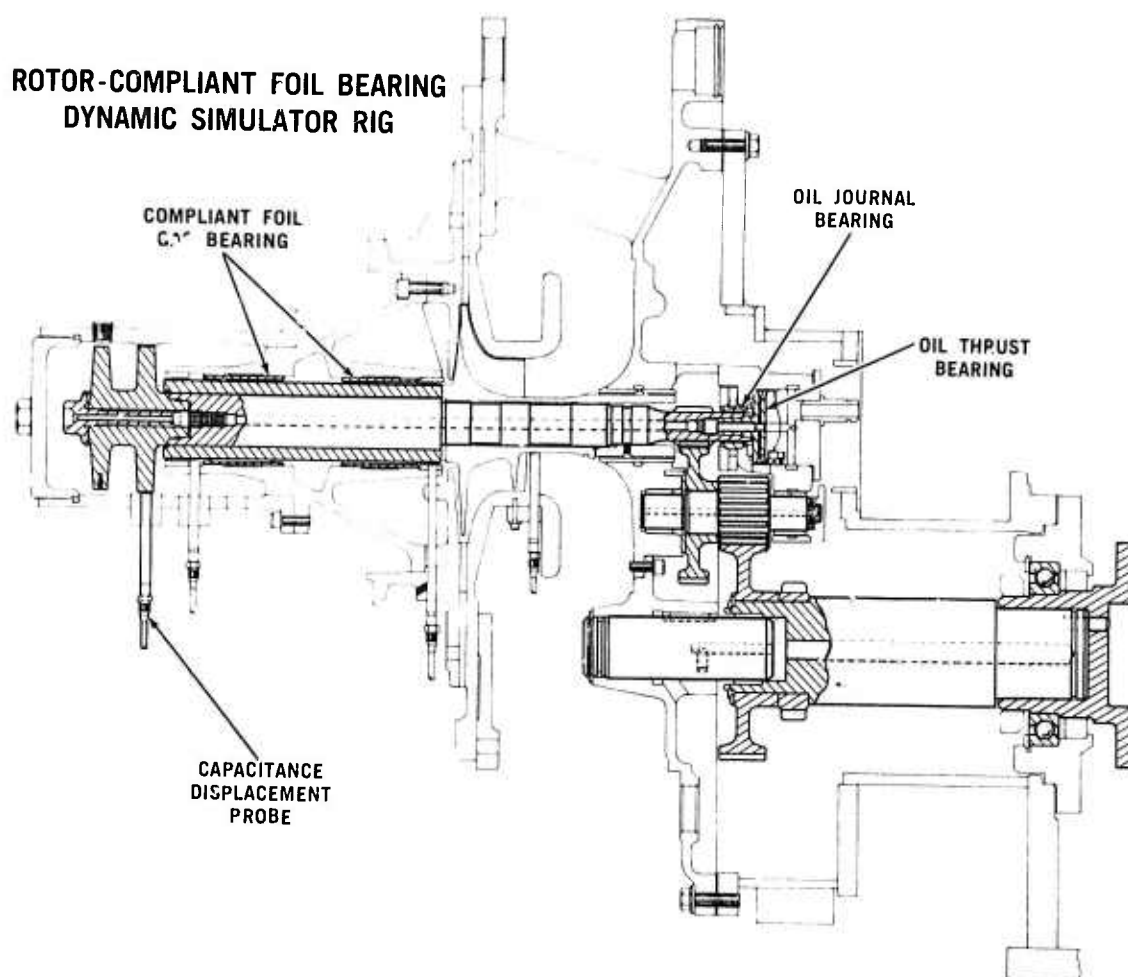
Figure 3.35   Dynamic Simulator Test Rig

The three leaf foil gas bearings tested to date were designed with three entry regions. The entry regions are formed from layers of shim stock and thus are very stiff as compared to the compliant characteristics of the other areas of the bearing. These stiff regions tend to excite the rotor system causing a triangular shaped orbit and therefore are deemed undesirable. For future development, the entry area would need to be redesigned to provide a smooth transition from one leaf to the next without any change in stiffness or compliance. In addition, various foil bearing geometry modifications need to be made to determine their effect on the rotor bearing system dynamics.

Improved Drive Line

Prior testing indicates that the foil gas bearings evaluated in the dynamic simulator rig have low damping capacity. With the intent of reducing external sources of vibration which may excite the high speed rotor bearing system of the dynamic simulator rig, a signature analysis was performed on the rig with the high speed rotor assembly removed.

72

**TURBINE END GAS BEARING
AXIAL LOCATION**
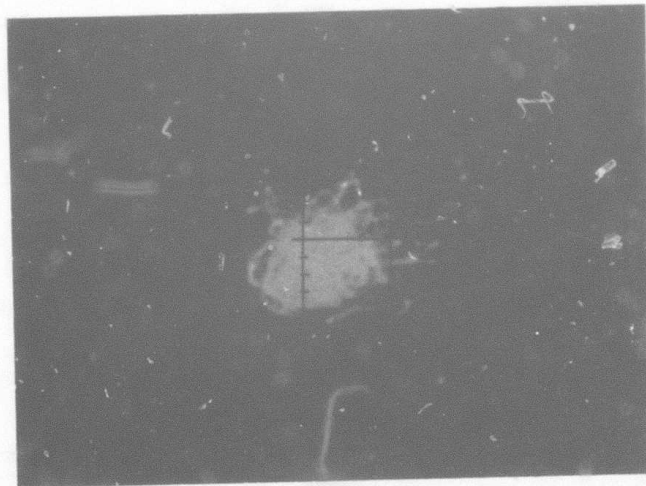
**COMPRESSOR END
AXIAL LOCATION**

SCALE 1 DIV = .001 IN

Figure 3.36   Oscilloscope Reading of Shaft Orbits

73

Velocity pickups were installed on the rig and a high speed visicorder was used to provide a record of the rig signature over its operating range. The original signature contained large amplitude low frequency beats. It was determined that these beats were generated by the electric drive motor and transmitted to the rig through the drive line and support structure.

Various drive shaft-flex coupling drive line combinations were installed and the corresponding rig signature compared with the original signature. A final drive line configuration was selected with a corresponding rig signature vastly improved over the original signature. The final configuration consists of a closely toleranced splined drive shaft supported between two precision universal joints. The drive shaft, universal joints and attachment flanges were balanced as an assembly to within 0.100 oz-in in two planes. In order to further reduce vibrations, the rig mounting system was changed from a three to a four stanchion mounting, which provided additional improvements to the rig signature.

While progress has been made on gas bearing development, it has been decided not to include further work in the ARPA program so that all available effort can be focussed on development of high temperature ceramic components.

74

4. PROGRESS ON MATERIALS TECHNOLOGY - VEHICULAR TURBINE PROJECT

SUMMARY

Materials technology is a very important portion of the systems approach employed in this project for the development of high temperature gas turbine engines. The generation of ceramic material property data, in progress since the beginning of the project, has been instrumental in component design modifications and failure analysis. As testing and fabrication experience was gained, improvements in materials have also been made. The properties of these improved materials are determined and fed back into design modifications and failure analysis, thus closing the loop. The work on determining material properties and material improvements for the vehicular ceramic turbine project, is reported in this section.

Reaction sintered Si_3N_4 components, made by the injection molding process, are inlet nose cones, stators, and rotor blade rings for use in the duo-density process. Work on developing of a 2.7 gm/cm^3 density moldable Si_3N_4 has continued. The viscosity and moldability of compositions of this density were measured and found to be equal to the lower density (2.55 gm/cm^3) presently being used for nose cones and stators. A composition was selected for fabrication of one piece stators. A problem of lower-than-predicted strength of 2.7 gm/cm^3 density molded Si_3N_4 was overcome by development of improved nitriding. The use of a relatively slow cycle, reaching a maximum temperature of 2550°F and using an atmosphere composed of 4% H_2/96% N_2, produced 4 point bend strengths averaging 43.2 ksi, which compare well with the predicted strength for this density.

A study of the nitriding of silicon was initiated, with the objective of identifying the rate limiting mechanisms. Particular emphasis was given to the high pressure nitriding concept, since experimental results (?) had been inconclusive. Calculations were made to determine what pressure would be needed to store enough nitrogen in the remaining pores at the point in the process where prior nitridation resulted in close-off of open porosity. These calculations show that a pressure of 10^5 psi or greater would be required for enough nitrogen to be contained within the closed pores. Since equipment limitations preclude nitriding at these high pressures, it is apparent that high pressure nitriding will not be feasible and further experimental work along this path was stopped.

The development of Sialon materials was continued, with emphasis on obtaining good high temperature properties using the sintering process. Some compositions containing yttrium additives were prepared and resulted in 4 point bend strengths as high as 80-86 ksi at room temperature, with some loss of strength at higher temperatures. However, upon reheating these materials in an oxidizing atmosphere, considerable glass was formed. Further work indicated this problem might be resolved by either using very low yttria contents or by using a heat treating process to crystallize the glassy material.

Work on non-destructive evaluation of ceramic components continues to rely primarily on x-ray radiography to locate internal flaws and voids in as-molded nose cones and stators. Ultrasonics may be useful to supplement radiography for detecting flaws in stator outer shrouds which are too small to be resolved by radiography. Dye penetrants have also proven useful on the higher density molded Si_3N_4 components. Sonic velocity measurements are being made routinely as a quality control test.

4.1 DEVELOPMENT OF HIGHER DENSITY MOLDED SILICON NITRIDE

Introduction

In the previous report [7], work was presented on the theory of developing a highly loaded silicon-polymer injection molding composition. The major innovation involved the use of a silicon metal powder with a very broad particle size distribution. Data was presented for both a 69.5 and a 73.5 volume percent loaded system (2.55 and 2.72 gm/cm^3 Si_3N_4 density respectively). During this reporting period, further work was done to qualitatively·compare molding compositions. Also, the effect of silicon particle size and nitriding cycles on the modulus of rupture was investigated.

Molding Properties

Table 4.1 compares the properties of the 74R, 2.55 gm/cm^3 molding composition currently being used to mold stators and nose cones with two experimental 2.72 gm/cm^3 compositions, 75P1 and 75Q. The 74R material shown in Figure 4.1 as distribution R, is a variation of the 74F material described in the last report [7], using a somewhat coarser silicon metal powder particle size distribution than 74F. The 75P1 composition is the same as described in the last report [7] with the exception of minor changes in organics. The 75Q composition utilized a coarse silicon particle size distribution as shown in Figure 4.1. As expected, the green strength of the 2.72 gm/cm^3 systems is less than the 2.55 gm/cm^3 system (due to higher silicon loading and therefore lower organics). For the same reason, the molding shrinkage is also less. The viscosity and moldability, as expressed by a capillary rheometer and spiral flow mold test respectively, are identical for the 74R and 75P1 composition. The viscosity of the 75Q material was not measurable and the spiral flow was lower because of the thixotropic nature of this material. This points out the importance of particle size distribution.

These results indicate that the moldability of the R distribution 2.55 gm/cm^3 density system is equivalent to the P distribution [7] 2.72 gm/cm^3 system. This was the conclusion qualitatively made in the previous report [7]. The 74R and 75P1 compositions also were found to behave in a similar fashion when molded in the one piece stator tooling. Both compositions are capable of producing components which are free of molding flaws when examined using x-ray radiography. Initially, problems with tooling alignment during the 75P1 molding trial caused severe blade cracking. This problem has since been corrected (see Section 3.2.1 of this report for details) and the 75P1 composition will be used as the initial composition for fabrication of 2.7 gm/cm^3 density Si_3N_4 one piece stators during the next reporting period.

Nitriding Parameters and Physical Properties

In the previous report [7], the strength of the 2.7 gm/cm^3 density Si_3N_4 was reported to be lower than the predicted value (35 ksi as opposed to 40 - 48 ksi). Various nitriding cycles were evaluated in an attempt to improve the strength values of the 2.7 gm/cm^3 Si_3N_4. Test bars of 75P1 composition were fabricated and nitrided according to the schedules in Table 4.2. The cycles can be grouped into two general classifications; those with only step-wise temperature increases, and those with constant rate temperature increases, both having holds at various temperatures.

TABLE 4.1   COMPARISON OF PROPERTIES OF MOLDING COMPOUNDS

Property	Test Method	74R	75P1	75Q
Si_3N_4 Density	ASTM C373-56	2.55 gm/cm^3	2.72 gm/cm^3	2.72 gm/cm^3
Green Strength	3 Point MOR L = 1-1/8"	2500 psi to 3400 psi	Estimate 1800 psi to 2800 psi	2230 psi to 2600 psi
Mold Shrinkage	Direct Measurement	0.6 to 0.75%	0.2 to 0.4%	0.4 to 0.5%
Viscosity	ASTM D1238-73	10 poises @ shear rate > 1.8 x 10^{-5}/ second	40 poises @ shear rate > 1.8 x 10^{-5}/ second	Thixotropic
Spiral Flow	ASTM D3123-72 Test conditions Material temperature = 200°F Die temperature = 90°F Injection Pressure 1750 psi	18 inches	19 inches	4 inches
One Piece Stator Molding Results	See Section 3.3.1 for details	Produces parts that are flaw free by x-ray	Problems encountered with die on first molding attempt. Will try this composition again in next reporting period.	Material too thixotropic to attempt molding.
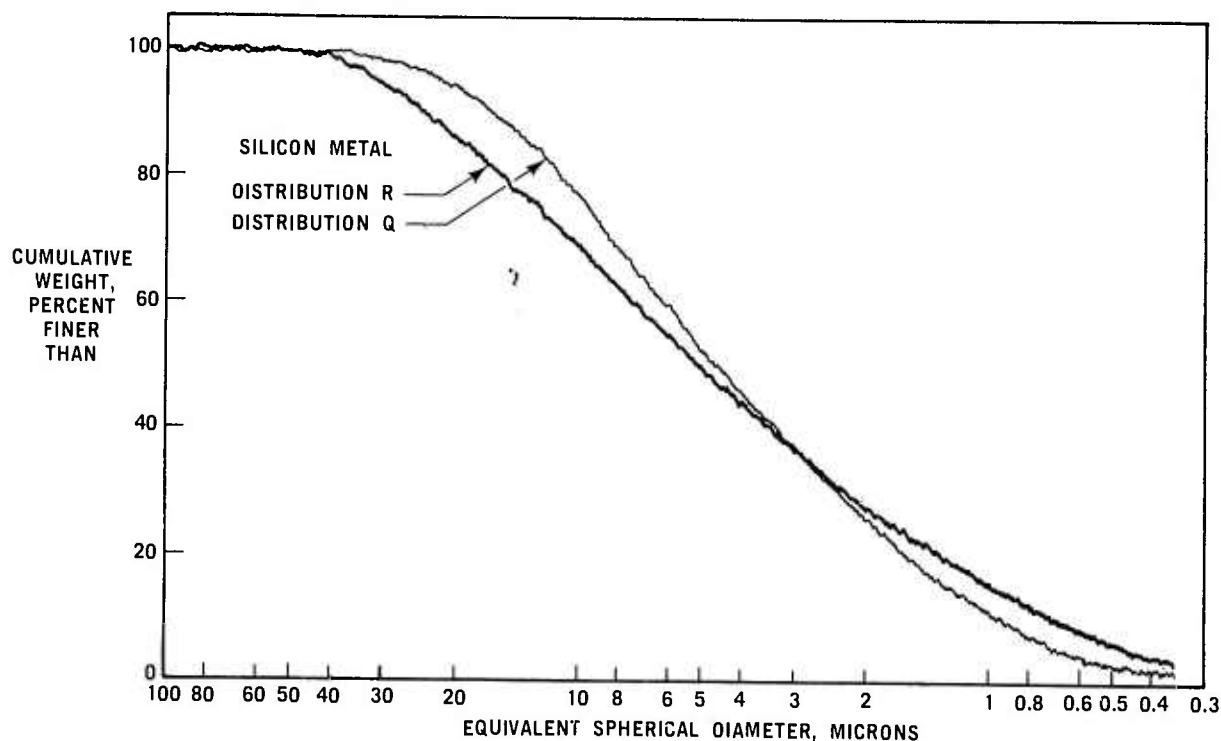
Figure 4.1   Particle Size Distribution of Silicon Metal Powders

TABLE 4.2   NITRIDING SCHEDULES

Designation	Descriptive (Time at Temperature)
AMMRC*	20 hrs at 1300$^{\rm o}$F, 3 hrs at 2282$^{\rm o}$F 20 hrs at 2416$^{\rm o}$F, 7 hrs at 2510$^{\rm o}$F 20 hrs at 2552$^{\rm o}$F
JM-1	20 hrs at 2300$^{\rm o}$F 7 hrs at 2415$^{\rm o}$F 20 hrs at 2510$^{\rm o}$F 7 hrs at 2552$^{\rm o}$F
JM-3A	RT-2100$^{\rm o}$F - furnace rate (500$^{\rm o}$F/hr) 2100-2550 $^{\rm o}$F at 7$^{\rm o}$F/hr
JM-3B	RT-2100$^{\rm o}$F - furnace rate (500$^{\rm o}$F/hr) 2100-2550$^{\rm o}$F at 14$^{\rm o}$F/hrs
JM-4	RT-2150$^{\rm o}$F - furnace rate (500$^{\rm o}$F/hr) hold 2150$^{\rm o}$F for approximately 72 hrs 2150-2550$^{\rm o}$F at 7$^{\rm o}$F/hr
HJ-2	24 hrs at 2000$^{\rm o}$F 24 hrs at 2300$^{\rm o}$F 24 hrs at 2660$^{\rm o}$F

*per Messier and Wong from AMMRC

Table 4.3 shows the effect of these various nitriding cycles on the modulus
of rupture of the 75Pl Si_3N_4. The strength of Si_3N_4 with nitriding cycles employing
step-wise increases in temperature are low, ranging from 26.7 to 33.4 ksi.
Improvements resulted when cycles using constant rate temperature increases were
evaluated. The best cycle on a maximum strength basis was JM-4, with a 3 day hold
at 2150$^{\rm o}$F followed by a gradual temperature increase from 2150 to 2550$^{\rm o}$F at 7$^{\rm o}$F/hr,
using a 4% H_2/96% N_2 atmosphere. This cycle yielded strengths averaging 43.2 ksi,
with individual high data points at 52.0 ksi and 58.0 ksi. These average strength
figures fall within the predicted band of 40-48 ksi for 2.72 gm/cm^3 Si_3N_4.

Earlier work showed that the strength of 2.55 gm/cm^3 Si_3N_4 depended upon
the silicon metal powder particle size. Experiments were conducted using 17 hr,
29 hr, 48 hr, and 140 hour grind silicon metal in a 2.72 gm/cm^3 Si_3N_4 composition.
The results, shown in Figure 4.2, indicate the effect of milling time on the strength
of the 2.55 gm/cm^3 Si_3N_4 for one nitriding cycle, and on the 2.72 gm/cm^3 Si_3N_4
number of nitriding cycles. An increase in milling time resulted in decreased
strength for the 2.55 gm/cm^3 material. However, with the exception of the results
obtained when using the AMMRC nitriding cycle, there is no apparent effect of
milling time on the strength of the 2.72 gm/cm^3 Si_3N_4. This is fortunate in that
the optimum particle size distribution for injection molding, Distribution P,
can be used without any apparent loss in room temperature strength.

TABLE 4.3   EFFECT OF NITRIDING CYCLE ON THE STRENGTH OF
75PI 2.72 gm/cm^3 DENSITY INJECTION MOLDED Si_3N_4

Nitriding Cycle	Nitriding Atmosphere	Average* MOR	MOR Range, ksi	Average Wt. Gain
AMMRC	N_2	26.7 ksi	21-33	59.5%
AMMRC	1% H_2/99% N_2	29.3 ksi	20-39	58.5%
HJ-2	N_2	33.4 ksi	30-36	60.0%
JM-1	N_2	32.6 ksi	31-35	59.5%
JM-3A	N_2	40.2 ksi	37-43	59.5%
JM-3A	4% H_2/96% N_2	38.8 ksi	36-42	58.5%
JM-3B	N_2	35.2 ksi	32-38	57.0%**
JM-4	N_2	35.1 ksi	32-39.5	58.5%
JM-4	4% H_2/96% N_2	43.2 ksi	33-58	59.0%

*   1/8 x 1/4 x 1-1/2" specimen, 3/8 x 1-1/8" fixture, .02 in/min load rate

**   Exuded silicon metal, center core of unreacted silicon
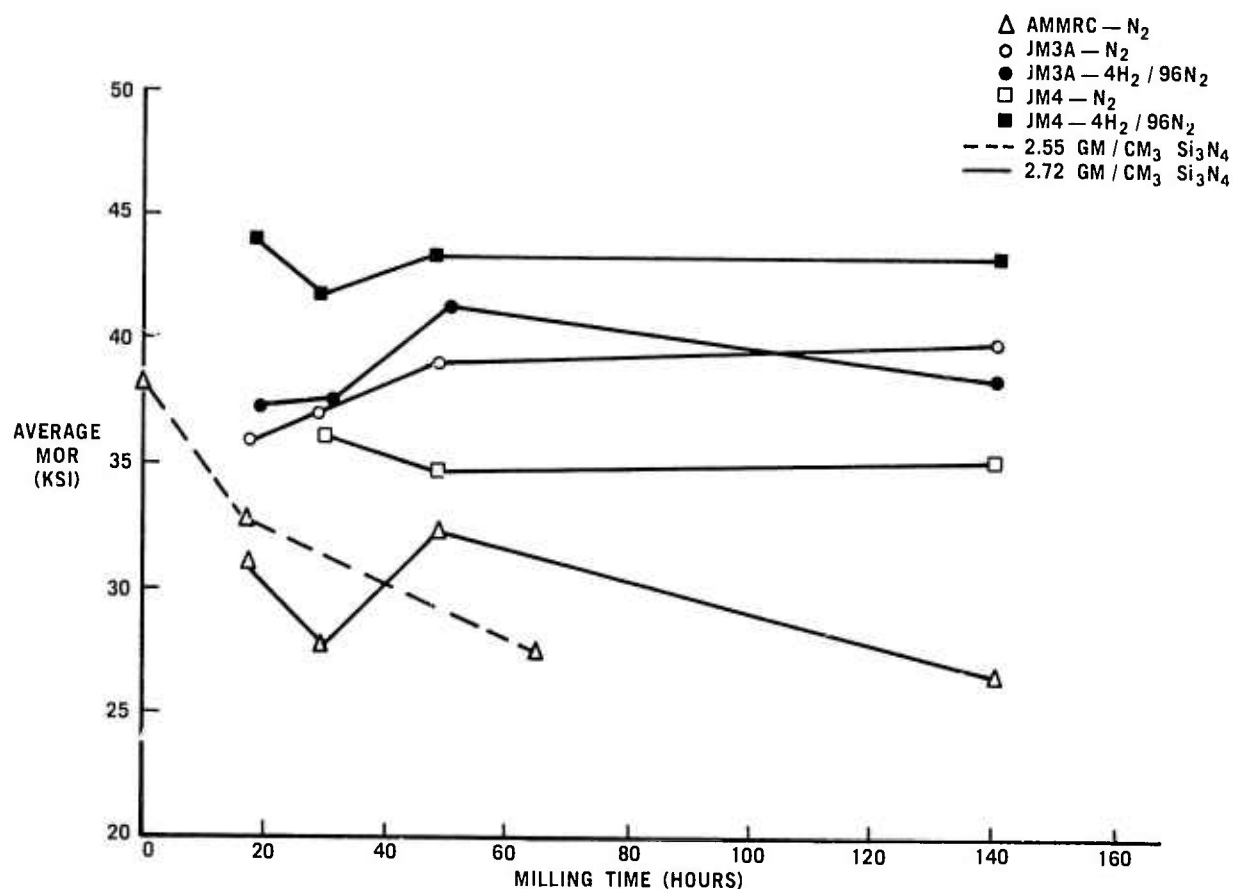
Figure 4.2   Strength vs Silicon Milling Time for Various Nitriding
Cycles

In summary, it has been shown that a 2.72 gm/cm^3 injection molding composition has been developed that has green strength, shrinkage and flow properties similar to the 2.55 gm/cm^3 material currently being used to fabricate one piece stators. This material is capable of being nitrided into Si_3N_4 with an average room temperature strength of 43 ksi compared to the 32 ksi currently being achieved in the 2.55 gm/cm^3 system.

4.2 STUDY OF THE NITRIDING OF SILICON

Introduction

A program to study the nitriding of silicon has been initiated, with the objective of identifying the rate limiting mechanisms in the nitriding process. The initial effort was a study of the reaction sintering of high density Si_3N_4 shapes by high pressure nitriding.

Parallel theoretical calculations and experiments have been carried out to determine how nitridation is affected by high nitrogen pressures. Mechanisms offering possible improvement considered to date are:

1.   Improved nitrogen diffusion into small silicon particles.

2.   Pore storage of nitrogen in the pore structure of the silicon compact.

3.   Improved flow of nitrogen through the pore structure of a partially nitrided body.

Diffusion of Nitrogen and Silicon in Small Particles

During the initial stages of nitridation, fine particles of silicon within the porous silicon compact form a surface skin of Si_3N_4. Further nitridation must continue either by outward diffusion of silicon or inward diffusion of nitrogen through the skin. Assuming both spherical geometry and that the diffusion coefficients of nitrogen and silicon in Si_3N_4 are equal, it was found that:

(a)   For nitrogen pressures experimentally possible, the outward rate of silicon diffusion is 10^2 to 10^4 times the inward rate of nitrogen diffusion.

(b)   If the nitridation rate is controlled by diffusion, the calculated time for complete nitridation of a 10μ diameter particle is a few minutes. This prediction compares favorably with observed nitridation times for small isolated silicon particles.

The diffusion rate into small nitriding particles thus is controlled mostly by silicon diffusion; nitrogen pressures in the 10 psi range will not speed up this process.

Pore Storage of Nitrogen in Porous Silicon Compacts

With high pressure nitridation, increased amounts of nitrogen will be stored in the pore structure of the green material after pores leading to the part exterior are closed off. Calculations of the nitrogen pressure required to complete nitridation with gas contained in the pore structure were made.

Considering a porous silicon compact of volume V and volume fraction f of silicon, it can be assumed that the pores are closed off after a volume fraction F of the silicon has been nitrided (note F<f). If T is absolute temperature, V_p the pore volume remaining at pore close off, and N the number

of moles of nitrogen required to nitride the remaining elemental silicon, the nitrogen pressure required to complete nitridation is, assuming ideal gas behavior,

$$P = \frac{NRT}{V_p} \qquad (1)$$

The initial volume of silicon is fV. At pore close off FV is nitrided and $(f-F)$ V is un-nitrided. The volume of the un-nitrided portion is unchanged, while the volume of the nitrided portion grows according to V (nitrided) = f_o^{-1} V (un-nitrided) where $f_o \simeq 0.8197$ is the value of f leading to fully dense nitrided material. Thus the volume of the nitrided material is f_o^{-1} FV, and the pore volume at pore close off is

$$V_p = \left\{ 1 - f - (f_o^{-1} - 1) \; F \right\} V \qquad (2)$$

N moles of nitrogen must nitride the remaining un-nitrided Si. If v is the atomic volume of silicon, the number of un-nitrided silicon atoms is $(f-F) \frac{V}{v}$, and the required number of moles of nitrogen to nitride these silicon atoms is

$$N = \frac{2}{3} \; (f - F) \; \frac{V}{N_o v} \qquad (3)$$

(N_o is Avogadro's number). Substituting (2) and (3) into (1) results in:

$$P = P_o \; \frac{f - F}{1 - f - (f_o^{-1} - 1) \; F} \qquad (4)$$

where $P_o = \frac{2}{3} \frac{kT}{v}$ and $k = R/N_o$ is Boltzmann's constant. Using numerical values $T = 1400^o C = 1673^o K$ and $v = 2.00 \times 10^{-23}$ cm^3, $P_o = 1.12 \times 10^5$ psi was calculated.

Figure 4.3 shows the pressure given by equation (4) as a function of F/f (the fraction of silicon nitrided at pore close off). Unless most of the silicon is nitrided by the time pores are closed off, extremely high pressures (10^5 psi or greater) will be required to complete nitridation using a pore storage mechanism.

If $f = fo$ (so that fully dense nitrided material results) equation (4) reduces to

$$P = P_o \; \frac{fo}{1-fo} \simeq 5.10 \times 10^5 \text{ psi} \qquad (5)$$

For samples approaching theoretical density the pressure required to complete nitridation is independent of the point when the pore structure is closed off.

Pore Flow

Incompletely nitrided, high density Si_3N_4 samples often show a fully nitrided skin with an un-nitrided interior. It is commonly supposed incomplete nitridation of the interior results from an insufficient nitrogen supply in the bulk of the sample. It was assumed that nitrogen cannot penetrate the fine pore structure of the fully nitrided skin.

82
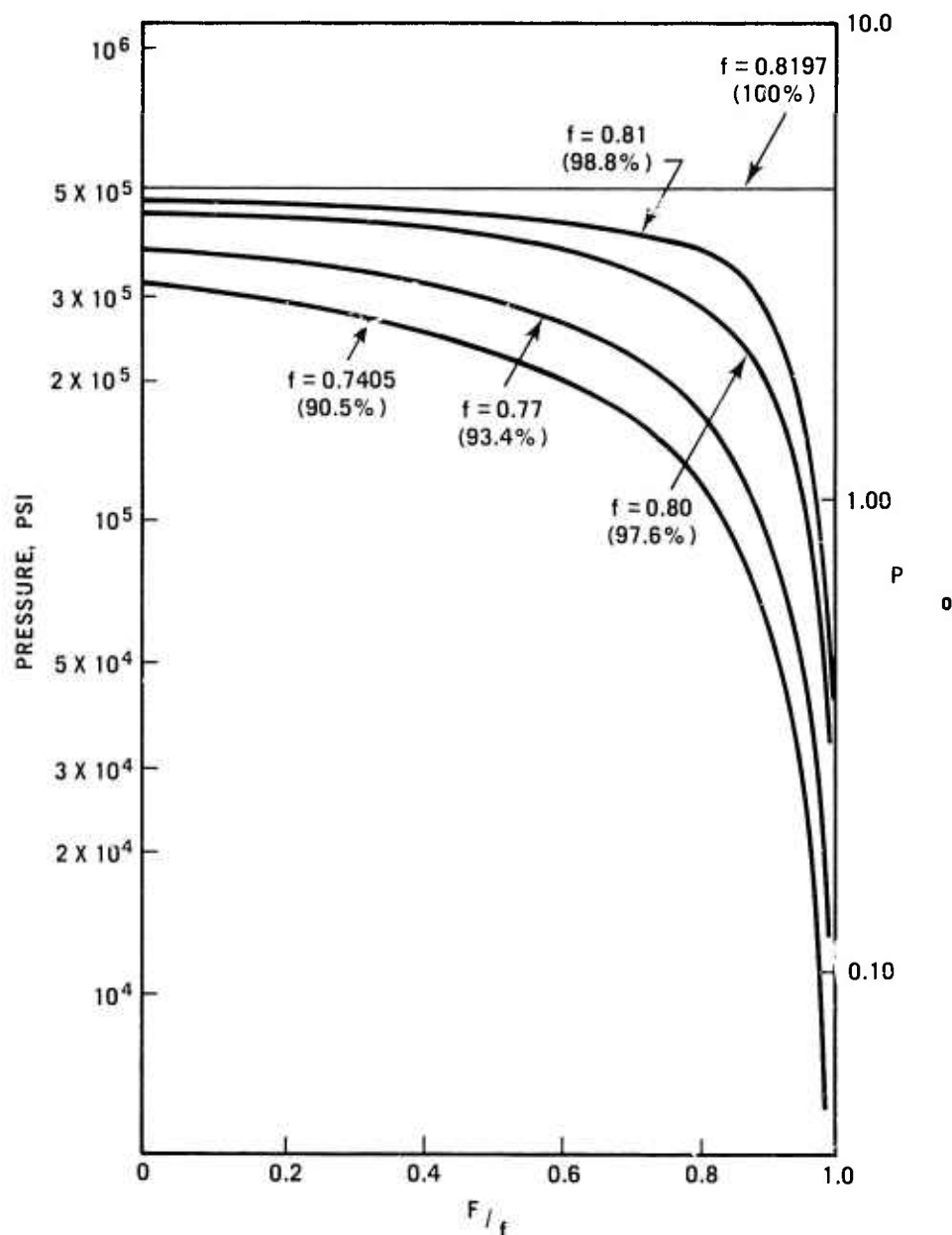
Figure 4.3   Nitrogen Pressure Required for Pore Storage to Complete
              Nitridation vs Fraction of Silicon Reacted at Pore
              Close-off

Experiments are in progress to measure flow rates through fully and
partially nitrided compacts. Results on fully nitrided slabs 1/8 inch thick
(density 2.7 gm/cm^3) give flow rates (corrected to 1400°C) sufficient to nitride
the 1/8 inch thick material in 3 to 4 hours. These times are somewhat shorter
than typical nitriding times of 25 hours or more for bulk samples.

Preliminary work on higher density, incompletely nitrided, samples with
high density skin (density 2.85 to 3.0 gm/cm^3) reveals much reduced flow through
pores. From flow data we estimate nitrogen pressures of 10^4 psi should signifi-
cantly speed nitridation for samples in the (full nitrided) density range 2.9
to 3.1 gm/cm^3. Higher Si_3N_4 densities would demand greatly increased nitrogen
pressure for much effect.

83

4.3 DEVELOPMENT OF SIALON MATERIALS

Introduction

Studies of sialon-type materials have continued, with the aim of producing a ceramic material suitable for turbine rotor tip shrouds. This material also has potential for application to other components, but this would require more time than is available under this contract. The goal is a strong, corrosion resistant, low-expansion ceramic material with good high temperature properties which can be fashioned by pressureless sintering.

Development of Yttria - Containing Sialons

The effects of yttria content and processing variables on some of the properties of pressureless sintered Si_3N_4 - Al_2O_3 - Y_2O_3 mixtures have been studied. Initial experiments, using a base mixture of 60 wt. % standard AME Si_3N_4 and 40% Linde Al_2O_3 with 1% and 3% added Y_2O_3, cold pressed and sintered under argon for 15 minutes at 1750°C, yielded quite ordinary materals. For this work, the Si_3N_4 and Al_2O_3 were arbitrarily taken on 100%, with additives accounted for as over and above 100%. However, when mixtures with 3 or 6% Y_2O_3 added were slip cast and sintered under argon for from 3 to 8 hours at temperatures ranging from 1550°C to 1700°C, rather substantial increases in room temperature strength were noted. Average MOR values, (measured in 4-point bending) as high as 63,000 psi were obtained, with individual specimens as high as 78,000 psi.

Materials sintered 4 hours at 1550°C contained alumina and α Si_3N_4, indicating incomplete reaction. Those sintered for 4 hours at 1650°C contained the extraneous phase, not identifiable by x-ray diffraction patterns. However, those sintered at 1600°C for 4 to 8 hours contained alumina, but no α Si_3N_4 or extraneous phase, suggesting that the alumina present was in excess of the solubility limit under these conditions. A systematic study of materials prepared with 3% Y_2O_3 and sintered at 1600°C for 8 hours showed that the final product contained alumina when the initial alumina content was greater than 16% by weight. No extraneous phase or unreacted silicon nitride was detected in these materials.

Materials were then prepared from mixtures containing from 16% to 40% alumina, with either standard AME or Plessey high purity Si_3N_4 and yttria additions ranging from 1% to 25%. Sintering temperatures ranged from 1600° to 1700°C, and times from 4 hours to 12 hours. Many of these had very promising room temperature strengths and showed only a single crystalline phase in their x-ray diffraction patterns. In general, the best materials were prepared from Plessey Si_3N_4 and contained 3% or 6% Y_2O_3 additive. A material prepared from 84% Plessey silicon nitride and 16% alumina with 3% Y_2O_3 additive by sintering for 12 hours at 1600°C contained a single crystalline phase, and had an average room temperature MOR of 82,000 psi in 4-point bending, the range being 80-86,000 psi. Another material, similarly prepared but containing 6% Y_2O_3 additive, had an average MOR of 74,000 psi. Samples of the same composition, sintered for 8 hours at 1600°C, contained a single crystalline phase and had an average MOR of 70,000 psi, with a range of 51-94,000 psi for seven specimens. A material prepared from standard AME Si_3N_4 with 16% Al_2O_3 and 3% Y_2O_3 additive contained a single crystalline phase and had an average MOR of 55,000 psi, with a range of 45-69,000 psi for 6 specimens. Generally, the densities of these strong materials were close to theoretical.

Materials containing a large proportion of Y_2O_3 were generally not as strong as those containing 3% or 6%. However, a material prepared from 64.4% AME Si_3N_4 and 35.6% Al_2O_3 with 16.1% Y_2O_3 added and sintered for 4 hours at 1600°C contained a single crystalline phase and had an average MOR of 45,000 psi, with a range of 32-61,000 psi on 7 specimens. Materials prepared from 66.7% AME Si_3N_4 and 33.3% Al_2O_3 with 25% Y_2O_3 added and sintered for from 3 to 12 hours at 1600°C and for 4 hours at 1650 and 1700°C had strengths ranging from 24,00 to 46,000 psi and often showed evidence of a glassy phase in their x-ray diffraction patterns.

Materials containing but 1% Y_2O_3 additive were also generally weaker than those containing 3 to 6%, but there was evidence that prolonging the sintering time or raising the sintering temperature improved matters. Thus, a material containing 84% AME Si_3N_4 with 1% Y_2O_3, sintered for 12 hours at 1600°C, contained no crystalline extraneous phase and had an average strength of 46,000 psi. Another, sintered for 4 hours at 1700°C, had an average strength of 50,000 psi and was similarly free of extraneous phase and alumina.

Because the room temperature strengths and phase compositions appeared promising, the strengths of a few materials were measured at elevated temperature. Some of the results are summarized in Figure 4.4. It can be seen that there is a substantial decrease in strength at temperatures above 1000°C. This, taken with the observation of a glassy phase in the x-ray patterns of the very high yttria materials, suggests, in general, the presence of a glassy phase in yttria containing sialons.

No.	Si_3N_4	Al_2O_3	Y_2O_3	
1.	60	40	+ 6	
2.	60	40	+ 3	
3.	84	16	+ 3	
4.	84	16	+ 6	
5.	64.4	35.6	+16.1	
6.	84	16	+ 6	Plessey
7.	84	16	+ 6	High Purity AME
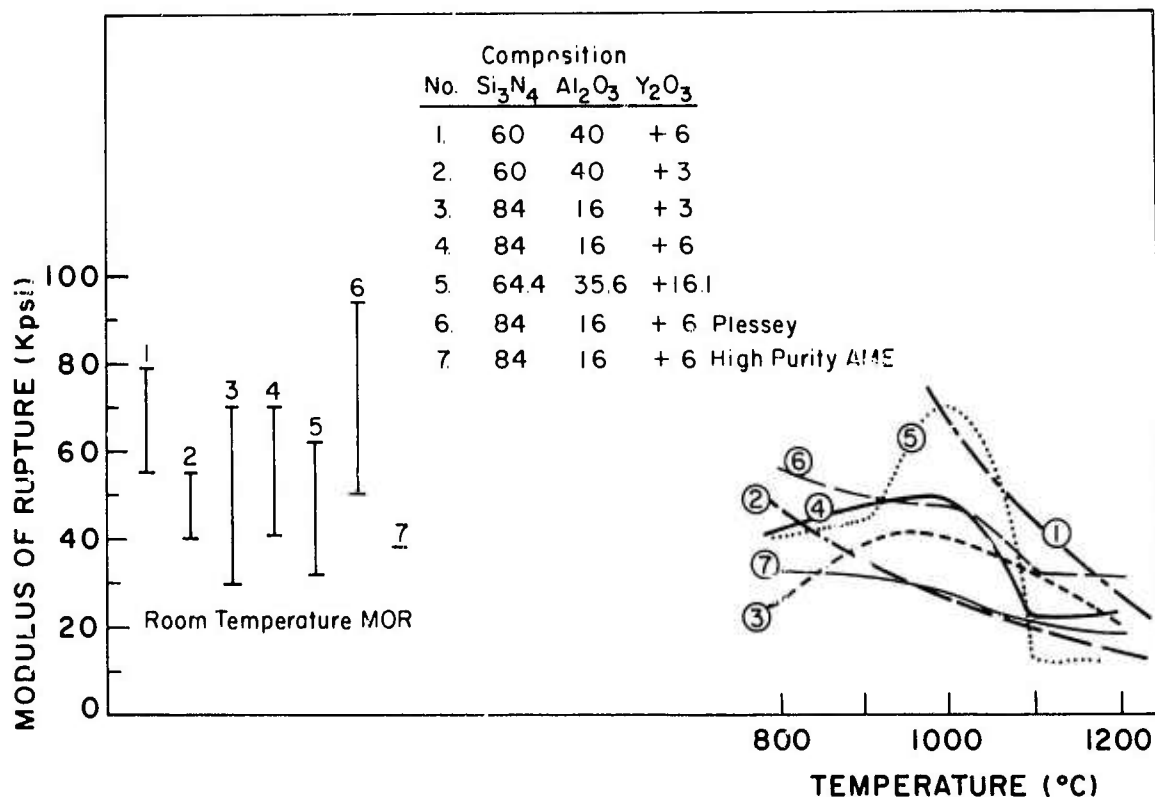
Figure 4.4   Effect of Temperature on Modulus of Rupture for Several Sialon Materials

Many of the materials prepared have been examined by optical and scanning electron microscopy on polished, etched, and fracture surfaces. The materials are extremely fine grained and give the appearance of having more than one phase present, even when x-ray patterns indicate a single phase material. This may be further evidence for the presence of a glassy phase.

When materials containing 3% or more Y_2O_3 were heated to $1260^{\circ}C$ in a gas-oxygen flame through 10 one-minute-on, one-minute-off cycles, substantial quantities of glass were formed; it appeared that the materials had melted. Those with little or no yttria formed no glass. However, many, though not all samples which did not melt in the flame did form a glassy surface on prolonged (70 hours) heating in a furnace at $1260^{\circ}C$ under either air or argon. Similar treatment under argon at $1600^{\circ}C$ for 4 hours produced no glassy surface at all. The significance of these observations is not yet completely clear, but a study aimed at improving the strengths of low Y_2O_3 and additive-free materials has been initiated. Sintering times have been extended to 24 hours at $1600^{\circ}C$ with promising results. Figure 4.5 shows the effect of sintering time on the room temperature MOR of a material with 84% AME Si_3N_4, 16% Al_2O_3 and 1% Y_2O_3 additive sintered at $1600^{\circ}C$.
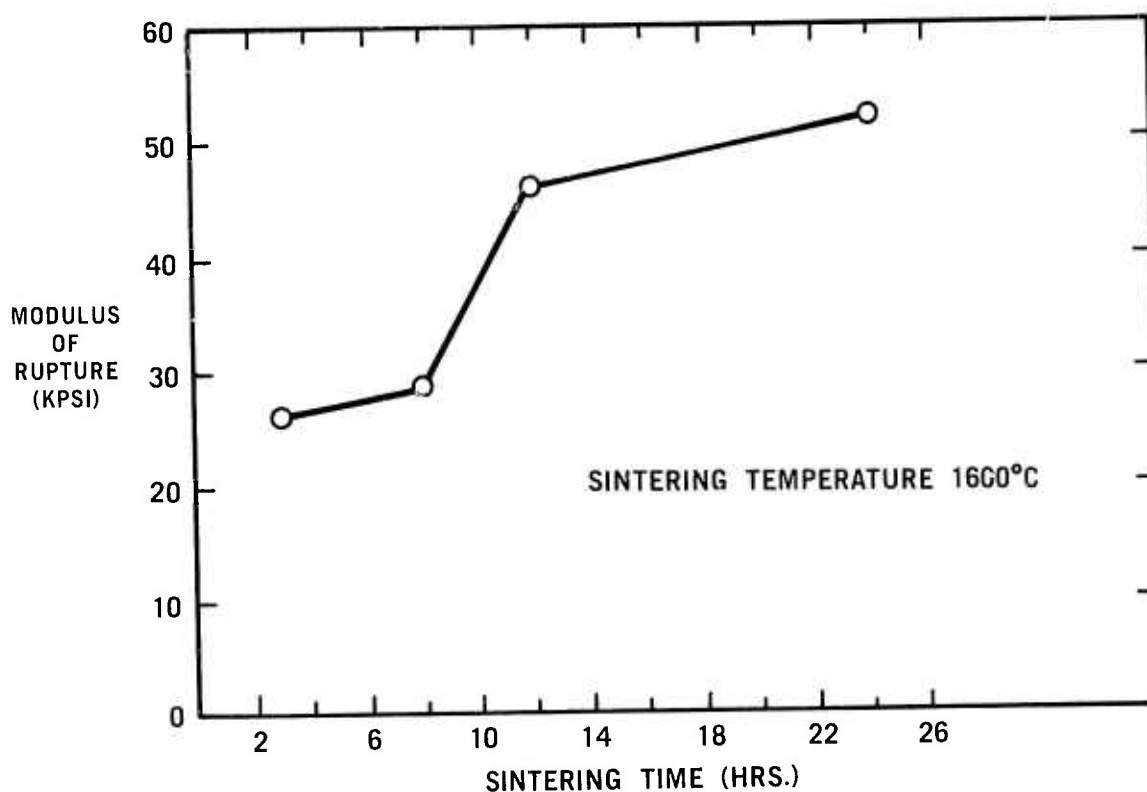
Figure 4.5   Effect of Sintering Time vs Modulus of Rupture of a Sialon Consisting of 84% Si_3N_4, 16% Al_2O_3, and 1% Y_2O_3

86

An investigation of the possibility of crystallizing the glass probably present in the Y_2O_3-doped materials showed that such crystallization could be achieved. Diffraction lines of new crystalline phases were observed in the x-ray patterns of materials receiving prolonged treatment at $1200°C$ in an inert atmosphere. Most of these lines were ascribable to yttrium silicates. Glass halos, which were present in the patterns of very high Y_2O_3 materials before treatment, disappeared after treatment. The change in x-ray pattern with heat treatment is shown in Figure 4.6. The room temperature MOR's were found to have decreased after crystallization, but were then much more nearly independent of temperature. Optimization of crystallization conditions with regard to strength is still to be achieved.
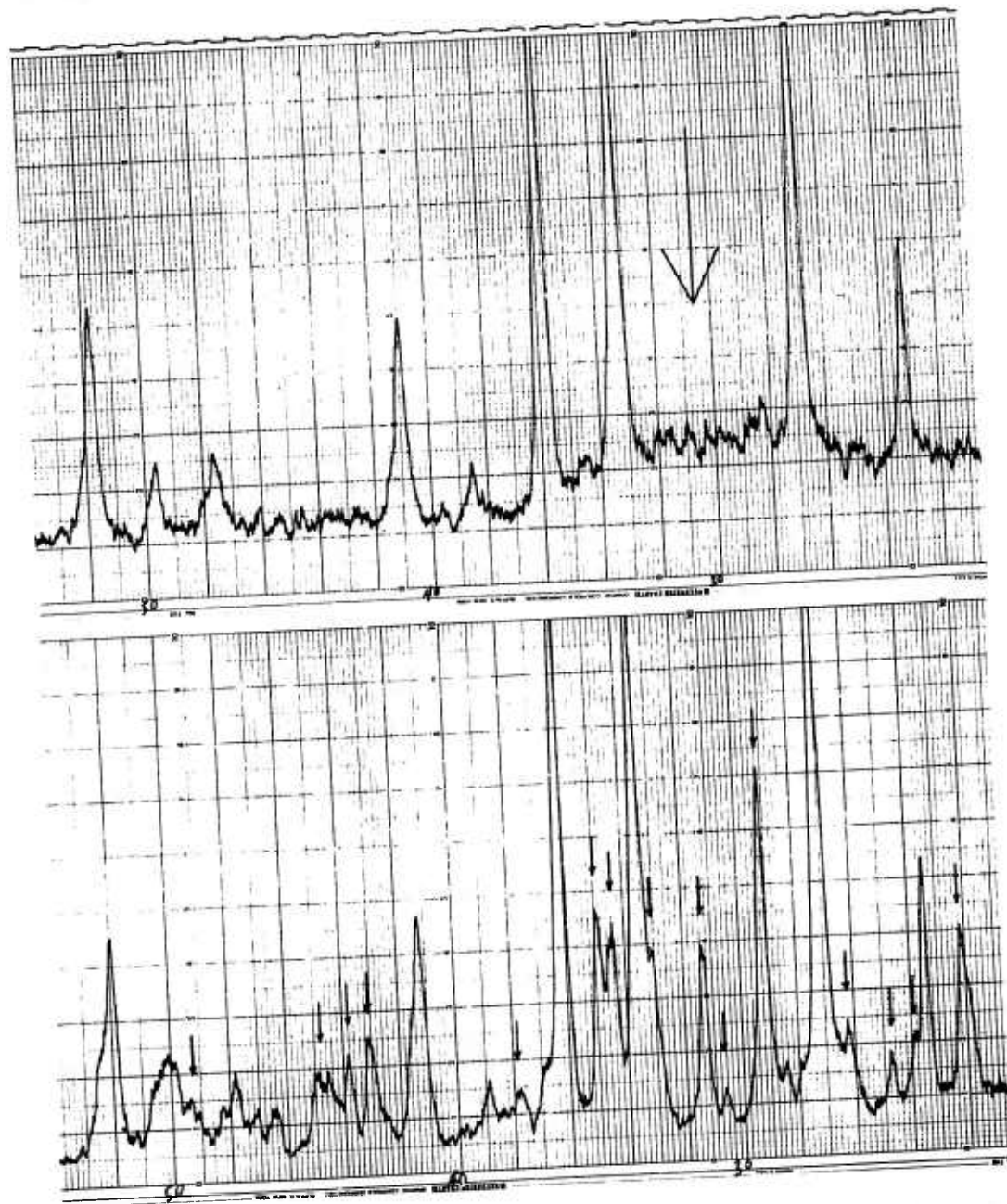
Figure 4.6   X-ray Diffraction Patterns of Sialon Prepared From 66.7% Si_3N_4, 33.3% Al_2O_3 With 25% Y_2O_3 By Sintering At $1600°C$ For 3 Hours Before (above) and After (below) Treatment At $1200°C$ For 185 Hours in Argon.

Most of the results reported here appear to be reasonably consistent with either of the two most frequently cited Sialon models. The original cation-vacancy model put forth by Oyama [12] and by Jack [13], with the general formula (6-3/4x)Si (2/3x)Al xO (8-x)N, does not account directly for the formation of extraneous or glassy phases, except as possibly arising from impurities, but no such accounting is really required. The currently popular vacancy-free model, with the general formula (6-x)Si xAl xO (8-x)N, represents a material which might be prepared in pure form by a reaction such as:

$$\left(2-\frac{x}{3}\right) Si_3N_4 \ + \ \left(\frac{x}{3}\right) Al_2O_3 \ + \ \left(\frac{x}{3}\right) AlN \to (6-x) \ Si \ xAl \ xO \ (8-x) \ N$$
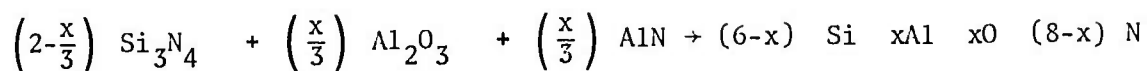
However, a reaction such as:

$$\left(2-\frac{x}{4}\right) Si_3N_4 \ + \ \left(\frac{x}{2}\right) Al_2O_3 \to \ (6-x) \ Si \ xAl \ xO \ (8-x) \ N \ + \ \left(\frac{x}{4}\right) SiO_2$$
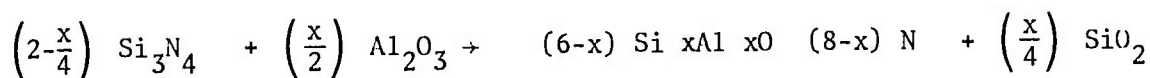
could produce it along with a glass. When additives and impurities are included, the possibilities of the pressure of fluxing extraneous crystalline products become considerable.

4.4 NON-DESTRUCTIVE EVALUATION OF CERAMIC COMPONENTS

Introduction

The use of established NDE techniques such as radiography and dye penetrants, and the more sophisticated techniques such as ultrasonics and acoustic emission, to detect flaws in ceramic turbine components has been previously reported [1-7]. During this reporting period, major emphasis was placed upon using x-ray radiography to monitor the molding of stators and nose cones to yield flaw-free components. The best combination of molding material and parameters was selected in this manner, and flaw free components were obtained for engine and rig testing.

Previous efforts resulted in obtaining 103 hours, in an operating turbine engine, on a one piece first stage stator [7]. Failure in the outer shroud was correlated to defects visible in the radiograph of this stator and the decision was made to continue to test only those components which were determined to be flaw-free by radiographic and visual inspection.

Radiographic NDE

Radiographic analysis was initially employed to evaluate material changes made during the molding of test bars and individual second stage stator vanes [6,7]. This information provided a starting point for molding the complex-shaped stator and nose cone. A discussion of the various changes made in the injection molding procedure appears in Section 3.2.1 of this report. All radiographic evaluations were accomplished in the as-molded stage for these components.

Although the radiographs of components selected for engine and rig testing revealed no visible internal flaws, small voids were observed in these parts after machining. These defects have been on the order of 0.030 inches (750μ) or less and their elimination would further prevent premature failures during testing. Future efforts will utilize molding under vacuum which should eliminate entrapped gas voids.

These small flaws present a problem, however, since these voids exceed the detection capability of radiography. As required in ASTM E94-68, radiographic quality must be at least 2% (2-2T). A stator shroud width of 0.7 inches requires a penetrameter hole diameter of 0.028 inches with a uniform depth of 0.014 inches to be observable in the radiograph in order to meet the 2% quality level. Spherical voids of 0.030 inches and less are therefore, extremely difficult to detect.

Ultrasonic NDE techniques have the potential to further improve structural integrity by detecting these smaller flaws. The characteristic longitudinal sonic velocity of the as-molded material is 4.0 cm/second using a 10 MHz transducer. Flaws on the order of one wavelength of sound or 0.016 inches (400μ) should be detectable in the as-molded material. Future efforts will determine the feasibility of detecting spherical voids of this size and define the limitations of ultrasonic evaluation in this material.

89

NDE-General

The recent increase in density of the components fabricated by injection molding has made possible surface crack detection using dye penetrants. Previously, surface crack detection was difficult due to the high level of surface porosity in the lower density silicon nitride. The retained dye penetrant tended to mask out the surface, preventing detection of cracks. With the lower surface porosity in the 2.55 gm/cm^3 material, very tight cracks have been detected using a graphite/volatile carrier penetrant which is simply applied to the surfaces to be inspected. The excess penetrant is subsequently rubbed off and cracks are highlighted by retaining the penetrant.

Sonic velocity and acoustic impedance data has been previously reported over the density range for silicon nitride [7]. Velocity data is continually compared to these curves to monitor changes made to the material systems and processes used to fabricate ceramic turbine components.

A significant improvement in the quality of recently molded components has been obtained, using NDE techniques to evaluate fabrication changes. Engine and rig testing in the near future should result in increased component reliability and further substantiate the usefulness of employing NDE in the ceramic fabrication process.

5. INTRODUCTION AND SUMMARY— STATIONARY TURBINE PROJECT

The principal objective of the Stationary Gas Turbine Project is to demonstrate the use of uncooled ceramic first stage stator vanes operating at a peak inlet temperature of 2500°F in a 30 MW size test turbine. Successful completion of this program objective will demonstrate that ceramic materials are viable engineering materials that can be used in demanding high temperature structural applications. While working toward the turbine demonstration, very significant developments have been made in the areas of brittle material design technology, materials science and technology, materials fabrication, and component testing. The baseline technology developed on the ARPA program thus becomes the keystone to further component and engine developments that will provide high performance gas turbines and, potentially, huge benefits to both the military and domestic sectors of the nation.

Gas turbine power generation is an existing, proven technology in this country, which today has the lowest capital cost per KW of installed capacity of any fossil fuel system. Currently, a major use of the stationary gas turbine is in electrical power generation to meet peaking power requirements. Available in sizes ranging from 19 to 70 megawatts, these units are applicable to DOD installations that require on-site power generation or they may be mounted on barges to supply remote locations that are accessible by way of natural water ways. As a prime mover in ship propulsion, the heavy duty gas turbine is gaining considerable attention because of its potential for lower cost and improved ship performance and reliability.

There is renewed interest today in the use of the combined cycle for electrical power generation as a result of the present "fuel crisis". Combined cycle is a gas turbine-steam turbine system capable of using a wide variety of fuels including coal derivatives. The major thrust of gas turbine technology in support of combined cycle development is directed toward an overall improvement of efficiency in the conversion of fuel to electrical energy where efficiency is directly related to the maximum operating temperature of the turbine.

Currently, stationary gas turbine inlet temperatures range from 1900°-2000°F, using convectively cooled superalloy components. When the present day turbo-generating machinery is operated in series with steam turbines via waste heat boilers in combined cycle operation, a thermal efficiency of 38-42% is attained making combined cycle plants competitive for intermediate load power generation. At 2500°F turbine inlet temperature uncooled, however, 50% efficiency can be achieved making combined cycle installations competitive for base load service. Herein lies the important role of ceramics because they provide the only direct materials approach to reaching 2500°F turbine inlet temperatures where this high thermal efficiency can be realized. In addition, the excellent hot corrosion-erosion resistance of ceramics such as silicon nitride and silicon carbide is expected to provide extended long-term reliability even when low grade, dirty fuels are used.

5.1 STATIONARY TURBINE PROJECT PLAN

The Stationary Turbine Project is directed toward the design and evaluation of first stage stator vanes as a first step in the development of ceramic components for a gas turbine one stage at a time.

Figure 5.1 illustrates the Westinghouse 30 MW turbine to be used in the ceramic stator vane demonstration. In this simple cycle machine, air is induced through a large intake silencer and filtered into an 18-stage axial compressor before entering the combustor housing. The combustor housing directs air at 650°F to combustion cans assembled in a circumferential array. Air is mixed with fuel and ignited in the primary zone of the combustor. The gas passes downstream through the combustion section mixing with secondary air. Flow continues from the combustor, through the transition zone, and enters the power turbine at the first stage stator vane location after which the hot gases expand through the three-stage turbine section and are either exhausted through a stack or ducted into a reheat boiler as part of a combined cycle power generating unit.

The first stage stator vane was selected for development and demonstration in the ARPA program because it represents the hottest material application ultimately affecting power and efficiency. Solving the design problems with the inlet stator vane and developing needed analytical tools are most important in establishing feasibility for the design of other turbine components, for example, first stage turbine blades.

Currently, the ceramic turbine concepts are designed and developed for the 30 MW frame size machine. Once feasibility and a performance base are achieved, adaptability to larger production machinery becomes a matter of modification and scale up. Material selection and optimum design depend upon several interrelated factors including the physical properties of materials, mass flow characteristics, heat transfer rates under steady state as well as transient conditions as well as the complex development of mechanical and thermal stress patterns in all components.
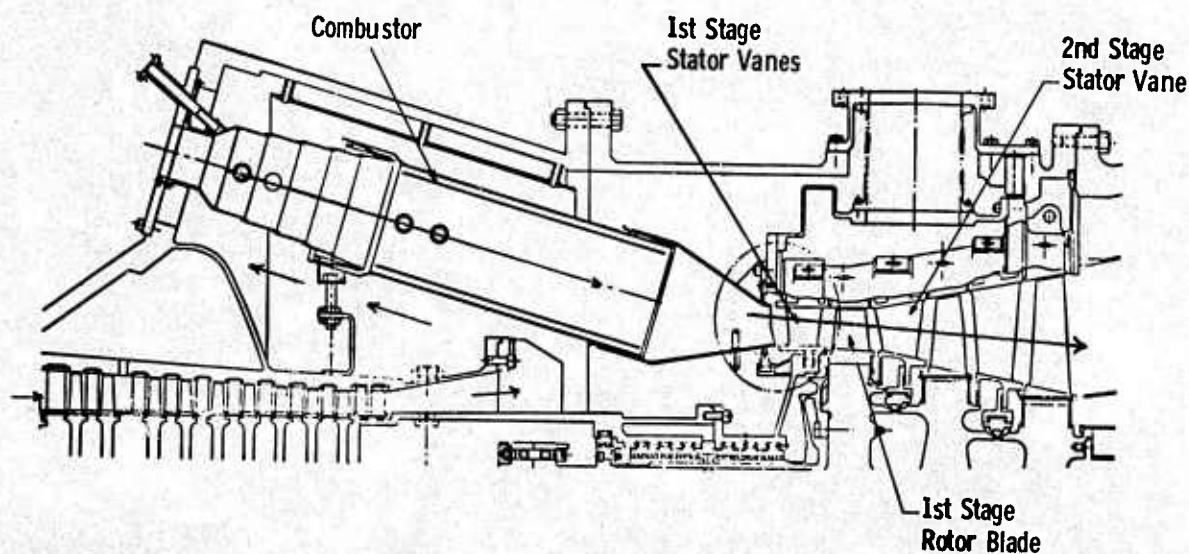
Figure 5.1   Stationary Power Turbine Flow Path 30 Mw Westinghouse 251

5.2 PROGRESS AND CUMULATIVE STATUS SUMMARY - STATIONARY TURBINE PROJECT

The objective of the ARPA Stationary Turbine Project is the design, development, evaluation and demonstration of ceramic stator vanes for 100 cycles simulating peaking service conditions at a peak temperature of 2500°F. While the original intention was to conduct this evaluation and demonstration in an actual 30 MW turbine engine after designs were verified in static rig tests, more recently a decision was made to focus efforts on demonstrating the objective exclusively in the static test rig. To achieve this, all activity is broken down into two major task areas subdivided as follows:

    I. Component Development

        (a) Design
        (b) Fabrication
        (c) Testing

    II. Material Technology

        (a) Material Engineering Data
        (b) Material Science
        (c) Non-Destructive Evaluation

The present status is summarized according to Task in Sections 5.2.1 and 5.2.2 of this report.

5.2.1 CERAMIC COMPONENT DEVELOPMENT

Component Development is concerned with the design and analysis of the first stage stator vane, fabrication of the first stage stator vane design iterations, and the testing of first stage stator vanes in the static rig at 2200° and 2500°F.

Design

A novel, power-generation size ceramic stator vane has evolved from a unique sandwich type multiple component concept. The concept utilizes a three-piece vane that is insulated, cushioned, and supported in such a manner as to minimize critical steady state and transient thermal stresses which would otherwise preclude the use of brittle materials in an industrial turbine. The configuration to be tested in the static rig at 2500°F represents the third design iteration featuring a tapered-twisted airfoil with modified end cap construction.

The problem of stress concentration is foremost in the design and use of brittle materials for engineering applications. To avoid stress concentration, the stress development in critical elements of a component must be defined. Two-dimensional finite element arrays such as triangles are adequate for the analysis of most of the stresses in the three-piece stator vane assembly but interfacial contact stresses and the stress developed in rotor blades require a more sophisticated volume element (3-dimensional) program for resolution. WISEC, the Westinghouse Isoparametric Element Code was partially developed on the Stationary Gas Turbine Project to meet this requirement.

Status

● A novel 3-piece, uncooled, simply-supported, ceramic stator vane assembly was selected and designed.[1,2,3,4]

● To minimize stresses, the cross-sectional size of the ceramic vane selected is only half that of the metal vane counterpart.[2]

● Critical stresses of the 3-piece ceramic vane assembly have been evaluated for both transient and steady state conditions expected during turbine operation at 2500°F.[2,3,4,5]

● A full scale kinematic model was built to show that the stator vane assembly was functional when subjected to thermally derived differential motion well in excess of design limits.[3]

● The detailed design of stator vane assembly, including compressive spring loading and the ceramic/metal insulation and support system was completed.[2,3]

● 3-D finite element code (WISEC) has been completed except for creep and contact stress analysis.[2,3,4,5,6]

● Preliminary analysis of a ceramic rotor blade using the 3-D finite element code has been completed.[4,5,6]

● A first stage air-cooled metal blade has been designed for the advanced test turbine. Design modifications for the air-cooled, metal second stage vanes and rotor blades are also complete.[7] However, turbine design and modification has been de-emphasized so that efforts can be focused in the static rig testing of the stator vane assemblies.

Fabrication

After design, fabrication is perhaps the most important aspect in the successful application of ceramics in gas turbines. Only fully dense, high-strength Si_3N_4 and SiC were selected for component development. Currently, these materials are made commercially by a process of hot-pressing, whereby powder is consolidated by the simultaneous application of pressure and temperature. The ARPA program has provided the first full-scale, power generation size, ceramic stator vanes fabricated from hot-pressed Si_3N_4 and SiC. These were made to Westinghouse specifications by the Norton Company of Worcester, Massachusetts and their subcontractors from hot-pressed billets. Diamond tools and tracer grinding machines were used to produce the stator vane geometry. This particular fabrication route was followed in order to assure the availability of components for testing.

Status

● Over 40 prototype vane sets for testing have been successfully fabricated by hot-pressing and machining.[3,4,5,6]

● 100 Si_3N_4 vane sets were ordered for completion of 2500°F static rig tests and for the test turbine demonstration.[6]

● 14 tapered-twisted airfoils and 24 end caps machined to the 3 in. radius and 3/8 nominal cavity depth specified for the 3rd generation (advanced turbine) design were received for the 2500°F static rig test.

● Experimental silicon nitride billets hot-pressed with yttria have been received for evaluation as an improved stator vane material.

Testing

A very important step in the ARPA program to develop ceramic vanes is the verification of design and materials by test of full scale parts under realistic conditions. The plan is to test in a highly instrumented static rig first at 2200°F and then 2500°F under conditions that nearly duplicate actual gas turbine conditions.

Status

● Design and construction of the instrumented static rig was completed after considerable delays due to procurement and start-up problems.[3,4]

● 2200°F static rig testing was successfully completed using Si_3N_4 vane assemblies (Fig. 5.2).[5]
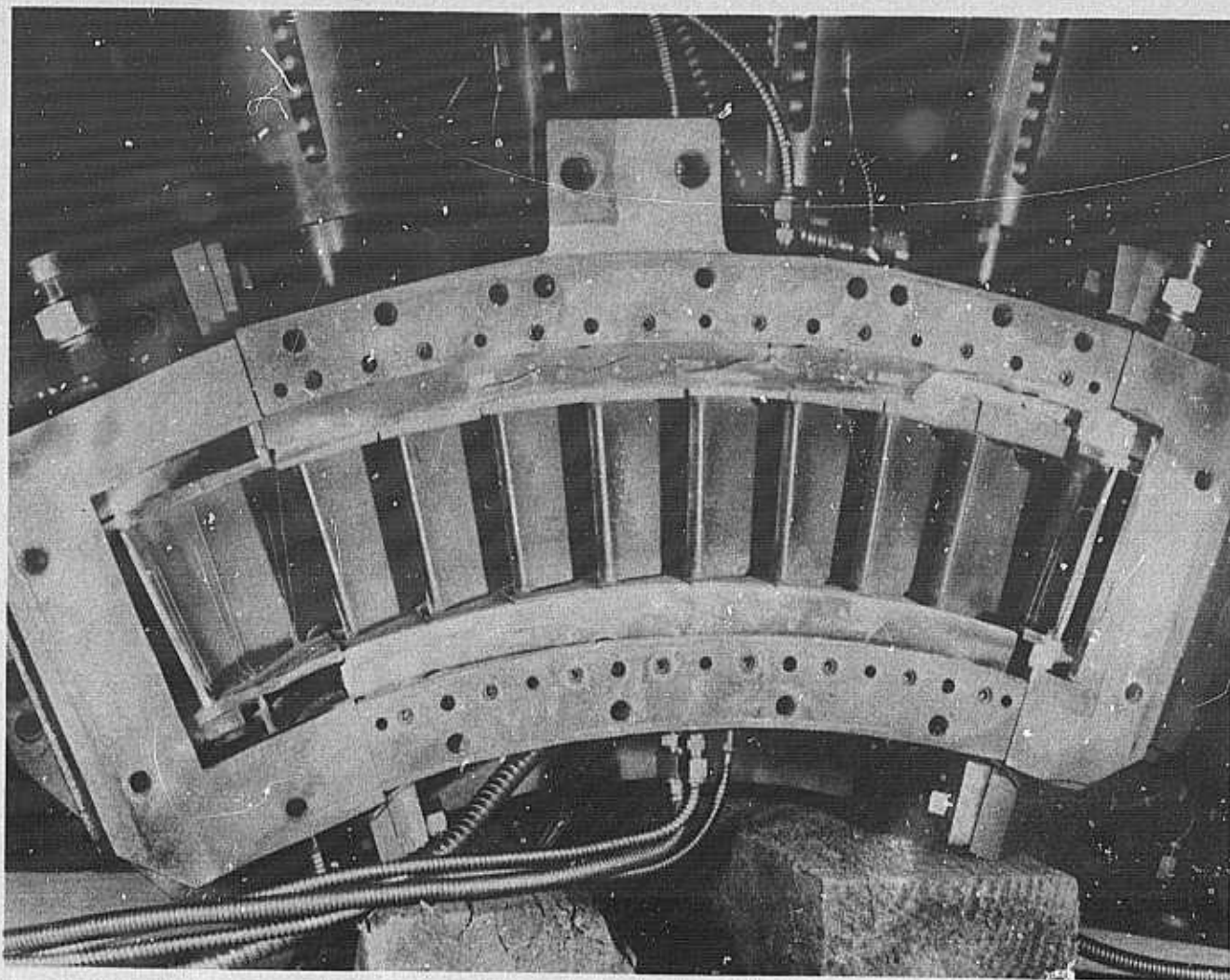
Figure 5.2   Stator Vane Assembly at the Completion of 2200°F Static
                  Rig Tests

● Silicon nitride stator vane assemblies were shown to be tougher,
more thermal shock resistant and generally more compatible with a
transient turbine environment than silicon carbide stator vanes of the
same design after 5 cycles of static rig testing at 2500°F. (Fig. 5.3)(7)

● The static rig has been rebuilt a second time to permit the
testing of silicon nitride stator vane assemblies with tapered-twisted
airfoils at 2500°F. A more extensively air-cooled Haynes 188 combustor,
a water-cooled exhaust duct and a water-cooled mixer were used to replace
components which failed during the fifth cycle of previous testing.(7)

SILICON NITRIDE STATOR VANES

SILICON CARBIDE STATOR VANES

2500°F STATIC RIG TEST
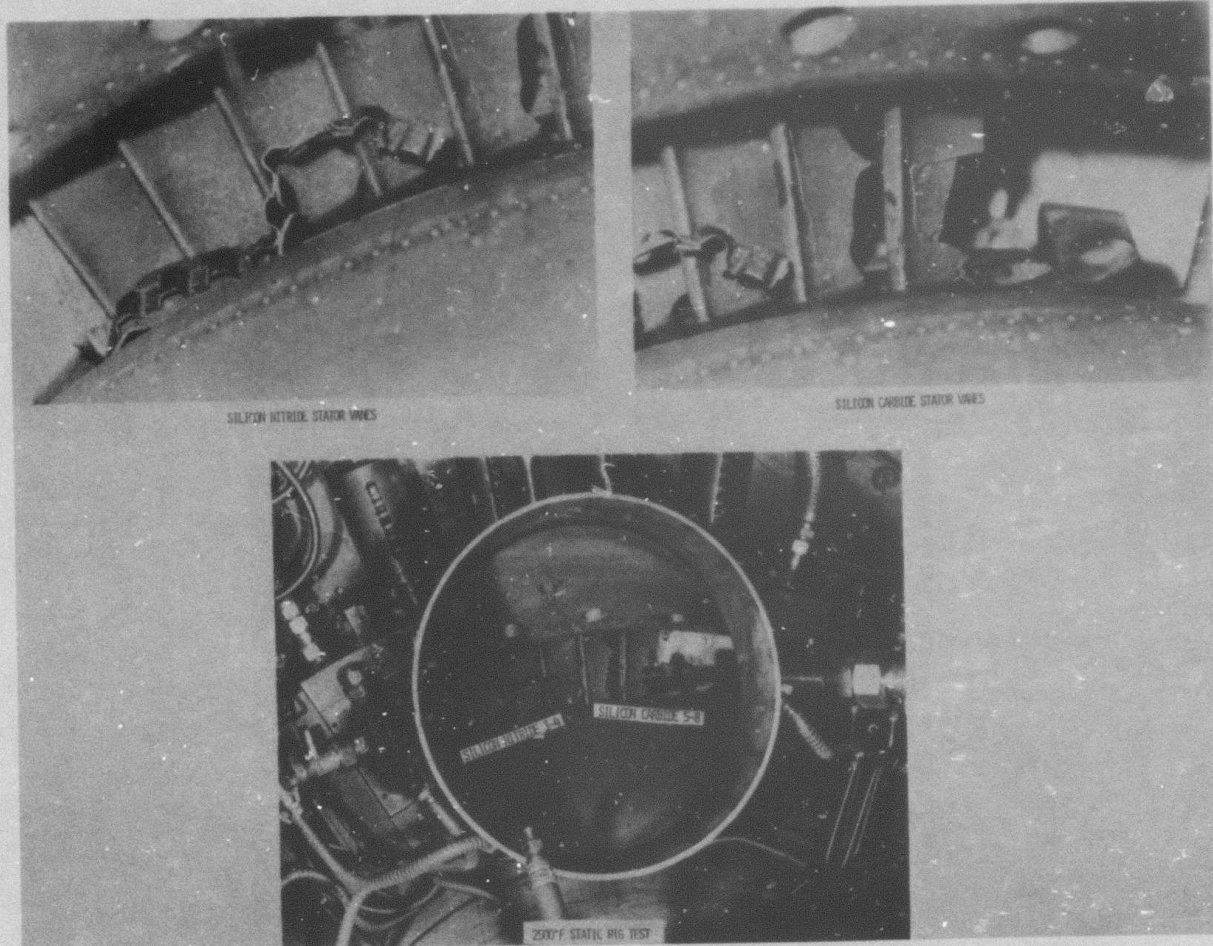
Figure 5.3   Static Rig Test Results After Five Cycles at 2500°F –
Catastrophic Rig Failure

5.2.2 MATERIALS TECHNOLOGY

Materials technology is considered a basic building block for design, fabrication and testing. The sub-tasks consist of Materials Engineering Data, Materials Science, and Non-Destructive Evaluation of Materials. The plan has been to continue this phase throughout the program in order to properly evaluate material improvements and design changes that evolve naturally in a focused engineering program.

Material Engineering Data

Design technology is highly dependent upon the thermal, physical and mechanical properties of the materials being used. A substantial effort has been expended to collect engineering property data for commercial hot-pressed Si3N4 and SiC to make the design code more comprehensive. The interaction between properties and design is shown in Fig. 5.4. Since the present design code uses an elastic-to-fracture criterion for stator vane ceramics and since the transient stresses are much larger than those of the steady state, thermal properties have been measured extensively in order to assure reliability. Both established and new testing procedures have been utilized to evaluate the physical and mechanical properties of gas turbine ceramics at temperatures up to 2500°F.
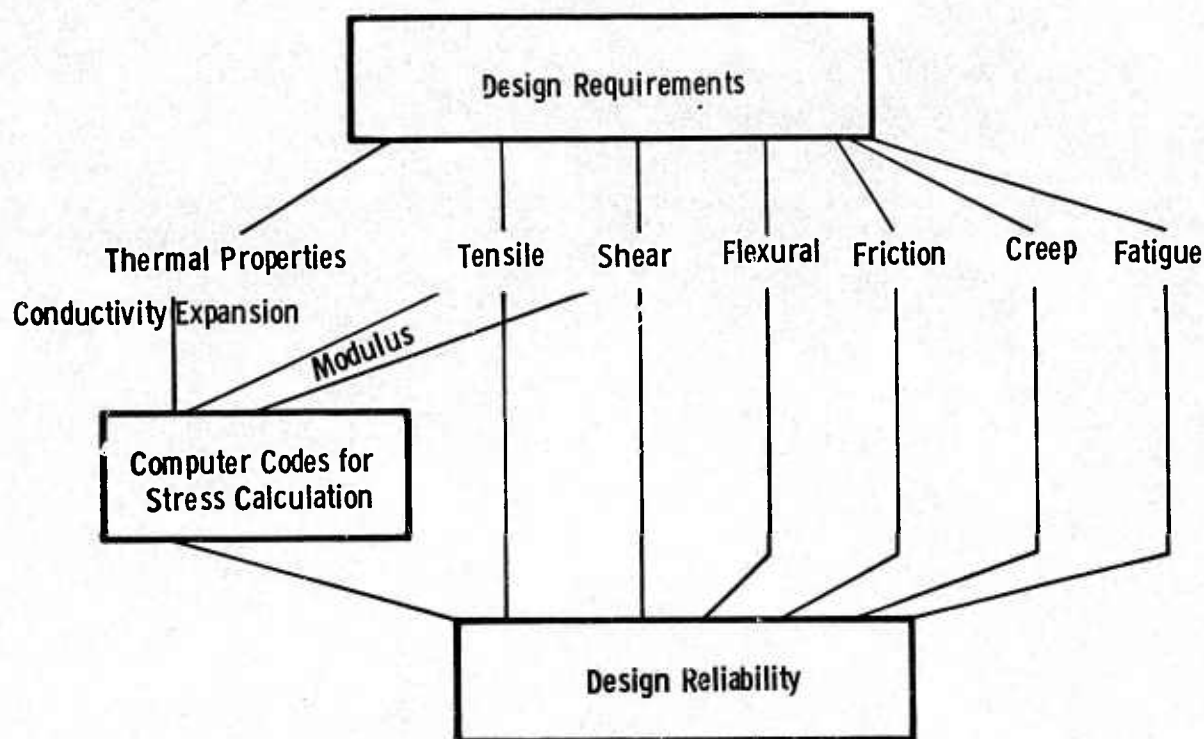
Figure 5.4   Flow Diagram Showing Design-Properties Interaction

Status

• Thermal properties (expansion, conductivity and specific heat) have been characterized from RT to 2500°F for hot-pressed Si3N4 (Norton HS-130) and hot-pressed SiC (Norton NC-203).[3,4]

● Flexural strength, tensile strength, shear strength, friction behavior, high cycle fatigue and elastic properties have been characterized from RT to 2500°F for both HS-130 Si_3N_4 and NC-203 SiC.[2,3,4,5,6]

● Creep, stress rupture, low cycle fatigue and corrosion-erosion behavior are evaluated continually because these properties relate to reliability and require longer term evaluation. Data will continue to be acquired to 2500°F.[3,4,5,6,7]

● Statistical treatment of engineering property data continues. Additional information is continually added to the data base.[2,3,4]

● Fracture mechanics studies as related to high temperature behavior has been initiated in order to assess component reliability and assign a practical fracture criterion for engineering use.

● Stress-strain data in the tensile mode indicate that Norton HS-130 (NC-132) silicon nitride is essentially elastic to failure up to 2200°F at loading rates in the range of 0.001 in/in/minute. Plastic deformation is apparent at temperatures of 2300°F and above.[7]

● 4000 hour static oxidation tests of silicon nitride and silicon carbide indicate significant flexural strength degradation after 100 hours due to surface reaction between the oxide film and substrate material.[8]

● An evaluation of hot-pressed silicon nitride hot-pressed with yttria shows improvements in high temperature strength and creep resistance. However, the material is subject to low temperature phase instability (at 1800°F) which causes decrepatation and subsequent loss of strength.[8]

Materials Science

Detailed investigations into materials science develop an understanding of material behavior which will hopefully lead to property improvements. This is particularly important since the ceramic materials being utilized in turbine engines are relatively new and appear capable of considerable improvement. The areas of material science cited for investigation have been defined by the engineering requirements of the system and thereby relate mainly to the commercial materials being used. They contribute to better control of the fabrication process, better properties, and tend to extend the useful life of the ceramic materials through property improvement.

The value of material science work has already been demonstrated by the property improvements that have been made since the onset of the ARPA program. By discovering that certain impurities and foreign inclusions were detrimental to the strength of hot-pressed Si_3N_4 above 1800°F and learning how to process starting powders to achieve a desired microstructure, strength at 2550°F has been improved by 400%.

Status

● Identification of microstructural details of commercial hot-pressed Si_3N_4 (Norton HS-110 and 130) and hot-pressed SiC (Norton NC-203) are complete.[1,2,3,4]

99

● Correlations between properties, microstructure, and fabrication processing for HS-130 Si3N4 and NC-203 SiC are complete.[3,4,5,6]

● Chemical analyses of Norton HS-130 Si3N4 and NC-203 SiC are complete.[6]

● Analyses of thermodynamic data for Si3N4 and SiC are complete.[1,2]

● Static oxidation kinetics of HS-130 Si3N4 and NC-203 SiC are complete.[3,4,5]

● The loss of strength in hot-pressed silicon nitride after prolonged oxidation at 2500°F is attributed to a surface reaction between the oxide film developed (MgO·SiO2· x CaO·etc.) and the substrate which appears soluble in it.[8]

● The poor low temperature oxidation resistance of yttria hot-pressed silicon nitride appears to be associated with a Si3N4·Y2O3 phase in the microstructure.[8]

Non-Destructive Evaluation

Uniformity of microstructure is necessary for reliable structural ceramics in gas turbine engine applications. The objectives of NDE are to identify and classify micro- and macro-structural defects and relate these to the component fabrication process. The ultimate goal is to define meaningful inspection methods that can be used to accept/ reject components prior to installation in the engine. Procedures utilizing ultrasonics, X-ray radiography, dye penetrants, and acoustic emission are currently being applied to ceramic systems for evaluation purposes.

Status

● Suitability of dye penetrants for detecting surface connected porosity and surface cracks has been established for ceramic gas turbine components.[5]

● Sensitivity of commercial techniques in ultrasonic A&C scanning to low density inclusions and segregated voids in hot-pressed Si3N4 and SiC has been established.[5,6]

● Detection limits and sensitivity by ultrasonic inspection has been established for hot-pressed ceramic turbine components.[5,6]

● Feasibility of applying acoustic emission to proof testing of ceramic components has been established.[4]

● Detection limits and sensitivity by X-ray radiographic inspection has been established for hot-pressed ceramic turbine components.[5,6]

● NDE of ceramic turbine components is continuing. The 14 Si3N4 vane sets for static rig testing at 2500°F have been qualified.[8]

5.3 FUTURE PLANS

In June 1975, a decision was made to de-emphasize the full stationary turbine demonstration of ceramic stator vanes and focus available effort on static rig testing to meet the demonstration objective. Work required to complete this plan is discussed briefly below.

Component Development

The static rig testing of the tapered-twisted stator vane design with boron nitride insulator components at 2500°F will be resumed later in the fall. Approximately six weeks will be required to complete 100 cycles of testing under conditions of controlled shutdown. Following this the rig will be assembled with instrumented metal vane components to establish heat transfer coefficients under actual static rig conditions up to 1800°F. The two parallel sided metal vanes will be tested with six ceramic components of similar geometry to permit the direct comparison of 3-dimensional stress analyses. The results will permit an accurate stress analysis of the tapered-twisted airfoil design.

Material Technology

Considering the long term effect of oxidation on the strength of hot-pressed silicon nitride, the Material Technology portion of the program will emphasize material improvement. This activity may be summarized as follows:

A) Accelerate development efforts to improve creep resistance and reduce or eliminate strength degradation in Si_3N_4 resulting from prolonged oxidation or corrosion/erosion at 2500°F.

B) Conduct a development program for coating both hot-pressed and reaction-sintered Si_3N_4 via chemical vapor deposition (CVD) to prevent long term strength degradation due to oxidation, corrosion and/or erosion.

C) Accelerate process development of the high purity Si_3N_4 powder required for material improvement and billet fabrication activities.

D) Conduct oxidation and hot corrosion experiments on improved candidate materials to determine environmental effects on mechanical properties.

E) Evaluate tensile engineering properties (strength, modulus, and stress rupture) of improved candidate materials.

F) Determine the pertinent thermal and mechanical properties of boron nitride insulator materials to confirm vendor data.

G) Complete microstructure, NDE, and failure analysis of stator vane assemblies and associated hardware from 2500°F static rig tests.

Material Fabrication

Since stator vane hardware will not be required for an advanced turbine demonstration, the order for 100 silicon nitride stator vane assemblies will be cancelled after 10 additional sets are fabricated to ensure the availability of replacement parts during static rig tests. Additional effort is required to develop hot-pressing schedules and produce fully dense billets of improved materials for evaluation. The Norton Company is expected to participate in this activity.

Since the stator vane demonstration in the advanced turbine has been de-emphasized in favor of static rig testing, the semi-production order for silicon nitride vane assemblies has been reduced from 100 to 28. This will satisfy the static rig assembly requirements and provide sufficient replacement parts to ensure the completion of static rig testing. Additional effort will be required to develop hot-pressing schedules and to produce fully dense billets of improved materials for evaluation.

6. PROGRESS ON CERAMIC COMPONENT DEVELOPMENT - STATIONARY TURBINE PROJECT

6.1 STATOR VANE DEVELOPMENT

SUMMARY

The static rig was completely rebuilt as a result of the catastrophic failure after the first 5 cycles of testing at 2500°F. A new combustor was designed and constructed to provide additional air-cooling in the secondary. A double-walled, baffeled metal duct with water cooling and a water spray cooled mixer section were also installed in the static rig. Instrumentation has been added to detect hot spots in hot gas path components to prevent future failures.

Some difficulties were encountered in the fabrication and delivery of the tapered-twisted airfoils and end caps which constitute the assemblies to be tested in the static rig. Airfoil tenons had to be remachined to correct an end cap alignment problem. Although the resumption of static rig testing at 2500°F was delayed beyond the report period as a result, the effort finally produced component parts of extremely high quality, the best received to date.

Accurate heat transfer data are a pre-requisite to reliable stress analysis. Two metal stator vane assemblies with parallel sided airfoils of first generation design have been instrumented with thermocouples and strain gauges, to provide heat transfer coefficients and collaborate stress measurements up to 1800°F and 850°F, respectively. The thermocouples and strain gauges have been calibrated. The instrumented components will be assembled at positions 3 and 5 in the eight vane test cascade to run in the static rig at the conclusion of the cyclic testing (October 1975).

6.1.1 DESIGN AND ANALYSIS

Introduction

The large size of the Westinghouse stationary power turbine permits a ceramic stator vane design which is particularly well suited to brittle materials. A three-piece vane assembly has been selected to minimize stress and simplify fabrication. This replaces the more conventional geometry in which the airfoil is integral with the shrouds. The use of silicon nitride or silicon carbide stator vanes is intended to increase the service temperature of the resultant machine to a peak temperature of 2500°F without a need to cool the first stage stator row.

With the decision to focus available effort on static rig testing to meet the demonstration objective, further work on design modifications for an advanced test turbine have been deferred. The project design activity is considered to be essentially complete with the development of the tapered-twisted airfoil which replaces the parallel sided non-tapered airfoil of the original three piece design.

Complete stress analysis of the third generation ceramic stator vane design with tapered-twisted airfoil remains to be accomplished. The boron nitride insulator design should also be examined with respect to stress and temperature distribution. These items will be considered to complete the design, analysis, performance loop at the end of static rig testing when ramp data and actual heat transfer coefficients are supplied.

6.1.2 STATIC RIG TESTING

Introduction

Last October, the static rig testing of silicon nitride and silicon carbide stator vane assemblies at 2500°F was terminated prematurely by total rig failure precipitated by an implosion of the Hastelloy X combustor.[7] The static rig has been rebuilt with a redesigned combustor section, water-cooled exhaust duct and spray water cooled mixer to permit the resumption of testing by the last quarter of 1975.

Static Rig Modification

The latest version of a modified static rig for the cyclic testing of silicon nitride vane assemblies and boron nitride insulators is presented in schematic plan view in Fig. 6.1. The combustor section was redesigned and fabricated with a new secondary section which contains two extra circumferential corrugations for additional wall cooling. The modification also required that a conical portion be inserted between the corrugations in order to avoid changing the downstream diameter. The size and location of the air scoops in the primary section of the combustor were altered to achieve more complete combustion in the
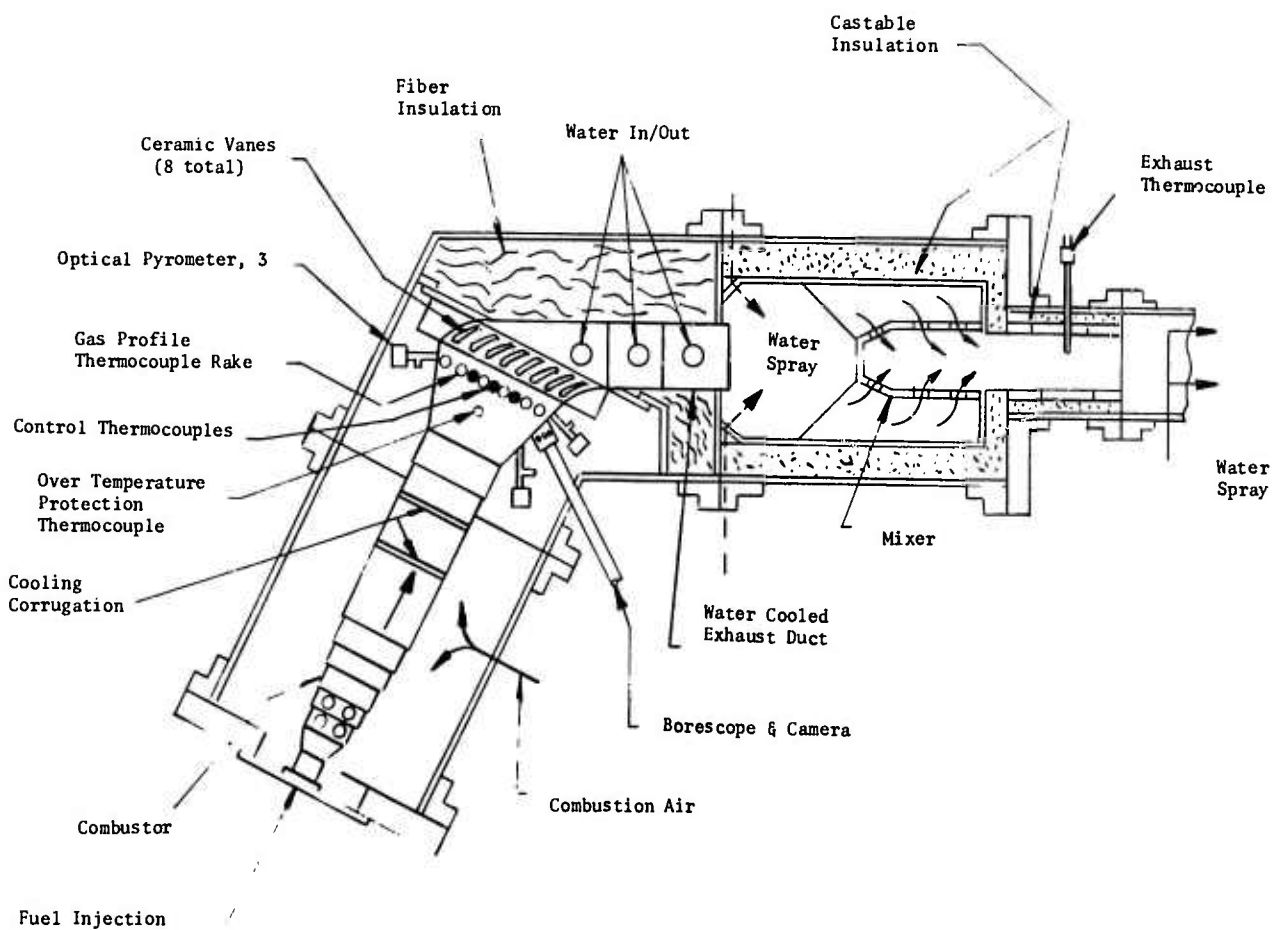
Figure 6.1   Plan View of 2500°F Static Rig - Water-Cooled Configuration

105

primary zone in an effort to eliminate flames which impinged upon the test vanes.(5) The exchange of dilution for extra cooling air was designed for no overall change in pressure drop. Additional thermocouples were added to the combustor primary and secondary sections to monitor wall temperature and prevent any possibility of combustor failure due to hot spots. The redesigned combustor is shown installed in the appropriate shell section of the static rig in Fig. 6.2.

The ceramic lined exhaust duct has been replaced by the water-cooled component illustrated in Fig. 6.3. Three independent cooling compartments are supplied with separate inlet and outlet, each controlled by a valve on the inlet side. Thirty-three thermocouples serve to monitor the metal wall and outlet water temperatures during operation. The water used for duct cooling drains into an open tank to avoid pressure build-up in the water-jacketed duct system. The miter shell section of the static rig was modified to permit entry and exit of cooling water for the exhaust duct.

The mixer section was redesigned to provide a stiffened metal shell structure which acts as an inner liner for the castable alumina with fiber foam insulation to protect the mixer section outer cylinder.
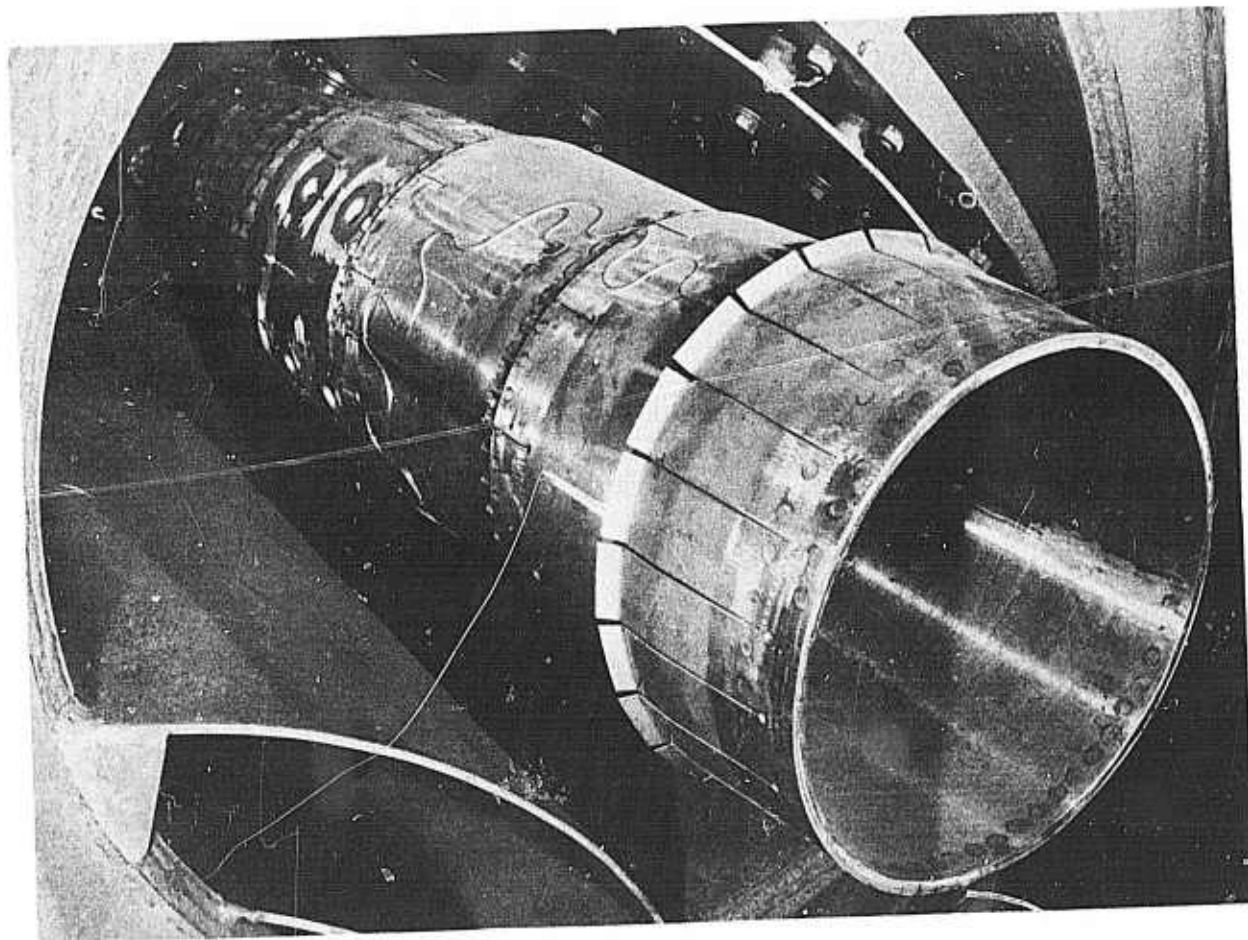
Figure 6.2   New Combustor with Additional Secondary Wall Cooling

106

The downstream mixer is now metal, similar in design to that used in the 2200°F static rig test.[5] The redesigned mixer section is cooled by a water spray introduced at six circumferentially located (60° apart) and radially directed nozzles much like those used in the spool piece. The spray water will cool the gas to 2000°F+ maximum at the mixer inlet when the vanes are operating at 2500°F. The mixer section appears in Fig. 6.4. Because of water spray injection in the mixer section, control of the rig has been transferred from the exhaust thermocouple location to three thermocouples located in the transition section immediately upstream of the stator vane cascade. The overtemperature protection thermocouple for emergency trip-out also remains in the transition. Each of these control thermocouples are of the adjustable low penetration type. Three optical pyrometers (suction side pyrometer is new) sight on airfoil #4. All critical metal components, i.e., the combustor, transition, exhaust duct, and mixer section elements were manufactured from Haynes 188 superalloy.
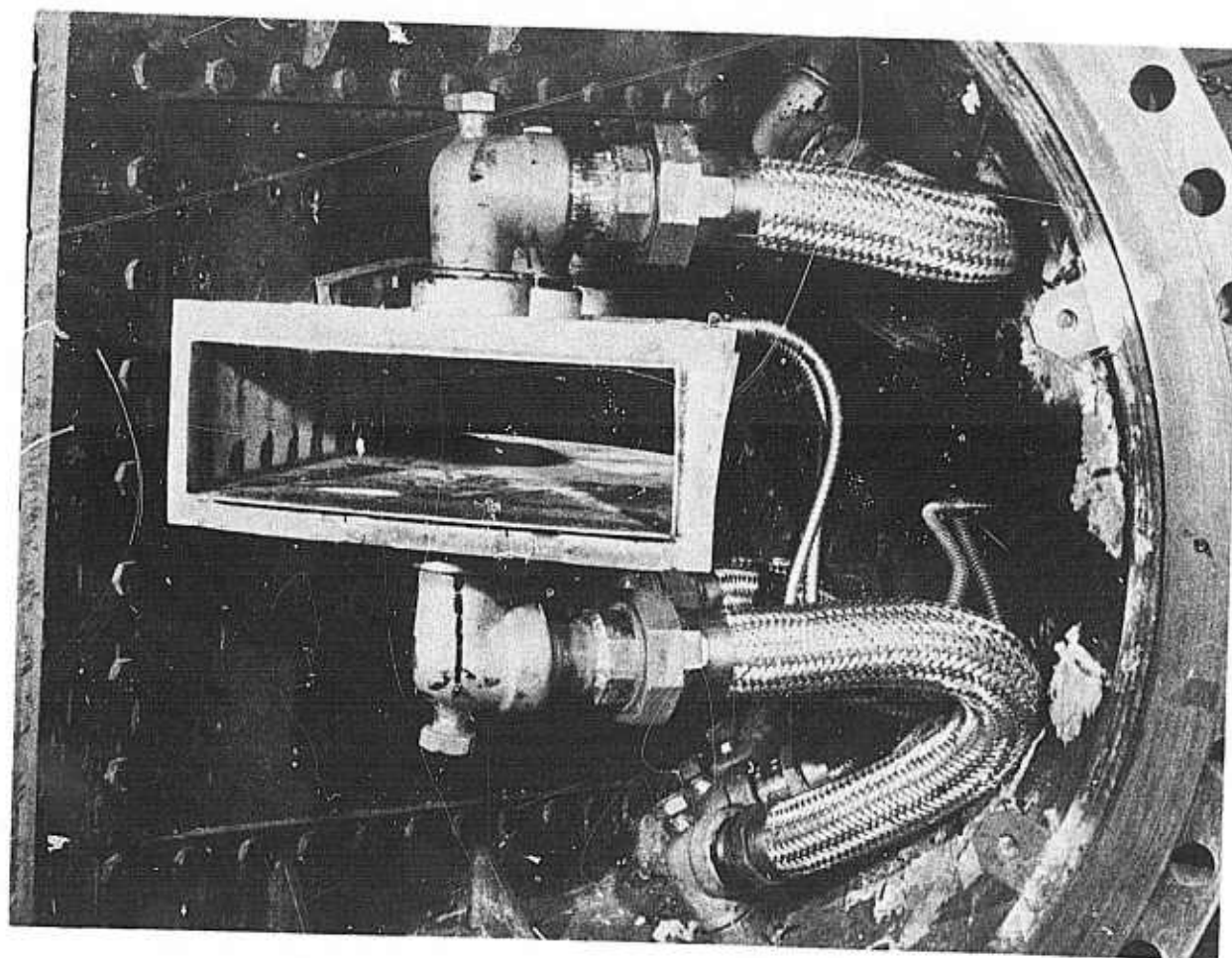
Figure 6.3   Water-Cooled Exhaust Duct
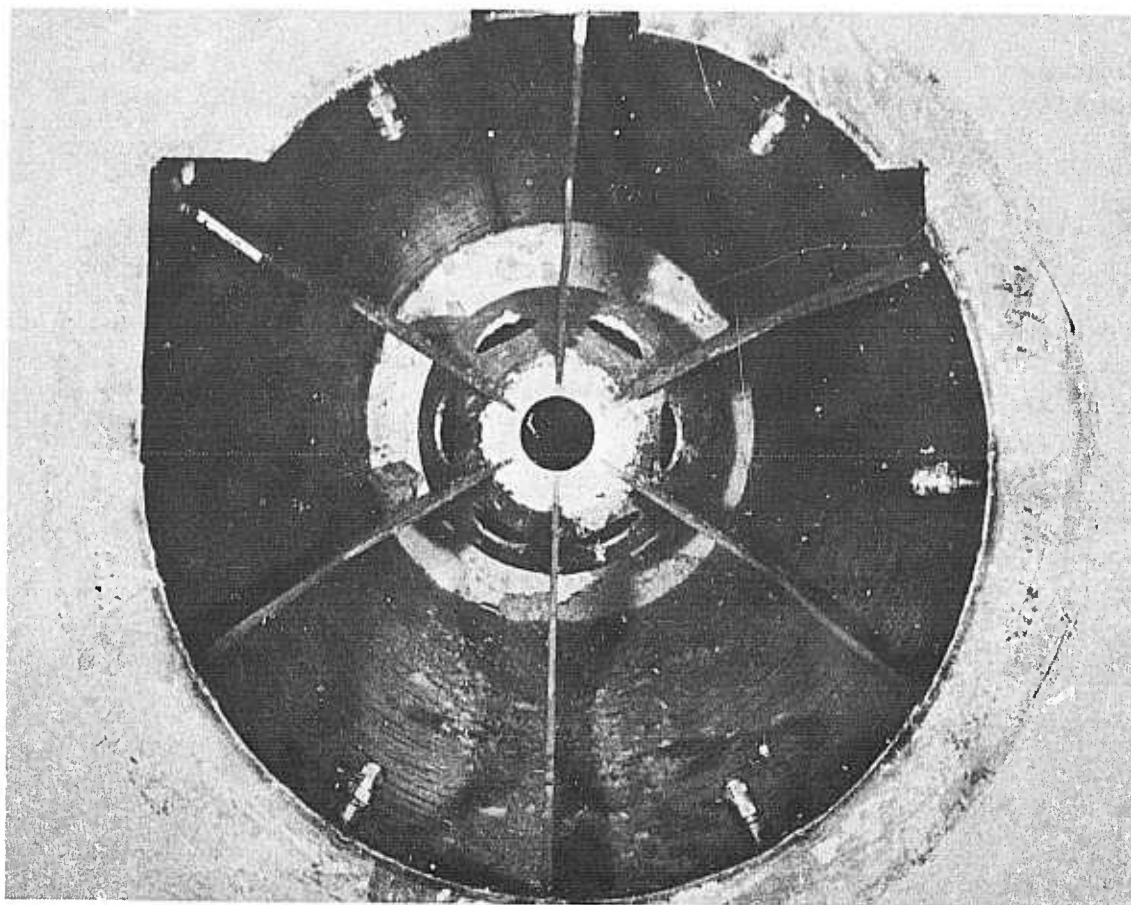
Figure 6.4   Water Spray-Cooled Mixer Section

Ceramic Vane Assembly Fixture

Details of the static rig test fixture (SRTF) have been described.[3-5]
A longitudinal section view of the assembly is shown in Fig. 6.5.   The
vane support structure was changed to substitute a 0.125" Haynes 188
air baffle for the 0.032 Hastelloy X baffle used previously.[5]   The
insulators to be tested are made of hot-pressed boron nitride Type M
(Carborundum) because this material survived the first phase of 2500°F
testing.   Because the insulator has higher temperature capability the
amount of cooling air across the shoe (Fig. 6.5) has been decreased to
reduce the steady state thermal gradients in the silicon nitride end caps.

The 3-piece vane assembly to be tested at 2500°F represents the
design modification with the tapered-twisted, half-size (chord and
thickness) airfoil described previously.[7]   The components are
illustrated in Fig. 6.6.   For the scheduled test series, all eight vanes
will be of hot-pressed silicon nitride (Norton NC-132) material.   Since
NC-132 material appears to degrade when oxidized for 150-400 hours at
2500°F two of the eight airfoils in the eight vane cascade will be
pre-oxidized at 2500°F for 103 hours prior to the transient thermal
test.   These airfoils will be located in vane positions 3 and 6 (looking
with flow and reading from left to right) in Fig. 6.1.
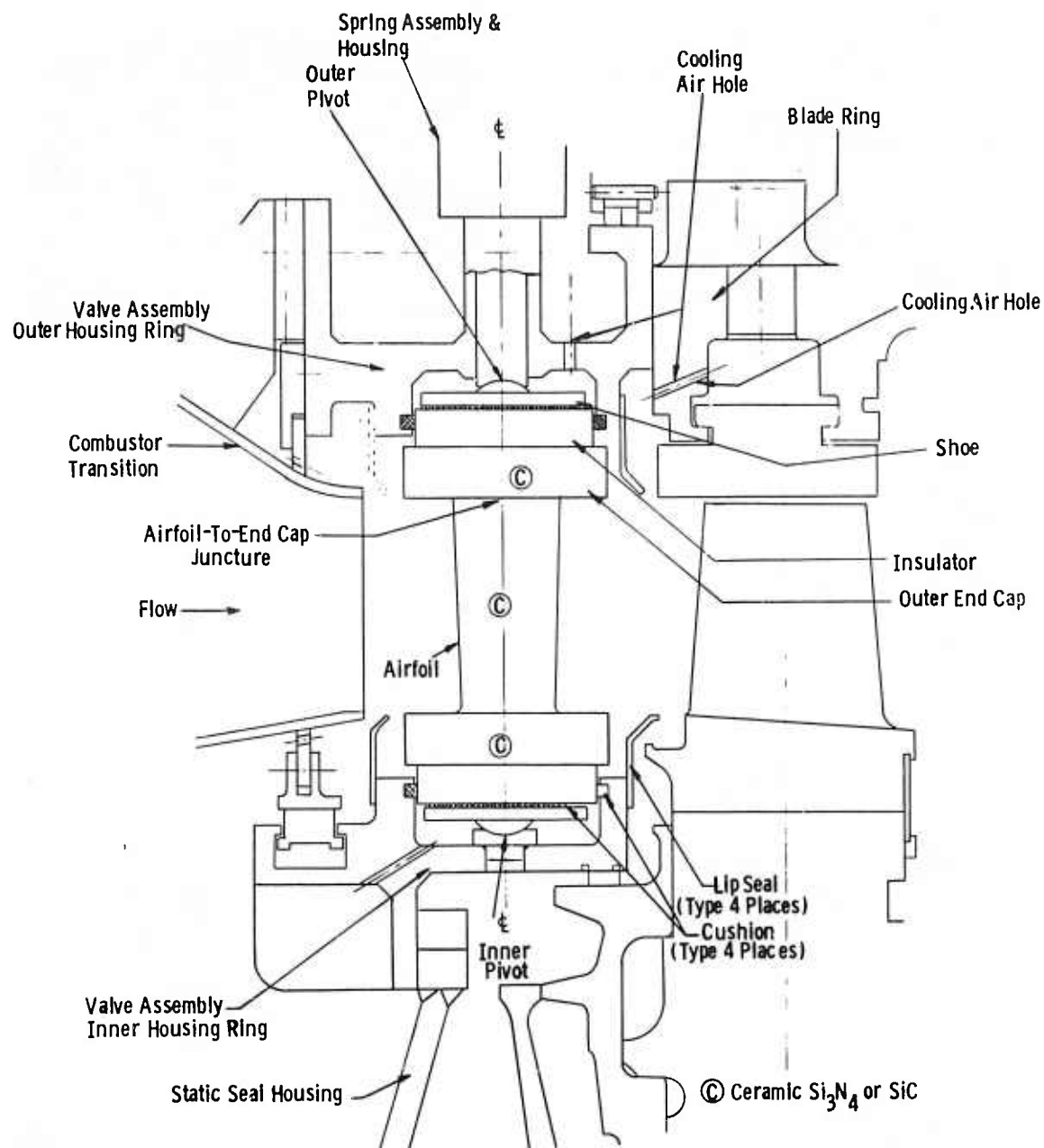
Figure 6.5   Three-Piece Ceramic Stator Vane with Insulator and Support Structure

2500°F Test Plan

Following 16 hours of mixer section insulation bake out at 1800°F, various steady state runs will be made with six aspirating thermocouple rakes to: (1) establish gas temperature profiles at 1200°F, 1800°F, 2000°F, and 2200°F, and (2) correlate rake temperature data with radiation pyrometer data and data from the three control thermocouples. Ramp rates will be established using the Veritrak Data Acquisition System. Critical metal parts, as monitored by thermocouples, will be observed for potential hot spot conditions.
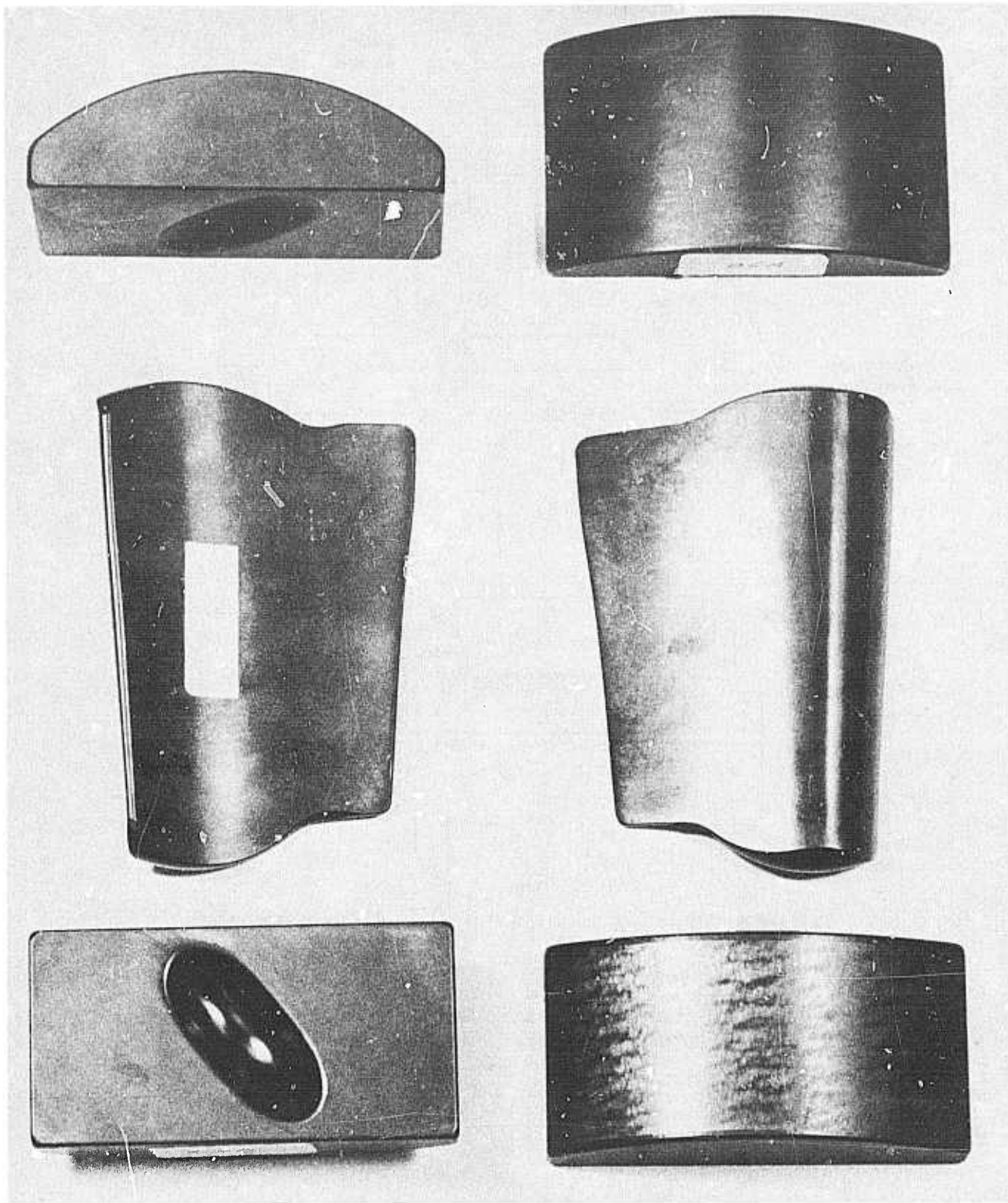
Figure 6.6   Third Generation Stator Vane Assembly Components

The following operating conditions are specified:

Airflow	:	31.5 lb/sec
Air Preheat Temperature:		600°F
Fuel Flow	:	0.85 lb/sec
Fuel Temperature	:	70°F
Shell Pressure	:	105 psig

After steady state calibration is complete, 100 transient thermal cycles similar to that shown in Fig. 6.7 will be run. The heat-up rate from 1200°F will be controlled at 10°F/sec. The 3 to 5 minute hold at 2500°F will permit data acquisition, vane viewing and/or photography through the boroscope. Cool down is represented by a ramp to 2000°F (from 2500°F), a 45 second hold to allow for vane maximum transient thermal stress decay, and controlled cooling from 2000°F to an idle temperature of 1200°F at 25°F/sec. The plan is to conduct the tests, 20 cycles at a time, with rig disassembly and check out of major components following each test segment. Prior to initial testing, critical airfoil-to-end cap contact (principally high spot) areas will be established and photographed using blueing and white spray powder techniques. At the end of the test program these contact areas will again be photographed to record the actual areas of contact. Based on prior experience with edge load type crack initiation this information will aid in post test analysis.
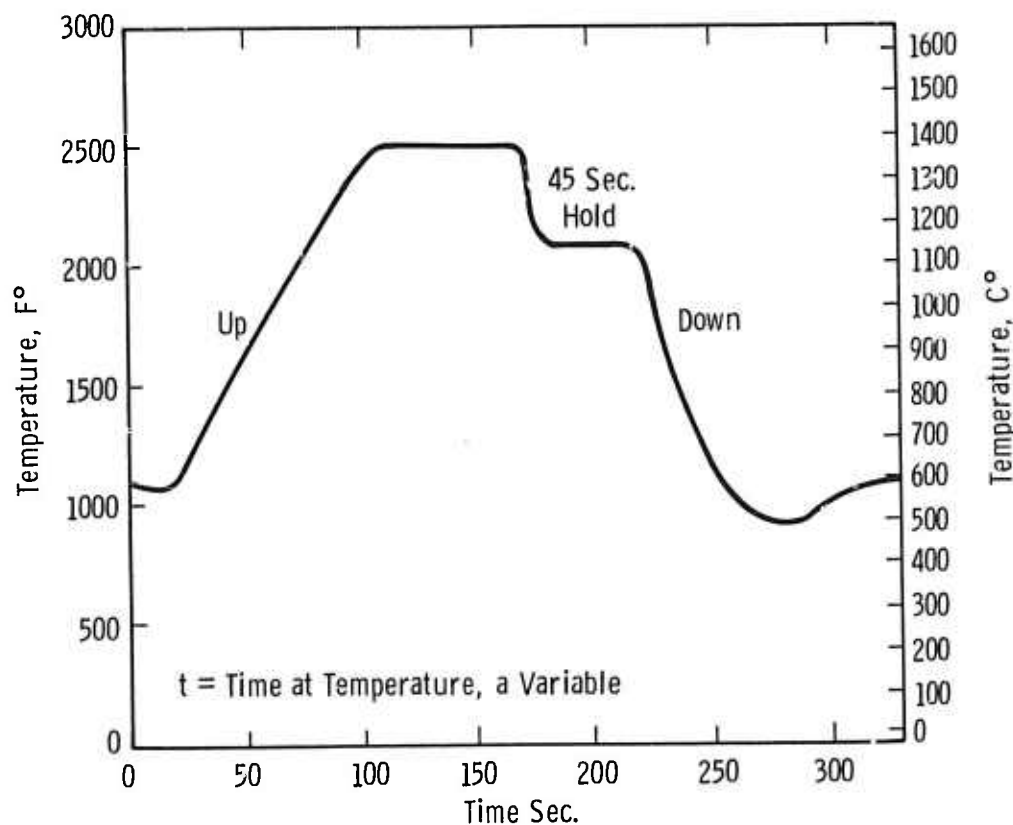
Figure 6.7   Proposed Cycle for Static Rig Tests at 2500°F

6.1.3 VANE FABRICATION

Introduction

The Norton Company continues as the sole source of hot-pressed materials for the fabrication of stator vane assemblies. Fourteen airfoils and twenty-two end caps, all part of the 100 stator vane set orders,[7] were manufactured for delivery during the report period. Unfortunate problems and mandatory rework made it impossible to start 2500°F static rig testing as scheduled.

Some difficulty has been encountered in the manufacture of Si_3N_4 billets hot-pressed with yttria. Billets containing 13.5 and $\sim$ 12.5 w/o Y_2O_3 were delivered, but these exhibited large low density areas. Norton was unable to press 16 w/o Y_2O_3 into billets exhibiting useful room temperature strength.

Static Rig Test Hardware

When the decision was made to test the tapered-twisted airfoil vane components in the static rig, Norton was contacted to expedite delivery of the test hardware. The activity was beset by difficulties, however. Ex Cello, the airfoil grinding subcontractor agreed to grind the tenon geometry after an original vendor was unable to perform the work. A drawing change increasing the tenon blend radius toward the trailing edge from 0.3 to 0.4 inches (Fig. 6.5) was required to make the work compatible with the machining process. Machine failure at Norton, made it necessary to locate an alternate machine shop to grind the end cap cavities on short notice. When planned procedures produced evidence of chatter on the 3 inch end cap radius and excessive diamond grinding wheel wear that operation had to be transferred to the Frank Cook Company, the original end cap machining vendor.

Fourteen airfoils and twenty-two end caps were delivered in May. Fluorescent dye penetrant techniques failed to disclose any cracks, chips or other serious surface defects on either airfoils or end caps. The 3 inch radius on the end caps had a somewhat mottled appearance reminiscent of a lapping operation in one direction which failed to remove all the evidence of coarser grinding marks in a direction normal to lapping (Fig. 6.6). Those end cap surfaces, however, did exhibit the 15 rms surface finish specified but the finish was not characteristic of the as-ground condition intended.

X-ray radiography revealed the airfoils to be remarkably free of internal indications or defects such as cracks, voids, or high and low density inclusions. Airfoils #16 and #17 were the only exceptions; 16 contained a single high density inclusion while 17 was cited for density variations. These airfoils will not be tested. End cap radiography produced a somewhat peculiar phenomenon best described as irregular light or dark lines in end caps #02A, 16B, 13B, 14B and 01A.

It is impossible to state whether these lines represent density variations at this time or to access the effect of significance of the indications with respect to component performance. Since eight vane sets must be selected in matched pairs some of these end caps must be

assembled for test. Great care will be taken to see whether the
indications influence test results.

Ultrasonic scanning did not disclose anything tangible in the way
of defects in any of the airfoils or end caps. There were, however,
areas of reduced back reflection at the large ends of airfoils #8, 9,
and 10. This phenomenon is not understood.

Westinghouse personnel first inspected the tapered-twisted
airfoil blanks for dimensional accuracy at Ex Cello in December 1975
when guillotine gauge tooling and the airfoil machining procedure was
reviewed, examined, and approved.[7] The only problem discussed at that
time was a non-linear trailing edge deviation at section AE (Fig. 6.8)
which appeared to be exaggerated because of variations in the trailing
edge blend radius.
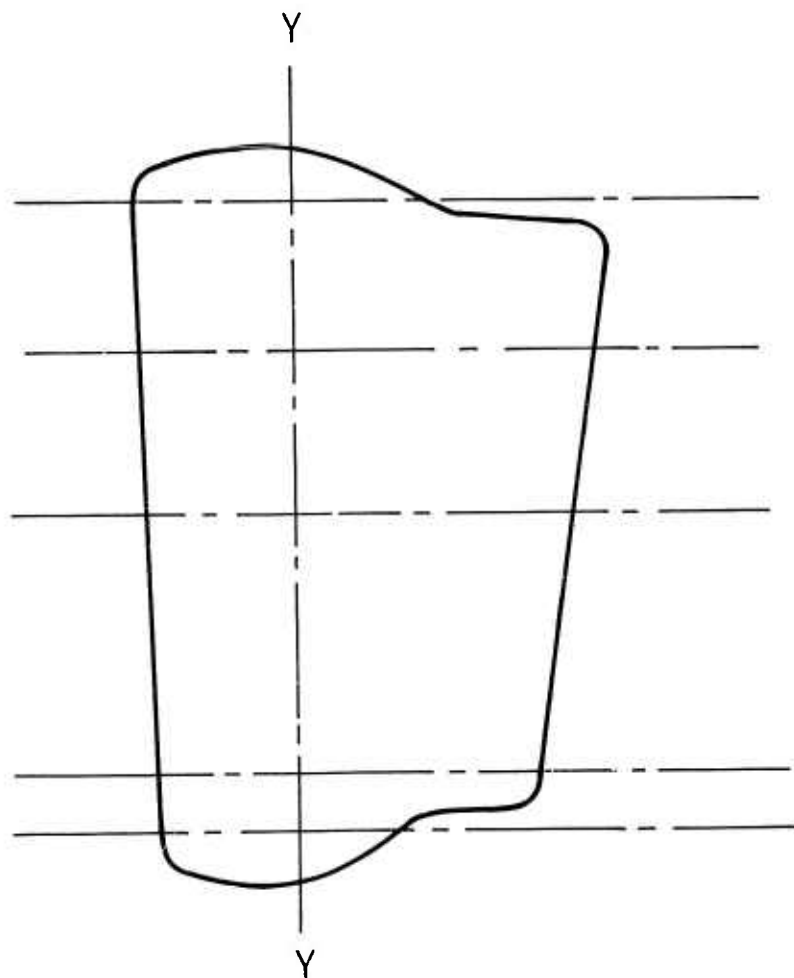
Figure 6.8   Tapered-Twisted Airfoil Drawing Showing Section Line
                  Positions

An airfoil blank was received at Westinghouse in January for more detailed examination. A plastic cast was made from the airfoil as shown in Fig. 6.9. The cast was machined on one end (nearest airfoil section AA-AA) for accurate location and alignment during inspection and actually sectioned by transverse slicing at each section location (AA-AA through AF-AF). Each cross-section was traced at 10X magnification for direct comparison with 10X Mylars. The results appear in composite Fig. 6.10 with the solid and dashed lines representing the Mylars and the section traces, respectively. The profile agreement is excellent attesting to the accuracy with which Ex Cello reproduced the airfoil. The center of the XX-YY axes (stacking axis of the airfoil) are also very accurate. The amount of taper and twist can be seen best when outer section AF-AF is superimposed upon inner section AA-AA (Fig. 6.11). Quality here is again excellent.

The only deviation worthy of comment appears to be variations in both the trailing and leading edge blending radii. For example, the trailing edge radius at section AE-AE (Fig. 6.10) is 0.030 or 0.020 inches too far inside the nominal whereas the trailing edge radius at section AC-AC is too small and outside the nominal. The non-linearity of the trailing edge discussed above is partially compensated for by the apparent error in section AE-AE which shortens the section. The Mylar reflects a drawing error in the actual trailing edge point location (too far out) which was originally identified on the airfoil drawings when second generation airfoils were machined. This defect in airfoil configuration is not expected to influence the mechanical performance of the airfoil in static rig testing at 2500°F. Its aerodynamic effect has not been assessed. Several radii appear as flats rather than true radii.

The first airfoil with the profiled, torroidal shaped tenon ends was received from Norton along with a prefinished inner and outer end cap set in early May. The end cap torroidal cavities were found to be within drawing tolerance with respect to radii, depth, location, and angularity.

The airfoil tenon end radii and shape were also within drawing tolerance. When end caps and airfoils were assembled, however, end cap misalignment approached 5° as shown in Fig. 6.12 indicating a serious error in airfoil tenon angularity. The maximum allowable misalignment, assuming that all angular tolerance build-up were to occur in the same direction, should not exceed 0° 50'. A machine set-up error had apparently occurred.

The specified angularities at the small and large ends of the airfoil are 36° ± 30' and 38° ± 30', respectively. When the airfoil tenon is machined the blank is placed in a shuttle with a 37° angle orientation built in. The shuttle is placed on a sine plate inclined 1° so that in one direction the total included angle is 37°-1° or 36° while 180° rotation of the shuttle produces 37° + 1° or 38°. In the original machine set up, the sine plate was inadvertently reversed to generate the 38° angle where the 36° angle was specified and 36° angle where the 38° angle was specified. Since the end cap cavities were machined correctly, 2° relative misalignment between an end cap and the airfoil occurred at each end when all elements of the stator vane assembly were put together.

114
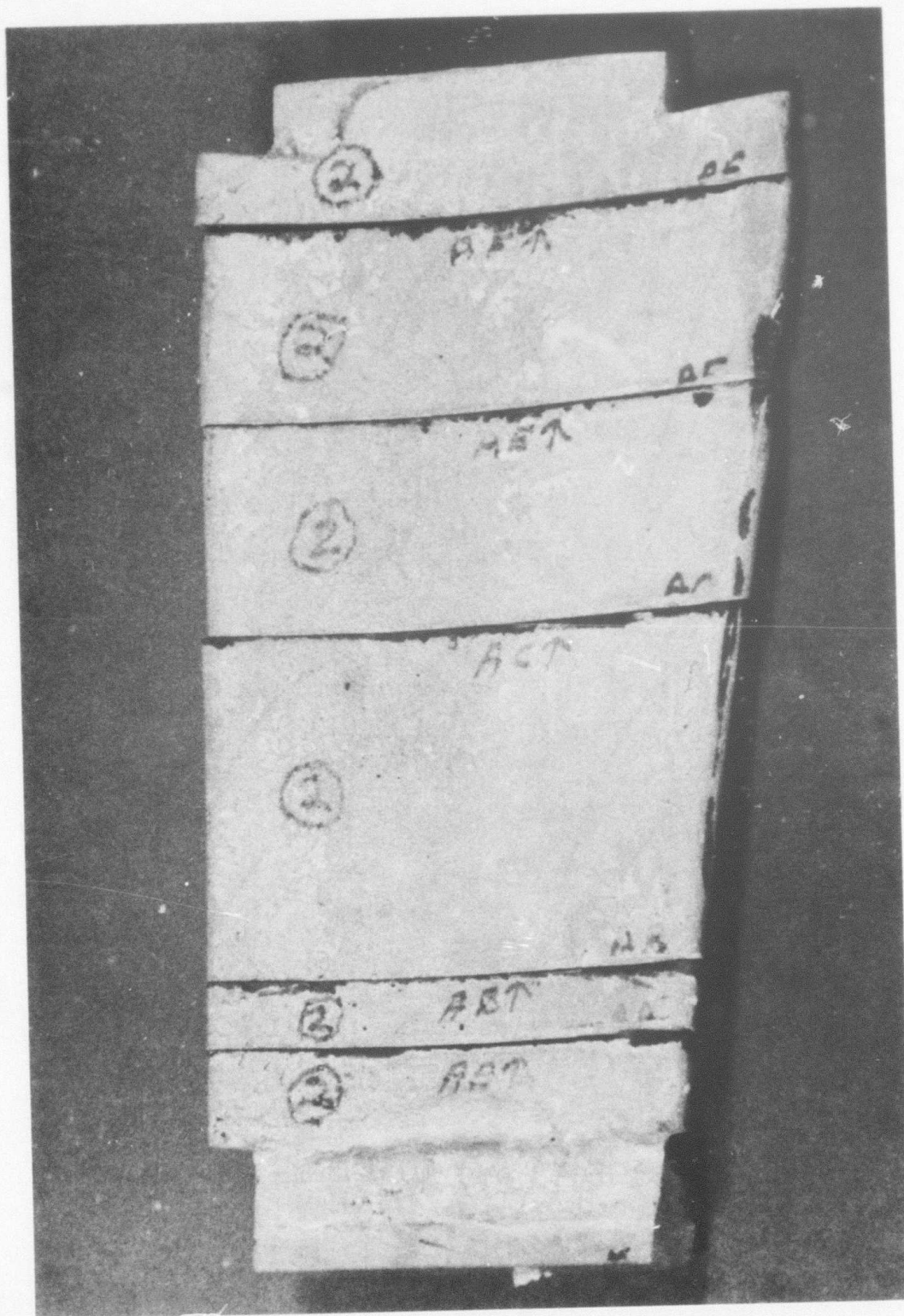
Figure 6.9   Sectioned Plastic Cast of Tapered-Twisted Airfoil Blank

115
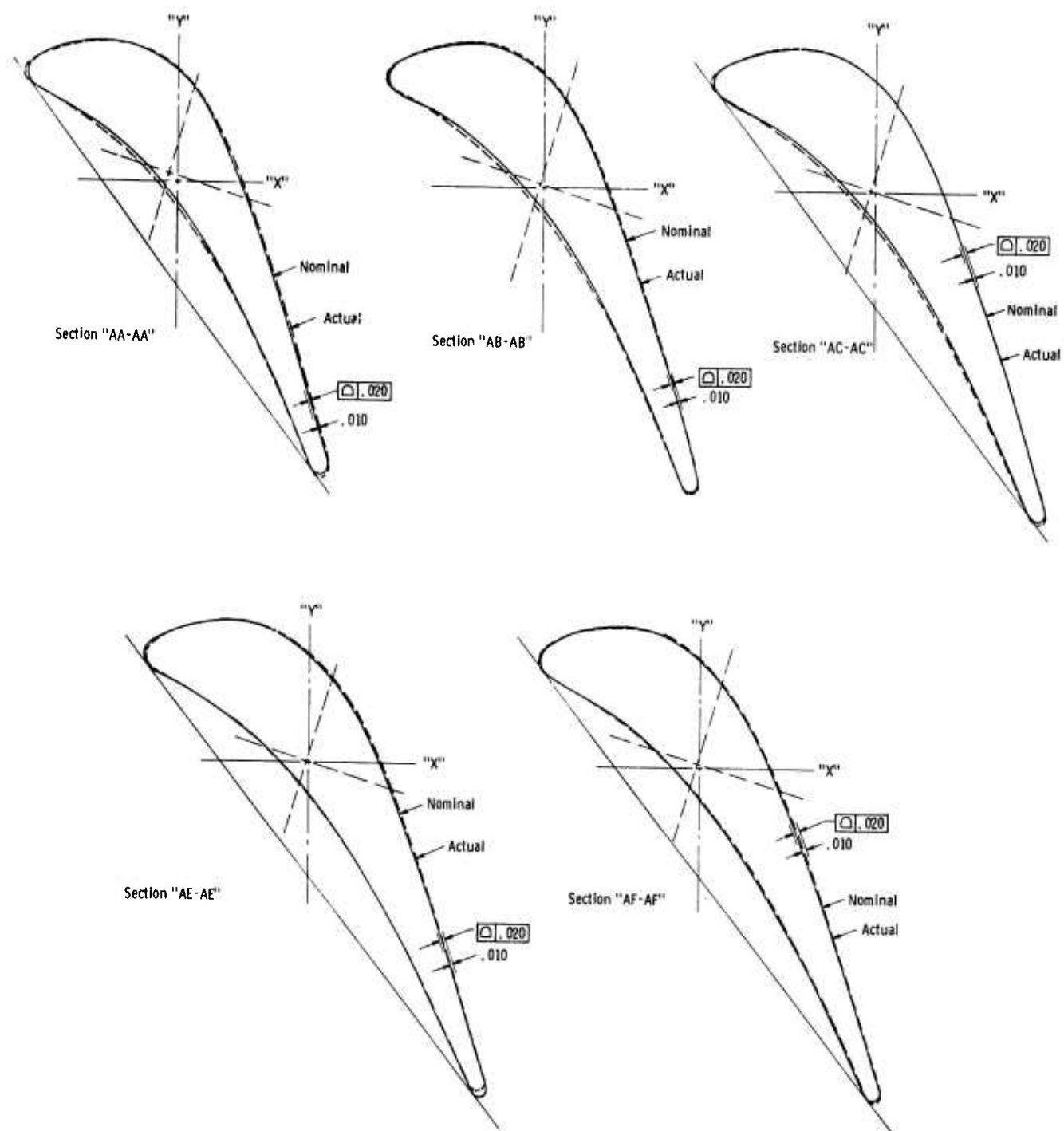
Figure 6.10   Section By Section Airfoil Inspection Record

116
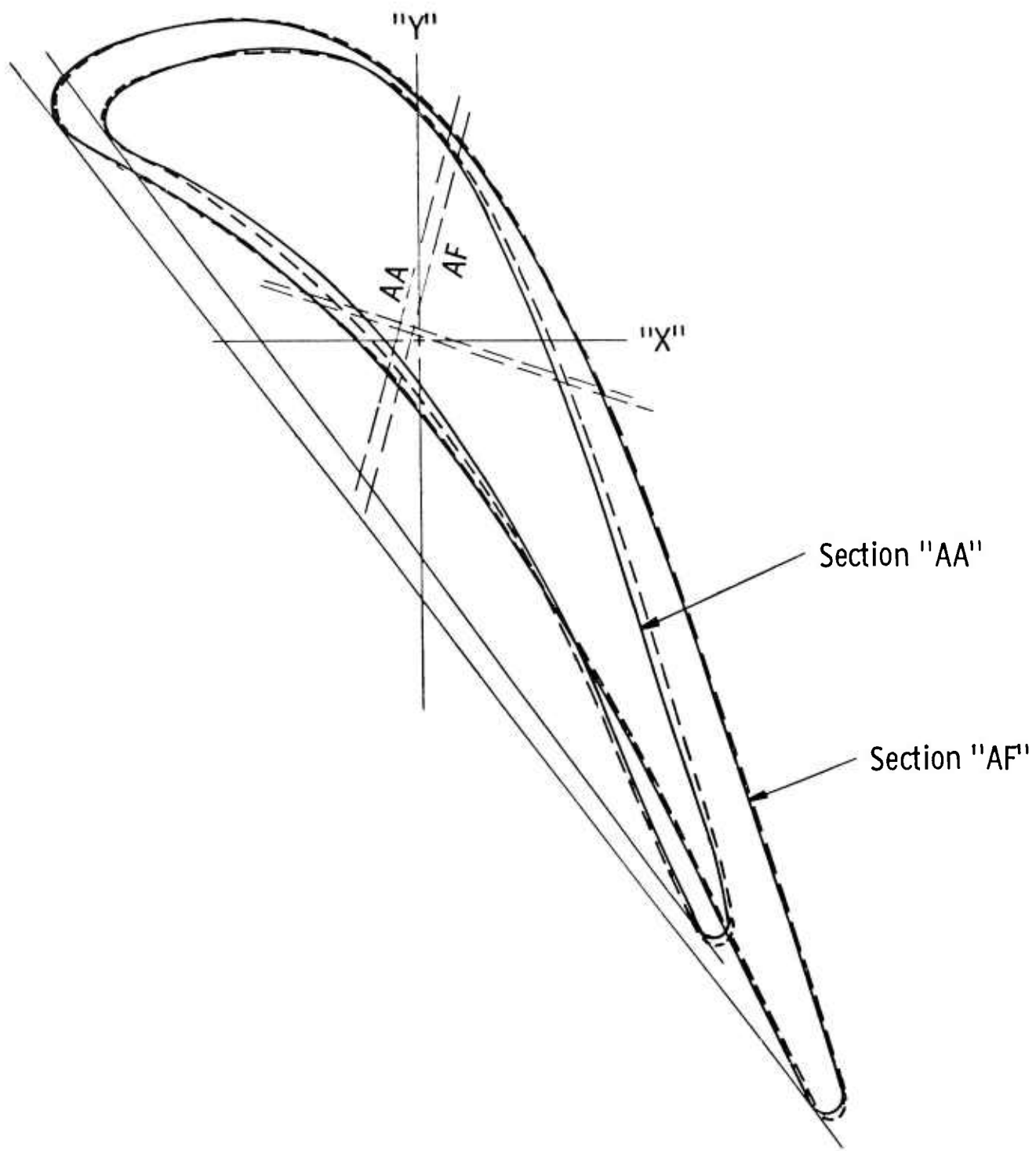
Figure 6.11   Airfoil Section Comparison Showing Typical Twist
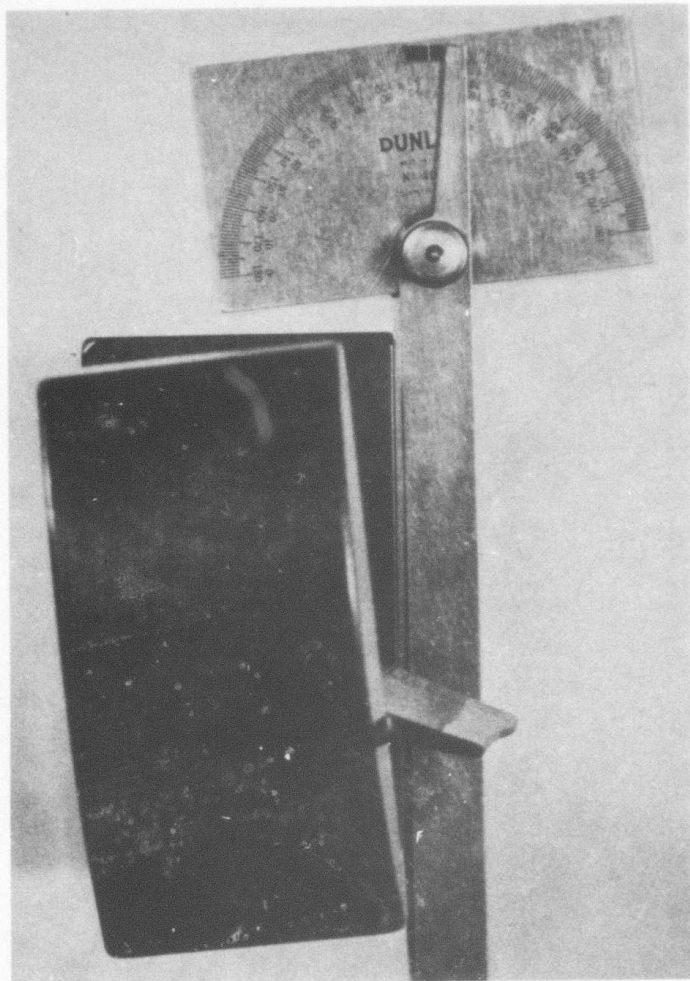
Figure 6.12   Effect of Airfoil Angularity Machining Error

Ex Cello was able to remachine the airfoil tenon ends by reshuttling all parts and removing only a few thousandths from each end. This was accomplished without decreasing the total airfoil length below tolerance. The properly aligned assembly is illustrated in Fig. 6.13.

A series of chatter rings were observed along the tenon surface when the airfoils were returned. These appeared as evenly spaced lines or high spots across the minor radius of the torroid at approximately 0.25 inch intervals or pitch. Experienced machinists estimated the amplitude of the undulating surface in angstroms or at most hundredths of a mil. Profilometer readings indicated that the band tolerance on the major torroidal radius did not exceed 0.00015 inches, however. An as-ground finish of 8 rms had been achieved on the tenon surfaces, the major surfaces of the airfoils were 12 rms. Measurements with a fixtured dial indicator and reference plate indicated a peak height of 0.0001 inches.

118
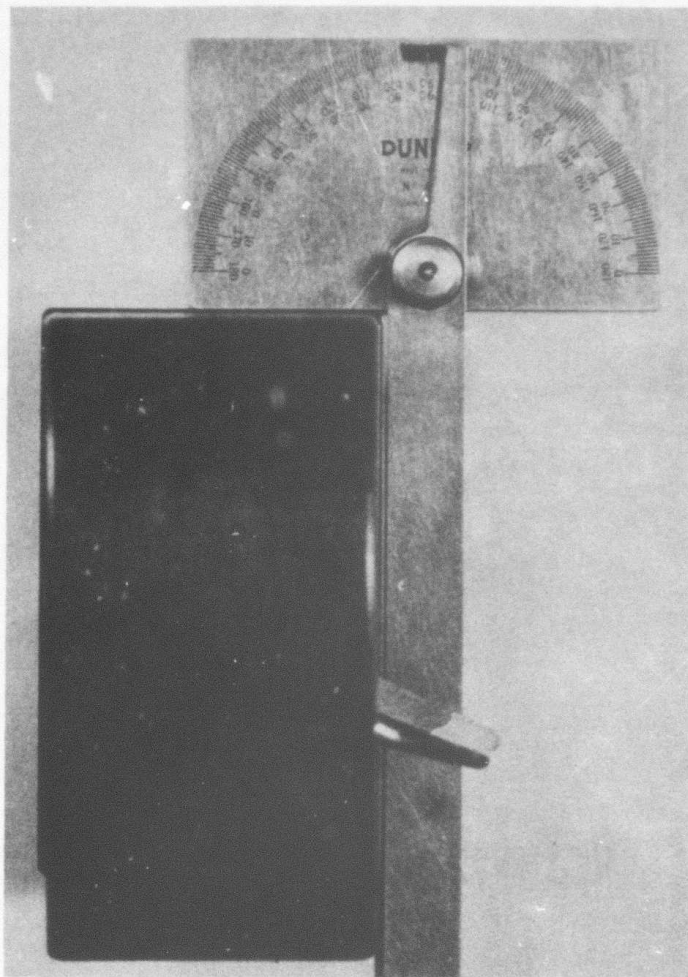
Figure 6.13   Correct End Cap to End Cap Orientation Resulting from
                Proper Airfoil Tenon Angularity

    The marks are typical of machined surfaces resulting from the
lightly loaded, high speed grinding operation which characterizes the
airfoil tenon clean up. When airfoils are mated with inner and outer
end caps as part of vane assembly, contact is established at these
high spots as shown by blueing and spray powder inspection techniques
(Fig. 6.14).

    The end caps were received in June, 1975 following inspection
at Norton Co. Several of these inspection procedures were witnessed
and accepted by Westinghouse in late May. Westinghouse verified the
inspection results. The end cap torroidal cavity major and minor radii
were finished to the maximum tolerance permitted. A surface finish
of 5 to 8 rms within the cavity area had been achieved by mechanical
lapping without disturbing cavity regularity and symmetry as specified.
The end cap edge contour radii, which are added by a hand operation,
were irregular especially around the periphery of the torroidal cavity.

119
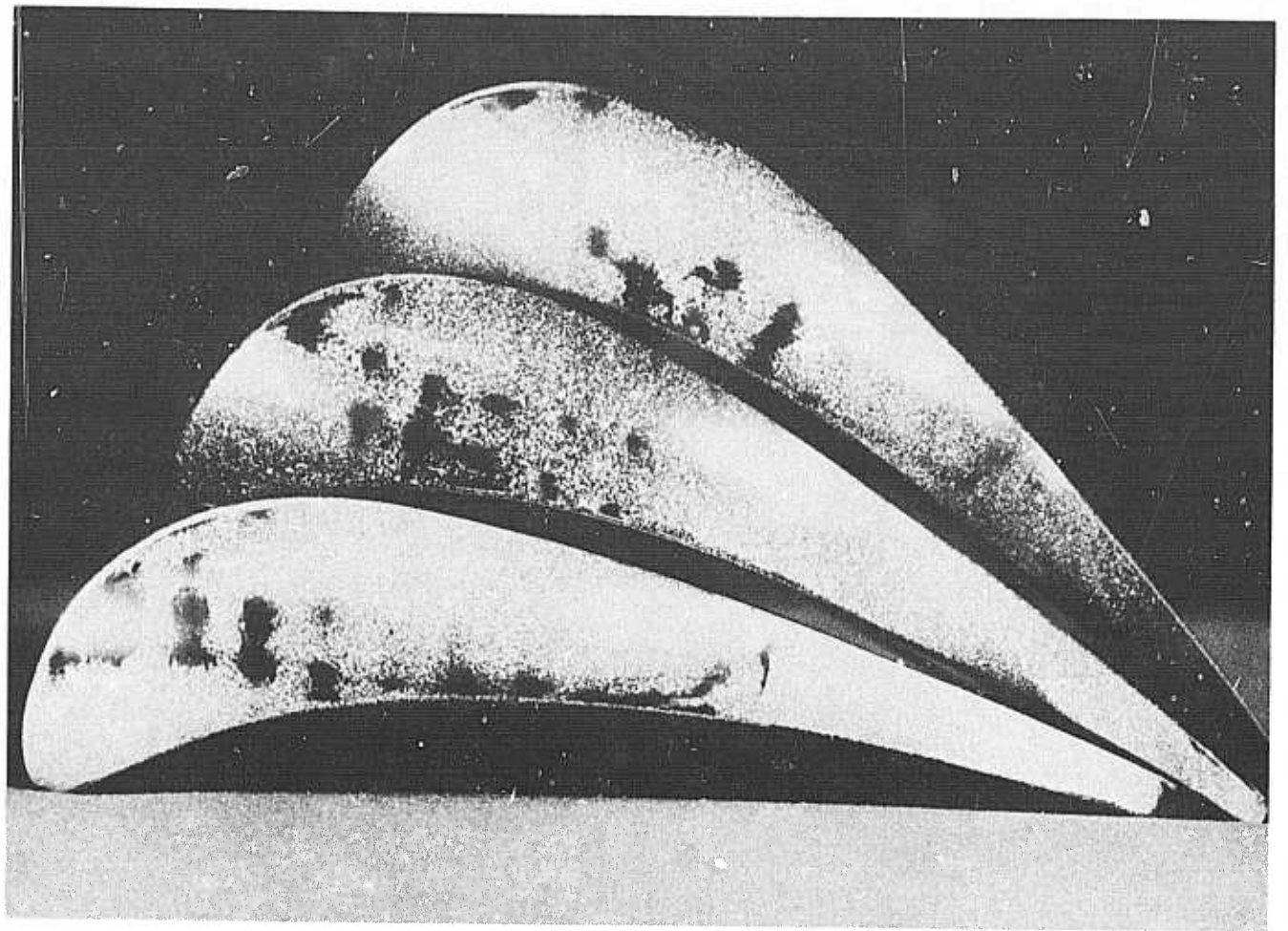
Figure 6.14   Blueing-Powder Display of Machine Chatter on Airfoil
                Tenon Surface

6.1.4 HEAT TRANSFER TESTS

Introduction

Heat transfer tests are required to establish reliable film heat transfer coefficients for accurate stress analysis. Two metal vane assemblies have been instrumented with thermocouples and strain gauges (on one vane only) to obtain temperature data during transients. Strain measurements are made for comparison with calculated strains to collaborate the results of stress analysis. Calibration has been completed and a test plan has been developed to acquire the desired data in the static rig at the conclusion of 2500°F ceramic vane testing.

Instrumentation

Twenty-three (23) locations on the airfoil surface and seventeen (17) locations on the outer end cap surfaces of the three-piece vane assembly were identified for the acquisition of temperature and strain information. One metal vane assembly has been instrumented with a high temperature thermocouple* at each location as illustrated in Fig. 6.15. The thermocouple lead wires are strapped and potted in grooves designed to minimize disturbances to the gas flow and heat transfer process itself.

A second metal vane assembly has been instrumented with thermocouples at twenty-one (21) locations only. High temperature strain gauges were placed at the nineteen locations remaining. Lead wires from the strain gauges are placed in grooves which terminate 0.250 inches from the gauge itself so as not to affect the measurement. The strain gauges are bonded in place with flame-sprayed aluminum oxide which is dressed to provide an aerodynamic shape which blends with the airfoil contour. The strain gauges used are of the wire type with dimensions approximately 0.250 in. long x 0.250 in. wide over a gauge length of 0.0625 in. These gauges were evaluated as the most reliable, most durable, and most stable gauge installations for measuring thermally induced strains up to 800°F over a distance (1/16 in.) that would make data comparisons with calculated strain values meaningful. It should be noted that the grain size of the vane material, Udimet 509, was measured to be approximately ASTM #5 (approximately 0.060 mm average characteristic length). A gauge can yield meaningful data by averaging the measurement over more than 10 grains. Strain measurements are converted to real strains by calibration. Each strain gauge was oriented to coincide with the greatest principal strain direction as calculated in previous analyses of ceramic vane assemblies to minimize measurement errors.

A small cantilevered beam specimen made of Udimet 500 was similarly instrumented with a single thermocouple and strain gauge to verify the supplier's application technique, to carry out the mechanical load-strain gauge calibration and to determine experimentally the maximum gauge excitation level at the maximum temperature in order to obtain the highest signal to noise ratio.

---

* The thermocouples are 0.040 in. diameter with mineral insulation. 0.040 in. Type "K" sheath wire with grounded measuring function provides long life (> 100 hours) up to 1850°F and may be used for short periods to 2300°F.
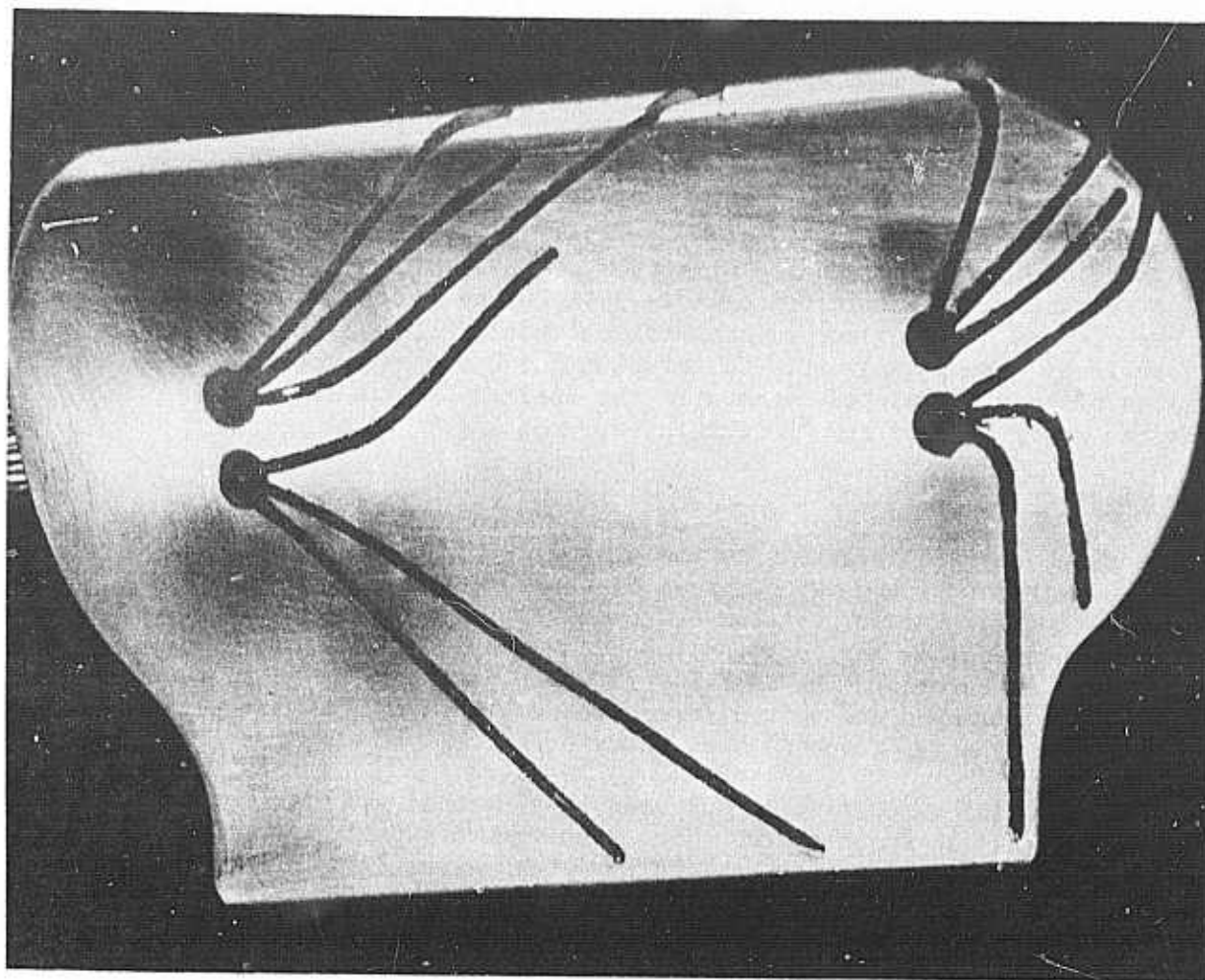
Figure 6.15   Thermocouple Instrumentation on Metal Airfoil for Heat
                Transfer Tests to 1800°F

Calibration

The vane assembly instrumented with both thermocouples and
strain gauges and the gauge calibration beam were placed in an electric
furnace with the assembly just resting on refractory bricks. The
cantilevered beam was fastened to a specially built rig which permits
mechanical loading from outside the furnace. The experimental set up
for calibration appears in Figs. 6.16 and 6.17 where the inside of the
furnace with instrumented parts and loading apparatus and the furnace
with data collection stations, respectively, are shown.

Steady state thermal strains were recorded at 100°F intervals
between 500°F and 800°F while the thermocouples readings, as checked
by furnace thermocouples, were used to indicate steady state conditions
in the furnace. Thus data were obtained to plot a calibration curve
for each strain gauge in the temperature range of interest. The elastic
strains caused by controlled loads on the cantilevered beam were recorded
at several temperatures for comparison with calculated values. All
data were collected in a manner consistent with that to be used for
static rig heat transfer tests.

Test Conditions

The optimum range and attainable increments have been determined for all variables affecting the transient temperature and strain distributions, within limits of static test rig capability, the data acquisition system, thermocouples, strain gauges, and vane assembly material capability. Temperature profiles, from previous static rig tests, indicate that vane locations three and five in the eight vane test cascade (as seen from upstream) experience similar temperature history. The hardware geometry at these locations should produce very similar flow conditions. The instrumented metal vanes will be positioned at vane locations 3 & 5. All rig modification have been made to accommodate the metal vanes with lead wires. The data logging system, including signal conditioners, is capable of recording forty signals every three seconds, in addition to the monitoring control thermocouples, a rate which establishes the steepest cooling ramp at which data may be gathered. The actual conditions for strain gauge and heat transfer tests are given in Tables 6.1 and 6.2. Heat transfer testing will be limited to 1850°F, the maximum useful service temperature of Udimet 500. Strain gauge tests, which will be performed first, will not exceed 850°F because of instrumentation limitations.
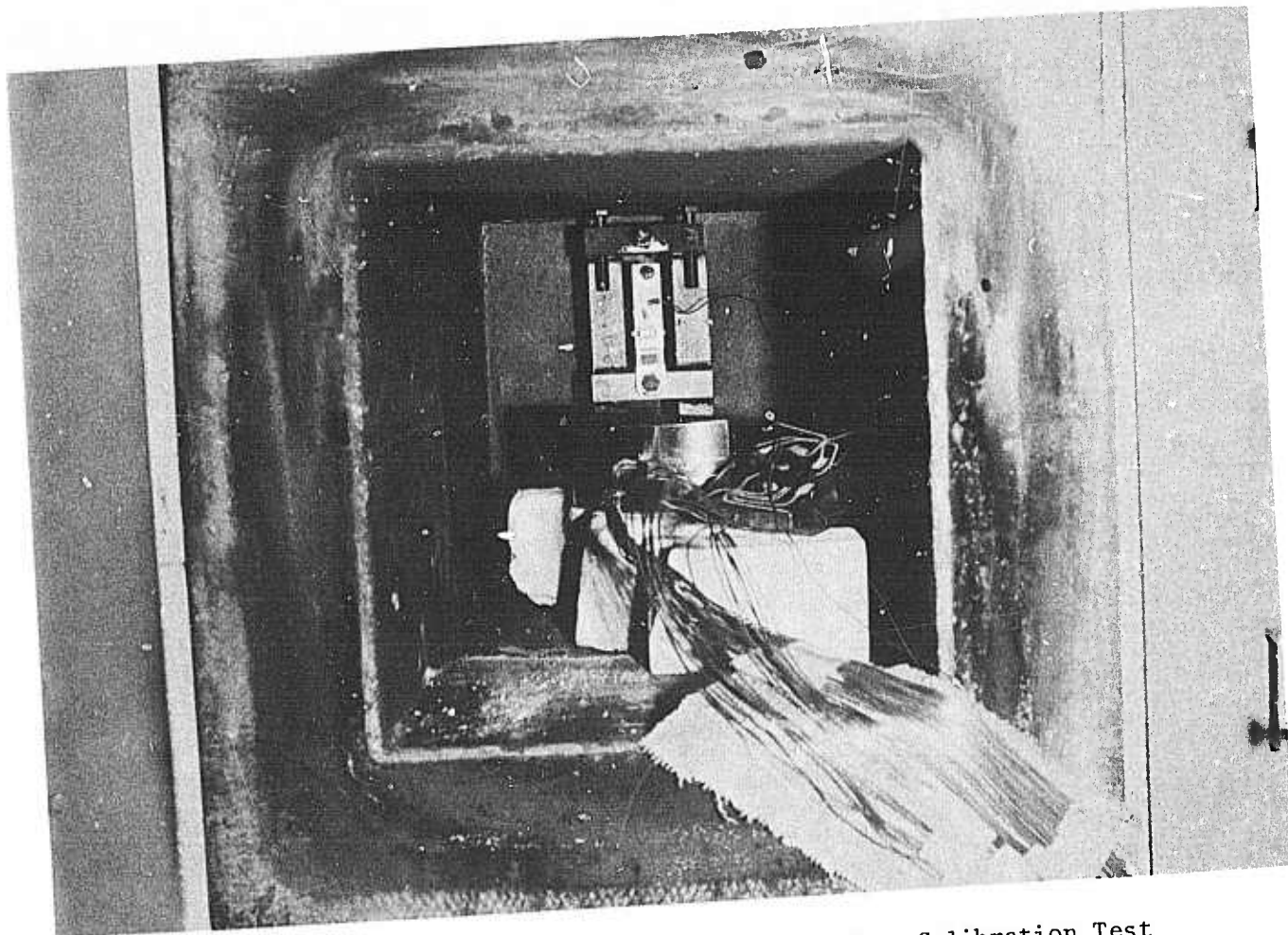
Figure 6.16   Instrumented Metal Vane Assembly Calibration Test
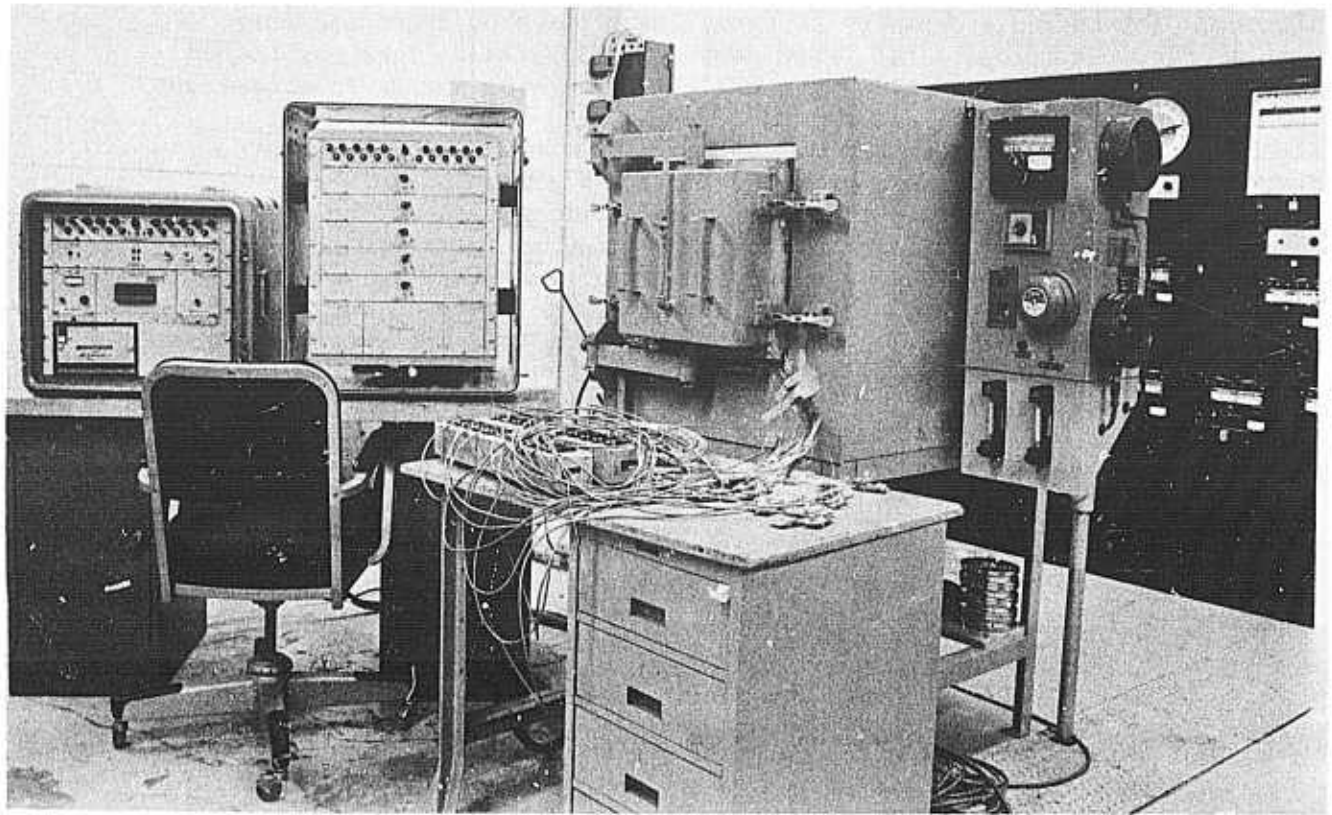
Figure 6.17   Laboratory View of Metal Vane Assembly Calibration
                Test and Equipment

TABLE 6.1

STRAIN GAUGE TEST

Test Conditions:

Air Flow	17.68 #/sec.
Fuel Flow	0.123 #/sec.
P_{shell}	45.7 psia
T_{shell}	230F
T_{exit}	730F
T_{peak}	850F

Test Configurations:

Fuel	Natural gas
Combustor Basket	Phase I configuration (2200F)
Exh. Temp. Con.	@ transition piece
Eliminate boroscope, pyrometers from the assembly	

Test Procedure:

1) Obtain steady state conditions - record initial values.
2) Flame-out.
3) Record the following data in the transient mode:
    Air Flow
    Shell Pressure
    Shell Temperature
    Strain Gauges
    Thermocouple Data
4) Repeat steps 1-3 for various "data" configurations
using 40 data points for each transient cycle.

Other:

Exhaust valve modulation for flame-out condition.
Flow area adjustments in transition piece, vane housing.

TABLE 6.2
STRAIN GAUGE HEAT TRANSFER TEST CONDITIONS

SS & GT Combustion Test # Strain Gauge/h-Test   Test Date

XL-1 Combustion Lab Rig # Ceramic Rig   Frame Size W-W251B

Combustor Configuration W251AA – Single Wall

Test Conditions: Run #	1	2	3	4	5	6
Run Description	S.G.		h-test	h-test	h-test	
Comb. Air Flow (pounds/sec)	17.68		11.72	19.55	31.30	
Comb. Simulation (ratio)	0.44		0.3	0.5	0.8	
Comb. Pressure P-6 (PSIG)	31.0		25.3	51.9	92.1	
Comb. Inlet Temp. T-4 (°F)	230.0		597.0	597.0	597.0	
Comb. Outlet Temp. T-14 (Mixer) (°F)	730.0		1600.0	1600.0	1600.0	
Air Flow Nozzle ΔP1-2 (H2O)	41.64		21.07	35.04	56.19	
9:1 Compressor Speed (RPM)	10,000		10,000	10,000	10,000	
9:1 3rd Stage Disch. Press. (PSIG)	36.0		30.0	58.90	102.59	
Air Flow Nozzle Press. P-1 (PSIG)	33.0		26.71	54.60	96.09	
Air Flow Nozzle Temp. T-1 (°F)	230.0		230.0	230.0	230.0	
Atomizing Air Press. (PSIG)	--		--	--	--	
Fuel Type	Nat. Gas		#2 Dis.	#2 Dist.	#2 Dist.	
Fuel Nozzle Size/Flow Capacity	W251B		170 GPH/80	170 GPH/80	170 GPH/80	
Fuel Nozzle Press. (PSIG)	50		63.45	158.03	364.2	
Fuel Flow (pounds/sec)	0.1237		0.1969	0.3284	0.5258	
Fuel Flow (gallon/hour)	--		105.01	175.14	280.44	
Comb. Temp. Rise (T14-T4) (°F ΔT)	500		1003	1003	1003	
Fuel/Air Ratio	0.007		0.0168	0.0168	0.0168	

Air Flow Nozzle: $G = 13.42 \sqrt{P\ \Delta P/T}$ $G = 54.82 \sqrt{P\ \Delta P/T}$

$\Delta P = H_2O$ $\Delta P = PSI\ \Delta P$

7. PROGRESS ON MATERIALS TECHNOLOGY-STATIONARY TURBINE PROJECT

7.1 MATERIALS ENGINEERING DATA

SUMMARY

In the stationary turbine project, commercially produced hot-pressed silicon nitride and silicon carbide have been under intensive investigation so that physical, mechanical, and thermal property data would be available to the design engineers and stress analysists, as required. This work is expected to continue throughout the program in order to up-date properties as material improvements evolve and to verify billet properties. The latter helps assure reliability of test components fabricated from the hot-pressed billets. This section deals with this continuing acquisition of property information.

Tensile testing of hot-pressed silicon nitride continued with emphasis on test modification and improvement. A new method of testing has evolved using powder support of the tensile specimen to obtain excellent alignment through the load train without using 3 to 9 strain gauges per specimen/test.

Norton NC-132 silicon nitride and NC-203 silicon carbide have been oxidized at 2500°F up to 4000 hours in air in a muffle furnace. Significant strength degradation was observed even after the first 100 hours of exposure. The flexural strength of silicon nitride was reduced to 30% of room temperature values after ∿ 100 hours. Loss of strength in silicon carbide is significant but far less dramatic.

Experimental billets of Si_3N_4 hot-pressed with yttria have been evaluated. Flexural strength at 2550°F approach 90,000 psi. Oxidation resistance at 2500°F also appears to be excellent. The material exhibited outstanding creep properties at 2550°F as compared to commercial NC-132 Si_3N_4 material. Non-uniform porosity was observed in the billet material. A low temperature phase instability apparently associated with $Si_3N_4 \cdot Y_2O_3$ in the microstructure at 1800°F led to material degradation.

7.1.1 TENSILE TESTING

Introduction

Load train alignment in uniaxial tensile testing has been accomplished by mechanical adjustment to reduce the differential strain indications within the gauge length of a specimen to 3% at room temperature.[2] It is possible to reduce the non-uniform stress distribution through the use of a powder cushion between the heads of a tensile specimen and each respective grip in a method that is self-aligning. The powder effectively transfers the load between grip and specimen by permitting the specimen to seat itself thereby insuring full area and uniform contact with the grips.

Experimental

A button-head tensile specimen 5.50 inches in length, with a 2.00 inch long, 0.250 inch diameter reduced gauge section was machined from 304 stainless steel. The gauge length of the steel specimen was instrumented with three EA-03-5000B-120 strain gauges at the center, 120° apart. Three EA-06-062AB-120 strain gauges were also attached at each end. The strain gauges were bonded to the specimen with an m-bond 20.0 adhesive.

The gripping arrangement is shown in Fig. 7.1. The split-seat, the key to this gripping device, is a diametric, split cylinder with a well for powder at one end and a tapered hole at the other end. The purpose of the tapered hole is to center the specimen and to keep the powder contained within the well, while providing sufficient angular precision ($\sim 7°$) of the button-head specimen around the axis of the split-seat.

The powder-cushion grip is assembled by first slipping the lower-grip end over the button head and then placing the split-seat within the lower-grip end. Keeping the button head above this arrangement, powder is loaded into the well of the split head with the aid of an eye-dropper. The button-head is frequently lowered to slightly tamp the powder. When the well contains a sufficient amount of powder, the specimen is seated and the upper-grip end is screwed into position.   A portion of the tensile loading train is then screwed into the upper-grip end to temporarily secure the specimen and powder. The specimen is turned upside down and this procedure is repeated to attach on the other end of the specimen. Contrary to expectations, the slightly tamped powder does not spill from either end of the split-seat while assembling the grips.

The instrumented specimen-grip assemblage was placed in a tensile load train consisting of one stationary end and one knife-edge fixtured end. No unusual care was taken to align the two ends of the load train. The specimen was loaded in increments of 100 lbs to 500 lbs and then in increments of 500 lbs to 1500 lbs. to keep within the elastic range of the steel specimen. After zeroing the strain gauges initially at zero load, strain measurements were made at each load increment. After completing each experiment, the specimen was disassembled from the grips; reassembly with fresh powder constituted a new test.

Testing was performed by two different operators using two different Satec universal testing machines. Table 7.1 describes eight different powders used in the demonstration.

128
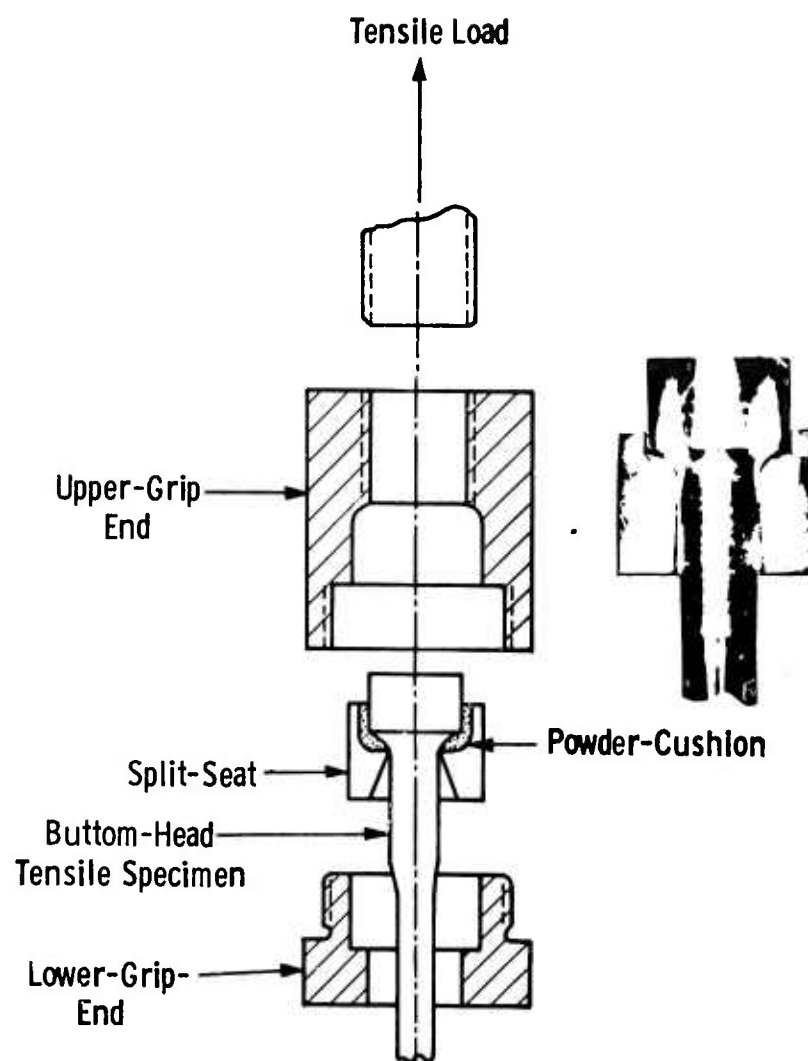
Figure 7.1   Powder Cushion Tensile Test

TABLE 7.1

DESCRIPTION OF POWDERS

POWDER	INTERNAL CODE	DESCRIPTION (Particle Size, etc.)
Nickel	Ni	Spherical particles, average 20 μm dia.
Silicon Carbide	SiC-280	Average 44 m
Silicon Carbide	SiC-1500	Average 9 m
Silicon Carbide	SiC-EK	Average 5 m
Silicon Carbide	SiC-PPG	submicron, 15 m^2/g
Tungsten Diselenide	WSe_2	- 100 mesh
Boron Nitride	BN	- 325 mesh
Graphite	G	- 325 mesh

Data Analysis

A vector analysis was used to define the resultant strain for each set of three strain gauges. The amount of misalignment at each set of gauges was calculated by dividing the absolute value of the resultant strain by the average strain of the three gauges:

$$\% \text{ misalignment} = 100x \frac{\sqrt{\varepsilon_1^2 + \varepsilon_2^2 + \varepsilon_3^2 - (\varepsilon_1\varepsilon_2 + \varepsilon_1\varepsilon_3 + \varepsilon_2\varepsilon_3)}}{1/3 (\varepsilon_1 + \varepsilon_2 + \varepsilon_3)}$$

A measure of the stress non-uniformity within the specimen's gauge length was obtained at each load increment by dividing the difference between the highest and lowest values $(\varepsilon_H - \varepsilon_L)$ of the nine strain gauges by their average value (ε_{AV}):

$$\% \text{ non-uniformity} = \frac{\varepsilon_H - \varepsilon_L}{\varepsilon_{AV}} \times 100 .$$

Summary of Results

Graphite and boron nitride formed the most effective powder cushions with graphite considered superior to boron nitride. Fig. 7.2 a,b,and c and Fig. 7.3 a,b, and c, report the results of eight experiments with graphite and three experiments with boron nitride, respectively. Error bars are used to indicate the highest and lowest values obtained. Closed circles represent mean values. Table 7.2 summarized typical results for the other six powders.

In general, the percentage misalignment and the percentage stress non-uniformity decrease with increasing load. For most cases, loads < 500 lbs (corresponding to < 10,000 psi) produced poor alignments. The shaded areas in Figs. 7.2 and 7.3 represent the suggested working range
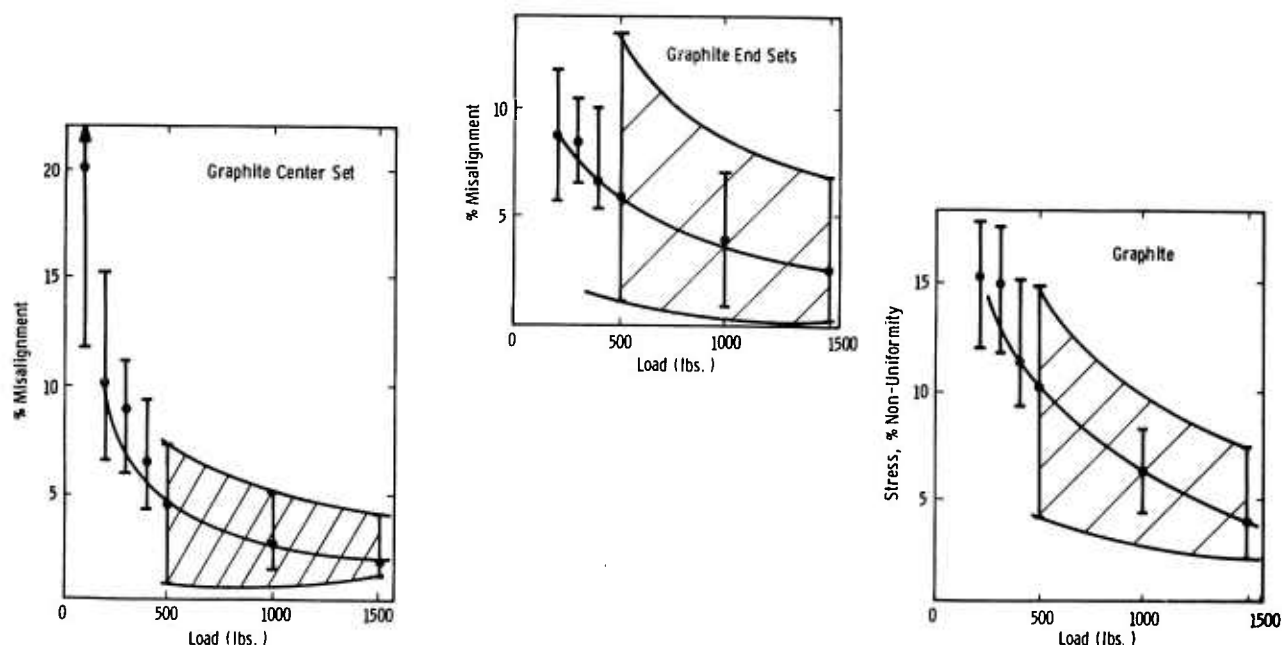
Figure 7.2   Effect of Graphite Powder in Powder Cushion Tensile Test

for graphite and boron nitride powders, respectively. Because all nine
strain gauges were considered in the analysis of stress uniformity, the
stress non-uniformity was higher relative to misalignment values obtained at
each gauge section. Better alignments and less data scatter were obtained
in the center of the gauge length than at the ends.

A correlation between the resultant strain vectors at each of the
three gauge sections showed that the axis of most specimens were parallel
to but not perfectly concentric with the loading axis.
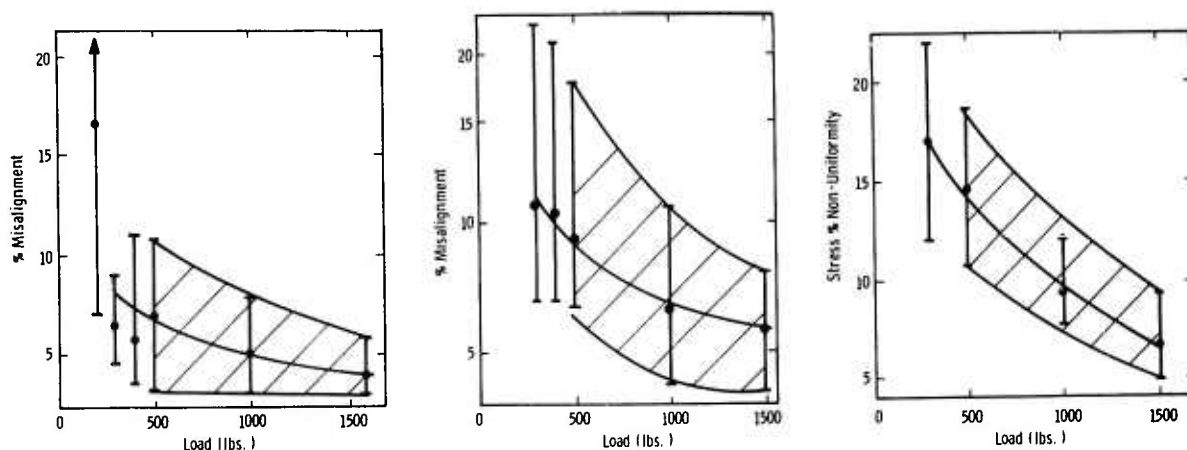
Figure 7.3   Boron Nitride Powder Performance in Powder Cushion
Tensile Test

TABLE 7.2

POWER PERFORMANCE IN UNIAXIAL TENSILE TESTS

POWDER	LOAD (lb)	MISALIGNMENT AT CENTER (%)
Ni (3)*	500	34 to 75
SiC - 280 (1)	1000	23
SiC - 1500 (1)	1000	9
SiC - EK (6)	1000	0 to 45
SiC - PPG (5)	1000	9 to 55
WSe$_2$ (4)	1000	0.9 to 9

*
( )   indicates number of tests

131

Discussion

Experience gained at Westinghouse strongly suggests that the powder-cushion gripping technique represents a simple and effective method for minimizing alignment problems in uniaxial tensile tests within the prescribed load range. The data reported show that similar or better alignment can be achieved using graphite powder cushions relative to other techniques* that require precisely machined specimens, gripping, and load train components.[8,9]

The simplicity of the powder-cushion technique is its main advantage. Since the powder forms a mold of both the specimen head and the grip surfaces while transferring the load, neither surface requires precise machining. This is a principal advantage when machining and testing ceramics. The second advantage is that specimen alignment occurs in the grips; i.e., alignment does not depend on load-train components.

Lubricating powders such as graphite, boron nitride and tungsten diselenide appear more effective in distributing load relative to other types of powder. Although this was generally found through trial and error, other powder characteristics such as particle size, size distribution, material compliance, deformability, etc., also appear to be important. For example, better alignments may be achieved at lower loads with either low compliance (e.g., polyethelene) or deformable (e.g., lead or indium) powders than those obtained with graphite.

Where the alignment is maintained within 3% the error due to bending is reduced below 1500 psi, thus improving the accuracy of the method to ± 3500 psi. The method is definitely recommended for ceramic materials and will be used to acquire additional test data for improved material systems.

---

* It should be noted that a conservative analysis was used to determine misalignments as compared with those reported for other alignment techniques, e.g., if the data reported here were analyzed using the technique described by Jones, et al.,[1] they would be reduced by ∿ 1/2.

132

7.1.2 EFFECT OF LONG-TERM OXIDATION ON THE STRENGTHS OF HOT-PRESSED SILICON NITRIDE AND SILICON CARBIDE

Introduction

Norton's hot-pressed Si_3N_4 and SiC materials were oxidized at 2500°F for different periods of time ranging up to 4,000 hrs in static air and 1 atm pressure, to determine the effect of long-term oxidation on mechanical properties. After oxidation, the flexural strengths were measured both at room temperature and at 2300°F, under conditions of 4-point loading using a strain rate of 0.002/min.

Results of Long-Term Static Tests

The flexural strengths of Si_3N_4 after different periods of oxidation are plotted in Fig. 7.4. The room temperature strength of unoxidized Si_3N_4 is in the range of 75 to 120 ksi. When tested at room temperature, strength of oxidized specimens falls off rapidly as a result of the first few hundred hours of oxidation. Minimum strength values of 35 ksi are reached after 1000 hours of oxidation. The dotted lines in Fig. 7.4 represent a statistical uncertainty of $\pm$ 10 ksi in the strength data. Similar reductions in the room-temperature strength of reaction bonded Si_3N_4 has been reported in the literature. The affect is attributed to the cracking of the oxide layer on cooling from oxidation temperature to room temperature.
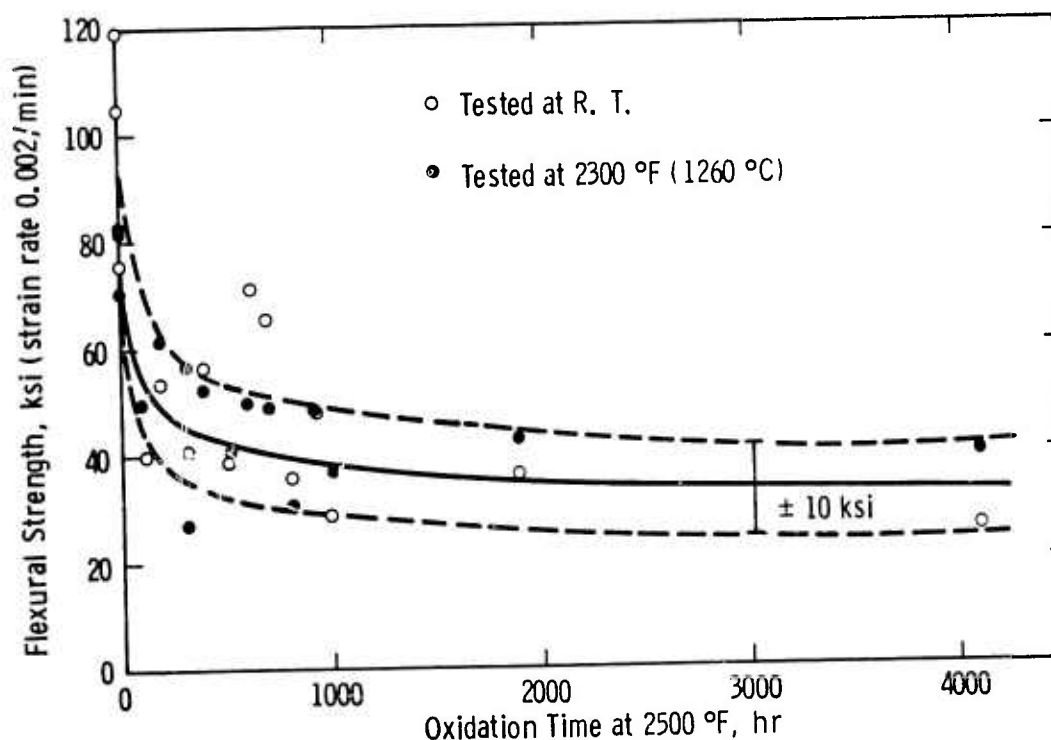
Figure 7.4   Effect of 4000 Hour Oxidation at 2500°F on The Flexural Properties of Norton NC-132 Silicon Nitride

The 2300°F strength of hot-pressed Si_3N_4 (Fig. 7.4) is also affected by time dependent oxidation. Both the RT and 2300°F flexural strength data fall within a similar scatter band. This reduction in strength is apparently caused by surface degradation occurring during oxidation. Degradation is evident in the surface appearance of the Si_3N_4 specimen shown in Fig. 7.5 after 4096 hrs of oxidation at 2500°F, both before and after removing the surface oxide. The specimen surface is characterized by microcavities which become visible when the oxide is removed. These microcavities are formed when $MgSiO_3$, the predominant oxidation product at temperatures above 2200°F, chemically dissolves Si_3N_4 from the surface. This phenomenon is more clearly illustrated in Fig. 7.6, where scanning electron micrographs of the fracture surface of an oxidized Si_3N_4 specimen appear. The fracture origin is indicated in the top micrograph. The area is magnified in the bottom micrograph. Energy-dispersive analysis indicates that $MgSiO_3$ forms a cavity on the surface as shown by the bottom micrograph. These microscopic cavities or pits act as fracture origins to produce reductions in strength. The effect on strength is strongly dependent on the temperature of oxidation. As reported earlier[3], no effect on strength was observed for Si_3N_4 exposed to pressurized hot combustion gases at 2000°F for up to 250 hrs. Since the degradiation in strength appears to be related to the formation of $MgSiO_3$, and since $MgSiO_3$ does not become the predominant oxidation product until about 2200°F, the degradation in strength by long term oxidation should not occur at oxidation temperatures lower than 2200°F. The actual oxidation temperature, above which the effect on strength becomes significant, is being determined experimentally at present.

The strength of hot-pressed SiC after different periods of oxidation at 2500°F is shown in Fig. 7.7. The room temperature strength is reduced somewhat compared to that of unoxidized specimens, due to the cracking of the oxide layer on cooling from oxidation temperature to room temperature. However, the 2300°F strength remains fairly stable even after 4000 hours of oxidation. The oxide formed on SiC is predominantly SiO_2 which developed as a very smooth surface layer (Fig. 7.8). This smooth oxide layer does not cause any surface degradation and the flexural strength, therefore, remains fairly constant.

Dynamic Corrosion-Erosion Tests

The pressurized turbine test passage was completely relined with reaction-sintered Si_3N_4 pre-forms for operation at 2500°F. Norton's hot-pressed Si_3N_4 and SiC, and an experimental Westinghouse Si_3N_4 hot-pressed with 20% Y_2O_3 were tested. After 50 hours of exposure to hot combustion gases at 2500°F, 3 atm pressure and 500 fps gas velocity, Norton's Si_3N_4 and SiC exhibited a net erosion loss on the surfaces identical to that reported previously.[4] These tests will continue for a total period of 250 hours.

Si_3N_4 with 20% Y_2O_3 developed cracks after 50 hours of oxidation. Yttria pressed silicon nitride material exhibits thermal instability at temperatures in the 1800°F range, apparently due to the instability of the $Y_2O_3 \cdot Si_3N_4$ and $Y_5O_{12}N$ phases in oxidizing ambience. This problem has been solved by choosing certain compositions in the $Si_3N_4 \cdot Y_2O_3 \cdot SiO_2$ ternary phase system.
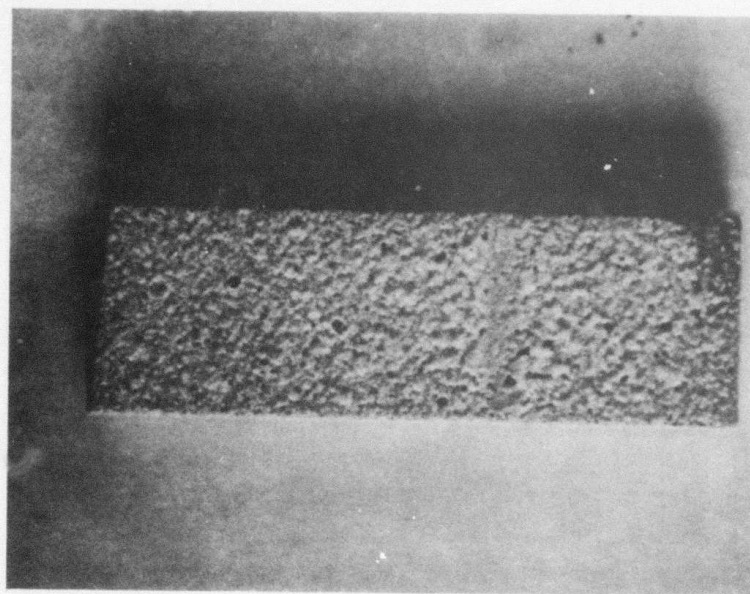
5 X
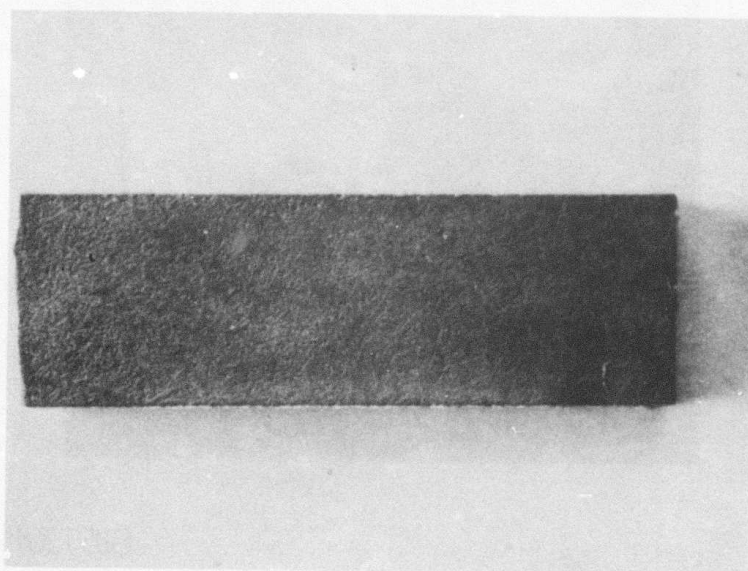
Figure 7.5   Surface Appearance of Si_3N_4 Specimen After 4096 Hours of
Oxidation at 2500°F Before (Top) and After (Bottom)
Removal of The Oxide
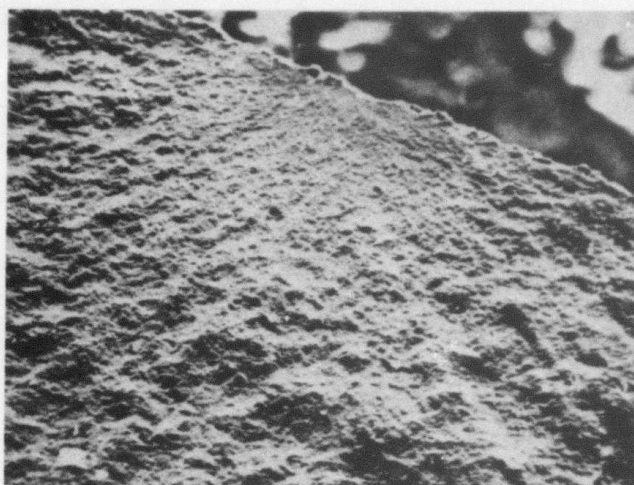
(105 X)
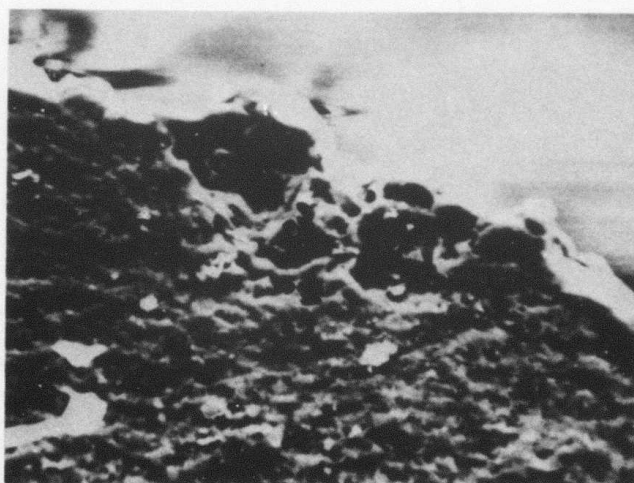
(1050 X)

Figure 7.6   SEM Microgaphs of Fracture Surface of Norton NC-132
Si_3N_4 Oxidized 625 Hours at $2500^\circ F$
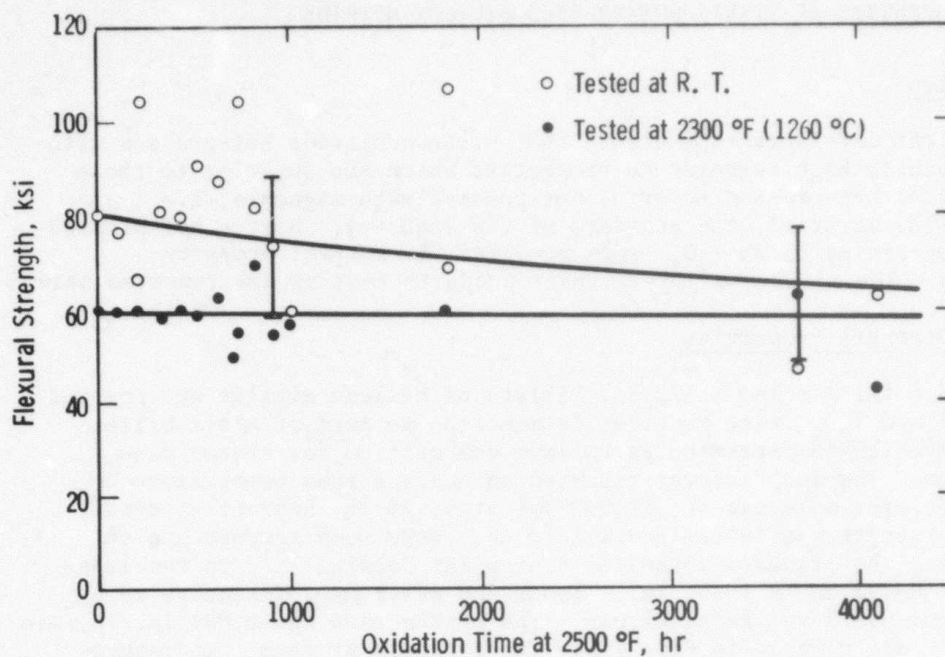
Figure 7.7   Effect of Static Oxidation at 2500°F on The Flexural Strength of Norton NC-203 SiC

Optical Picture (6x)
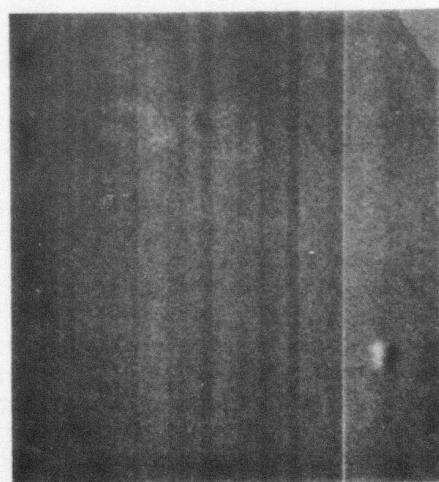
Scanning Electron Micrograph (5000x)

Figure 7.8   Surface Appearance of a SiC Specimen Oxidized for 1203 Hours at 2500°F

137

7.1.3 PROPERTIES OF YTTRIA HOT-PRESSED SILICON NITRIDE

Introduction

Recent developments indicate that silicon nitride hot-pressed with yttria exhibits high temperature properties which are superior to those of commercial hot-pressed material hot-pressed with magnesia; i.e., Norton NC 132 material, the standard of the industry. Norton hot-pressed billets containing 13.5% Y_2O_3 were received for initial property evaluation. The results of preliminary property testing are reported here.

Flexural Strength Properties

Two 6 in. x 6 in. x 1/2 in. billets of silicon nitride hot-pressed with 13.5 w/o Y_2O_3 were received from Norton as part of a six billet order from which to determine an optimum composition for stator vane fabrication. The manufacturer reported an average room temperature strength for the material of 141000 psi at 98.2% of theoretical density. Flexural strength was determined within the range room temperature to 2550°F using the standard method of four point loading [2]. on specimens 0.250 in x 0.125 in. x 1.125 in. Inner and outer span distances were 0.375 in and 0.875 in., respectively. The strain rate was 0.001 in./in./min. The results are plotted in Fig. 7.9. The strength at room temperature tends to confirm Norton data. The high temperature flexural strength is excellent although some low values were recorded at 1800°F.

The strength degradation at 1800°F was confirmed by subsequent tests which indicate poor oxidation resistance for the material at that temperature. When oxidized at 1800°F for 100 hours, the silicon nitride hot-pressed with yttria expanded 8% due to cracking. Strength had degraded to the point where specimens failed upon loading. The problem is attributed to a $Si_3N_4 \cdot Y_2O_3$ phase within the material which appears to be very susceptible to oxidation. At higher temperature, the oxidation resistance of $Si_3N_4 \cdot Y_2O_3$ is superior to NC 132. This is apparently due to the development of an SiO_2 layer which protects the substrate. At 1800°F a sufficient SiO_2 forms as a layer to protect the material from internal oxidation of the $Si_3N_4 \cdot Y_2O_3$ phase.

An incremental flexural creep experiment was run to assess the relative creep and stress rupture properties of the $Si_3N_4 \cdot 13.5 \ Y_2O_3$ at 2552°F. The results appear in Fig. 7.10. The creep behavior as indicated here is vastly superior to NC 132 at similar test temperatures under similar conditions. These data are not intended to imply an equivalent creep strength in the tensile mode, however, The specimen tested is small, a 0.25 in x 0.125 in x 1.125 in rectangular bar loaded in the four point bending mode and the incremental aspect of the test may affect the test results. Norton reported an 80 hr stress rupture life at 45000 psi outer fiber stress, for a material of similar composition. The steady state creep rate was 5×10^{-4} in./in./hrs. on a 1.5 in. x 0.125 in. x .125 in. specimen in the four point, quarter point bending mode.
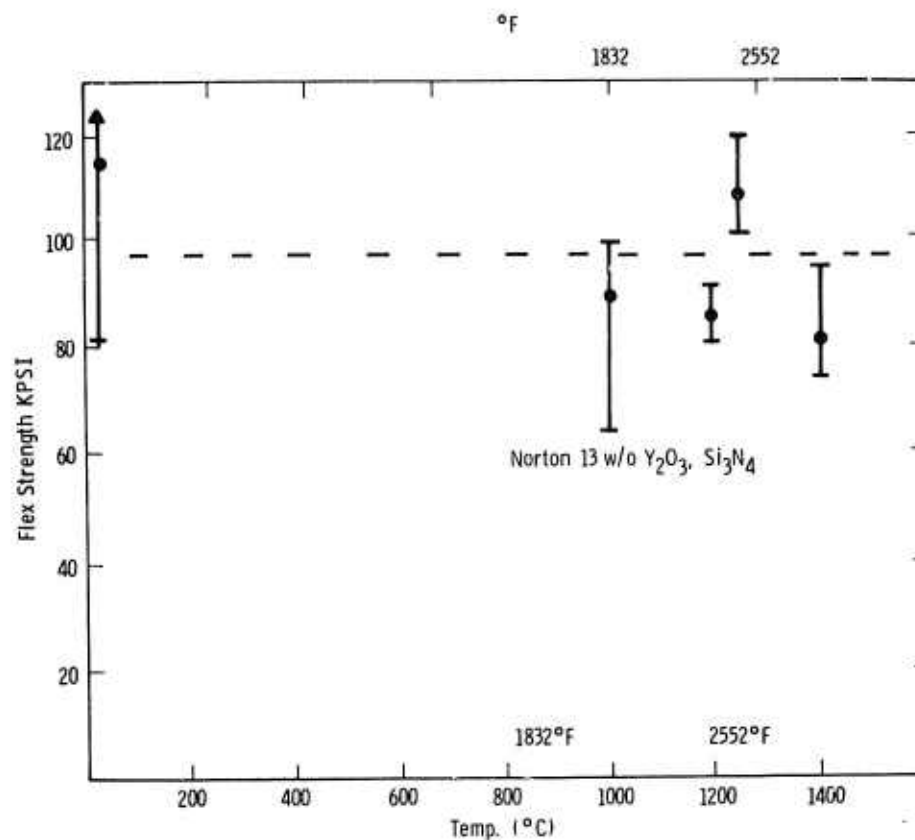
Figure 7.9   Flexural Strength of Silicon Nitride Hot-Pressed with Yttria
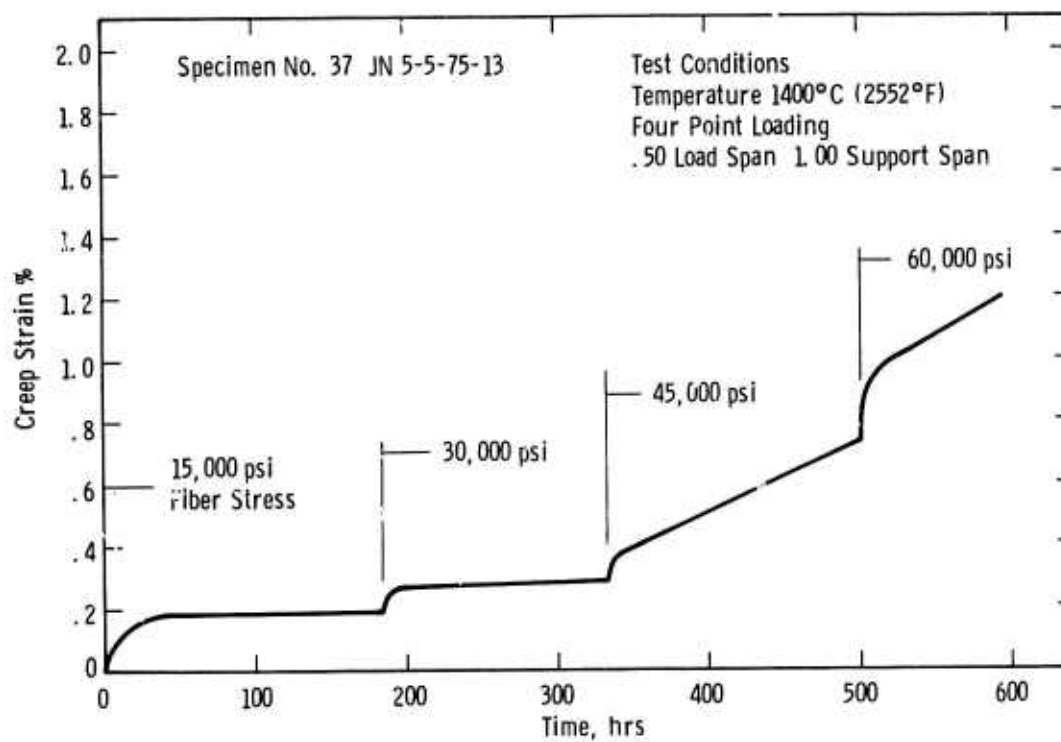
Figure 7.10   Flexural Creep Properties of Silicon Nitride Hot-Pressed with Yttria

8. REFERENCES

1. McLean, A. F., Fisher, E. A., Harrison, D. E., "Brittle Materials Design, High Temperature Gas Turbine". AMMRC-CTR-72-3, Interim Report, March, 1972.

2. McLean, A. F., Fisher, E. A., Bratton, R. J., "Brittle Materials Design, High Temperature Gas Turbine". AMMRC-CTR-72-19, Interim Report, September, 1972.

3. McLean, A. F., Fisher, E. A., Bratton, R. J., "Brittle Material Design, High Temperature Gas Turbine". AMMRC-CTR-73-9, Interim Report, March, 1973.

4. McLean, A. F., Fisher, E. A., Bratton, R. J., "Brittle Materials Design, High Temperature Gas Turbine". AMMRC-CTR-73-32, Interim Report, September, 1973.

5. McLean, A. F., Fisher, E. A., Bratton, R. J., "Brittle Materials Design, High Temperature Gas Turbine". AMMRC-CTR-74-26, Interim Report, April, 1974.

6. McLean, A. F., Fisher, E. A., Bratton, R. J., "Brittle Materials Design, High Temperature Gas Turbine". AMMRC-CTR-74-59, Interim Report, September, 1974.

7. McLean, A. F., Fisher, E. A., Bratton, R. J. Miller, D. G., "Brittle Materials Design, High Temperature Gas Turbine". AMMRC-CTR-75-8, Interim Report, April, 1975.

8. McLean, A. F., Fisher, E. A., Bratton, R. J. Miller, D. G., "Brittle Materials Design, High Temperature Gas Turbine". Interim Report September, 1975.

9. Katsanis, Theodore: "Fortran Program for Calculating Transonic Velocities on a Blade-to-Blade Stream Surface of a Turbomachine". NASA TN D-5427, 1969.

10. McNally, William D.: "Fortran Program for Calculating Compressible Laminar and Turbulent Boundary Layers in Arbitrary Pressure Gradients". NASA TN D-5681, 1970.

11. Zienkiewicz, O. C., "On the Principle of Repeatability and its Application in Analysis of Turbine and Pump Impellers", International Journal for Numerical Methods in Engineering, Volume 4, pp 445-452 (1972).

12. Oyama, Y., "Solid Solution in the System Si_3N_4 - Ga_2O_3 -Al_2O_3", Japanese J. Appl. Phys., $\underline{12}$, pp 500-508 (1973).

13. Jack, K. H. and Wilson, W. I., "Ceramics Based on the Si-Al-O-N and Related Systems", Nature Physical Sciences $\underline{238}$, pp 28-29 (1972).

14. M.H. Jones, R.T. Bubsey, G. Succop and W.F. Brown, Jr., J. of Testing and Evaluation, JTEVA $\underline{2}$ [5], 378, (1974).

15. M.H. Jones and W.F. Brown, Jr., JTEVA $\underline{3}$ [3], 179 (1975).

ARMY MATERIALS AND MECHANICS RESEARCH CENTER
WATERTOWN, MASSACHUSETTS 02172

TECHNICAL REPORT DISTRIBUTION

No. of Copies	To
1	Office of the Director, Defense Research and Engineering, The Pentagon, Washington, D.C. 20301
12	Commander, Defense Documentation Center, Cameron Station, Building 5, 5010 Duke Street, Alexandria, Virginia 22314
1	Metals & Ceramics Information Center, Battelle Memorial Institute, 505 King Avenue, Columbus, Ohio 43201
2	Dr. James I. Bryant, Office of the Chief of Research, Development and Acquisition, ATTN: DAMA-CSS, The Pentagon, Washington, D.C. 20310
1	Commanding Officer, Army Research Office (Durham), Bx CM, Duke Station Durham, North Carolina 27706 ATTN: Dr. H. M. Davis
2	Commanding General, U.S. Army Material Command, Washington D.C. 20315 AMCRD-TC (Dr. El-Bisi) ANCDL (Dr. Dillaway)
1	Commanding General, U.S. Army Missile Command, Redstone Arsenal, Alabama 35809 ATTN: Technical Library
4	Commanding General, U.S. Army Tank-Automotive Command, Warren, Michigan 48090, ATTN: AMSTA-BSL, Research Library Br, ATTN: AMSTA-RKM (Mr. C. Green), ATTN: AMSTA-RGR (Mr. Engel), ATTN: AMSTA (Dr. Banks)
1	Commanding General, U.S. Army Weapons Command, Research and Development Directorate, Rock Island, Illinois 61201, ATTN: AMSWE-RDR
1	Commanding Officer, Aberdeen Proving Ground, Maryland 21005, ATTN: Technical Library, Building 313
1	Commanding Officer, U.S. Army Aviation Material Laboratories, Fort Eustis, Virginia 23604
1	Librarian, U.S. Army Aviation School Library, Fort Rucker, Alabama 36360 ATTN: Bldg. 5907
1	Commanding Officer, USACDC Ordnance Agency, Aberdeen Proving Ground, Maryland 21005 ATTN: Library, Building 350

TECHNICAL REPORT DISTRIBUTION

No. of Copies	To
1	U.S. Army Air Mobility Research and Development Laboratory ATTN: J. White, Assistant Technical Director, Eustis Directorate, Ft. Eustis, Virginia 23604
1	U.S. Army Air Mobility Research and Development Laboratory ATTN: R. Berrisford, Chief, Structures Division, Eustis Directorate, Ft. Eustis, Virginia 23604
1	U.S. Army Air Mobility Research and Development Laboratory ATTN: T. Coleman, Director, Langley Directorate, Langley Research Center, Langley Field, VA 23365
2	U.S. Army Air Mobility Research and Development Laboratory ATTN: J. Accurio, Director, Lewis Directorate, NASA, Lewis Research Center, 21000 Brookpark Road, Cleveland, Ohio 44135
1	Commanding General, U.S. Army Aviation Systems Command, ATTN: R. Long, Deputy Director RD&E, P.O. Box 209, St. Louis, MO 63166
1	Office Chief Research & Development, Department of Army, ATTN: Col. J. Barnett, Physical & Engineering Sciences Division, Washington, D.C. 20315
1	Commanding General, Army Missile Command, ATTN: AMCDL, Webb Taylor, 5001 Eisenhower Avenue, Alexandria, VA 22304
1	Commanding General, Army Missile Command, ATTN: AMCRD-F, J. Beebe, Washington, D.C. 20315
1	Office, Chief Research & Development, Department of the Army, ATTN: R. Ballard, Physical & Engineering Sciences Division, Washington, D.C. 20315
1	Commander, USA Foreign Science & Technology Center, ATTN: AMXST-SD3, Mr. C. Petschke, 220 7th Street NE, Charlottesville, VA 22901
1	Mr. Irving Machlin, High Temperature Materials Div., Materials and Processes Branch, (NAIR-52031D), Naval Air Systems Command, Department of the Navy, Washington, D.C. 20360

TECHNICAL REPORT DISTRIBUTION

No. of Copies	To
1	Commanding Officer, U.S. Army Engineer Waterways Experiment Station, Vicksburg, Mississippi 39180 ATTN: Research Center Library
4	Commanding Officer, U.S. Army MERDEC, Fort Belvoir, Virginia 22060
	ATTN: STSFB-EP (Mr. Frank Jordan)
	STSFB-EP (Mr. W. McGovern)
	AMCPM-FM (Mr. Allen Elkins)
	AMXFB-EM (Mr. George F. Sams

Director, Army Materials and Mechanics Research Center, Watertown, Massachusetts 02172

2	ATTN: AMXMR-PL
1	AMXMR-PR
1	AMXMR-CT
1	AMXMR-AP
1	AMXMR-X (Dr. Gorum)
1	AMXMR-EO (Dr. Katz)
2	AMXMR-TM (Dr. Lenoe)
2	AMXMR-D (Dr. Priest)
1	AMXMR-EO (Dr. Messier)
2	AMXMR-P (Dr. Burke)
1	AMXMR-MS (Mr. MacDonald)
1	AMXMR-E (Dr. Larson)
1	Lt. Col. E. E. Chick

Advanced Research Projects Agency, 1400 Wilson Blvd., Arlington, Virginia 22209

2	ATTN: Director
1	Dep Director
1	Director of Materials Sciences - Dr. Stickley
1	Dep. Director Materials Sciences - Dr. van Reuth
1	Tech. Information Office - Mr. F. A. Koether

1	Mr. R. M. Standahar, Office of the Director of Defense, Research and Engineering, Room 3D1085, Pentagon, Washington, D.C. 20301
1	Mr. Charles F. Bersch, Department of the Navy, Naval Air Systems Command, Washington, D.C. 20360
1	Dr. A. M. Diness, Metallurgy Branch, Code 471, Office of Naval Research, 800 N. Quincy Street, Arlington, Virginia 22217
2	U.S. Army Air Mobility Research and Development Laboratory, Advanced Systems Research Office, Ames Research Center, Moffett Field, California 94035 ATTN: F. Immen, J. Wheatly

ARMY MATERIALS AND MECHANICS RESEARCH CENTER
WATERTOWN, MASSACHUSETTS 02172

TECHNICAL REPORT DISTRIBUTION

No. of Copies	To
1	Mr. Keith Ellingsworth, Office of Naval Research, Power Program, Arlington, VA 22217
1	Mr. John Fairbanks, Naval Ships Engineering, Prince George Center, Hyattsville, Maryland 20782
1	Capt. D. Zabierek, Air Force Aeropropulsion Lab, Wright-Patterson Air Force Base, Ohio 45433
1	Capt. Smyth, Air Force Materials Laboratory, Wright-Patterson Air Force Base, Ohio 45433
1	Mr. S. Lyons, Wright-Patterson Air Force Base, Ohio 45433
4	Aerospace Research Laboratory, ATTN: ARL-LL, Wright-Patterson Air Force Base, Ohio 45433 ATTN: Dr. Henry Graham Dr. James Wimmer Maj. L. Jacobson Mr. Larry Hjelm
4	NASA Lewis Research Center, 21000 Brookpark Road, Cleveland, Ohio 44135 ATTN: Mr. W. Sanders Dr. Hubert Probst Dr. Robert C. Bill Mr. Donald Guentert
1	Dr. G. C. Deutsch, Ass't Director of Research (Materials), Code RR-1 NASA, Washington, D.C. 20546
1	Mr. George Staber, Office of Coal Research, U.S. Department of the Interior, Washington, D.C. 20240
1	Dr. S. Wiederhorn, Physical Properties Section, Institute for Materials Research, National Bureau of Standards, Washington, D.C. 20234
1	Mr. R. Reynik, Director, Div. of Materials Research, National Science Foundation, 1800 G. Street, N.W., Washington, D.C. 20550
1	Dr. Robb Thomson, Senior Research Scientist, Rm B109, Bld. 225, National Bureau of Standards, Washington, D.C. 20234
1	Mr. H. Morrow, Eustis Directorate, AMRDL, Fort Eustis, VA 23604
1	Dr. R. Warren, Contact Officer, Defense Research & Development Staff, British Embassy, 3100 Massachusetts Avenue N.W., Washington, D.C. 20008

ARMY MATERIALS AND MECHANICS RESEARCH CENTER
WATERTOWN, MASSACHUSETTS 02172

TECHNICAL REPORT DISTRIBUTION

No. of Copies	To

3	Div. of Transportation & Energy Conservation Energy Research and Development Administration, 20 Massachusetts Avenue, NW Washington, D.C. 20545
	ATTN: Mr. George Thur
	           Mr. Robert Schulz
	           Mr. Thomas Sebestyen

1	Dean Daniel C. Drucker, Engineering College, University of Illinois, Urbana, Illinois 61801
1	Professor Merton Flemings, Massachusetts Institute of Technology, Cambridge, Massachusetts 02139
1	Professor Edward E. Hucke, Materials and Metallurgical Engineering, The University of Michigan, Ann Arbor, MI 48104
1	Professor Frank A. McClintock, Department of Mechanical Engineering, Massachusetts Institute of Technology, Cambridge, Massachusetts 02139
1	Dr. R. M. Spriggs, Assistant to the President, Lehigh University, Bethlehem, Pennsylvania 18015
1	Mr. J. D. Walton, Jr., EES, Georgia Tech., Atlanta, Georgia 30332
1	Mr. Y. Baskin, Manager Inorganic Chemical Research, Technical Center, Ferro Corporation, 7500 East Pleasant Valley Road, Independence, Ohio 44131
3	Mr. Robert Beck, Dept. Head, Development Materials, Teledyne CAE, 1330 Laskey Road, Toledo, Ohio 43601 Dr. Eli Benstien, Director of Engineering Mrs. Marlene S. Dowdell, Librarian
1	Dr. J. E. Burke, General Electric Company, Corporate Research & Development, P.O. Box 8, Schenectady, New York 12301
1	Dr. C. A. Bruch, Manager, Advanced Studies, General Electric Company, Aircraft Engine Group, Cincinnati, Ohio 45215
1	Mr. A. R. Canady, Caterpillar Tractor Company, Technical Center Building F, Peoria, Illinois 61602
1	Mr. Seymour Bortz, IIT Research Institute, 10 West 35th Street, Chicago, Illinois 43601

TECHNICAL REPORT DISTRIBUTION

No. of Copies	To
1	Mr. L. M. Donley, Owens Illinois Glass, 1900 North Westwood Avenue, Toledo, Ohio 43601
1	Mr. E. J. Dulis, President, Colt Industries, Materials Research Center, Box 88, Pittsburgh, PA 15230
1	Mr. O. Prachar, Passenger Car Turbine Department, Engineering Staff, General Motors Technical Center, Warren, MI 48090
1	Mr. Winston Duckworth and Mr. Lewis E. Hulbert, Battelle Columbus Laboratories, 505 King Avenue, Columbus, Ohio 43201
1	Energy Research Corporation, Bethel, Connecticut 06801
1	Dr. Peter L. Fleischner, National Beryllia Corp., Haskell, New Jersey 07420
1	Mr. O. I. Ford, Technical Manager, Combustor Systems, Aerojet Liquid Rocket Company, P.O. Box 18222, Sacramento, Calf. 95813
1	Mr. Chester T. Sims, Manager, Advanced Materials General, Electric Company, Gas Turbine Products Div., Schenectady, N.Y. 12301
1	Mr. E. W. Hauck, Market Manager, Engine Components, Norton Company, 1 New Bond Street, Worcester, Massachusetts 01606
1	Mr. M. Herman, Detroit Diesel Allison Division, General Motors Corporation, Indianapolis Operations, P.O. Box 894, Indianapolis, Indiana 46206
1	Mr. J. B. Mann, Director of Research, Chrysler Corporation, P.O. Box 1118, Detroit, MI 48231
1	Mr. James F. Holloway, Materials Project Engineer, Pratt & Whitney Corporation, 400 Main Street, E. Hartford, Connecticut 06108
1	Dr. Paul Jorgensen, Associate Director, Materials Laboratory, Stanford Research Institute, Menlo Park, California 94025
1	Dr. A. V. Illyn, Technical Director, Refractories Division, Babcock & Wilcox, Old Savannah Road, Augusta, Georgia 30903
1	Mr. Paul F. Jahn, Vice President, Fiber Materials, Inc., Broadway and Main Streets, Graniteville, Massachusetts 01829

TECHNICAL REPORT DISTRIBUTION

No. of Copies	To
1	Dr. Robert F. Kirby, Materials Engineering Dept. 93-393M, AiResearch Manufacturing Company, Div. of the Garrett Corporation, Sky Harbor Airport, 402 South 36th Street, Phoenix, Arizona 85034
1	Mr. John G. Lanning, Corning Glass Works, Corning, NY 14830
1	Mr. William D. Long, Manager, Product Development, K-Ramics, Kaman Sciences Corporation, Garden of the Gods Road, Colorado Springs, Colorado 80907
1	Mr. James Lynch, Metals & Ceramics Information Center, Battelle Columbus Laboratories, 505 King Avenue, Columbus Ohio 43201
1	Mr. C. H. McMurtry, Project Manager, Research and Development Div., The Carborundum Company, Niagara Falls, New York 14302
1	Mr. Deo Mattoon, Sing Sing Road, Horseheads, New York 14845
1	Mr. G. Kookootsedes, Market Development, Resins and Chemicals, Dow Corning, Midland, Michigan 48640
1	Professor Burton Paul, Dept. of Mechanical Engineering, University of Pennsylvania, Philadelphia, Pennsylvania 19104
1	Mr. Y. K. Pei, Owens Illinois Glass, 1020 North Westwood Avenue, Toledo, Ohio 43607
1	Dr. Jerry D. Plunkett, President, Materials Consultants, Inc., 2150 South Josephine Street, Denver, Colorado 80210
1	Mr. J. A. Rubin, President, Ceradyne Incorporated, 8948 Fullbright Avenue, Chatsworth, California 91311
1	Mr. Jack W. Sawyer, Gas Turbine International, 4519 Eighteen Street North, Arlington, VA 22207
1	Mr. D. W. McLaughlin, Research & Development Div., Mechanical Technology, Inc., 968 Albany-Shaker Road, Latham, New York 12110

ARMY MATERIALS AND MECHANICS RESEARCH CENTER
WATERTOWN, MASSACHUSETTS 02172

TECHNICAL REPORT DISTRIBUTION

No. of Copies	To
1	Mr. A. R. Stetson, Chief, Process Research Laboratories, Mail Zone R-1, Solar Div. of Int. Harvester Company, 2200 Pacific Highway, San Diego, California 92112
1	Dr. M. L. Torti, Norton Company, 1 New Bond Street, Worcester Massachusetts 01606
1	Dr. T. Vasilos, Applied Technology Division, Avco Corp., Lowell Industrial Park, Lowell, Massachusetss 01851
1	Mr. Francis L. VerSnyder, Manager, Materials Engineering and Research Lab, Pratt & Whitney Corporation, 400 Main Street, E. Hartford, Connecticut 06108
1	Mr. McCoy, Materials Engineering, Garrett-AiResearch Dept. 93-393M, 412 South 36th Street, Phoenix, Arizona 85034
1	Mr. Donald E. Weyer, Dow Corning Corporation, Midland, MI 48640
1	Dr. Michael Guinan, B. Div./L-24, P.O. Box 808, Lawrence Livermore Laboratory, Livermore, California 94550
1	Dr. Mark Wilkins, B Div./L-24, P.O. Box 808, Lawrence Livermore Laboratory, Livermore, California 94550
1	Dr. Charles J. McMahon, Jr., Assoc. Prof. Materials Science, School of Metallurgy & Materials Science, University of Pennsylvania, 3231 Walnut Street, Philadelphia, Pennsylvania
1	Mr. Gaylord D. Smith, The International Nickel Co., Inc., 1 New York Plaza, New York, New York 10004
1	Mr. H. R. Schelp, Garrett Corporation, 9851 Sepulveda Blvd., Los Angeles, California 90009
1	Dr. Robert Widmer, President, Industrial Materials Technology 19 Wheeling Avenue, Woburn, Massachusetts
1	Prof. R. P. Kroon, University of Pennsylvania, Philadelphia, Pennsylvania
1	Dr. Paul G. Shewmon, D212, Argonne National Laboratory, 9700 South Cass Avenue, Argonne, Illinois 60439

TECHNICAL REPORT DISTRIBUTION

No. of Copies	To
1	Dr. Thomas D. McGee, Professor of Ceramic Engineering, Iowa State University, Ames, Iowa 50010
1	Mr. Joe Glotz, Department of the Navy, Naval Air Propulsion Test Center, Trenton, New Jersey 08628
1	Mr. John Miguel, Naval Underwater System Center, Newport, Rhode Island
1	Mr. Robert Benham, AEP-22, U.S. Naval Air Propulsion Test Center (AE), Philadelphia, PA 19112
1	Mr. R. Barry Strachan, Williams Research Corp., Walled Lake, Michigan 48088
1	Mr. S. Walosin, Curtis-Wright Corp. One Passaic Street, Woodridge, N.J. 07075
1	Prof. Marc Richman, Engineering Division, Brown University, Providence, Rhode Island 02912
1	Mr. R. Rice, Naval Research Laboratory, Washington, D.C. 20390
1	Mr. George A. Wacker, Head Metal Physics Br., Naval Ships Research & Development Center, Annapolis, Md. 21402, ATTN: Code 2812
1	Dr. R. Charles, Manager Ceramics Branch, General Electric Co., Corporate R & D Center, P.O. Box 8, Schenectady, New York 12301
1	Mr. C. F. Cline, Manager, Strength Physics Department, Allied Chemical Corporation, P.O. Box 1021R, Morristown, New Jersey 07960
1	Dr. J. T. Bailey, American Lava Corp., Chattanoga, Tennessee 37405
1	Mr. S. T. Wlodek, Cabot Corp. Stellite Div., 1020 West Park Avenue, Kokomo, Indiana 46901
2	Cummins Engine Company, Inc., Columbus, Indiana 47201 Mr. R. Kano, Mr. K. J. Mather
1	Mr. J. D. Mote, EF Industries, Inc., 1501 Courtesy Rd. Louisville, Colorado 80027
1	Mr. William E. Gurwell, Eaton Corporation, Research Center 26201 Northwestern Highway, Southfield, MI 48076

TECHNICAL REPORT DISTRIBUTION

No. of Copies	To
1	Mr. Robert W. Gibson, Jr., Head, Library Dept. General Motors Corporation GM Technical Center, Warren, MI 48090
1	Mr. R. L. Lormand, Lawrence Radiation Lab, P.O. Box 808, Livermore, California 94550
2	Ms. Bolick, National Aeronautics and Space Adminstration Goddard Space Flight Center, Greenbelt, Maryland 20771
1	Mr. Neil T. Saunders, Ch. Mat'ls Appl'n Branch, National Aeronautics and Space Administration, Lewis Research Center, Cleveland, Ohio 44135
1	Ms. Rayna Lee Caplan, Librarian, Northern Research and Engineering Corp., 219 Vassar Street, Cambridge, Mass. 02139
1	Mrs. Jame Bookmyer, Info. Services Div., PPG Industries, Inc., P.O. Box 11472, Pittsburgh, Pennsylvania 15238
1	Mr. P. W. Parsons, Manager, Commercial Research Dept., Stackpole Carbon Company, St. Marys, Pennsylvania 15857
1	Ms. Lucille Steelman, Order Librarian, Stanford Research Institute ATTN: G-037 Library, Menlo Park, Calif. 94025
1	Technical Library, TRW Equipment, TRW Inc., 23555 Euclid Avenue, Cleveland, Ohio 44117
1	Dr. E. P. Flint, U.S. Department of Interior, Bureau of Mines, Room 4513, Interior Bldg., Washington, D.C. 20240
1	Mr. W. Wheatfall, Naval Ship R & D Lab, Code 2812, Annapolis, Maryland 21402
1	Dr. Joseph E. Motherway, University of Bridgeport, Bridgeport, Connecticut 06602
1	Dr. Soloman Musikant, Manager, Metallurgy & Ceramics Lab General Electric Valley Forge, Valley Forge, PA
1	Mr. Louis J. Fiedler, Mat'ls & Process Technology Lab., Avco Corporation, 550 S. Main Street, Stratford, Connecticut 06497
1	Mr. Donald Lapades, The Aerospace Corporation, P.O. Box 92957, Los Angeles, California 90009

ARMY MATERIALS AND MECHANCIS RESEARCH CENTER
WATERTOWN, MASSACHUSETTS 02172

TECHNICAL REPORT DISTRIBUTION

No. of Copies	To
1	Mr. Thomas J. Ahrens, Assoc. Prof. of Geophysics, California Institute of Technology, Seismological Laboratory, 295 San Rafael Avenue, P.O. Bin 2, Arroyo Annex, Pasadena, California 91109
1	Mr. Victor de Biasi, Editor, Gas Turbine World, P.O. Box 494, Southport, Connecticut 06490
1	SKF Industries, Inc., Engineering & Research Center, 1100 1st Avenue, King of Prussia, PA 19406, ATTN: Warren E. Jameson & Harish Dalal
1	Dr. Edward Reynolds, General Motors Technical Center, Passenger Car Turbine Division, Warren, MI 48090
1	Dr. Wm. R. Freeman, Jr., V.P. and Technical Director, Howmet Corporation, Superalloy Group, One Misco Drive, Whitehall, Michigan 47461
1	Mr. D. William Lee, Arthur D. Little, Inc. Acorn Park, Cambridge, Massachusetts 02140
1	Dr. L. Kaufman, Project Director, Manlabs, Inc., 21 Erie Street, Cambridge, Massachusetts 02139
1	Prof. Morris E. Fine, Northwestern University, The Technological Institute, Dept. of Materials Science, Evanston, Illinois
1	Raytheon Company, Research Division Library, Foundry Avenue, Waltham, Massachusetts 02154, ATTN: Ms. Madaleine Bennett, Librarian
1	Prof. T. L. Chu, Southern Methodist University, Institute of Technology, Electronic Sciences Center, Dallas, Texas 75222
1	Mr. H. Stuart Starrett, Head, Mechanics Section, Southern Research Institute, 2000 Ninth Avenue South, Birmingham, Alabama 35205

ARMY MATERIALS AND MECHANICS RESEARCH CENTER
WATERTOWN, MASSACHUSETTS 02172

TECHNICAL REPORT DISTRIBUTION

No. of Copies	To
1	Dr. O. Conrad Trulson, Union Carbide Corporation, Carbide Products Division, 270 Park Avenue, New York, New York 10017
1	Prof. Earl R. Parker, University of California, Department of Materials Science and Engineering, 286 Hearst Mining Building, Berkeley, California 94720
1	Mr. Willard H. Sutton Manager, Ceramics Projects, Special Metals Corporation, New Hartford, New York 13413
1	Dr. Maurice J. Sinnott, Department of Chemical & Metallurgical Engineering, The University of Michigan, Ann Arbor, MI 48104
1	Mrs. R. J. Benacquista, R.I.A.S., 9616 Labrador Lane, Cockeysville, MD 21030
1	Prof. M. C. Shaw, Head, Department of Mechanical Engineering, Cornegie-Mellon University, Pittsburgh, Pennsylvania 15213
1	Mr. Gail Eichelman, Manufacturing Processes Div., Air Force Mateials Laboratory, Wright-Patterson AFB, Ohio 45433
1	Dr. J. C. Lewis, Metals & Minerals Economics Div. Battelle Memorial Institute, 505 King Avenue, Columbus, Ohio 43201
1	Massachusetts Institute of Technology, Cambridge, Massachusetts, 02139, ATTN: Prof. D. W. Kingery, Rm. 13-4090
1	Prof. Michael F. Ashby, Gordon McKay Professor of Metallurgy, Pierce Hall, Harvard University, Cambridge, Massachusetts 02138
1	Prof. I. B. Cutler, University of Utah, College of Engineering Division of Materials Science and Engineering, Salt Lake City, Utah 84112
1	Mr. J. A. Alexander, Manager, Materials Research Department, TRW 23555 Euclid Avenue, Cleveland, Ohio 44117
1	Airesearch Manufacturing Company, Sky Harbor Airport, 402 South 36th Street, Phoenix, Arizona 85034, Attn: Supervisor, Propulsion Engine Advanced Technology Dept., 93-12M
1	Mr. M. Blake, Norton Company, One New Bond Street, Worcester, Mass. 01606

TECHNICAL REPORT DISTRIBUTION

No. of Copies	To
1	Dr. H. P. Kirchner, Ceramic Finishing Company, P.O. Box 498, State College, Pennsylvania 16801
1	Dr. Morris Berg, General Motors Corporation, AC Spark Plug Division Flint, Michigan 48556
1	Dr. Michael J. Noone, General Electric Company, Space Sciences Laboratory, Box 8555, Philadelphia, Pennsylvania 19101
1	Dr. Richard Kliener, GTE Sylvania, Tonawanda, Pennsylvania 18848
1	Mr. F. E. Krainess, Rockwell International Corporation, D/391-204 AB70 12214 Lakewood Boulevard, Downey, California 90241
1	Mr. David Cormier, Nuclear Planning Division, Stone & Webster Engineering Corporation, 87 Nash Memorial Road, Abington, Ma. 02351
1	Mr. V. A. Chase, Chief of Development Laboratory, Whittaker Corporation, Research and Development Division, 3540 Aero Court, San Diego, Cal. 92123
1	Dr. Stanley Waugh, Research Division, Raytheon Corporation, Research Division, 28 Seyon Street, Waltham, Massachusetts 02154
1	Coors Porcelain Company, Research Department, 17750 West 32nd Avenue, Golden, Colorado 80401
1	Professor Robert F. Davis, North Carolina State University, Department of Materials Science, Box 5427, Raleigh, North Carolina 27607
1	Dr. H. von E. Doering, Manager, Fuels/Corrosion Unit, General Electric Company, Gas Turbine Products Division, Building 53-311, Schenectedy, New York 12345
1	Dr. R. Ruh, AFML/LLS, Air Force Materials Laboratory, Wright-Patterson AFB, Ohio 45433
1	Mr. Michael E. Naylor, General Motors Technical Division, Passenger Car Turbine Division, Warren, Michigan 48090
1	Dr. John V. Milewski, ESSO Research and Engineering Company, Government Research Laboratory, P.O. Box 8, Linden, New Jersey 07036
1	Mr. M. J. Klein, Research Staff Specialist, Mail Zone R-1, Solar, 2200 Pacific Highway, P.O. Box 80966, San Diego, California 92138

ARMY MATERIALS AND MECHANICS RESEARCH CENTER
WATERTOWN, MASSACHUSETTS 02172

TECHNICAL REPORT DISTRIBUTION

No. of Copies	To
1	Dr. Frank Galasso, United Aircraft Research Laboratories, East Hartford Conn. 06108
8	Lt. Col. James Kennedy, Chief, Materials Branch, European Research Office U. S. Army R&D Group, (EUR), Box 15, FPO New York 09510
1	Dr. Joseph Griffo, U. S. Atomic Energy Commission Space Nuclear Systems Division, Century XXI Building, Mail Station F-309, Washington, D.C. 20545
1	Mr. Joseph Simpson, Rohr Industries, Inc., Technical Library P.O. Box 1516, Chula Vista, California 92012
1	Mr. Philip J. Willson, Chemical Research, Chrysler Corporation, Box 1118, CIMS 418-19-18, Detroit, Michigan 48231
1	Mr. William Combs, Battelle Memorial Institute, 2030 M Street N.W. Washington, D.C. 20036
1	Mr. M. A. Schwartz, U.S. Department of the Interior, Bureau of Mines Tuscaloosa Metallurgy Research Laboratory, P.O. Box 1, University, Alabama 35486
1	Turbo Power and Marine Systems, Inc., ATTN: Mr. Carl Merz, Farmington, Connecticut 06032
1	Mr. R. N. Singh, Argonne National Laboratory, Materials Science Division 9700 South Cass Avenue, Argonne, Illinois 60439
1	Mr. Richard E. Engdahl, Deposits & Composites, Inc., 1821 Michael Faraday Drive, Reston, Virginia 22090
1	Mr. Leonard Topper, Office of Energy Policy, National Science Foundation 1800 G Street N. W., Washington, D.C. 20550
1	Mr. Ron Lowrey, U.S. Bureau of Mines, P.O. Box 70, Albany, Oregon 97321
1	Materials Science Corporation, Technical Library, Blue Bell Office Campus, Merion Towle Building, Blue Bell, Pennsylvania 19422
1	Ms. Sharon Wright, Creare Inc., Technical Library, Hanover, New Hampshire 03755

ARMY MATERIALS AND MECHANICS RESEARCH CENTER
WATERTOWN, MASSACHUSETTS 02172

TECHNICAL REPORT DISTRIBUTION

No. of Copies	To
1	Mr. John Polyansky, Gas Turbine Design Engineering, Turbodyne Corporation, 626 Lincoln Avenue S E, St. Cloud, Minnesota 56301
1	Mr. Donald J. Legacy, Turbodyne Corporation, Wellsville, New York 14895
1	Mr. P. R. Miller, NASA Headquarters, Code RPD, 600 Independence Avenue S. W., Washington, D.C. 20546
1	Dr. Charles Berg, Chief Engineer, Federal Power Commission, Room 2100 825 North Capital Street, N.E., Washington, D.C. 20426
1′	Mr. Michael Lauriente, Department of Transportation, 400 Seventh Street, S. W., Washington, D.C. 20590
1	Dr. Donald Vieth, National Bureau of Standards, Administration Bldg., Room A1002, Washington, D.C. 20234
1	Dr. Leonard Topper, National Science Foundation, Office of Energy R & D Policy, Room 537, 1800 G Street NW, Washington, D.C. 20550
2	Electric Power Research Institute, P.O. Box 10412, Palo Alto, California 94304 ATTN: Dr. Richard E. Balzhiser, Dr. Arthur Cohn
1	W. C. Christensen, Assistant for Resources, Directorate for Energy, OASD (I&L), Room 2B341 Pentagon, Washington, D.C. 20301
1	Mr. Tyler Port, Special Assistant, OASA (I&L), Room 3E620 Pentagon, Washington, D.C. 20301
1	Major Jose Baca, Hdqtrs., Air Force Systems Comman/DLFP, Propulsion and Power Branch, Andrews Air Force Base, Washington, D.C. 20034
1	Mrs. Patricia Mooney, Office of Management and Budget, Energy R&D Coordination Branch, Room 8001, New Executive Office Bldg., Washington, D.C. 20503
1	James Johnson, Environmental Protection Agency, Air Technology Branch, RD-681, Room 621 W, 401 M Street, N.W., Washington, D.C. 20490
1	Mr. Thomas Gross, Staff Member, Office of Energy Conservation, Federal Energy Office, Room 4234, Columbia Plaza Bldg., Washington, D.C. 20461

ARMY MATERIALS AND MECHANICS RESEARCH CENTER
WATERTOWN, MASSACHUSETTS 02172

TECHNICAL REPORT DISTRIBUTION

No. of Copies	To
1	Dr. John S. Foster, Jr., Vice President for Energy Research and Development, TRW Incorporated, One Space Park, Redondo Beach, California 90278
1	Dr. Raymond Bisplinghoff, Deputy Administrator, National Science Foundation, 1800 G. Street, N.W., Washington, D.C. 20550
1	Dr. Alan Womack, Assistant Director, Gas Cooled Reactors, Atomic Energy Commission, Washington, D.C. 20545
1	Dr. Donald Weidhuner, Chief, Power Division, Research Development & Engineering Directorate, Army Materials Command Headquarters, 5001 Eisenhower Avenue, Alexandria, Virginia 22304
1	Dr. A. Lovelace, Deputy Assistant Secretary (R&D), Office of Assistant Secretary of the Air Force (Research & Development), Room 4E973, Pentagon, Washington, D.C. 20330
1	Dr. Neal Richardson, TRW Incorporated, One Space Park, Redondo Beach, California 90278
1	Mr. Roy Peterson, Chief, Pollution Abatement & Gas Turbine Research, Ship Research & Technology Division, Naval Ship Systems Command Hqtrs., 2531 Jefferson Davis Highway, Arlington, Virginia 20362
1	Dr. Eugene C. Gritton, The Rand Corporation, Physical Sciences Department, 1700 Main Street, Santa Monica, California 90406
1	Mr. C. A. Vassilakis, Turbo Power & Marine Systems, New Britain Ave., Farmington, Conn. 06032
1	Mr. P. E. McConnell, Owens-Corning Fiberglas Corporation, Technical Center, Granville, Ohio 43023
1	Turbodyne Corporation, 711 Anderson Avenue North, St. Cloud, Minnesota 56301, ATTN: Diane Konsor
1	Mr. N. B. Elsner, General Atomics Corporation, Box 81608, San Diego, California 92037
1	Mr. Eldor R. Herrmann, Ceramic Systems, Inc., 11402 Schaefer Highway, Detroit, Michigan 48227
1	Dr. William H. Rhodes, GTE Laboratories, Waltham Research Center, 40 Sylvan Road, Waltham, Massachusetts 02154

ARMY MATERIALS AND MECHANICS RESEARCH CENTER
WATERTOWN, MASSACHUSETTS 02172

TECHNICAL REPORT DISTRIBUTION

No. of Copies	To
1	Anne M. Theil, Avco Everett Research Laboratory, Inc., 2385 Revere Beach Parkway, Everett, Massachusetts, 02149
1	Mr. William Oldfield, Materials Research and Computer Simulation, 634 Berkeley Place, Westerville, Ohio 43081
1	Dr. Wilfred H. Dukes, Assistant Director Engineering for Development Bell Aerospace, P.O. Box 29307, New Orleans, Louisiana 70189
1	Dr. Keith E. McKee, Director of Research Engineering Mechanics Div., IIT Research Institute, 10 West 35th Street, Chicago, Illinois 60616
1	Dr. Donald R. Uhlmann, Associate Professor of Ceramics, Department of Metallurgy and Materials Science, Massachusetts Institute of Tech., Cambridge, Massachusetts 02139
1	Dr. John B. Wachtman, Jr., Division Chief, Inorganic Materials Div. National Bureau of Standards, Room A359, Materials Building, Washington, D.C. 20234
1	Mr. Donald G. Groves, Staff Engineer, National Materials Advisory Board, National Academy of Sciences, 2101 Constitution Ave., N.W., Washington, D.C. 20418
1	Major Roger Austin, Air Force Materials Laboratory, Wright-Patterson Air Force Base, Ohio 45433
1	Mr. James J. Gangler, Advanced Research & Technology Div., Code RRM, Room B556, National Aeronautics and Space Adminstration, Headquarters, Washington, D.C. 20546
1	Dr. W. Bunk, DFVLR - Institut fur Werkstoff-Forshung, 505 Porz-Wahn, Linder Hohe, Germany
1	Mr. Karl Koyama, General Atomic Company, Box 81608, San Diego, Ca 92138
1	Mr. M. Allen Magid, Materials Marketing Engineer, Florida R & D Center Pratt & Whitney Aircraft, P.O. Box 2691, West Palm Beach, Fla 33402
1	Mr. Nelson R. Roth, Bell Aerospace Company, P.O. Box #1, Dept. V70, Buffalo, NY 14240
1	Mr. F. G. Stroke, Asst. Mgr. Mrkt. Dev., PPG Industries, Inc., 1 Gateway Center, Pittsburgh, Pa 15222

TECHNICAL REPORT DISTRIBUTION

No. of Copies	To
1	Mr. Leslie Hypnarowski, Carborundum Co., Carborundum Center, Niagara Falls, Ny 14302
1	Dr. Mike Buckley, AFML - LLP, Wright Patterson AFB, Dayton, Ohio 45433
1	Dr. Don Thompson, Rockwell International Corporation, Science Center, 1049 Camino Dos Rios, Thousand Oaks, Ca 91360
1	Dr. W. Thielbaln, Code 4061, Naval Weapons Center, China Lake, Ca 93555
1	Dr. Arthur Cohn, EPRI, P.O. 10412, 3412 Hillview Avenue, Palo Alto, Ca 94304
1	Mr. A. E. Leach, Mgr., Process Development Engineering, Mail Zone C-33, Bell Aerospace Company, P.O. Box 1, Buffalo, NY 14240
1	Dr. Robert K. Thomas, FA4-4, Reactor Engineering, General Atomic Company, P.O. Box 81608, San Diego, Ca 92138
1	Mr. Arthur L. Ross, Valley Forge Space Center, General Electric Company, P.O. Box 8555, Philadelphia, Pennsylvania 19101
1	Mr. Dennis W. Swain, Department 93-19 M, Airesearch Manufacturing Company, P.O. Box 5217, Pheonix, Arizona 85010
1	Mr. Wayne Everett, Wyman-Gordon Company, Research and Development, North Grafton, MA 01536
1	Mr. William A. Edmiston, Jet Propulsion Laboratory, California Institute of Technology, 4800 Oak Grove Drive, Pasadena, Ca 91103
2	Kawecki-Berylco Industries Inc., P.O. Box 1462, Reading, Pa 19603 ATTN: Mr. R. J. Longenecker, Mr. E. Laich

4 Authors

306 Total Copies Distributed

D18

Key Words

Gas Turbine Engine
Brittle Design
Ceramics
High Temperature Materials
Silicon Nitride
Silicon Carbide
Non-Destructive Tests
Mechanical Properties

ABSTRACT

The "Brittle Materials Design, High Temperature Gas Turbine" program objective is to demonstrate successful use of brittle materials in demanding high temperature structural applications. A small vehicular gas turbine engine and a static test rig, each using uncooled ceramic components, will be utilized in this iterative design and materials development program. Both the contractor, Ford Motor Company, and the subcontractor, Westinghouse Electric Corporation, have had in-house research programs in this area prior to this contract.

In the vehicular turbine project, design work was completed and tooling ordered for a revised Design D silicon nitride duo-density turbine rotor using radially stacked airfoil sections which reduced blade stresses by 16%. Press bonding of duo-density rotors continues to show excellent bonding between the hot pressed hub and the reaction sintered blade ring when hub-forming and bonding are accomplished in the same operation. Two hot pressed silicon nitride hubs were successfully tested through ten cycles to 1950°F and 35,000 rpm in the turbine rotor test rig with no observable deterioration in the curvic coupling rotor-to-shaft attachment. Stators of 2.55 gm/cm³ density silicon nitride were injection molded which were free from flaws as determined visually and by x-ray radiography. Further development of 2.7 gm/cm³ density (84.5% T.D.) injection molded silicon nitride resulted in improved moldability; test samples nitrided in an atmosphere of 4% H₂/96% N₂ had an average modulus of rupture of 43.2 ksi. This material will be used for molding of engine components.

In the stationary turbine project, a decision was made to de-emphasize the 30 MW size turbine demonstration of ceramic stator vanes and to focus available efforts on static rig testing. The static rig was rebuilt following catastrophic failure, and incorporates a new metal combustor with additional air cooling as well as other improvements. Tensile testing of Si₃N₄ continues, with the development of a method of powder support for the specimens which considerably improved alignment. Long term static oxidation testing of hot pressed Si₃N₄ resulted in strength degradation, due to the formation of MgSiO₃ which chemically attacks the Si₃N₄. Hot pressed Si₃N₄ made with yttria additives was found to have poor oxidation resistance at 1800°F, although oxidation resistance was good when measured at higher temperatures.

AD _____

Army Materials and Mechanic Research Center,
Watertown, Massachusetts 02172

BRITTLE MATERIALS DESIGNS
HIGH TEMPERATURE GAS TURBINE

Arthur F. McLean, Eugene A. Fisher, Ford
Motor Company, Dearborn, Michigan 48121
Raymond J. Bratton, Donald G. Miller,
Westinghouse Electric Corporation, Pittsburgh,
Pennsylvania 15235

Key Words

Gas Turbine Engine
Brittle Design
Ceramics
High Temperature Materials
Silicon Nitride
Silicon Carbide
Non-Destructive Tests
Mechanical Properties

ABSTRACT

The "Brittle Materials Design, High Temperature Gas Turbine" program objective is to demonstrate successful use of brittle materials in demanding high temperature structural applications. A small vehicular gas turbine engine and a static test rig, each using uncooled ceramic components, will be utilized in this iterative design and materials development program. Both the contractor, Ford Motor Company, and the subcontractor, Westinghouse Electric Corporation, have had in-house research programs in this area prior to this contract.

In the vehicular turbine project, design work was completed and tooling ordered for a revised Design D silicon nitride duo-density turbine rotor using radially stacked airfoil sections which reduced blade stresses by 16%. Press bonding of duo-density rotors continues to show excellent bonding between the hot pressed hub and the reaction sintered blade ring when hub-forming and bonding are accomplished in the same operation. Two hot pressed silicon nitride hubs were successfully tested through ten cycles to 1950°F and 35,000 rpm in the turbine rotor test rig with no observable deterioration in the curvic coupling rotor-to-shaft attachment. Stators of 2.55 gm/cm³ density silicon nitride were injection molded which were free from flaws as determined visually and by x-ray radiography. Further development of 2.7 gm/cm³ density (84.5% T.D.) injection molded silicon nitride resulted in improved moldability; test samples nitrided in an atmosphere of 4% H₂/96% N₂ had an average modulus of rupture of 43.2 ksi. This material will be used for molding of engine components.

In the stationary turbine project, a decision was made to de-emphasize the 30 MW size turbine demonstration of ceramic stator vanes and to focus available efforts on static rig testing. The static rig was rebuilt following catastrophic failure, and incorporates a new metal combustor with additional air cooling as well as other improvements. Tensile testing of Si₃N₄ continues, with the development of a method of powder support for the specimens which considerably improved alignment. Long term static oxidation testing of hot pressed Si₃N₄ resulted in strength degradation, due to the formation of MgSiO₃ which chemically attacks the Si₃N₄. Hot pressed Si₃N₄ made with yttria additives was found to have poor oxidation resistance at 1800°F, although oxidation resistance was good when measured at higher temperatures.

REPORT DOCUMENTATION PAGE	READ INSTRUCTIONS BEFORE COMPLETING FORM

1. REPORT NUMBER AMMRC CTR-75-28	2. GOVT ACCESSION NO.	3. RECIPIENT'S CATALOG NUMBER

4. TITLE (and Subtitle) Brittle Materials Design, High Temperature Gas Turbine	5. TYPE OF REPORT & PERIOD COVERED Interim Report Number 8 1/1/75 to 6/31/75
	6. PERFORMING ORG. REPORT NUMBER

7. AUTHOR(s) A. F. McLean, Ford Motor Company E. A. Fisher, Ford Motor Company R. J. Bratton, Westinghouse Elec. Corp. D. G. Miller, Westinghouse Elec. Corp.	8. CONTRACT OR GRANT NUMBER(s) DAAG 46-71-C-0162

9. PERFORMING ORGANIZATION NAME AND ADDRESS Ford Motor Company, Dearborn, Mi 48121	10. PROGRAM ELEMENT, PROJECT, TASK AREA & WORK UNIT NUMBERS D/A Project: ARPA Order-1849 Agency Accession: DA OD 4733

11. CONTROLLING OFFICE NAME AND ADDRESS Army Materials and Mechanics Research Center Watertown, Massachusetts 02172	12. REPORT DATE October, 1975
	13. NUMBER OF PAGES 158 p.

14. MONITORING AGENCY NAME & ADDRESS(if different from Controlling Office)	15. SECURITY CLASS. (of this report) Unclassified
	15a. DECLASSIFICATION/DOWNGRADING SCHEDULE

16. DISTRIBUTION STATEMENT (of this Report)

Distribution limited to U.S. ▉▉▉▉ Government agencies, ▉▉▉ ▉▉▉▉▉ only: Test and Evaluation data; October, 1975. Other requests for this document must be referred to the Director, Army, Materials and Mechanics Research Center, ATTN: AMXMR-PL, Watertown, Massachusetts 02172

17. DISTRIBUTION STATEMENT (of the abstract entered in Block 20, if different from Report)

Interim rept. no. 8, 1 Jan - 31 Jun 75;

18. SUPPLEMENTARY NOTES

19. KEY WORDS (Continue on reverse side if necessary and identify by block number)

Gas Turbine Engine	Silicon Nitride
Brittle Design	Silicon Carbide
Ceramics	Non-Destructive Tests
High Temperature Materials	Mechanical Properties

20. ABSTRACT (Continue on reverse side if necessary and identify by block number)

(See reverse side)

DD FORM 1473 1 JAN 73   EDITION OF 1 NOV 65 IS OBSOLETE

141 250

ABSTRACT

The "Brittle Materials Design, High Temperature Gas Turbine" program objective is to demonstrate successful use of brittle materials in demanding high temperature structural applications. A small vehicular gas turbine engine and a static test rig, each using uncooled ceramic components, will be utilized in this iterative design and materials development program. Both the contractor, Ford Motor Company, and the subcontractor, Westinghouse Electric Corporation, have had in-house research programs in this area prior to this contract.

In the vehicular turbine project, design work was completed and tooling ordered for a revised Design D silicon nitride duo-density turbine rotor using radially stacked airfoil sections which reduced blade stresses by 16%. Press bonding of duo-density rotors continues to show excellent bonding between the hot pressed hub and the reaction sintered blade ring when hub-forming and bonding are accomplished in the same operation. Two hot pressed silicon nitride hubs were successfully tested through ten cycles to 1950°F and 35,000 rpm in the turbine rotor test rig with no observable deterioration in the curvic coupling rotor-to-shaft attachment. Stators of 2.55 gm/cm^3 density silicon nitride were injection molded which were free from flaws as determined visually and by x-ray radiography. Further development of 2.7 gm/cm^3 density (84.5% T.D.) injection molded silicon nitride resulted in improved moldability; test samples nitrided in an atmosphere of 4% H_2/96% N_2 had an average modulus of rupture of 43.2 ksi. This material will be used for molding of engine components.

In the stationary turbine project, a decision was made to de-emphasize the 30 Mw size turbine demonstration of ceramic stator vanes and to focus available efforts on static rig testing. The static rig was rebuilt following catastrophic failure, and incorporates a new metal combustor with additional air cooling as well as other improvements. Tensile testing of Si_3N_4 continues, with the development of a method of powder support for the specimens which considerably improved alignment. Long term static oxidation testing of hot pressed Si_3N_4 resulted in strength degradation, due to the formation of $MgSiO_3$ which chemically attacks the Si_3N_4. Hot pressed Si_3N_4 made with yttria additives was found to have poor oxidation resistance at 1800°F, although oxidation resistance was good when measured at higher temperatures.